Calcium and Zirconium Oxide Based Solid Catalysts for the Transesterification of Low Quality Triglycerides

Submitted in partial fulfillment of the requirement

for the Degree of

Doctor of Philosophy

by

Navjot Kaur

(Roll No. 901009002)

Under the supervision of

Dr. Amjad Ali

(Associate Professor)

SCHOOL OF CHEMISTRY AND BIOCHEMISTRY
THAPAR UNIVERSITY
PATIALA – 147004

December-2014

DEDICATED TO

MY

BELOVED PARENTS

ACKNOWLEDGEMENTS

I would like to express my deepest gratitude to my Supervisor and mentor Dr. Amjad Ali, School of Chemistry and Biochemistry, Thapar University, Patiala for his immense encouragement, guidance and unwavering support from the preliminary to the concluding levels of my Doctoral Research. He supported me throughout my work with patience and knowledge whilst allowing me the room to work in my own way. He has always been a pillar of support and constant source of inspiration. His commitment and sense of mission has molded my work to provide it direction and substance.

I am extremely thankful to the Director, Thapar University, Dean (Research & Sponsored Projects) and Head, School of Chemistry & Biochemistry for extending the opportunity to undertake this doctoral research.

I would be failing in my duties if I do not mention Council of Scientific & Industrial Research (CSIR), New Delhi and School of Chemistry & Biochemistry for providing fellowship. I am highly obliged to the doctoral committee members Dr. Ranjana Prakash, Dr. Manmohan Chibber & Dr. Raj Kumar Gupta for monitoring my research work from time to time and giving their valuable suggestions.

I would like to acknowledge School of Chemistry and Biochemistry (Thapar University, Patiala) and DST-FIST for FT-IR and GC-MS, SAI laboratories (Thapar University, Patiala) for NMR, SEM and XRD, SAIF (Panjab University, Chandigarh) for powder XRD, FT-IR, TEM and NMR, IIT Ropar for SEM, SAIF (IIT Bombay) for ICP-AES and CHNS analysis, AVANSA Technology and Services (Kanpur) for XPS and surface area analysis, We are very thankful to Dr. Nakka Linghiah for the sample analysis

of CO_2-TPD, Dr. Nitin Kumar Singhal (NABI, Mohali) for the sample analysis of ICP-AES, Dr. Bhupendra Chudasama the sample analysis of TGA. In lab I have been aided for many years in running the equipment by Mr. Chander Singh, a fine technician.

This journey would not have been the same without my seniors Grateful acknowledgement is made to my seniors Dr. Dinesh Kumar, Dr. Vishal Mutreja, Dr. Joginder Singh, Dr. Madhu Katiyar, Dr. Mandeep Kaur, Dr. Rupinder Kaur, Dr. Inderpreet Singh, Dr. Rohit Singh, and my friends Shilpa Narang, Ruchika Thakur, Alka Sharma, Shweta Sareen, Sandeep Kaur Bhupinder, Bindu, Abida and Rashi.

I am also thankful to all the teaching and non-teaching staff members of the department for their invaluable cooperation and help during the entire tenure of my studies in the department.

In the end, I wish to express my deep sense of gratitude to my family, for supporting and encouraging me at every step of my work. It is power of their blessings, which has given me the courage, confidence and zeal for hard work.

Navjot Kaur

Navjot Kaur

CERTIFICATE

This is to certify that thesis entitled "CALCIUM AND ZIRCONIUM OXIDE BASED SOLID CATALYSTS FOR THE TRANSESTERIFICATION OF LOW QUALITY TRIGLYCERIDES", being submitted by Navjot Kaur, to the School of Chemistry and Biochemistry, Thapar University, Patiala for the award of degree of DOCTOR OF PHILOSOPHY, is a record of bonafide research work carried out by her. Ms. Navjot Kaur has worked under my guidance and supervision and has fulfilled the requirements for the submission of this thesis, which to my knowledge has reached the requisite standard.

The results embodied in the thesis have not been submitted in part or full to any other University or Institute for the award of any degree or diploma.

Dr. Amjad Ali
Associate Professor
School of Chemistry and Biochemistry,
Thapar University, Patiala.

TABLE OF CONTENTS

LIST OF ABBREVIATIONS

Abbreviation	*Description*
FAAE	Fatty acid alkyl ester
FAME	Fatty acid methyl ester
FAEE	Fatty acid ethyl ester
VOs	Vegetable oils
FFA	Free fatty acids
OA	Oleic acid
MO	Methyl oleate
EO	Ethyl oleate
CO	Cottonseed oil
WO	Waste cottonseed oil
JO	Jatropha oil
KO	Karanja oil
BD	Biodiesel
A.V.	Acid value
MeOH	Methanol
EtOH	Ethanol
XRD	X-ray diffraction
XPS	X-ray photoelectron spectroscopy
FT-IR	Fourier transform infra red
DRIFT	Diffuse reflectance infra red fourier transform
SEM	Scanning electron microscopy
TEM	Transmission electron microscopy
EDS	Energy Dispersive X-ray spectroscopy
BET	Brunauer- Emmett-Teller
BJH	Barret-Joyner-Halenda
NH_3-TPD	Ammonia Temperature Programmed Desorption
CO_2-TPD	Carbon dioxide Temperature Programmed Desorption
XPS	X-ray Photoelectron Spectroscopy
FT-NMR	Fourier transform nuclear magnetic resonance
GC-MS	Gas chromatography mass spectrometry
ICP-AES	Inductively coupled plasma-atomic emission spectroscopy
CHNS	Carbon Hydrogen Nitrogen Sulfur Analyzer
TMS	Tetramethyl silane
TOF	Turn over frequency
NIST	National Institute of Standards and Technology
JCPDS	Joint Committee for Powder Diffraction Standards
ATR	Attenuated total reflectance
ASTM	American Society for Testing and Materials
EN	European standards
$\%C_{ME}$	Conversion of methyl ester
$\%C_{EE}$	Conversion of ethyl ester
cm	Centimetre
mmol g^{-1}	Millimole per gram
IU	International unit
kJ mol^{-1}	Kilo joule per mole

kJ K^{-1} mol^{-1}	Kilo joule per mole per kelvin
min	minute
ml	Millilitre
MHz	Mega hertz
Mol	Mole
MW	Molecular weight
mg	Milligram
mg L^{-1}	Milligram per litre
µmol	Micro mole
N_2	Nitrogen
nm	nanometre
ppm	Parts per million
rpm	Rotation per minute
v/v	Volume by volume
wt%	Weight percentage
NR	Not reported
ND	Not determined

LIST OF SYMBOLS

Symbols	*Description*
Å	Angstrom
A	Pre–exponential factor
C	Celsius
E_a	Activation energy
$\Delta G^{\ddagger}$	Gibbs free energy
$\Delta H^{\ddagger}$	Enthalpy
$\Delta S^{\ddagger}$	Entropy
g	Gram
h	Hour
K	Kelvin
k	Rate constant
m	Metre
%	percentage
μ	Micro
θ	Theta
α	Alpha
°	Degree
R	Gas constant
T	Temperature
t	Time
v	Volume
pK_a	Hammett acidity or basicity
B	Bronsted sites
L	Lewis sites
f_m	Active sites
v	vander Waals radii
X	Conversion

LIST OF FIGURES

LIST OF TABLES

LIST OF SCHEMES

ABSTRACT

In present thesis five different series of catalysts *viz.*, Ce/ZrO_2-TiO_2/SO_4^{2-}, Zr/CaO, Mo/CaO, Li/ZrO_2 and Sr:Zr were prepared by wet chemical route and/or co-precipitation method to catalyze the esterification and/or transesterification of free fatty acid containing VOs in heterogeneous mode. The structure of catalysts was established by powder XRD study, while the surface morphology and particle size by SEM and TEM studies. The acidic/basic active sites present in catalysts were quantified by Hammett indicator test method.

For the esterification of fatty acids, in presence of triglycerides, sulfated Ce/ZrO_2–TiO_2 was employed as solid catalyst. The catalyst activity was found to be a function of its Bronsted acidic sites which in turn depends on the cerium concentration in catalyst. The catalyst was able to catalyze the fatty acid esterification even in presence of up to 12 wt% moisture contents (with respect to fatty acids). The catalyst has shown excellent stability as negligible sulfate leaching was observed and recovered catalyst was reused in five successive runs without significant loss in activity. However, the catalyst was not found to be active to carry out the transesterification of triglycerides.

In order to replace highly toxic and non renewable methanol with nontoxic as well as renewable ethanol for biodiesel production, Zr/CaO catalyst was employed as heterogeneous catalyst for the transesterification of jatropha oil which contain up to 15.6 wt% FFA content. The catalytic activity was found to be a function of basic sites which in turn depend on calcination temperature and zirconium concentration. The activity of the catalyst was lost after two successive runs mainly due to the leaching of active metal. To further improve the reusability and stability of CaO based catalyst, Mo impregnated CaO catalyst was prepared (Mo/CaO) and employed as reusable catalyst for the ethanolysis of non edible oils (having up to 18 wt% FFA content), to obtain > 99% fatty acid ethyl ester (FAEE) yield. The catalyst was recovered and reused five times without significant loss in activity.

In order to develop a catalyst for simultaneous esterification as well as transesterification, Li/ZrO_2 was prepared and successfully employed for one-pot production of biodiesel via esterification and transesterification from vegetable oil having FFA content as high as 18.1 wt%. No significant loss in catalyst activity was observed even during 9 consecutive runs as > 90 % fatty acid alkyl ester yield was maintained. Another catalyst, Sr:Zr was also found to catalyze simultaneous esterification and transesterification of high free fatty acid containing vegetable oils with ethanol. The catalyst has been recovered and recycled without any significant loss in activity during four successive catalytic cycles.

Besides catalytic activity, kinetics and thermodynamic parameters of the reactions catalyzed by prepared catalyst, were also evaluated. The transesterification reaction catalyzed by all catalysts has followed (pseudo) first order kinetic equation. For all catalysts, the heterogeneous mode of action has been proved by performing hot filtration test. Koros-Nowak test was performed to demonstrate that catalytic activity was free from internal mass diffusion limitations. Few physicochemical properties of the prepared FAME and FAEE have also been studied and compared with EN 14214 and ASTM standard values.

Keywords: Biodiesel, Transesterification, Esterification, Methanolysis, Ethanolysis, Leaching, Kinetics, Koros-Nowak test and Mass transfer.

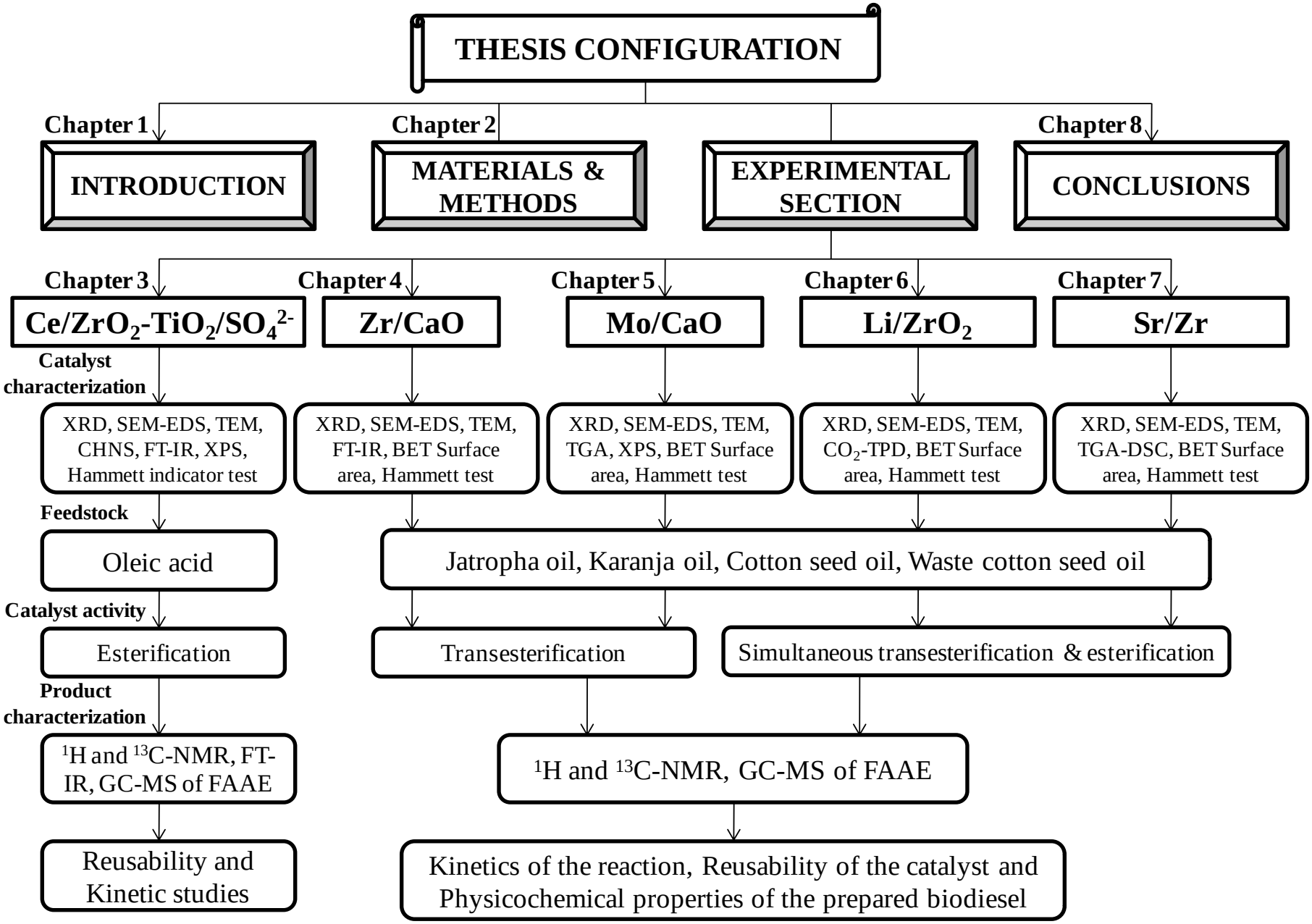
THESIS CONFIGURATION
Chapter 1
INTRODUCTION
Chapter 2
MATERIALS & METHODS
EXPERIMENTAL SECTION
Chapter 8
CONCLUSIONS
Chapter 3
Ce/ZrO2-TiO2/SO4 2-
Chapter 4
Zr/CaO
Chapter 5
Mo/CaO
Chapter 6
Li/ZrO2
Chapter 7
Sr/Zr
Catalyst characterization
XRD, SEM-EDS, TEM, CHNS, FT-IR, XPS, Hammett indicator test
XRD, SEM-EDS, TEM, FT-IR, BET Surface area, Hammett test
XRD, SEM-EDS, TEM, TGA, XPS, BET Surface area, Hammett test
XRD, SEM-EDS, TEM, CO2-TPD, BET Surface area, Hammett test
XRD, SEM-EDS, TEM, TGA-DSC, BET Surface area, Hammett test
Feedstock
Oleic acid
Jatropha oil, Karanja oil, Cotton seed oil, Waste cotton seed oil
Catalyst activity
Esterification
Transesterification
Simultaneous transesterification & esterification
Product characterization
1H and 13C-NMR, FT-IR, GC-MS of FAAE
1H and 13C-NMR, GC-MS of FAAE
Reusability and Kinetic studies
Kinetics of the reaction, Reusability of the catalyst and Physicochemical properties of the prepared biodiesel

Introduction and literature review

Abstract: Biodiesel, defined as fatty acid alkyl esters, is a renewable, biodegradable, and non-toxic alternate to conventional diesel fuel. The replacement of mineral diesel with biodiesel would be beneficial from environmental point of view, as later fuel does not contain aromatic and sulfur compounds, and upon combustion causes lower emissions of hydrocarbon and CO_x in comparison to conventional diesel fuel. At present, edible vegetable oils are the main feedstock for the commercial scale biodiesel production. Due to scarcity of edible oil, however, in India use of non edible or waste cooking oils is encouraged for biodiesel production. These oils are much cheaper than refined edible vegetable oil and hence, their application as feedstock may also reduce the biodiesel production cost to significant extent. However, due to the presence of high free fatty acids (2.5-40 wt%) and moisture contents, such feedstock could not be used in homogeneous catalyzed process for biodiesel production. Additionally homogeneous catalysts required subsequent neutralization, separation, and purification steps which are time consuming and generate huge quantity of industrial effluents. Recently more attention has been paid for the development of heterogeneous catalyst for biodiesel production due to the advantages of separation, reusability, and high FFA and moisture tolerance. A wide variety of heterogeneous acid/base catalysts for biodiesel production have been reported in literature including sulfated metal oxides, heteropolyacids, sulfonic ion exchange resins, zeolites, mesoporous silica, sulfonated carbon based, and miscellaneous solid acid catalysts, alkali or alkaline earth oxides, alkali doped mixed oxides, transition metal oxides, basic zeolites and clays such as hydrotalcites, and immobilised organic bases.

1.1. Introduction

Spiralling fossil fuel consumption in past three decades, due to severe industrialization, is exhausting the limited fossil fuel resources at a great pace and causing the environmental distress due to the emission of greenhouse gases and other pollutants (Aransiola *et al.*, 2014). Thus for a sustainable future non renewable fuel resources must be replaced with alternative and renewable one. From energy security point of view it is extremely important for a country like India, which supplement 60-70% of its demand with imported crude oil, to find out the alternative and renewable fuel resources derived from locally grown sources.

Biodiesel, defined as fatty acid alkyl esters (FAAE), is a renewable, biodegradable, and non-toxic alternate to conventional diesel fuel. The replacement of mineral diesel with biodiesel would also be beneficial from environmental point of view, as later fuel does not contain aromatic and sulfur compounds, and on burning causes lower emissions of hydrocarbon and CO_x than fossil based diesel fuel (Singh *et al.*, 2014). Transesterification of vegetable oils (VOs) and animal fat with short chain alcohols in presence of alkali catalysts (NaOH, KOH, etc.) leads to the generation of biodiesel and glycerol as shown in Scheme 1 (Srinivas and Satyarthi, 2011).

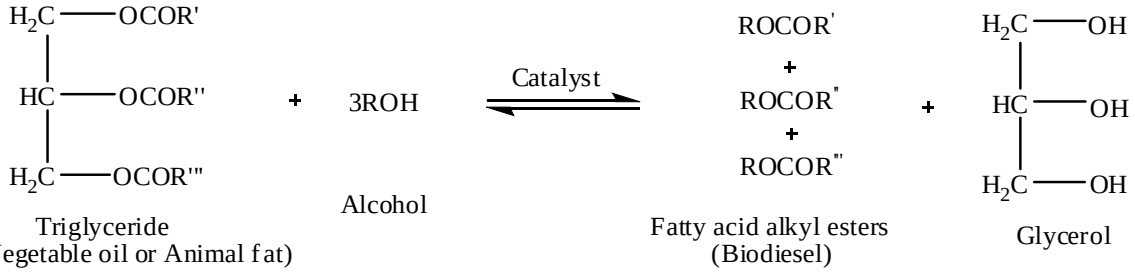

Scheme 1.1. Transesterification of triglycerides with alcohol to form methyl esters of fatty acids (biodiesel) in the presence of acid, base or enzyme as catalyst. R', R'' and R''' are the straight hydrocarbon chains of fatty acids, usually having 14-20 carbon atoms.

At present, edible VOs are the main feedstock for the commercial scale biodiesel production. Currently, more than 95% biodiesel across the globe is produced from edible oil which is easily available on large scale from the agricultural industry (Teo *et al.*, 2014). Due to scarcity of edible oil, however, in India use of non edible or waste cooking oils is encouraged for biodiesel production. These oils are much cheaper than refined edible VOs and hence, their application as feedstock may also reduce the biodiesel production cost to significant extent.

1.2. Biodiesel

The name Biodiesel was introduced in United States during 1992 by the National Soy diesel Development Board (presently national biodiesel board) which has pioneered the commercialization of Biodiesel (Vyas *et al.*, 2010). Biodiesel properties mainly depend on the characteristics of the VOs from which it has been derived.

1.2.1. Feedstock for biodiesel production

Theoretically any vegetable oil could be employed for biodiesel production, however, choice of feedstock is mainly restricted by the cultivation of vegetable oil in a particular geographical area. For example, soybean oil is main feedstock in South America and United States, rapeseed oil in European countries, canola oil in Canada, palm oil in Malaysia and Indonesia, jatropha oil in India and African region (Kiakalaieh *et al.*, 2013). Soybean and rapeseed oils account for ~ 85% of global biodiesel production. Edible refined oils (e.g., soya, rapeseed, sunflower, etc.) are the feedstock for the production of ***first-generation*** biodiesel fuel. However, application of refined VOs is unviable in many countries including India due to their limited availability and high cost (McLaughlin, 2011). On the other hand, s***econd-generation*** biodiesel is produced from non edible VOs (e.g., castor, jatropha, karanja, animal fats, microalgae etc.), waste frying oils and animal fats, which are much cheaper than edible oils (Sheldon, 2014). Nevertheless, these low-quality feed stocks generally contain a relatively high concentration of free fatty acids (FFA; > 2.5 wt%) and water (> 0.3 wt%), which may negatively influence homogeneous base catalyzed transesterification of triglycerides.

Biodiesel production, in recent past, has gained a lot of criticism as it has mainly utilized edible vegetable oil which has not only caused the global vegetable oil scarcity but also escalated its price to significant extent. Additionally, the cost of biodiesel is not competitive to petroleum diesel fuel due to high price of feedstock and expensive processing. Therefore, it is essential to explore the use of alternate feedstock for biodiesel production, such as non edible oil, waste cooking oils and animal fat, as they are much cheaper than conventional feedstock and hence their application may reduce biodiesel production cost. The oil yield from non edible jatropha seed (up to 40%) is significantly higher than edible seeds (20-30%) and former plant can grow in poor quality soil and waste land, thus avoiding the competition with arable land (Achten *et al.*, 2008). Approximately 15 million tons of waste cooking oil is disposed of annually worldwide, which could also be employed as a cheap feedstock for the

biodiesel production. As per the estimates, biodiesel production cost could be halved using waste oils for biodiesel production. Nevertheless, waste cooking and non edible oils usually contains relatively higher concentration of FFA (2.5-40 wt%) and/or moisture contents (0.3-61 wt%) (Chung *et al.*, 2008; Atadshi *et al.*, 2012). Current biodiesel production technology mainly utilizes homogeneous alkali catalysts which get deactivated via saponification in presence of fatty acid and/or moisture contents. Thus it is desired to develop new technologies which could utilize low quality feedstock for the biodiesel production.

Another triglyceride source, algal oil, has also received significant attention as a biodiesel feedstock. Microalgae are fast growing, produce higher oil yield than vegetable plants, and can be grown on waste land without requiring fresh water. However, biodiesel produced from algal oil, due to the presence of high saturated fatty acid contents, show poor low temperature operability (Tran *et al.*, 2010).

Fatty acid profile of feedstock influences the chemical composition as well as physicochemical properties of biodiesel fuel. VOs usually comprise five major fatty acid components viz., palmitic (16:0), stearic (18:0), oleic (18:1), linoleic (18:2) and linolenic (18:3).Usually saturated fatty acid rich biodiesel is thermally more stabile but at the same time it demonstrates poor cold flow properties. On the other hand high concentration of unsaturated fatty acid is beneficial to achieve better cold flow properties but at the cost of thermal stability of fuel. Table 1.1 demonstrates the fatty acid composition of commonly used VOs as feedstock for biodiesel production (Aransiola *et al.*, 2014).

Table 1.1. The common feed stocks with their chemical composition and physicochemical properties (Aransiola *et al.*, 2014).

Feedstock	Country	Fatty acid composition (Cxx:y)							
		Saturated				*Monounsaturated*		*Polyunsaturated*	
		C16:0	C18:0	C20:0	C22:0	C20:1	C18:1	C18:2	C18:3
Cottonseed *(Gossypium spp.)*	Canada, Cambodia	20.10	2.60	-	-	-	19.20	55.20	0.60
Pea nut *(Arachis hypogaea)*	China, India	8.23	2.46	1.83	3.89	-	58.69	21.77	0.34
Soybean *(Glycine max)*	USA, Brazil, China	11.0	4.0	-	-	-	23.40	53.20	7.80
Rapeseed *(Brassica napus)*	Germany	3.5	0.9	-	-	-	64.1	22.3	8.2
Sunflower *(Helianthus annuus)*	Brazil	-	4.50	0.30	-	2.0	21.10	66.20	-
Canola *(Brassica campestris)*	Canada	4.0	2.0	-	-	-	62.0	20.0	9.0
Corn *(Zea mays)*	USA	11.67	1.85	0.24	-	-	25.16	60.6	0.48
Palm *(Elaeis guineensis)*	Malaysia, Costa Rica	44.0	4.50	-	-	-	39.20	10.10	0.40
Camelina *(Camelina sativa)*	USA	5.4	2.6	0.25	1.4	16.8	14.3	2.9	38.4
Jatropha *(Jatropha Curcas)*	India	14.20	7.0	-	-	-	44.70	32.80	0.20
Karanja (*Pongamia pinnata)*	India, Brazil	3.7-7.9	2.4-8.9	-	-	-	45-71	11-18.3	-
Tallow	USA, India, Brazil	23.30	19.40	-	-	-	42.40	2.90	0.90
Poultry	USA, India, Russia	22.20	5.10	-	-	-	42.30	19.30	1.0
Used cooking oil	USA	Depends upon fresh cooking oil							

xx:y = no. of carbon atoms: unsaturated centres. 16:0 - palmitic acid, 18:0 - stearic acid, 18:1- oleic acid, 18:2 - linoleic acid, 18:3 - linolenic acid, 20:0 - arachidic acid, 20:1- eicosenoic acid, 22:0 - behenic acid.

Biodiesel produced from various feedstock sources must satisfy ASTM 6751 or EN 14214 specifications (Table 1.2) prior to application in diesel engine. Kinematic viscosity is one of the most important property of biodiesel as it affects the operation of fuel injector, particularly at low temperatures (Atabani *et al.*, 2013). On the other hand low cetane number causes the diesel fuel knocking which increases gaseous and particulate exhaust emissions due to incomplete combustion of biodiesel fuel.

Table 1.2. ASTM-6751 and EN 14214 specifications of biodiesel fuels (Atabani *et al.*, 2013).

Property specification	Units	Biodiesel			
		ASTM D6751		EN 14214	
		Limits	Test method	Limits	Test method
Ester content	% mass	-	-	96.5 min	EN 14103
Density at 15 °C	kg/m^3	880	D 1298	860-890	EN ISO 3675/12185
Kinematic viscosity at 40 °C	mm^2/s	1.9-6.0	ASTM D445	3.5-5.0	EN ISO 3104
Flash point	°C	130 min	ASTM D93	101 min	EN ISO 3679
Cloud point	°C	-3 to -12	ASTM 2500	-	-
Pour point	°C	-15 to -16	ASTM 97	-	-
Cetane number		47 min	ASTM D613	51 min	EN ISO 5165
Cold filter plugging point	°C	+5 max	ASTM 6371	-	EN 14214
Iodine number	g I_2/g	-	-	120	EN 14111
Acid number	mg KOH/g	0.5 max	ASTM D664	0.5 max	EN 14014
Oxidation stability		-	-	3 h min	EN 14112
Carbon residue	% m/m	0.050 max	ASTM D4530	0.3 max	EN ISO 10370
Ash content	% mass	0.002 max	ASTM D874	0.02 max	EN ISO 3987
Lubricity (HFRR)	M	520 max	ASTM D6079		
Water and sediment		0.005 vol% max	ASTM D2709	500 mg/kg max	EN ISO 12937
Moisture	wt%	-	-	0.05 max	EN 1412
Free glycerine	% mass	0.02 max	ASTM D6584	0.02 max	EN 1405/14106
Total glycerin	% mass	0.24	ASTM D6548	0.25	EN 14105
Methanol content	% mass	-	-	0.2 max	EN 14110
Na and K	mg/kg	-	-	5 max	EN 14108, EN 14109
Total contamination	mg/kg	24	ASTM D 5452	24	EN 12662

1.2.2. Alcohols used for biodiesel production

Methanol is most frequently employed alcohol in existing technologies for biodiesel production due to its suitable physicochemical properties, low cost, mild reaction conditions and easy phase separation of fatty acid methyl esters (FAME) from glycerol. However, there are few disadvantages associated with the use of methanol such as toxicity, explosion risk (due to low boiling point) and non-renewability as it is mainly derived from the refining of crude oil (Stamenkovic *et al.*, 2011). During last few years researchers are striving to replace methanol with nontoxic and renewable alcohol such as ethanol for biodiesel production.

Bioethanol is not only nontoxic and a "green" reactant but also renewable as it is mainly derived by the fermentation of biomass. Produced fatty acid ethyl esters (FAEE) have better low temperature operability than corresponding methyl esters. However, at present ethanol is costlier than methanol, less reactive, and FAEE are difficult to separate from glycerol. Due to less reactivity, ethanol is not frequently employed for biodiesel production in presence of heterogeneous catalysts and hence, more efficient solid catalysts are essential to utilize ethanol for biodiesel production (Brunschwig *et al.*, 2012).

1.3. Catalysis in transesterification

The transesterification of VOs mainly utilizes two different types of catalysts viz., chemical and enzyme based (Scheme 2) which further could be categorized as homogeneous and heterogeneous catalysts (Lam *et al.*, 2010). Due to extremely high cost of lipase catalyzed transesterification, it is mainly explored at lab scale for academic purpose. At present, biodiesel industry is dominated by homogeneous acid or alkali catalyzed transesterification process due to cost effectiveness, simple usage, higher activity and forming the acceptable biodiesel yield under mild reaction conditions. Heterogeneous catalysts although have the advantages of easy separation and reusability, however, very few biodiesel production plants across the globe utilizes them, owing to their low reactivity which requires high temperature and pressure to achieve acceptable FAME yield.

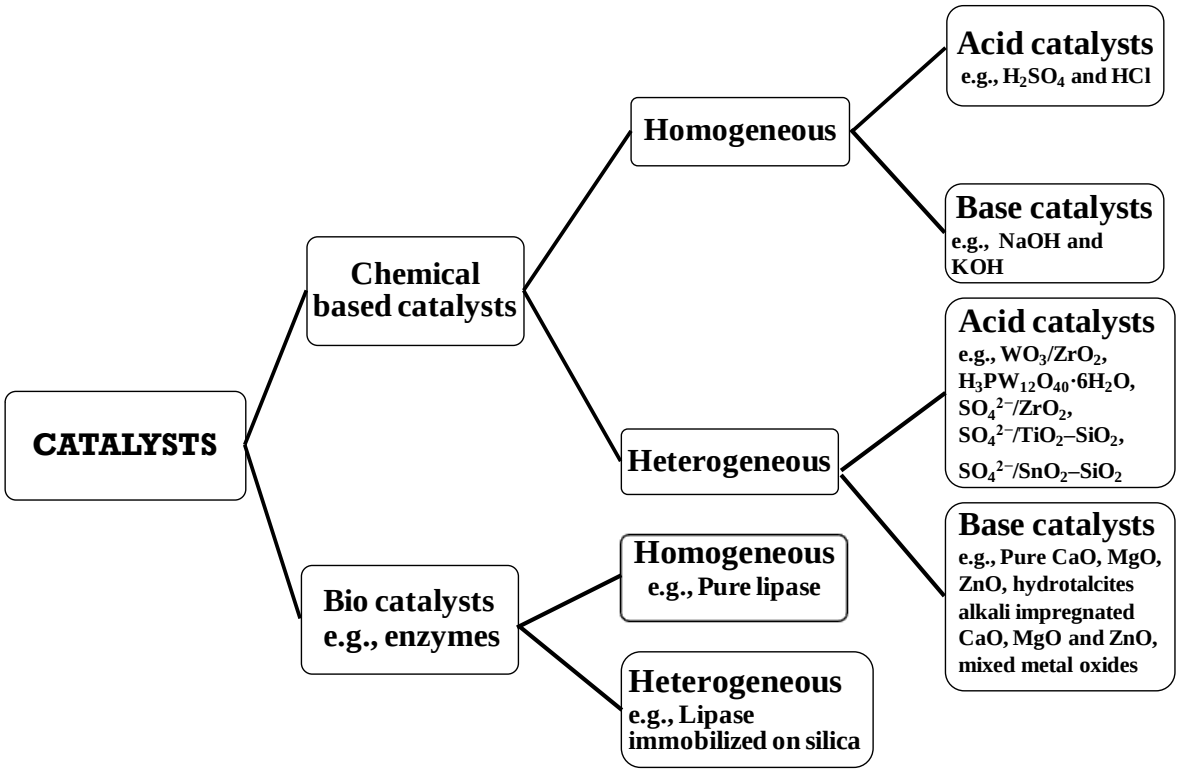

Scheme 1.2. Catalysts used for biodiesel production.

1.3.1 Homogeneous catalysis

At industrial scale, biodiesel is commonly produced in homogeneous alkali (e.g., NaOH, KOH and CH_3ONa etc.) catalyzed reaction as these catalysts are low cost and yielded high conversion rate even under less energy intensive ambient reaction conditions. Homogeneous base catalysts are used for those VOs having < 0.5 wt% FFA and/or < 0.3 wt% moisture content. Alkali catalysts, if employed for the transesterification of feedstock having > 0.5

wt% FFA contents, gets deactivated via saponification reaction. The presence of water in the reaction mixture could hydrolyze the fatty esters which can further react with alkali to form soap. Thus, excessive soap formation resulted the catalyst deactivation, reduced biodiesel yield and increased biodiesel purification and separation cost (Meher *et al.*, 2006).

Homogeneous acid (*e.g.*, H_2SO_4 and HCl) catalysts could be used for biodiesel production from high FFA containing VOs as they can catalyze the simultaneous esterification of fatty acid and transesterification of triglycerides. However, acid catalysts are sensitive to the presence of water; a by-product of esterification reaction and less reactive as rate of acid catalyzed transesterification is ~ 4000 times slower as compared to alkali catalyzed reaction (Lam *et al.*, 2010). The major drawbacks of using homogeneous catalysts are the subsequent neutralization, separation, and purification steps which are time consuming and lead to generate huge quantity of industrial effluents which can pollute the environment.

1.3.2. Heterogeneous acid catalysts

A wide range of solid acid catalysts have been explored for the transesterification of oils to produce biodiesel. Solid acid catalysts are generally less active than their alkali counterparts and hence, usually required high temperature, pressure and alcohol to oil molar ratio to achieve acceptable conversion levels. In spite of their poor activity, solid acids have the advantage as (i) they are less sensitive to FFA contents, (ii) they can catalyze simultaneous esterification and transesterification, (iii) their application can eliminate the need of neutralization and washing of biodiesel, (iv) they are easy to separate from reaction medium and reusable, (v) their application can reduce corrosion of reactor, thus simplifying the reactor design (Helwani *et al.*, 2009).

The ideal solid acid catalyst could catalyze simultaneous esterification of fatty acids and transesterification of triglycerides over Bronsted and/or Lewis acid centres. A wide variety of heterogeneous acid catalysts for biodiesel production have been reported in literature (Su and Guo, 2014) including sulfated metal oxides (SO_4^{2-}/ZrO_2, SO_4^{2-}/SnO_2, SO_4^{2-}/SiO_2 and SO_4^{2-}/TiO_2), heteropolyacids ($H_3PW_{12}O_{40}\cdot 24H_2O$ and $H_4SiMo_{12}O_{40}\cdot 13H_2O$), and heteropolyacids supported on TiO_2, ZrO_2, SnO_2, SiO_2 and Al_2O_3, sulfonic ion exchange resins (Nafion and Amberlyst), zeolites (H–ZSM-5, Y and Beta), mesoporous silica (SO_3H-SBA-15, ZnO/SBA-15 and SO_3H-KIT-6), sulfonated carbon based (sulfonated D-glucose derived sugar and sulfonated bearing cellulose-derived carbon), and miscellaneous solid acid catalysts such as $Fe(HSO_4)_3$, and WO_3/SnO_2.

1.3.2.1. Sulfated metal oxides

Sulfuric and sulfonic acids have shown excellent activity as homogeneous acid catalyst and in order to prepare solid acid catalysts, a variety of metal oxides have been explored as support material for the sulfate or sulfonic acid group immobilization. Sulfated metal oxides such as phenyl and propyl sulfonic acid supported SBA-15, SO_4^{2-}/ZrO_2, SO_4^{2-}/SnO_2, SO_4^{2-}/SiO_2 and SO_4^{2-}/TiO_2 are frequently used solid super acid catalysts in literature, due to their capability of catalyzing the esterification and transesterification of VOs having high FFA concentration (Petchmala *et al.*, 2010; Jitputti *et al.*, 2006; Perin *et al.*, 2008; Chen *et al*., 2007). Metal oxides such as ZrO_2, SnO_2, SiO_2 and TiO_2 possess both Bronsted and Lewis acid sites as they can simultaneously protonate pyridine as well as coordinatively bind to pyridine (Alsalme *et al.*, 2010). The surface modification of these oxides with sulfate groups can enhance the Bronsted acid sites which in turn resulted in improved catalytic activity. As shown in Fig. 1.1, in a typical SO_4^{2-}/ZrO_2 unit, two oxygen atoms from S–O bonds are linked to Zr atoms, and one oxygen atom from S=O group is bonded to the Zr—OH group. The acidic proton from Zr —OH group can be released easily to form total three S–O–Zr bonds between SO_4^{2-} group and ZrO_2 matrix. The addition of water to the catalyst hydrolyzes one of the S-O-Zr bond to form Bronsted acid sites which further enhances Lewis acid sites (Arata, 2009).

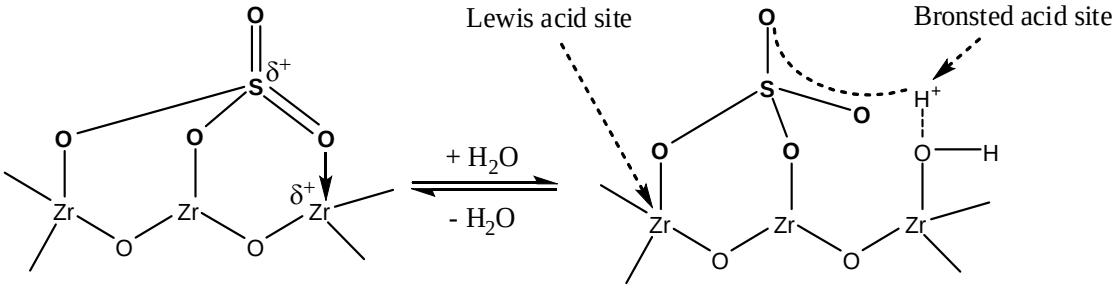

Fig.1.1. Illustration of Lewis and Bronsted acidic sites in SO_4^{2-}/ZrO_2 (Arata, 2009).

Kiss *et al.* (2006) demonstrated that SO_4^{2-}/ZrO_2 showed high catalytic activity and selectivity for the esterification of dodecanoic acid with methanol at 150 °C. The catalyst was reused during five consecutive runs to maintain 90% FAME yield. Garcia *et al.* (2010) used sulfated zirconia for the methanolysis as well as ethnaolysis of soybean oil to achieve 98.6 and 92 % FAME and FAEE yield, respectively, in 1 h. Chen *et al.* (2007) found that SO_4^{2-}/TiO_2 showed 95 % FAME yield from cotton seed oil at relatively high reaction temperature of 230 °C, and longer reaction duration of 10 h. Jittiputi *et al.* (2006) reported SO_4^{2-}/SnO for the

transesterification of crude kernel oil at high reaction temperature of 200 °C. Mixed metal oxides, due to the presence of structural defects, are found to be better catalytic support than single metal oxide. Although it is not often well understood which of the constituent metal cation plays a role of active center in mixed metal oxides (Gawande *et al.*, 2012). Sulfate group immobilize ZrO_2-TiO_2/La^{3+} mixed oxide was also observed to be an effective catalyst for simultaneous esterification and transesterification of VOs containing 60 wt% FFA. The role of lanthanum was to strengthen the interaction of SO_4^{2-} with the ZrO_2-TiO_2 support material to reduce the loss of SO_4^{2-} in reaction mixture. Lanthanum although enhances the catalyst stability as an assistant component, but itself remain silent during the catalytic process. The developed catalyst was reused during five runs without any regeneration process to maintain 90.2% FAME yield after fifth cycle (Li *et al.*, 2010a; Li *et al.*, 2010b). Few, other sulfated mixed oxides employed for biodiesel production is illustrated in Table 1.3 along with their reaction conditions.

Table 1.3. Literatures reported sulphated metal oxides heterogeneous acidic catalysts.

Catalyst	Feedstock	Reaction conditions					Reusability	Ref.
		Catalyst amount (wt%)	Alcohol to oil molar ratio (m/m)	Reaction temp. (°C)	Reaction time (h)	FAAE Yield (%)		
Methanolysis								
SO_4^{2-}/ZrO_2	Dodecanoic acid	3	3:1	150	0.1	90	5	Kiss *et al.*, 2006
SO_4^{2-}/ZrO_2	Palm	0.5	25:1	250	0.16	90	2	Petchmala *et al.*, 2010
S-ZrO_2	Soybean	5	20:1	120	1	98.6	2	Garcia *et al.*, 2010
SO_4^{2-}/TiO_2	Cotton seed	2	12:1	230	10	95	5	Chen *et al.*, 2007
SO_4^{2-}/SnO	Kernel oil	3	6:1	200	4	95.4	NR	Jitputti *et al.*, 2006
SO_4^{2-}/ZrO_2-Al_2O_3	Sea mango	5	8:1	180	NR	83.8	NR	Kansedo *et al.*, 2009
$SO_4^{2-}/ZT/La^{3+}$	Rapeseed	5	6.3:1	80	5	97.8	5	Li *et al.*, 2010a
$SO_4^{2-}/ZT/La^{3+}$	Acid oil	5	15:1	200	2	96.24	5	Li *et al.*, 2010b
SO_4^{2-}/ZrO_2-SiO_2	Lauric acid	20	10:1	68	6	97.4	NR	Chen *et al.*, 2007
SO_4^{2-}/SnO_2-TiO_2	Waste cooking	6	15:1	150	1.5	88.2	NR	Lam *et al.*, 2009
Ethanolysis								
S-ZrO_2	Soybean oil	5	20:1	120	1	92	NR	Garcia *et al.*, 2010
SO_4^{2-}/SiO_2	Castor	10	6:1	60	6	95	1	Perin *et al.*, 2008

S = Sulfated, ZT = ZrO_2-TiO_2

1.3.2.2. Mesoporous silicas

Mesoporous silica owing to its insolubility in most of the organic solvents, tuneable pore size, and ease of surface modification has been proved a versatile support for the preparation of a variety of industrial catalysts (Sierra and Guth, 1999). To develop solid catalysts for biodiesel production, sulfonic acid, phenyl and propyl sulfonic acid groups have been incorporated over various categories of silica supports. In order to tune the pore size of mesoporous material, to reduce the internal mass transfer limitations, poragens such as trimethyl-, triethyl-

or triisopropyl-benzene are employed as pore swelling agents (Chen *et al.*, 2006; Cao *et al.*, 2009). To further enhance the stability/activity of the catalyst instead of pure silica, Ti or Al-doped silica material was used for the impregnation of active species. For example, Ti-doped SBA-15 was employed for the simultaneous esterification and transesterification of high FFA containing VOs with methanol (Chen *et al.*, 2014). The catalyst was found effective even in presence of common oil impurities, and up to 5 wt% water or 30 wt% FFA contents. Superior catalytic activity can be achieved in case of mesoporous based catalysts by incorporating more acid sites, tuning pore diameter (5-20 nm), and adjusting the surface hydrophilic/hydrophobic property. High temperature requirement to achieve the acceptable oil conversion levels and leaching of the sulfate group in reaction medium are the common drawbacks of the mesoporous based catalysts.

1.3.2.3. Heteropolyacids

Heteropolyacids are another category of acid catalysts which posses super acid sites (pK_H > 12) and flexible structure, although in native form, they are not suitable as heterogeneous catalysts for biodiesel production due to their high solubility in polar media (Mizuno and Misono, 1998; Kozhevnikov, 1998). To reduce the solubility of polyacids during the reaction, they are often impregnated over support material of high surface area. Proton exchange with large cations, such as Cs^+, into Keggin type phospho- ($Cs_xH_{(3-x)}PW_{12}O_{40}$) and silicotungstic ($Cs_yH_{(4-y)}SiW_{12}O_{40}$) acids can also increase their chemical stability. Although acidic proton is lost, both $Cs_xH_{(3-x)}PW_{12}O_{40}$ and $Cs_yH_{(4-y)}SiW_{12}O_{40}$ remain active towards palmitic acid esterification as well as tributyrin transesterification (Narasimharao *et al.*, 2007; Pesaresi *et al.*, 2009). To make the catalyst separation easier, Duan *et al.* (2013) have reported the immobilization of $H_3PW_{12}O_{40}$ over Fe_2O_3 to prepared magnetic catalyst for the esterification of palmitic acid under mild conditions. Water resistance of the catalyst was further improved by incorporating nonyl chains over the catalyst surface.

1.3.2.4. Miscellaneous solid acids

A variety of other solid acid catalysts have also been investigated for biodiesel production such as sulfonated carbonaceous material (carbon is mainly derived from sugar, cellulose and crop waste), supported tungsten oxides (WO_3/SnO_2,WO_3/ZrO_2), ferric hydrogen sulphate ($Fe(HSO_4)_3$), ferric zinc metal cyanide, supported partially substituted heteropolytungstates, and bifunctional catalysts, such as Mo-Mn/Al_2O_3-15 wt% MgO, ZnO-La_2O_3 having the advantages of acid well as base catalysis (Sivasamy *et al.*, 2009; Zong *et al.*, 2007; Okamura

et al., 2006; Xie and Wang, 2013; Laosiripojana *et al.*, 2010; Alhassan, 2013; Sreeprasanth *et al.*, 2006; Shiekh *et al.*, 2013; Farooq *et al.*, 2013; Yan *et al.*, 2009b) A few heterogeneous catalysts used for the simultaneous transesterification and esterification of high FFA containing vegetable oils are compared in Table 1.4.

Table 1.4. Comparison of catalytic activity for simultaneous transesterification and esterification by heterogeneous catalysts.

Catalyst	Reaction conditions						Ref.
	FFA/ Moisture content (wt%)	Catalyst amount (wt%)	Reaction temp. (°C)	Methanol to oil molar ratio	Reaction time (h)	FAME yield (%)	
Sr/ZrO_2	2.5/N.R	2.7	60	6:1	5	40	Omar and Amin, 2011
	2.5/ N.R	2.7	111.5	29:1	2.8	79.7	
TPA/HZ[a]	20/ N.R	3	200	9:1	10	90	Kulkarni *et al.*, 2006
$ZnO\text{-}La_2O_3$	5.4/5.1	2.3	200	36:1	3	96	Yan *et al.*, 2009b
Fe-Zn metal cyanide	5.4/ N.R	3	170	15:1	8	98	Sreeprasanth *et al.*, 2006
SO_4^{2-}/ZrO_2	10/ N.R	3	170	20:1	1	86	Rattanaphra *et al*., 2010
Mg-Al-CO_3	43/3.5	1	200	6:1	3	99	Barakos *et al.*, 2008
$SO_4^{2-}/ZrO_2\text{-}TiO_2/La^{3+}$	60/ N.R	5	200	15:1	6	96.24	Li *et al.*, 2010a
$SO_4^{2-}/SiO_2\text{-}TiO_2$	50/ N.R	3	200	9:1	6	92	Peng *et al.*, 2008
ZS/Si	15/ N.R	3	200	18:1	10	98	Jacobson *et al.*, 2008
Sr:Zr	4.7/4.0	5	75	12:1	7	>99	Kaur and Ali, 2014d
	18.1/0.3	5	75	12:1	15	>99	
Li/ZrO_2	4.7/4.0	5	65	12:1	1.25	99	Kaur and Ali, 2015
	18.1/0.3	5	65	12:1	6	99	

[a]Tungstophosphoric acid supported on hydrous zirconia; N.R- Not Reported

1.3.3. Heterogeneous base catalysts

Heterogeneous base catalysts are generally more active than heterogeneous acid catalysts, and hence are suitable for the transesterification of high purity oils with low FFA content. The advantages of solid base catalyzed reaction includes, (i) relatively faster reaction rate than acid-catalyzed transesterification, (ii) achievement of acceptable FAME yield even under mild reaction condition, (iii) less energy intensive process and (iv) easy separation of catalyst from product and hence, high possibility to reuse and regenerate the catalyst (Helwani *et al.*, 2009).

Esterfip process, developed by the French Institute of Petroleum, utilizes Zn/Al mixed-oxide as a heterogeneous catalyst for industrial scale biodiesel production but requires relatively higher pressure (3–5 Mpa) and temperature (483–523 K) compared to conventional homogeneous catalyzed process (Chen *et al.*, 2014). A variety of solid base catalysts are reported for transesterification reaction *viz.*, alkali or alkaline earth oxides, alkali doped

mixed oxides, transition metal oxides, basic zeolites and clays such as hydrotalcites, and immobilised organic bases.

1.3.3.1. Alkaline earth oxides

Alkaline earth oxides due the cost effectiveness and ease of preparation were widely used as solid base catalysts for the transesterification of a variety of triglycerides. The Lewis basic sites in such catalysts are due to the presence of oxide ion (O^{2-}) in M–O ion pairs (Hattori, 1995). Lewis basic sites were found to be more active towards transesterification than corresponding Bronsted basic sites. The strength of the basic sites could be further enhanced by creating these sites at low coordination defect, corners and edges, or on high Miller index surfaces (Lee *et al.*, 2014). The alkaline earth metal oxides employed for the transesterification reaction follow the order of their activity:- BaO > SrO > CaO > MgO (Yan *et al.*, 2008). Single metal oxides either demonstrate low activity and/or leached out into the reaction mixture to cause the homogeneous contribution in catalytic activity. In order to improve the stability as well as reactivity, mixed metal oxides of alkali earth oxides were prepared and employed for the transesterification reaction. The active centres in such catalysts are either oxide ion or impregnated metal oxide or the defect created due to metal impregnation. Mixed oxide of Sr/Al was prepared as $Sr_3Al_2O_6$ nanocomposites and used as a heterogeneous catalyst for transesterification of soybean oil to form corresponding methyl esters. The utilization of methanol to oil molar ratio of 25 in presence of 1.3 wt% catalyst produced FAME yield of 95.7 % in 1 h of reaction duration (Rashtizadeh *et al.*, 2014). CaO due to nontoxic nature, wide availability and cost effectiveness has been widely studied in literature as a catalyst or solid catalyst matrix to support other active metals. Furthermore, CaO can also be prepared from the waste matters consisting of calcium carbonate, such as mollusk shells, egg shells, etc (Kouzu and Hidaka, 2012). Thitsartarn and Kawi (2011) synthesized CaO-CeO_2 catalyst and observed that vacancies are created due to the substitution of Ca^{2+} in ceria. These vacancies bring about the lattice distortions to form defects that are favourable for heterogeneous catalysis. The catalyst was active for the transesterification of palm oil to yield > 90% conversion levels. The catalyst show excellent stability, excellent reusability during 18 successive cycles and negligible metal leaching in reaction media. Dehkordi and Ghasemi (2012) prepared CaO-ZrO_2 mixed oxide as stable catalyst due to the formation of homogeneous solid solution. An increase in Ca to Zr ratio was found to increase catalyst activity, however, with a compromise in catalyst stability due to the leaching of Ca from catalyst surface. TeO *et al.* (2014) used CaO-NiO and CaO-Nd_2O_3

mixed oxides for the transesterification of jatropha oil claiming > 80 % FAME yield. In CaO-Nd_2O_3 binary system, strong interaction between CaO and Nd_2O_3 was observed due to the transfer of electrons from metal neodymium oxide to CaO. The active sites of high basic strength were formed in both catalysts due to presence of unbounded oxide anion. Table 1.5 illustrates the few alkaline earth oxide based catalyst used for the transesterification of VOs.

Table 1.5. Comparison of activity of alkaline earth oxide based heterogeneous catalysts.

Catalyst	Oil	Reaction conditions						Ref.
		Catalyst dosage (wt%)	Reaction temp. (°C)	Alcohol to oil molar ratio	Reaction time (h)	FAEE yield (%)	Reusability	
Methanolysis								
Commercial CaO	Soybean	8	65	12:1	3	95	20	Liu *et al.*, 2008a
Nanocystalline CaO	Soybean	1.8	Room temp.	33:1	24	99	9	Reddy *et al.*, 2006
MgO	Jatropha	4	65	15:1	6	10	NR	Yap *et al.*, 2011
SrO	Soybean	3	65	12:1	0.5	95	10	Liu *et al.*, 2007
Sr/MgO	Soybean	5	65	12:1	0.5	93	1	Tantirungrotechai *et al.*, 2013
SrO/MgO	Soybean	5	67	9:1	3	94	2	Dias *et al.*, 2012
Mg/La	Sunflower	5	65	53:1	0.3	100	No	Babu *et al.*, 2008
$Sr_3Al_2O_6$	Soybean	1.3	60	25:1	1.01	95.7	NR	Rashtizadeh *et al.*, 2014
SrO/SiO_2	Olive	5	65	6:1	1	98.3	4	Chen *et al.*, 2012
CaMgO, CaZnO	Jatropha	4	65	15:1	6	83,81	6	Yap *et al.* 2011
Zn/CaO	Waste cooking	5	65	9:1	0.75	99	3	Kumar and Ali, 2013
$CaO-Al_2O_3$	Palm	3.5	65	12:1	5	94		Zabeti *et al.*, 2009
$CaTiO_3$, $CaMnO_3$, $Ca_2Fe_2O_5$, $CaZrO_3$, $CaCeO_3$	Rapeseed	NR	60	6:1	10	90	3	Kawashima *et al.*, 2008
$CaO-CeO_2$	Palm	5	85	20:1	6	>90	18	Thitsartarn and Kawi, 2011
$CaO-ZrO_2$	Waste cooking	10	65	30:1	2	92.1	NR	Dehkordi and Ghasemi, 2012
$CaO-La_2O_3$	Waste oil	5	58	20:1	1	94.3	NR	Yan *et al.*, 2009
$CaO-La_2O_3/CeO_2$	Soybean	8	65	10:1	3.5	97	NR	Kim *et al.*, 2011
$CaO-MoO_3$-SBA-15	Soybean	6	65	50:1	50	83.2	77.2	Xie and Zhao, 2014
$CaO-Nd_2O_3$, CaO-NiO	Jatropha	5	65	15:1	6	80,85	4	Teo *et al.*, 2014
Ethanolysis								
CaO	Sunflower	20	75	18:1	6	100	N.R	Phiri *et al.*, 2010
Zr/CaO	Jatropha	5	75	21:1	7	> 99	N.R.	Kaur and Ali, 2014c
$CaO-La_2O_3$	Soybean	8	65	10:1	6	71.6	N.R	Kim *et al.*, 2010
CaO-ZnO	Sunflower	3	78	20:1	3	> 95	2	Caballero *et al.*, 2013
$Ca(OCH_2CH_3)$	Soybean	3	75	12:1	3	91.8	N.R	Liu *et al.*, 2008b
$MgO/SBA-15^a$	Edible oil	2	220	6:1	5	96	N.R	Li and Rudolf, 2008

1.3.3.2. Alkali doped metal oxides

In another approach, alkali metal doping in CaO and MgO was found to improve the basicity as well as activity due to the formation of defects in the form of O^- on replacement of alkali metal (M^+) for alkaline earth metal (M^{2+}) (Montero *et al.*, 2010). Table 1.6 illustrates the alkali metal doped heterogeneous catalysts employed for the transesterification of VOs. Kumar and Ali (2010) prepared M/CaO (M= Li, Na, K) for the transesterification of used cotton seed and found better performance of Li/CaO to achieve >98% FAME yield in 45 min. The same catalyst was also found to be effective for the VOs

transesterification even in presence of 15 wt% water content. Alkali metal leaching was established as major cause for the loss of catalytic activity and poor reusability. To improve the catalyst stability, Wang *et al.* (2012) immobilized Li over silica to form lithium orthosilicate (Li_4SiO_4) for the production of biodiesel from soybean oil. Li_4SiO_4 was found to be less basic than CaO but more stable as well as more tolerant towards air, moisture and carbon dioxide. Sodium silicate, Na_2SiO_3, was also found to be an active catalyst for biodiesel production from rapeseed and jatropha oils under conventional and microwave heating to give 98% FAME yield (Guo *et al.*, 2010). The loss of catalytic activity, during reusability experiments, was attributed to the Si–O–Si bond cleavage and sodium leaching on exposure to the moisture.

Table 1.6. Comparison of activity of alkali metal doped heterogeneous catalysts.

Catalyst	Oil	Reaction conditions						Ref.
		Catalyst dosage (wt%)	Reaction temperature (°C)	Alcohol to oil molar ratio	Reaction time (h)	FAAE yield (%)	Reusability	
Methanolysis								
Li/CaO	Used cotton seed	5	65	12:1	0.75	>98	NR	Kumar and Ali, 2010
Li/MgO	Muttton fat	5	65	12:1	0.66	>99	NR	Kaur and Ali, 2013
Li/MgO	Soybean	9	60	12:1	2	93.9	3	Wen *et al.*, 2010b
K/CaO	Waste cotton seed	7.5	65	12:1	1.25	98	3	Kumar and Ali, 2012
K/La-Mg	Used cotton seed	5	65	54:1	0.33	96	3	Mutreja *et al.*, 2014
Li_4SiO_4	Soybean	6	65	18:1	2	98.1	10	Wang *et al.*, 2012
Na_2SiO_3	Soybean	3	60	7.5:1	1	100	5	Guo *et al.*, 2010
Na/SiO_2	Jatropha	65	65	15:1	0.75	99	3	Akbar *et al.*, 2009
KF/Al_2O_3	Palm	4	65	12:1	3	90	NR	Bo *et al.*, 2007
Cs/MgO	Glyceryl tributyrate	6	60	30:1	3	100	NR	Montero *et al.*, 2010
Mesoporous Li/ZrO_2	Soybean	3	65	13:1	3	98.2	NR	Ding *et al.*, 2011
Na_2ZrO_3	Soybean	3	65	NR	3	98.3	4	Torres *et al.*, 2014
K/ZrO_2	Soybean	10	60	NR	24	89	NR	Georgogianni *et al.*, 2009
KF/CaO-NiO	Waste cotton seed	5	65	15:1	4	>99	4	Kaur and Ali, 2014b
Ethanolysis								
Li/CaO	Waste cotton seed	5	65	12:1	2.5	98	4	Kaur and Ali, 2011

1.3.3.3. Transition metal oxides

Transition metal based catalysts were found to be effective for catalyzing a wide range of chemical reaction, and also find industrial application owing to their cost effectiveness, ease of regeneration and selectivity in action. Their catalytic activity is mainly coupled to the presence of partially filled transition metal *d*-orbitals and splitting of these orbitals under the influence of the oxide ligand field (Gawande *et al.*, 2012). Transition metal oxides afford higher transesterification activity than solid acids, hence a variety of such catalysts of varying Lewis base character have been explored in biodiesel production

including MnO, MoO_3, TiO_2 and ZrO_2 (Gombotz *et al.*, 2012; Xie and Zhao, 2014; Kaur and Ali, 2015). Table 1.7 illustrates few transition metal oxide based heterogeneous catalysts, employed for the transesterification of VOs. Among them, MnO and TiO_2 are soft bases which have demonstrated activity for the simultaneous transesterification and esterification of high FFA containing (up to 15 wt%) VOs. Major advantage of these catalysts are less soap formation, even in presence of high FFA contents, by the leached metal from the catalyst surface than that observed in presence of conventional homogeneous alkali catalysts (Gombotz *et al.*, 2012). However, Mn or Ti oxidation state in either fresh or reused catalysts were not established and hence, the nature of catalytic centre remains a mystery.

Zirconia possesses both acidic and basic properties, hence, successfully employed for catalyzing simultaneous esterification and transesterification of high fatty acid containing VOs (Li *et al.*, 2002). Use of zirconia as support material resulted distinctive interaction between the active metal and support material which resulted enhanced activity and selectivity of the prepared catalysts. Torres *et al.* (2014) synthesized Na_2ZrO_3 catalyst *via* a solid-state reaction and tested its activity as a solid basic catalyst (3 wt%) for the transesterification of soybean oil to produce 98.3% FAME yield at 65 °C in 3 h of reaction time. Omar and Amin (2011) prepared a series of alkaline earth doped zirconia catalysts (Mg/ZrO_2, Ca/ZrO_2, Sr/ZrO_2, and Ba/ZrO_2) for the biodiesel production from waste cooking oil. Among these catalysts, Sr/ZrO_2 exhibited higher catalytic activity due to the presence of stronger basic as well as acid sites to facilitate simultaneous transesterification and esterification. However, the methyl ester yield, even at relatively high reaction temperature of 115.5 °C, was significant less (79.7%) than the acceptable limit of 96.5%. Xie and Zhao (2014) prepared CaO-MoO_3-SBA-15 catalyst by wet impregnation method and employed for the transesterification of soybean oil with methanol. Authors proposed that interaction between the basic CaO and the acidic MoO_3 in the solid catalyst promoted a homogeneous dispersion of catalytically active sites to enhance the stability of catalyst. The catalyst was reused during 5 runs without significant loss in activity.

Table 1.7. Comparison of activity of transition metal oxide based heterogeneous catalysts.

Catalyst	Oil	Reaction conditions						Ref.
		Catalyst dosage (wt%)	Reaction temp. (°C)	Alcohol to oil molar ratio	Reaction time (h)	FAAE yield (%)	Reusability	
Methanolysis								
Li/ZrO_2	Waste cotton seed	5	65	12:1	1.25	99	9	Kaur and Ali, 2015
Na_2ZrO_3	Soybean	3	65	NR	3	98.3	4	Torres *et al.*, 2014
K/ZrO_2	Soybean	10	60	NR	24	89	NR	Georgogianni *et al.*, 2009
$SrZrO_3$	Soybean	3	60	12:1	3	98	NR	Lima *et al.*, 2012
Sr/ZrO_2	Waste cooking	2.7	115.5	29:1	2.8	79.7	NR	Omar and Amin, 2011
$CaO\text{-}MoO_3$-SBA-15	Soybean	6	65	50:1	50	83.2	77.2	Xie and Zhao, 2014
MoO_3/Al_2O_3	Sunflower	5	100	9:1	24	96	5	Sankaranarayanan *et al.*, 2011
Na_2MoO_4	Soybean	5	120	54:1	3	95.6	2	Nakagaki *et al.*, 2008
TiO_2-MgO	Waste cooking	5	150	30:1	6	92.3	4	Wen *et al.*, 2010a
Ethanolysis								
Li/NiO	Waste cotton seed	5	65	12:1	3	98	7	Kaur and Ali, 2014a
Li/ZrO_2	Waste cotton seed	5	75	15:1	2.5	98	NR	Kaur and Ali, 2015
Sr:Zr	Waste cotton seed	5	75	12:1	7	>99	4 (98)	Kaur and Ali, 2014d

1.3.3.4. Hydrotalcites

Hydrotalcites, also known as layered double hydroxides (LDHs), are a class of anionic clays composed of brucite like layers of $Mg(OH)_2$, separated by anions (A^{n-}) in which a portion of octahedrally coordinated M^{2+} cations are replaced by M^{3+} cations (Cosimo *et al.*, 1998). The general formula of hydrotalcites can be written as: $([M^{2+}_{1-x}M^{3+}_{x}(OH)_2]^{x+}\ (A^{n-})_{x/n}\cdot mH_2O)$, where $M^{2+} = Mg^{2+}$, Zn^{2+} or Ni^{2+}; $M^{3+} = Al^{3+}$, Fe^{3+} or Cr^{3+}; $A^{n-} = OH^-$, Cl^-, NO_3^- or SO_4^{2-}; and $x \sim 0.1$- 0.5. Hydrotalcites can be prepared by co-precipitation method employing appropriate metal nitrates and alkali carbonates as pH regulators and carbonate source. Many reports suggested that hydroxide ion in hydrotalcites exhibits basic properties (Choudary, 1999). As-prepared hydrotalcites are often inactive owing to the presence of physically adsorbed water molecules in their pores which hinder access of substrates to the basic sites. Hence, thermal treatment of as-prepared hydrotalcites is necessary to produce active solid base catalysts for the transesterification reaction (Winter *et al.*, 2006). Mg-Al hydrotalcites have been reported to catalyze the transesterification of triglycerides having 9.5 wt% FFA and 45 wt% moisture contents to yield 99% conversion within 3 h at 200 °C (Barakos *et al.*, 2008). Liu *et al*. (2014) prepared Zn-Al hydrotalcite by co-precipitation method at 8.5 pH using Na_2CO_3 and NaOH as precipitating agents followed by the heating at 150 °C to remove interlayer water. Later, prepared hydrotalcite was calcined at 400 °C to incorporate the smaller Al^{3+} cations into the lattice of ZnO. The incorporation of Al^{3+} into the ZnO framework creates cationic vacancies. These vacancies are compensated with surface Zn^{2+} cations, which eventually lead to the generation of M^{n+}–O^{2-} (M = Zn or Al) pairs and isolated

oxide ion. The dehydrated Zn–Al hydrotalcites obtained at 200 °C exhibited the highest activity, with a 76% FAME yield at 150 °C, 1.7 MPa, and 1:1 methanol to soybean oil molar ratio. The catalyst was not found to be deactivated even after150 h of continuous run.

During hydrotalcite preparation Na or K hydroxides or carbonates are employed as precipitating agent and their complete removal is difficult. Thus, presence of Na or K ions is always suspected to cause homogeneous contribution in catalytic activity (Fraile, 2009). To overcome this problem NH_4OH or $(NH_4)_2CO_3$, are employed as precipitating agent for the preparation of Mg-Al hydrotalcites by varying *x* in the range of 0.25-0.55. An increase in Mg/Al ratio was found to increase catalyst surface area, basic strength as well as activity towards tributyrin transesterification (Cantrell *et al.*, 2005).

Thus in short, a host of inorganic solid acid and base catalyst were developed and employed for the triglyceride transesterification in literature. However, most of the literature reported heterogeneous catalysts were employed for the transesterification of edible oils with methanol. Limited reports are available for the application of solid catalysts for simultaneous transesterification and esterification of VOs having high FFA contents, which is essential to produce second generation biodiesel from low quality feedstock.

1.4. Conclusions

1. Biodiesel is a non-toxic, biodegradable fuel and its application in diesel engines can reduce the greenhouse gas emissions to significant extent. At industrial scale, biodiesel is commonly produced by the transesterification of vegetable oils with methanol in presence of homogeneous catalysts.
2. The conventional method of biodiesel production utilizes methanol, which is a highly toxic chemical and a refinery residue. Bioethanol is not only non toxic but also renewable alcohol as it is produced through the fermentation of biomass, thus making bioethanol a more sustainable reactant than methanol.
3. Homogeneous catalysts could be used only for costly refined edible oils having FFA content < 0.5 wt%. The cultivation of edible oils for biodiesel production may reduce the availability of agricultural land and enhance the vegetable oil price to significant extent. Hence, it is necessary to employ alternative feedstock for biodiesel production such as waste cooking oil or non edible VOs (eg. Jatropha and karanja oil).
4. In this regard use of heterogeneous catalysts for biodiesel production could be advantageous as they are effective even for the transesterification of low quality

feedstock, are reusable, are easy to separate from reaction medium, do not generate huge amount of effluents and do not require extensive biodiesel and glycerol purification step after the reaction.

5. Mixed metal oxides are reported to be more active solid catalysts towards transesterification than single metal oxides, mainly due to the presence of defects in catalyst structure.
6. The activity of the mixed metal oxide based catalysts could be further improved by supporting them with active species such as alkali metal ions, transition metal ions, or sulfate ions. Presence of acidic as well basic sites on catalyst was found to be effective for simultaneous esterification as well transesterification of high FFA containing VOs.

1.5. Objectives

1. To prepare a series of calcium oxide and zirconia based solid catalysts by co-precipitation and wet impregnation method.
2. Application of the prepared catalysts for the transesterification of low quality triglycerides (*e.g.* waste and non-edible) with methanol/ethanol and to study the kinetics of the reactions.
3. To study the leaching of the catalytic species of the catalyst in biodiesel and their reusability.
4. To study the physicochemical properties of the biodiesel.

References

Achten, W. M. J.; Verchot, L.; Franken, Y. J.; Mathijs, E.; Singh, V. P.; Aerts, R.; Muys, B.; Jatropha bio-diesel production and use. *Biomass Bioenerg.*, **2008**, 32, 1063-1084.

Akbar, E.; Binitha, N.; Yaakob, Z.; Kamarudin, S. K.; Salimon, J.; Preparation of Na doped SiO_2 solid catalysts by the sol-gel method for the production of biodiesel from jatropha oil. *Green Chem.*, **2009**, 11, 1862-1866.

Alhassan, F. H.; Yunus, R.; Rashid, U.; Sirat, K.; Islam, A.; Lee, H. V.; Yap, Y. H. T.; Production of biodiesel from mixed waste vegetable oils using ferric hydrogen sulphate as an effective reusable heterogeneous solid acid catalyst. *Appl. Catal. A: Gen.*, **2013**, 456, 182-187.

Alsalme, A. M.; Wiper, P. V.; Khimyak, Y. Z.; Kozhevnikova, E. F.; Kozhevikov, I. V.; Solid acid catalysts based on $H_3PW_{12}O_{40}$ heteropoly acid: acid and catalytic properties at a gas-solid interface. *J. Catal.*, **2010**, 276, 181-189.

Aransiola, E. F.; Ojumu, T. V.; Oyekola, O. O.; Madzimbamuto, T. F.; Omoregbe, D. I. O.; A review of current technology for biodiesel production: State of the art. *Biomass Bioenerg.*, **2014**, 61, 276-297.

Arata, K.; Organic syntheses catalyzed by superacidic metal oxides: sulfated zirconia and related compounds. *Green Chem.*, **2009**, 11, 1719-1728.

Atabani, A. E.; Silitonga, A. S.; Ong, H. C.; Mahlia, T. M. I.; Masjuki, H. H.; Badruddin, I. A.; Fayaz, H.; Non-edible vegetable oils: A critical evaluation of oil extraction, fatty acid compositions, biodiesel production, characteristics, engine performance and emissions production. *Renew. Sus. Energ. Rev.*, **2013**, 18, 211-245.

Atadashi, I. M.; Aroua, M. K.; Aziz, A. R. A.; Sulaiman, N. M. N.; The effects of water on biodiesel production and refining technologies: A review. *Renew. Sust. Energ. Rev.*, **2012**, 16 3456-3470.

Babu, N. S.; Sree, R.; Prasad, P. S. S.; Lingaiah, N.; Room-temperature transesterification of edible and nonedible oils using a heterogeneous strong basic Mg/La catalyst. *Energy Fuel*, **2008**, 22, 1965-1971.

Barakos, N.; Pasias, S.; Papayannakos, N.; Transesterification of triglycerides in high and low quality oil feeds over an HT2 hydrotalcite catalyst. *Bioresour. Technol.*, 2008, 99, 5037-5042.

Bo, X.; Guomin, X.; Lingfeng, C.; Ruiping, W.; Lijing, G.; Transesterification of palm oil with methanol to biodiesel over a KF/Al_2O_3 heterogeneous base catalyst. *Energy Fuel*, **2007**, 21, 3109-3112.

Brunschwig, C.; Moussavou, W.; Blin, J.; Use of bioethanol for biodiesel production. *Prog. Energ. Combust. Sci.*, **2012**, 38, 283-301.

Caballero, J. M. R.; Gonzalez, J. S.; Robles, J. M.; Tost, R. M.; Castillo, M. L. A.; Alonso, E. V; Lopez, A. J.; Torres, P. M.; Calcium zincate derived heterogeneous catalyst for biodiesel production by ethanolysis. *Fuel*, **2013**, 105, 518-522.

Cantrell, D. G.; Gillie, L. J.; Lee, A. F.; Wilson, K.; Structure-reactivity correlations in MgAl hydrotalcite catalysts for biodiesel synthesis. *Appl. Catal. A: Gen.*, **2005**, 287, 183-190.

Cao, L.; Man, T.; Kruk, M.; Synthesis of ultra-large-pore SBA-15 silica with two-dimensional hexagonal structure using triisopropylbenzene as micelle expander. *Chem. Mater.*, **2009**, 21, 1144-1153.

Chen X. R.; Ju, Y. H.; Mou, C. Y.; Direct synthesis of mesoporous sulfated silica-zirconia catalysts with high catalytic activity for biodiesel via esterification. *J. Phys. Chem. C*, **2007**, 111, 18731-18737.

Chen, C. L.; Huang, C. C.; Tran, D. T.; Chang, J. S.; Biodiesel synthesis via heterogeneous catalysis using modified strontium oxides as the catalysts. *Bioresour. Technol.*, **2012**, 113, 8-13.

Chen, D.; Li, Z.; Wan, Y.; Tu, X.; Shi, Y.; Chen, Z.; Shen, W.; Yu, C.; Tu, B.; Zhao, D.; Anionic surfactant induced mesophase transformation to synthesize highly ordered large-pore mesoporous silica structures. *J. Mater. Chem.*, **2006**, 16, 1511-1519.

Chen, S. Y.; Mochizuki, T.; Abe, Y.; Toba, M.; Yoshimura, Y.; Ti-incorporated SBA-15 mesoporous silica as an efficient and robust Lewis solid acid catalyst for the production of high-quality biodiesel fuels. *Appl. Catal. B: Environ.*, **2014**, 148-149, 344-356.

Choudary, B. M.; Kantam, M. L.; Reddy, V.; Rao, K. K.; Figueras, F.; Henry reactions catalysed by modified Mg–Al hydrotalcite: an efficient reusable solid base for selective synthesis of β-nitroalkanols. *Green Chem.*, **1999**, 187-189.

Chung, K. H; Chang, D. R.; Park, B. G.; Removal of free fatty acid in waste frying oil by esterification with methanol on zeolite catalysts. *Bioresour. Technol.*, **2008**, 99, 7438-7443.

Cosimo, J. I. D.; Diez, V. K.; Xu, M.; Iglesia, E.; Apesteguia, C. R.; Structure and surface and catalytic properties of Mg-Al basic oxides. *J. Catal.*, **1998**, 178, 499-510.

Dehkordi, A. M.; Ghasemi, M.; Transesterification of waste cooking oil to biodiesel using Ca and Zr mixed oxides as heterogeneous base catalysts. *Fuel Process. Technol.*, **2012**, 97, 45-51.

Dias, A. P. S.; Bernardo, J.; Felizardo, P.; Correia, M. J. N.; Biodiesel production by soybean oil methanolysis over SrO/MgO catalysts the relevance of the catalyst granulometry. *Fuel Process. Technol.*, **2012**, 102, 146-155.

Ding, Y.; Sun, H.; Duan, J.; Chen, P.; Lou, H.; Zheng, X.; Mesoporous Li/ZrO_2 as a solid base catalyst for biodiesel production from transesterification of soybean oil with methanol. *Catal. Comm.*, **2011**, 12, 606-610.

Duan, X.; Liu, Y.; Zhao, Q.; Wang, X.; Li, S.; Water-tolerant heteropolyacid on magnetic nanoparticles as efficient catalysts for esterification of free fatty acid. *RSC Adv.*, **2013**, 3, 13748-13755.

Farooq, M.; Ramli, A.; Subbarao, D.; Biodiesel production from waste cooking oil using bifunctional heterogeneous solid catalysts. *J. Cleaner Prod.*, **2013**, 59, 131-140.

Fraile, J. M.; Garcıa, N.; Mayoral, J. A.; Pires, E.; Roldan, L.; The influence of alkaline metals on the strong basicity of Mg–Al mixed oxides: the case of transesterification reactions. *Appl. Catal. A: Gen.*, **2009**, 364, 87-94.

Garcia, C. M; Teixeira, S.; Marciniuk, L. L; Schuchardt, U.; Transesterification of soybean oil catalyzed by sulfated zirconia. *Bioresour. Technol.*, 2**008**, 99, 6608-6613.

Gawande, M. B.; Pandey, R. K.; Jayaram, R. V.; Role of mixed metal oxides in catalysis science-versatile applications in organic synthesis. *Catal. Sci. Technol.*, **2012**, 2, 1113-1125.

Georgogianni, K. G.; Katsoulidis, A. P.; Pomonis, P. J.; Kontominas, M. G.; Transesterification of soybean frying oil to biodiesel using heterogeneous catalysts. *Fuel Process. Technol.*, **2009**, 90, 671-676.

Gombotz, K.; Parette, R.; Austic, G.; Kannan, D.; Matson, J. V.; MnO and TiO solid catalysts with low-grade feedstocks for biodiesel production. *Fuel*, **2012**, 92, 9-15.

Guo, F.; Peng, Z. G.; Dai, J. Y.; Xiu, Z. L; Calcined sodium silicate as solid base catalyst for biodiesel production. *Fuel Process. Technol.*, **2010**, 91, 322-328.

Hattori, H.; Heterogeneous basic catalysis. *Chem. Rev.*, **1995**, 95, 537-558.

Helwani, Z.; Othman, M. R.; Aziz, N.; Fernando, W. Z. N.; Kim, J.; Technologies for production of biodiesel focusing on green catalytic techniques: A review. *Fuel Process. Technol.*, **2009**, 90, 1502-1514.

Jacobson, K.; Gopinath, R.; Meher, L. C.; Dalai, A. K.; Solid acid catalyzed biodiesel production from waste cooking oil. *Appl. Catal. B: Environ.*, **2008**, 85, 86-91.

Jitputti, J.; Kitiyanan, B.; Rangsunvigit, P.; Bunyakiat, K.; Attanatho, L.; Jenvanitpanjakul, P.; Transesterification of crude palm kernel oil and crude coconut oil by different solid catalysts. *Chem. Eng. J.*, **2006**, 116, 61-66.

Kansedo, J.; Lee, K. T.; Bhatia, S.; Cerbera odollam (sea mango) oil as a promising non-edible feedstock for biodiesel production. *Fuel*, **2009**, 88, 1148-1150.

Kaur, M.; Ali, A.; An efficient and reusable Li/NiO heterogeneous catalyst for ethanolysis of waste cottonseed oil. *Eur. J. Lipid Sci. Technol.*, **2014a**, 116, 1-11.

Kaur, M.; Ali, A.; Lithium ion impregnated calcium oxide as nano catalyst for the biodiesel production from karanja and jatropha oils. *Renew. Energ.*, **2011**, 36, 2866-2871.

Kaur, M.; Ali, A.; Potassium fluoride impregnated CaO/NiO: An efficient heterogeneous catalyst for transesterification of waste cottonseed oil. *Eur. J. Lipid Sci. Technol.*, **2014b**, 116, 80-88.

Kaur, N.; Ali, A.; Kinetics and reusability of Zr/CaO as heterogeneous catalyst for the ethanolysis and methanolysis of *Jatropha crucas* oil. *Fuel Process. Technol.*, **2014c**, 119, 173-184.

Kaur, N.; Ali, A.; Lithium ions-supported magnesium oxide as nano-sized solid catalyst for biodiesel preparation from mutton fat. *Energ. Sourc. Part A*, **2013**, 35, 2, 184-192.

Kaur, N.; Ali, A.; Lithium zirconate as solid catalyst for simultaneous esterification and transesterification of low quality triglycerides. *Appl. Catal. A: Gen.*, **2015**, 489, 193-202.

Kaur, N.; Ali, A.; One-pot transesterification and esterification of waste cooking oil via ethanolysis using Sr:Zr mixed oxide as solid catalyst. *RSC Adv.*, **2014d**, 4, 43671-43681.

Kawashima, A.; Matsubara, K.; Honda, K.; Development of heterogeneous base catalysts for biodiesel production. *Bioresour. Technol.*, **2008**, 99, 3439-3443.

Kiakalaieh, A. T.; Amin, N. A. S.; Mazaheri, H.; A review on novel processes of biodiesel production from waste cooking oil. *Appl. Energ.*, **2013**, 104, 683-710.

Kim, M.; Dimaggio, C.; Yan, S.; Salley, S. O.; Ng, K. Y. S.; The effect of support material on the transesterification activity of CaO-La_2O_3 and CaO-CeO_2 supported catalysts. *Green Chem.*, **2011**, 13, 334-339.

Kim, M.; Dimaggio, C.; Yan, S.; Salley, S. O.; Ng, K. Y. S.; The synergistic effect of alcohol mixtures on transesterification of soybean oil using homogeneous and heterogeneous catalysts. *Appl. Catal. A: Gen.*, **2010**, 378, 134-143.

Kiss, A. A.; Dimian, A. C.; Rothenberg, G.; Biodiesel by catalytic reactive distillation powered by metal oxides, *Energy Fuel*, **2008**, 22, 598-604.

Kouzu, M.; Hidaka, J.; Transesterification of vegetable oil into biodiesel catalyzed by CaO: A review. *Fuel*, **2012**, 93, 1-12.

Kozhevnikov, I. V.; Catalysis by heteropoly acids and multicomponent polyoxometalates in liquid-phase reactions. *Chem. Rev.*, **1998**, 98, 171-198.

Kulkarni, M. G.; Gopinath, R.; Meher, L. C; Dalai, A. K.; Solid acid catalyzed biodiesel production by simultaneous esterification and transesterification. *Green Chem.*, **2006**, 8, 1056-1062.

Kumar, D.; Ali, A.; Nanocrystalline K-CaO for the transesterification of a variety of feedstocks: Structure, kinetics and catalytic properties. *Biomass Bioenerg.*, **2012**, 46, 459-468.

Kumar, D.; Ali, A.; Nanocrystalline lithium ion impregnated calcium oxide as heterogeneous catalyst for transesterification of high moisture containing cotton seed oil. *Energy Fuel*, **2010**, 24, 2091-2097.

Kumar, D.; Ali, A.; Transesterification of low-quality triglycerides over a Zn/CaO heterogeneous catalyst: kinetics and reusability studies. *Energy Fuel*, **2013**, 27, 3758-3768.

Lam, M. K.; Lee, K. T.; Mohamed, A. R.; Homogeneous, heterogeneous and enzymatic catalysis for transesterification of high free fatty acid oil (waste cooking oil) to biodiesel: A review. *Biotechnol. Adv.*, **2010**, 28, 500-518.

Lam, M. K.; Lee, K. T.; Mohamed, A. R.; Sulfated tin oxide as solid superacid catalyst for transesterification of waste cooking oil: An optimization study. *Appl. Catal. B: Environ.*, **2009**, 93, 134-139.

Laosiripojana, N.; Kiatkittipong, W.; Sutthisripok, W.; Assabumrungrat, S.; Synthesis of methyl esters from relevant palm products in near-critical methanol with modified-zirconia catalysts. *Bioresour. Technol.*, **2010**, 101, 8416-8423.

Lee, A. F.; Bennett, J. A.; Manayil, J. C.; Wilson, K.; Heterogeneous catalysis for sustainable biodiesel production via esterification and transesterification. *Chem. Soc. Rev.*, **2014**, 43, 7887-7916.

Li, E.; Rudolph, V.; Transesterification of vegetable oil to biodiesel over MgO-functionalized mesoporous catalysts. *Energy Fuel*, **2008**, 22, 145-149.

Li, Y.; He, D.; Yuan, Y.; Cheng, Z.; Zhu, Q.; Influence of acidic and basic properties of ZrO_2 based catalysts on isosynthesis. *Fuel*, **2002**, 81, 1611-1617.

Li, Y.; Zhang, X. D.; Sun, L.; Xu, M.; Zhou, W. G.; Liang, X. H.; Solid superacid catalyzed fatty acid methyl esters production from acid oil. *Appl Energ.*, **2010a**, 87, 2369-2373.

Li, Y.; Zhang, X. D.; Sun, L.; Zhang, J; Xu, H. P.; Fatty acid methyl ester synthesis catalyzed by solid superacid catalyst $SO_4^{2-}/ZrO_2–TiO_2/La^{3+}$. *Appl. Energ.*, **2010b**, 87, 156-159.

Lima, J. R. O.; Ghani, Y. A.; Silva, B.; Batista, F. M. C.; Bini, R. A.; Varanda, L. C.; Oliveira, J. E.; Strontium zirconate heterogeneous catalyst for biodiesel production: Synthesis, characterization and catalytic activity evaluation. *Appl. Catal. A: Gen.*, **2012**, 445-446, 76-82.

Liu, Q.; Wang, B.; Wang, C.; Tian, Z.; Qu, W.; Maa, H.; Xua, R.; Basicities and transesterification activities of Zn–Al hydrotalcites-derived solid bases. *Green Chem.*, **2014**, 16, 2604-2613.

Liu, X.; He, H.; Wang, Y.; Zhu, S.; Piao, X.; Transesterification of soybean oil to biodiesel using CaO as a solid base catalyst. *Fuel*, **2008a**, 87, 216-221.

Liu, X.; He, H.; Wang, Y.; Zhu, S.; Transesterification of soybean oil to biodiesel using SrO as a solid base catalyst. *Catal. Comm.*, **2007**, 8, 1107-1111.

Liu, X.; Piao, X.; Wang, Y.; Zhu, S.; Calcium ethoxide as a solid base catalyst for the transesterification of soybean oil to biodiesel, *Energy Fuel*, **2008b**, 22, 1313-1317.

McLaughlin, D. W.; Land, food and biodiversity. *Conserv. Biol.*, **2011**, 25, 1117-1120.

Mizuno, N.; Misono, M.; Heterogeneous catalysis. *Chem. Rev.*, **1998**, 98, 199-218.

Meher, L. C.; Kulkarni, M. C.; Dalai, A. K.; Naik, S. N.; Transesterification of karanja *(Pongamia pinnata)* oil by solid basic catalysts. *Eur. J. Lipid Sci. Technol.*, **2006**, 108, 389-397.

Montero, J. M.; Wilson, K.; Lee, A. F.; Cs promoted triglyceride transesterification over MgO nanocatalysts. *Top Catal.*, **2010**, 53, 737-745.

Mutreja, V.; Singh, S.; Ali, A.; Potassium impregnated nanocrystalline mixed oxides of La and Mg as heterogeneous catalysts for transesterification. *Renew. Energ.*, **2014**, 62, 226-233.

Nakagaki, S.; Bail, A.; Santos, V. C. D.; Deouza, V. H. R.; Vrubel, H.; Nunes, F. S.; Ramos, L. P.; Use of anhydrous sodium molybdate as an efficient heterogeneous catalyst for soybean oil methanolysis. *Appl. Catal. A: Gen*., **2008**, 351, 267-274.

Narasimharao, K.; Brown, D.; Lee, A. F.; Newman, A. D.; Siril, P. F.; Tavener, S. J.; Wilson, K.; Structure–activity relations in Cs-doped heteropolyacid catalysts for biodiesel production. *J. Catal.*, **2007**, 248, 226-234.

Okamura, M.; Takagaki, A.; Toda, M.; Kondo, J. N.; Tatsumi, T.; Domen, K.; Hara, M.; Hayashi, S.; Acid-catalyzed reactions on flexible polycylic aromatic carbon in amorphous carbon. *Chem. Mater.*, **2006**, 18, 3039-3045.

Omar, W. N. N. W.; Amin, N. A. S.; Biodiesel production from waste cooking oil over alkaline modified zirconia catalyst. *Fuel Process. Technol.*, **2011**, 92, 2397-2405.

Peng, B. X.; Shu, Q.; Wang, J. F.; Wang, G. R.; Wang, D. Z.; Han, M. H.; Biodiesel production from waste oil feedstocks by solid acid catalysis. *Process. Saf. Environ. Prot.*, **2008**, 86, 441-447.

Perin, G.; Alvaro, G.; Westphal, E.; Viana, L. H.; Jacob, R. G.; Lenardao, E. G.; Doca, M. G. M.; Transesterification of castor oil assisted by microwave irradiation. *Fuel*, **2008**, 87, 2838-2841.

Pesaresi, L.; Brown, D. R.; Lee, A. F.; Montero, J. M.; Williams, H.; Wilson, K.; Cs-doped $H_4SiW_{12}O_{40}$ catalysts for biodiesel applications. *Appl. Catal. A: Gen.*, **2009**, 360, 50-58.

Petchmala, A.; Laosiripojana, N.; Jongsomjit, B.; Goto, M.; Panpranot, J.; Mekasuwandumrong, O.; Shotipru, A.; Transesterification of palm oil and esterification of palm fatty acid in near and super-critical methanol with SO_4-ZrO_2 catalysts. *Fuel*, **2010**, 89, 2387-2392.

Phiri, H. K.; Matsumura, Y.; Miniwa, T.; Fujimoto, S.; Heterogeneously catalyzed ethanolysis of groundnut crude oil using activated calcium oxide and surface-modified activated calcium oxide. *J. Jpn. Inst. Energy*, **2010**, 89, 53-58.

Rashtizadeh, E.; Farzaneh, F.; Talebpour, Z.; Synthesis and characterization of $Sr_3Al_2O_6$ nanocomposite as catalyst for biodiesel production. *Bioresour. Technol.*, **2014**, 154, 32-37.

Rattanaphra, D.; Harvey, A.; Srinophakun, P.; Simultaneous conversion of triglyceride/free fatty acid mixtures into biodiesel using sulfated zirconia. *Top Catal*., **2010**, 53, 773-782.

Reddy, C.; Reddy, V.; Oshel, R.; Verkade, J. G.; Room-temperature conversion of soybean oil and poultry fat to biodiesel catalyzed by nanocrystalline calcium oxides. *Energy Fuel*, **2006**, 20, 1310-1314.

Sankaranarayanana, T. M.; Pandurangana, A.; Banub, M.; Sivasanker, S.; Transesterification of sunflower oil over MoO_3 supported on alumina. *Appl. Catal. A: Gen*., **2011**, 409-410, 239- 247.

Sheikh, R.; Choi, M. S.; Im, J. S.; Park, Y. H.; Study on the solid acid catalysts in biodiesel production from high acid value oil. *J. Ind. Eng. Chem.*, **2013**, 19, 1413-1419.

Sheldon, R. A.; Green and sustainable manufacture of chemicals from biomass: state of the art. *Green Chem*., **2014**, 16, 950-963.

Sierra, L.; Guth, J. L.; Synthesis of mesoporous silica with tunable pore size from sodium silicate solutions and a polyethylene oxide surfactant. *Micropor. Mesopor Mat.*, **1999**, 27, 243-253.

Singh, D.; Bhoi, R.; Ganesh, A.; Mahajani, S.; Synthesis of biodiesel from vegetable oil using supported metal oxide catalysts. *Energy Fuel*, **2014**, 28, 2743-2753.

Sivasamy, A.; Cheah, K. Y.; Fornasiero, P.; Kemausuor, F.; Zinoviev, S.; Miertus, S.; Catalytic applications in the production of biodiesel from vegetable oils. *Chem. Sus. Chem.*, **2009**, 2, 278-300.

Sreeprasanth, P. S.; Srivastava, R.; Srinivas, D.; Ratnasamy, P.; Hydrophobic, solid acid catalysts for production of biofuels and lubricants. *Appl. Catal. A: Gen.*, **2006**, 314, 148-159.

Srinivas, D.; Satyarthi, J. K.; Biodiesel production from vegetable oils and animal fat over solid acid double-metal cyanide catalysts. *Catal. Surv. Asia*, **2011**, 15, 145-160.

Stamenkovic, O. S.; Velickovic, A. V.; Veljkovic, V. B.; The production of biodiesel from vegetable oils by ethanolysis: Current state and perspectives. *Fuel*, **2011**, 90, 3141-3155.

Su, F.; Guo, Y.; Advancements in solid acid catalysts for biodiesel production. *Green Chem.*, **2014**, 16, 2934-2957.

Tantirungrotechai, J.; Thepwatee, S.; Yoosuk, B.; Biodiesel synthesis over Sr/MgO solid base catalyst. *Fuel*, **2013**, 106, 279-284.

Teo, S. H.; Rashid, U.; Yap, Y. H. T.; Biodiesel production from crude *Jatropha Curcas* oil using calcium based mixed oxide catalysts. *Fuel*, **2014**, 136, 244-252.

Thitsartarn, W.; Kawi, S.; An active and stable CaO-CeO_2 catalyst for transesterification of oil to biodiesel. *Green Chem.*, **2011**, 13, 3423-3430.

Torres, N. S.; Ibarra, I. C. R.; Pfeiffer, H.; Sodium zirconate (Na_2ZrO_3) as a catalyst in a soybean oil transesterification reaction for biodiesel production. *Fuel Process. Technol.*, **2014**, 120, 34-39.

Tran, N. H.; Bartlett, J. R.; Kannangara, G. S. K; Milev, A. S.; Volk, H.; Wilson, M. A.; Catalytic upgrading of biorefinery oil from micro-algae. *Fuel*, **2010**, 89, 265–274.

Vyas, A. P.; Verma, J. L.; Subrahmanyam, N.; A review on FAME production processes. *Fuel*, **2010**, 89, 1-9.

Wang, J. X.; Chen, K. T.; Wu, J. S.; Wang, P. H.; Huang, S. T.; Chen, C. C.; Production of biodiesel through transesterification of soybean oil using lithium orthosilicate solid catalyst *Fuel Process. Technol.*, **2012**, 104, 167-173.

Wen, Z.; Yu, X.; Tu, S. T.; Yan, J.; Dahlquist, E.; Biodiesel production from waste cooking oil catalyzed by TiO_2–MgO mixed oxides. *Bioresour. Technol.*, **2010b**, 101, 9570-9576.

Wen, Z.; Yu, X.; Tu, S. T.; Yan, J.; Dahlquist, E.; Synthesis of biodiesel from vegetable oil with methanol catalyzed by Li-doped magnesium oxide catalysts. *Appl. Energ.*, **2010a**, 87, 743-748.

Winter, F.; Xia, X. Y.; Hereijgers, B. P. C.; Bitter, J. H.; Dillen A. J. V.; Muhler, M.; Jong, K. P.; On the nature and accessibility of the bronsted-base sites in activated hydrotalcite catalysts. *J. Phys. Chem. B.*, **2006**,110, 9211-9218.

Xie, W.; Wang, T.; Biodiesel production from soybean oil transesterification using tin oxide-supported WO_3 catalysts. *Fuel Process. Technol.*, **2013**, 109, 150-155.

Xie, W.; Zhao, L.; Heterogeneous CaO-MoO_3-SBA-15 catalysts for biodiesel production from soybean oil, *Energ. Convers. Manag.*, **2014**, 79, 34-42.

Yan, S.; Kim, M; Salley, S. O.; Ng, K. Y. S.; Oil transesterification over calcium oxides modified with lanthanum. *Appl. Catal. A: Gen.*, **2009**, 360, 163-170.

Yan, S.; Lu, H.; Liang, B.; Supported CaO catalysts used in the transesterification of rapeseed oil for the purpose of biodiesel production. *Energy Fuel*, **2008**, 22, 646-651.

Yan, S.; Salley, S. O; Ng, K. Y. S.; Simultaneous transesterification and esterification of unrefined or waste oils over ZnO-La_2O_3 catalysts. *Appl. Catal. A: Gen.*, **2009**, 353, 203-212.

Yap, Y. H. T.; Lee, H. V.; Hussein, M. Z.; Yunus, R.; Calcium-based mixed oxide catalysts for methanolysis of *Jatropha curcas* oil to biodiesel, *Biomass Bioenerg.*, **2011**, 35, 827-834.

Zabeti, M.; Daud, W. M. A. N.; Aroua, M. K.; Optimization of the activity of CaO/Al_2O_3 catalyst for biodiesel production using response surface methodology. *Appl. Catal. A: Gen.*, **2009**, 366, 154-159.

Zong, M. H.; Duan, Z. Q.; Lou, W. Y.; Smith, T. J.; Wu, H.; Preparation of a sugar catalyst and its use for highly efficient production of biodiesel. *Green Chem.*, **2007**, 9, 434-437.

Materials and Methods

Abstract: This chapter includes the list of chemicals and materials, and detailed description of methods and analytical techniques which are frequently employed in present thesis.

2.1. Chemicals

Karanja and jatropha oils were obtained from Medors Biotech Pvt. Ltd. New Delhi (India). Waste cottonseed oil has been procured from the restaurants located in Patiala. Fresh cottonseed oil was purchased from local shops located in Patiala. $ZrOCl_2.8H_2O$, ZrO_2 and CaO were purchased from Sigma Aldrich (U.S.A). $TiCl_4$, $Ce(NO_3)_3.6H_2O$, H_2SO_4, LiOH, $NaNO_3$, KNO_3, $Sr(NO_3)_2$, $Ca(NO)_3.4H_2O$, $Mg(NO_3)_2.6H_2O$, $Ba(NO_3)_2$, $(NH_4)_6Mo_7O_{24}.4H_2O$, ammonia, NaOH, HCl and silica gel for thin layer chromatography (TLC) of reagent grade quality, diethyl ether, ethanol and potassium hydroxide used for the determination of acid value were purchased from S D Fine Chemical Ltd. (India) and used as such without further purification. Hexane, ethyl acetate, acetic acid, benzene (HPLC grade), butyl amine and trichloroacetic acid used for Hammett indicator titration was purchased from Loba Chemie Pvt. Ltd. (India). Methanol and ethanol of analytical grade quality were obtained from Merck (India). Propionic, butyric, caproic caprylic, lauric, palmitic, stearic, oleic acid, propanol, butanol, pentanol, hexanol, heptanol, octanol, nonanol and decanol were purchased from Spectrochem Pvt. Ltd. (India). Hammett indicators *viz.*, crystal violet (H_ = 0.8), methyl orange (pK_a = 3.3), methyl red (pK_a = 4.8), neutral red (pK_a = 6.8), bromthymol blue (pK_a = 7.2), phenolphthalein (pK_a = 9.3), nile blue (pK_a = 10.1), tropaeolin-O (pK_a = 11.1), 2, 4-dinitroaniline (pK_a = 15.0), and 4- nitroaniline (pK_a = 18.4) were purchased from Qualigens Fine Chemicals (India).

2.2. Chemical analysis of various vegetable oils

The free fatty acid (FFA) contents, moisture content, saponification and iodine values of the fresh cottonseed oil (CO), waste cottonseed oil (WO), karanja oil (KO) and jatropha oil (JO) were determined by following the methods as reported in literature (Plummer, 1988) and obtained values are given in Table 2.1.

Table 2.1. The chemical analysis of the vegetable oils.

Feedstock	FFA content (wt%)	Moisture content (wt%)	Saponification value (mg of KOH/g of sample)	Iodine value (mg of I_2/g of sample)
CO	0.3-1.2	0.24	181.4	88.2
WO	4.0-5.0	0.27	192.3	94.3
JO	7.0-9.0	0.36	186.2	98.2
KO	15.0-18.1	0.30	194.1	103.5

2.3. Conversion of free fatty acids

Percentage conversion of FFA into respective ester at specific time was determined (Marchetti and Errazu, 2008) by substituting the acid values (A.V.) in equation 2.1.

$$\text{Conversion of FFA (\%)} = \left(\frac{\text{A.V.}_{\text{initial}} - \text{A.V.}_{\text{final}}}{\text{A.V.}_{\text{initial}}}\right) \times 100 \qquad (2.1)$$

All results are an average of three experiments with a relative standard deviation of ±2 %. A.V (mg of KOH/g of sample) of the reaction mixture at specific time was determined by following equation 2.2.

$$\text{A.V.} = (\text{V} \times 1000 \times \text{MW} \times \text{C})/\ \text{W} \qquad (2.2)$$

where V = volume of KOH solution employed for titration (ml); MW = molecular weight of KOH; C = molar concentration of the KOH solution used for titration (0.01 M in present case); and W = weight (in mg) of the reaction mixture to be analyzed.

2.4. Reaction kinetics and thermodynamics

Transesterification is generally assumed to follow a pseudo first order rate law as alcohol in this reaction is employed in excess to the required stoichiometric molar ratio of 3:1 (alcohol to oil). To calculate the activation energy, reactions were carried by varying the temperatures between 35 and 85 ºC. The conversion of VO at different reaction times was obtained and apparent first order rate constants (Song *et al.*, 2011) and activation energy (Balbino *et al.*, 2011) were calculated by fitting the appropriate values in equations 2.3 and 2.4, respectively.

$$-\ln(1-X) = k\,t \qquad (2.3)$$

$$k = A.\, e^{-Ea/RT} \qquad (2.4)$$

where k is the apparent first order rate constant (min^{-1}), X is mole fraction of FAAE at time t, E_a is the activation energy (kJ mol^{-1}), A is the pre-exponential factor (min^{-1}), R is the gas constant (8.314×10^{-3} kJ K^{-1} mol^{-1}) and T is the reaction temperature (°K).

Thermodynamic parameters *viz.*, enthalpy ($\Delta H^{\ddagger}$), entropy ($\Delta S^{\ddagger}$), and the Gibb's free energy of activation ($\Delta G^{\ddagger}$), were calculated (Ong *et al.*, 2013) from Eyring-Polanyi equation 2.5.

$$k = \frac{k_B T}{h} \exp\left(-\frac{\Delta G^{\ddagger}}{RT}\right) \qquad (2.5)$$

Taking the natural logarithm of equation 2.5 and substituting the value of $\Delta G^{\ddagger} = \Delta H^{\ddagger} - T\Delta S^{\ddagger}$, equation 2.6 is obtained.

$$\ln\left(\frac{k}{T}\right) = -\frac{\Delta H^{\ddagger}}{R}\left(\frac{1}{T}\right) + \left[\ln\left(\frac{k_B}{h}\right) + \frac{\Delta S^{\ddagger}}{R}\right] \quad (2.6)$$

where k_B and h are the Boltzmann (1.38×10^{-23} J K^{-1}) and Planck (6.63×10^{-34} Js) constants, respectively. The slope and intercept of 1/T *vs* ln (k/T) plot would be equals to $-\Delta H^{\ddagger}/R$ and $\ln(k_B/h) + \Delta S^{\ddagger}/R$, respectively. The superscript ‡ notation refers to the value of interest in the activation complex or transition state.

2.5. Hammett indicator titration

The acidic strengths of the catalysts were determined by Hammett indicator-amine titration method (Yamanaka and Tanabe, 1975). In 5 mL benzene, 50 mg solid catalyst was suspended and to this five drops of methanolic solution of Hammett indicators (0.02 M) of pK_a between 0.8 to 6.8 was added. The resulted suspension was titrated with 0.1 M *n*-butyl amine solution, till appropriate color change was observed. In order to make sure that excess amine is not present on the solid surface, 0.1 M solution of trichloroacetic acid (prepared in benzene) was added after amine titration. Finally, the amount of *n*-butylamine consumed by the catalyst was determined and represented as acidity of the catalyst in terms of mmol/g of catalyst.

The basic strengths of the catalysts were determined by Hammett indicator-carboxylic acid titration method (Yamanaka and Tanabe, 1975). In 5 mL benzene, 50 mg solid catalyst was suspended and to this five drops of methanolic solution of Hammett indicator (0.02 M) of pK_a between 6.8 and 18.4 was added. The resulted suspension was titrated with 0.1 M trichloroacetic acid solution, till appropriate color change was observed. In order to make sure that excess acid is not present on the solid surface, 0.1 M solution of *n*-butyl amine (prepared in benzene) was added after acid titration. Finally, the amount of trichloroacetic acid consumed by the catalyst was determined and represented as basicity of the catalyst in terms of mmol/g of catalyst.

2.6. Turn over frequency

The turnover frequency (TOF) of the catalyst (Tao *et al.*, 2012) is calculated from equation 2.7.

$$TOF = \frac{mol_{actual}}{f_m \times m_{cat} \times t} \quad (2.7)$$

where mol_{actual} is the moles of FAAE at 25 % conversion; m_{cat} is the mass of catalyst; *t* is the reaction time and f_m is active sites (basic/acidic sites) of catalyst (in mmol) calculated by Hammett indicator titration method.

2.7. Instruments

2.7.1. Powder X-ray diffraction (XRD)

Powder X-ray diffraction patterns were recorded on a PANalytical's X'Pert Pro diffractometer operating at 40 kV using nickel-filtered monochromatic Cu Kα radiation (λ = 1.54060 Å). The samples were scanned over a 2θ range of 5–80° at the scanning speed of 2º/min. The phases present in the samples were identified with the help of JCPDS (Joint Committee of the Powder Diffraction Standards) database files.

2.7.2. X-ray photoelectron spectroscopy (XPS)

The binding energy and electronic state of the elements present in catalysts were determined by X-ray photoelectron spectroscopy using KRATOS-AXIS Ultra DLD spectrometer instrument (Kratos Analytical, UK) equipped with monochromator alumina source (Al Kα radiation; $h\nu$ = 1486.69 eV). The instrument was operated at 10 kV and 15 mA with pass energy of 160 eV and an increment of 1 eV. For analysis, powdered samples were deposited on carbon tape and degassed for 2 h in XPS chamber to minimize the air contamination at sample surface. To overcome the charging problem, a charge neutralizer of 2 eV was applied and binding energy of C 1s core level (284.6 eV) was taken as a reference.

2.7.3. Fourier transformation infra-red spectroscopy (FT-IR)

Fourier transform-infrared spectra of the samples were recorded in KBr or ATR accessory on Agilent Cary-660 spectrophotometer in the range of 400-4000 cm^{-1}.

To quantify the Bronsted and Lewis acid sites in catalysts, pyridine adsorption method was employed. For the analysis, samples were saturated with pyridine at room temperature, dried under vacuum at 50 °C for 2 h, and further heated for 10 min at 300 °C to desorb the pyridine. Finally the diffuse reflectance FT-IR (DRIFT) spectra of these samples were recorded in KBr pellet using Agilent Cary-660 spectrophotometer in the range of 1400–1700 cm^{-1}.

2.7.4. Fourier transform-nuclear magnetic resonance (FT-NMR)

Fourier transform-nuclear magnetic resonance spectra of vegetable oils and FAAEs were recorded on a JEOL ECS-400 (400 MHz) spectrophotometer in $CDCl_3$ solvent using tertramethyl silane (TMS) as internal reference and chemical shifts (δ) were expressed in parts per million (ppm).

FAME and FAEE were quantified by ^{1}H-NMR technique (Knothe, 2000; Ghesti *et al.*, 2007) following the equation 2.8 and 2.9, respectively.

$$\%C_{ME} = 100 \left(\frac{2\, I_{OCH_3}}{3\, I_{\alpha CH_2}} \right) \quad (2.8)$$

where $I_{OCH3\ and}$ $I_{\alpha CH2}$ are the integrated area of methoxy and methylene protons at 3.7 ppm and 2.3 ppm respectively.

$$\%C_{EE} = 100 \left(\frac{4(I_{TAG+EE} - I_{TAG})}{4(I_{TAG+EE} - I_{TAG}) + 6(2I_{TAG})} \right) \quad (2.9)$$

where I_{TAG} = integration of glyceryl methylenic hydrogens at 4.15-4.35 ppm; $I_{(TAG+EE)}$ integration of glyceryl methylenic hydrogens and -OCH_2 of ethoxy hydrogens superimposed at 4.10- 4.20 ppm.

2.7.5. Gas chromatography-Mass spectroscopy (GC-MS)

Gas chromatography-Mass spectroscopy of FAAEs was performed on Bruker GC-45X coupled with Scion MS-TQ/SQ system. For GC-MS study samples were diluted with hexane and one µL sample solution was injected (injection temperature 250 °C) in GC (15 m × 0.25 mm × 0.25 mm RTX -5MS sil capillary column) in split/splitless mode (split ratio 1:20 for 0.01 s). Helium was used as a carrier gas with a flow rate of 1 ml/min. The column temperature was increased from 60 °C to 300 °C with the heating rate of 10 °C/min. The output from the GC column was entered into the ionization chamber of mass spectrometer *via* a transfer line maintained at 260 °C. Mass spectrum (EI 70 eV, ion source temperature 280°C, solvent delay 2.5 min) was scanned in the m/z range of 50-800. The National Institute of Standard and Test (NIST) library match software was used to identify the individual FAAE. Composition as well as FAEE yield was quantified by following the literature reported method (Li *et al*., 2010).

2.7.6. Scanning electron microscopy-Energy Dispersive X-ray Analysis (SEM-EDS)

Scanning electron microscopy coupled with energy dispersive X-ray spectrometry was performed on JEOL JSM 6510LV instrument. For analysis, initially sample was ultrasonicated in ethanol for 2 h. A drop of this suspension was mounted on a sample holder with the help of carbon tape. The sample was then sputter coated with gold and visualized with instrument to assess the particle morphology.

2.7.7. Transmission electron microscopy (TEM)

Transmission electron microscopy images of the sample were recorded on HITACHI 7500 instrument. For sample preparation, powdered sample was mixed with ethanol and ultrasonicated for 1 h to suspend the particles in solvent. A small drop of this suspension was placed on a copper grid and solvent was dried prior to the analysis.

2.7.8. Brunauer-Emmett-Teller (BET) surface area

The surface area of the catalysts was determined at 77 K by the standard Brunauer-Emmett-Teller method using Micromeritics TriStar -3000 surface area analyzer. Prior to analysis, all samples were degassed at 473 K for 2 h under a nitrogen atmosphere to remove the physisorbed moisture from the catalysts.

2.7.9. Temperature programmed desorption (TPD)

In a typical experiment of CO_2-TPD, 0.1 g of catalyst was loaded in a quartz reactor between two quartz plugs. Prior to CO_2 adsorption, the catalyst was pretreated with He gas at 300 °C for 2 h and then cooled to room temperature. The adsorption of CO_2 was carried out by passing a mixture of 10% CO_2-balanced He gas over the catalyst for 1 h. To remove the physisorbed CO_2, He gas was flushed over catalyst surface at 100 °C for 2 h. Then sample was heated upto desired temperature with a ramp of 10 °C/min under the flow of He gas (flow rate of 30 mL/min). The CO_2 desorption was monitored using the thermal conductivity detector (TCD) of a gas chromatograph (Varian, 8301).

2.7.10. Thermo-gravimetric–Differential Scanning Calorimetry analysis (TG-DSC)

Thermo-gravimetric-Differential scanning calorimetry analysis was performed on NETZSCH STA 449F3 instrument. Samples were heated between 25 to 800 °C, at a heating rate of 10 °C min^{-1} under normal atmosphere.

2.7.11. Inductively coupled plasma -Atomic emission spectrometry (ICP-AES)

The metal concentration in FAAEs and glycerol was estimated by Inductively coupled plasma-Atomic emission spectroscopy on Spectro ARCOS instrument. For sample preparation, 0.5 g of sample was digested in 5 ml HNO_3 (16 M) in a beaker and then $HClO_4$ (11 M) was added drop-wise to destroy all organic matter. Prior to analysis, the solution is filtered in a 50 mL volumetric flask and volume was made up with de-ionized water.

2.7.12. Carbon hydrogen nitrogen sulfur analyzer (CHNS)

The sulfate content in methyl oleate and catalysts was analyzed by Thermo Finnigan FLASH EA 1412 series CHNS analyzer.

References

Balbino, J. M.; Menezes, E. W. D.; Benvenutti, E. V.; Cataluna, R.; Ebelinga G.; Dupont, J.; Silica supported guanidine catalyst for continuous flow biodiesel production. *Green Chem.*, **2011**, 13, 3111-3116.

Ghesti, G. F.; Macedo, J. L.; Resck, I. S.; Dias, J. A.; Dias, S. C. L.; FT-Raman spectroscopy quantification of biodiesel in a progressive soybean oil transesterification reaction and its correlation with 1H-NMR spectroscopy methods. *Energy Fuel*, **2007**, 21, 2475-2480.

Knothe, G.; Monitoring a progressing transesterification reaction by fiber-optic near infrared spectroscopy with correlation to ^{1}H nuclear magnetic resonance spectroscopy. *J. Am. Oil Chem. Soc.*, **2000**, 77, 489-493.

Li, Y.; Zhang, X. D.; Sun, L; Xu, M.; Zhou W. G.; Liang, X. H.; Solid superacid catalyzed fatty acid methyl esters production from acid oil. *Appl. Energ.*, **2010**, 87, 2369-2373.

Marchetti, J. M; Errazu, A. F.; Comparison of different heterogeneous catalysts and different alcohols for the esterification reaction of oleic acid. *Fuel*, **2008**, 87, 3477-3480.

Ong, L. K.; Kurniawan, A.; Suwandi, A. C; Lin, C. X.; Zhao, X. S.; Ismadji, S.; Transesterification of leather tanning waste to biodiesel at supercritical condition: Kinetics and thermodynamics studies. *J. Supercrit. Fluids*, **2013**, 75, 11-20.

Plummer, D. T.; An introduction to practical biochemistry. Tata McGraw-Hill: New Delhi, India. **1988**, pp 195-197.

Song, R.; Tong, D.; Tang, J; Hu, C; Effect of composition on the structure and catalytic properties of KF/Mg_La solid base catalysts for biodiesel synthesis via transesterification of cottonseed oil. *Energy Fuel*, **2011**, 25, 2679-2686.

Tao, G.; Hua, Z.; Gao, Z.; Chen, Y.; Wang, L.; He, Q.; Chenaand, H.; Shi, J.; Synthesis and catalytic activity of mesostructured $KF/Ca_xAl_2O_{(x+3)}$ for the transesterification reaction to produce biodiesel. *RSC Adv.*, **2012**, 2, 12337-12345.

Yamanaka, T.; Tanabe, K.; A new determination of acid-base strength distribution of a common scale on solid surfaces. *J. Phys. Chem.*, **1975**, 79, 2409-2411.

Preparation and Application of Ce/ZrO_2-TiO_2/SO_4^{2-} as Solid Catalyst for the Esterification of Fatty Acids

Contents *Page No.*

Abstract: To develop heterogeneous and reusable catalyst for the esterification of fatty acids, in presence of triglycerides, sulfate species has been incorporated over $Ce/ZrO_2–TiO_2$ support. The catalyst activity was found to be a function of its Bronsted acidic sites which in turn depends on the cerium concentration in catalyst. The esterification of oleic acid with methanol or ethanol in presence of prepared catalyst has followed the first order kinetics and Koros-Nowak test has demonstrated that reaction rates are independent from diffusion limitations. An increase in acid or alcohol alkyl chain length (steric factor) was found to show negative effect on the esterification activity of catalyst. Although, the catalyst was able to catalyze the esterification even in presence of up to 12 wt% moisture (with respect to fatty acids), however, a decrease in turn over frequency (TOF) was observed. The catalyst has shown excellent stability as negligible sulfate leaching was observed and recovered catalyst was reused in five successive runs without significant loss in activity.

Even in presence of triglyceride (vegetable oil) the catalyst was able to convert > 98% free fatty acids into respective esters. The esterified oils were fruitfully employed, without any pre-neutralization and water washing, in homogeneous alkali catalyzed transesterification to achieve > 98% fatty acid methyl ester (FAME) yield.

3.1. Introduction

The major hurdle for the commercialization of biodiesel in India is non availability of adequate feedstock for the transesterification. Further, application of costly refined edible oils would not only create the scarcity of the cooking oil but also increases the biodiesel production cost (Sarkar *et al.*, 2010). Both the problems could be circumvented by employing non edible or waste cooking oils as feedstock for the biodiesel production. However, such oils usually contain high concentrations of FFA and moisture contents (Kaur and Ali, 2014) and hence, homogeneous alkali catalyst could not be directly employed for the transesterification. Biodiesel production from high FFA (> 0.5 wt%) containing feedstock usually involve two steps *viz*., (i) acid catalyzed esterification to reduce the FFA contents followed by (ii) base catalyzed transesterification of the ester rich feedstock to produce biodiesel (Zhang and Jiang, 2008). Homogeneous mineral acids (e.g. H_2SO_4) employed for the esterification of FFA are nonreusable, difficult to separate from the products, highly corrosive, require high temperature (> 100 °C), and promoted the reverse reaction (hydrolysis of ester) in presence of water: a by-product of esterification (Park *et al.*, 2010a). Moreover, after the completion of esterification acid is neutralized by alkali and generated salt must be washed away with water from the reaction mixture. Product washing required huge amount of water and generate vast quantity of industrial effluents to cause the disposal problem (Thiruvengadaravi *et al.*, 2012).

To overcome the limitations of the homogeneous catalysts, in literature, a variety of solid catalysts were employed for the fatty acid esterification. Sulfated zirconia as well as other reported sulfated catalysts for the fatty acid esterification was found to be moisture sensitive and unstable due to the leaching of the sulfate group from the catalyst (Sudarsanam *et al.*, 2013). In most of the sulfated catalysts a single metal oxide was employed as a support, although a combination of two or more mixed metal oxides is expected to be more efficient (Das *et al.*, 2002). To improve the versatility, stability and reusability of sulfated catalysts, in current study, Ce/Zr/Ti mixed oxide was prepared and employed as support for the sulfate group immobilization. Prepared Ce/ZrO_2-TiO_2/SO_4^{2-} was employed as heterogeneous catalyst for the esterification of a variety of carboxylic acids (C_2-C_{18}) and alcohols (C_1-C_{10}). Further, to test the sensitivity of catalyst towards moisture, oleic acid esterification was performed in presence of up to 12 wt% water (with respect to oleic acid). The effect of reaction parameters, such as alcohol to acid molar ratio, reaction temperature, catalyst concentration and stirring speed were studied on the course of reaction. Finally to demonstrate the practical application,

the prepared catalyst was employed for the esterification of VOs having 2.8–15.2 wt% FFA. The catalyst was found to be effective even in presence of triglycerides as > 98 % FFA in VOs was esterfied. Esterified VOs was successfully employed, without any prior purification step, during base (NaOH) catalyzed transesterification reaction to produce biodiesel.

3.2. Experimental section

3.2.1. Catalyst preparation

The mixed oxide of zirconium and titanium ($Zr(OH)_4$–$Ti(OH)_4$) was prepared *via* co-precipitation method. In a typical preparation, 5.5 mL of $TiCl_4$ and 8.05 g of $ZrOCl_2.8H_2O$ (corresponding to theoretical Ti/Zr atomic ratio of 1:1) were dissolved in 100 ml deionized water and stirred in a 250 mL beaker for 5 min. To this, NH_3 solution (25 wt%) was added drop wise to maintain a final pH ~10 and resulting suspension was stirred for 3 h at 30 °C. Finally the precipitate was filtered out, washed with deionised water to remove chloride ions, and dried at 120 °C for 24 h to obtain a white powder of $Zr(OH)_4$–$Ti(OH)_4$.

To prepare the targeted catalyst, 1 g of powdered $Zr(OH)_4$–$Ti(OH)_4$ was mixed in 20 mL deionized water in a 100 mL beaker. To this, appropriate amount of 1 M sulfuric acid and desired amount of $Ce(NO)_3.6H_2O$ was added and resulted mixture was stirred for 24 h at 30 °C. This mixture was dried at 120 °C for 12 h and finally calcined at desired temperature to obtain Ce/ZrO_2-TiO_2/SO_4^{2-} catalyst.

Prepared catalysts were labelled as *x*-Ce/ZrO_2–TiO_2/SO_4^{2-}-T, where *x* and T represent the Ce concentration (wt%) and calcination temperature (ºC), respectively.

3.2.2. Esterification of fatty acids

Esterification reactions were carried out in a 50 mL two–neck round bottom flask equipped with an oil bath, magnetic stirrer and a water–cooled reflux condenser. In a typical reaction 10 g of oleic acid (OA) was mixed with desired molar concentrations of alcohol and catalyst, and stirred (500 rpm) at desired temperature to achieve the esterification of fatty acid into corresponding ester. The conversion of FFA at specific time was calculated by the method given in Section 2.3 in Chapter 2. The prepared fatty acid alkyl esters were characterized by FT-IR, ^{1}H-NMR, ^{13}C-NMR and GC-MS techniques.

3.3. Results and Discussion

3.3.1. Catalyst characterization

3.3.1.1. Powder X–ray diffraction (XRD)

Powder XRD study was performed to establish the effect of cerium loading and calcination temperature on catalysts structure. As shown in Fig. 3.1(a), presence of a broad peak at 2θ ~ 30° in the XRD patterns of $Zr(OH)_4$–$Ti(OH)_4$ indicate its poor crystalline nature and no significant difference was observed even upon 2 wt% cerium impregnation in support material. However, upon sulfate impregnation over the same support, weak diffraction patterns corresponding to *orthorhombic* zirconium sulfate ($Zr(SO_4)_2$; JCPDS card no. 72-2192) and intense peaks of *hexagonal* titanium sulfate ($Ti_2(SO_4)_3$; JCPDS card no. 42-0230) were observed. A gradual increase in zirconium sulfate phase was observed on increasing cerium concentration (0.5-2.0 wt%) in catalyst. The catalyst prepared by using lanthanum in place of cerium also found to show similar results as reported by Li *et al.* (2010). A further increase in cerium concentration (3 wt%) was not found to make any significant change in catalyst structure.

The effect of calcination temperature on catalyst structure was evaluated in the temperature range of 400–700 °C. As shown in Fig. 3.1(b), the *monoclinic* zirconia phase was also observed along with zirconium sulfate, titanium sulfate and cerium oxide (CeO_2; JCPDS card no. 81-0792) up to 500 °C calcination temperature. The ratio between zirconium sulfate and titanium sulfate increases from 1.71 to 2.15 on increasing the calcination temperature from 400–600 °C. A further increase in calcination temperature (700 °C) was found to generate a new phase of $ZrTiO_4$ (JCPDS card no. 42-0230) due to the decomposition of zirconium and titanium sulfate. The crystallite size of the 2-Ce/ZrO_2–TiO_2/SO_4^{2-}-600 catalyst was found to be ~ 16 nm by the Debye-Sherrer method.

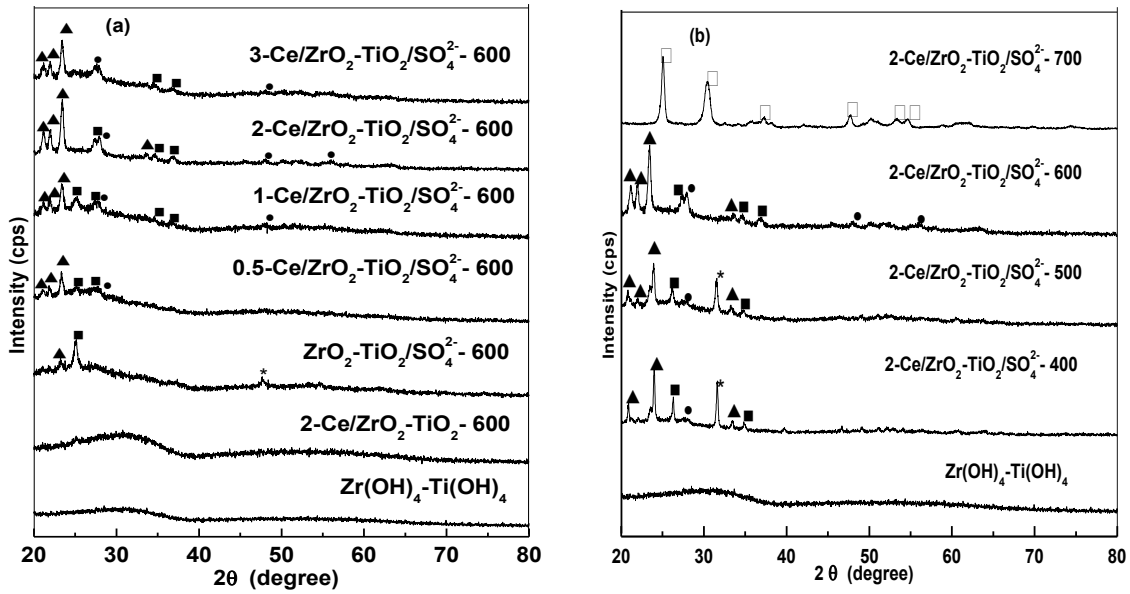

Fig. 3.1. XRD of varying (a) cerium concentration and (b) calcination temperature. (*- *m*-ZrO_2,•- CeO_2,▲- $Zr(SO_4)_2$, ■ - $Ti_2(SO_4)_3$, □ - $ZrTiO_4$).

3.3.1.2. SEM-EDS, TEM and elemental analysis

The surface morphology of the prepared samples was studied by SEM and their images are demonstrated in Fig. 3.2. The SEM image (Fig. 3.2(a)) of catalyst support $Zr(OH)_4$-$Ti(OH)_4$ shows the formation of ~ 5 µm sized particles in irregular geometries. Incorporation of cerium and sulfate on this support resulted the flake like structure in irregular shape and sizes as shown in Fig. 3.2(b). The thickness of these flakes was measured ~ 0.5 µm.

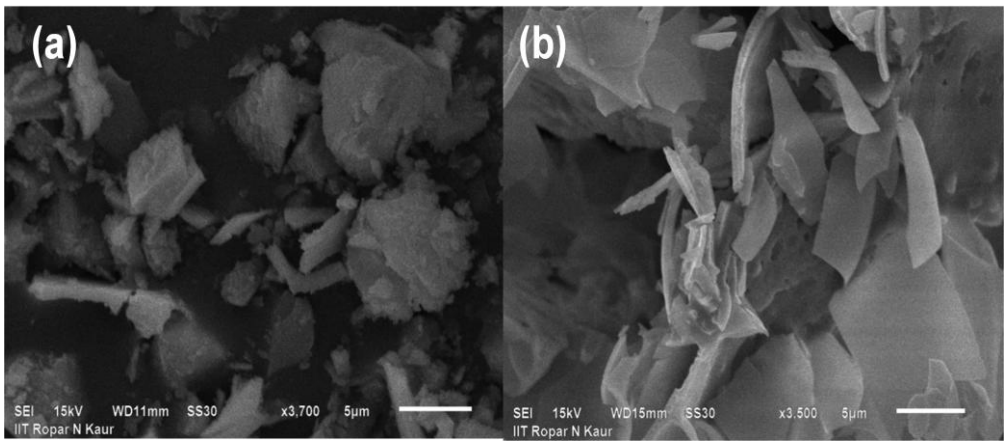

Fig. 3.2. Comparison between the SEM images of (a) $Zr(OH)_4$–$Ti(OH)_4$ and (b) 2-Ce/ZrO_2–TiO_2/SO_4^{2-}-600.

Atomic ratio of Zr and Ti in $Zr(OH)_4$–$Ti(OH)_4$ was observed as ~1:1 during EDS analysis as given in Table 3.1. The sulfated $Zr(OH)_4$–$Ti(OH)_4$ without and with cerium was found to have 10.21 and 16.69 wt% sulfur contents (by elemental analysis), respectively. Thus

presence of cerium was found to enhance the sulfate impregnation over the catalyst support. The catalyst calcined at 700 °C (2-Ce/ZrO_2–TiO_2/SO_4^{2-}-700) was found to have only 0.86 wt% sulfur content (by element analysis) due to the major decomposition of sulfate moiety.

Table 3.1. EDS analysis of $Zr(OH)_4$-$Ti(OH)_4$, SO_4^{2-}/ZrO_2-TiO_2-600 and 2-Ce/ZrO_2-TiO_2/SO_4^{2-}-600 catalysts.

Elements →	**O**		**Ti**		**Zr**		**S**		**Ce**	
Catalysts	**Wt%**	**At%**	**Wt%**	**At%**	**Wt%**	**At%**	**Wt%**	**At%**	**Wt%**	**At%**
$Zr(OH)_4$-$Ti(OH)_4$	60.69	86.60	15.72	7.10	23.59	6.30	-	-	-	-
SO_4^{2-}/ZrO_2-TiO_2-600	41.90	8.31	22.22	12.62	26.07	7.78	9.81	71.29	-	-
2-Ce/ZrO_2-TiO_2/SO_4^{2-}-600	61.63	9.29	9.70	4.36	13.10	3.07	13.73	83.00	1.84	0.28

TEM imaging of 2-Ce/ZrO_2–TiO_2/SO_4^{2-}-600 also shows the formation of catalyst in flake like structure as demonstrated in Fig. 3.3. These flakes are actually the aggregates of smaller particles with an average particle size of ~15 nm. The crystallite size measured by powder XRD study (~16 nm) shows an agreement with the size calculated by TEM study.

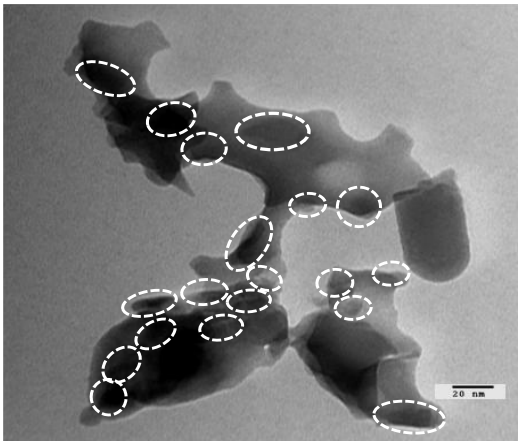

Fig. 3.3. TEM image of 2-Ce/ZrO_2–TiO_2/SO_4^{2-}-600.

3.3.1.3. FT-IR Spectroscopy

To demonstrate the sulfate impregnation over $Zr(OH)_4$–$Ti(OH)_4$, FTIR spectra of 2-Ce/ZrO_2–TiO_2-600, 2-Ce/ZrO_2–TiO_2/SO_4^{2-}-600 and 2-Ce/ZrO_2–TiO_2/SO_4^{2-}-700 is compared in Fig. 3.4. The presence of sulfate functional group in 2-Ce/ZrO_2–TiO_2/SO_4^{2-}-600 was supported by the appearance of bands at 990 (ν_s(S—O)), 1041(ν_{as}(S—O)), 1162 (ν_s(S=O)) and 1236 cm^{-1} (ν_{as}(S=O)). These are the characteristic bands corresponding to the bidentate bridging of sulfate group with Zr^{4+} and/or Ti^{4+} (Li *et al.*, 2012). The sample prepared at 700 °C calcination temperature didn't show the characteristic sulfate bands to support the catalyst decomposition.

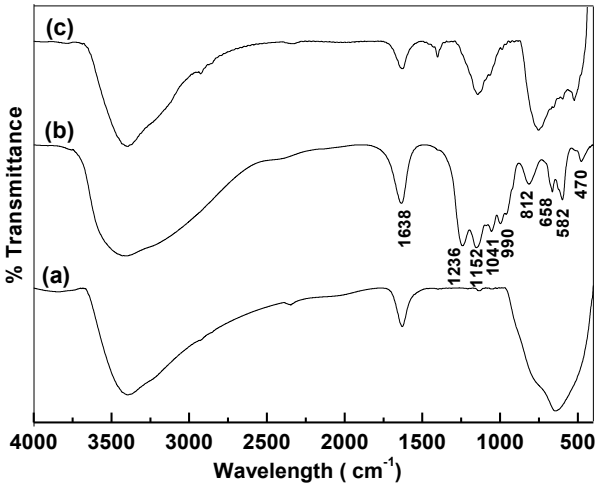

Fig. 3.4. Comparison of FTIR spectra of (a) 2-Ce/ZrO_2–TiO_2-600, (b) 2-Ce/ZrO_2–TiO_2/SO_4^{2-}-600, and (c) 2-Ce/ZrO_2–TiO_2/SO_4^{2-}-700.

3.3.1.4. Pyridine adsorption DRIFT study

In DRIFT spectra (Fig. 3.5) of catalyst saturated with pyridine, characteristic bands of pyridinium ion (Bronsted (B) acid sites) were observed at ~1638 and 1540 cm^{-1} and covalently bonded pyridine (Lewis (L) acid cites) was observed at ~1616 cm^{-1}. The peak observed at ~1490 cm^{-1} is due to the presence of total acidic (B+L) sites in the catalyst (Yang *et al.*, 2005). The bands corresponding to pyridine adsorption remain absent from catalyst support (Fig. 3.5(a)) $Zr(OH)_4$-$Ti(OH)_4$ and catalyst prepared with cerium (Fig. 3.5(b)) 2-Ce/ZrO_2-TiO_2-600, to rule out the presence of strong acidic sites. Incorporation of sulfate group without cerium although generate the acidic sites (Fig. 3.5(c)), but immobilization of sulfate group along with cerium was found to further strengthen these sites. An increase in cerium concentration (0.5-2 wt%) was found to enhance the sulfate loading over the catalyst support which resulted enhancement in L and B acid sites (Table 3.2). Maximum acidic sites were observed for the catalyst with 2 wt% cerium concentration and a further increase in cerium concentration was not found to enhance the acidic sites on catalyst surface (Table 3.2). The catalyst prepared at 700 °C calcination temperature shoe merely weak pyridine bands due to the loss of acidic sites owing to the sulfate group decomposition.

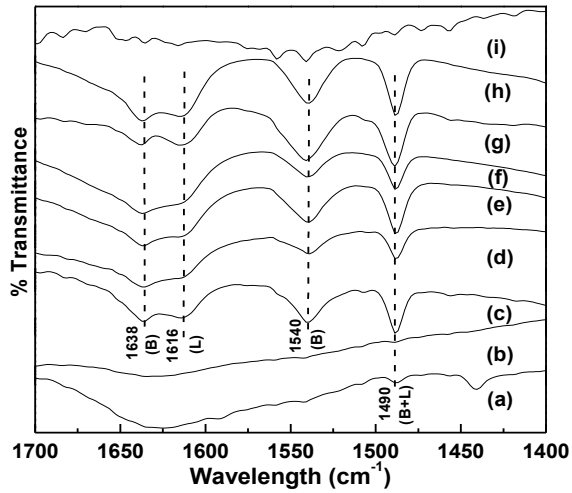

Fig. 3.5. DRIFT spectra of pyridine absorbed on (a) support $Zr(OH)_4$-$Ti(OH)_4$, (b) 2-Ce/ZrO_2-TiO_2-600, (c) SO_4^{2-}/ZrO_2-TiO_2-600, (d) 0.5-Ce/ZrO_2–TiO_2/SO_4^{2-}-600, (e) 2-Ce/ZrO_2–TiO_2/SO_4^{2-}-600, (f) 3-Ce/ZrO_2–TiO_2/SO_4^{2-}-600, (g) 2-Ce/ZrO_2–TiO_2/SO_4^{2-}-400, (h) 2-Ce/ZrO_2–TiO_2/SO_4^{2-}-500 and (i) 2-Ce/ZrO_2–TiO_2/SO_4^{2-}-700 at 300 °C.

3.3.1.5. XPS analysis

The electronic state of the metal ions present in catalyst was determined by XPS analysis as shown in Fig. 3.6. The peaks observed at 884.9, 168.9, 184.2, 458.9 and 531.9 eV could be assigned to the presence of Ce^{4+} (3d), S^{2-} (2p) Zr^{4+} (3d), Ti^{4+} (2p) and O^{2-} (1s), respectively (Reddy *et al.*, 2009a; Reddy *et al.*, 2009b). Qualitative analysis by XPS study supported the presence of 2.11 wt% Zr, 3.32 wt% Ti, 0.06 wt% Ce, 47.77 wt% O and 16.91 wt% S over catalyst surface.

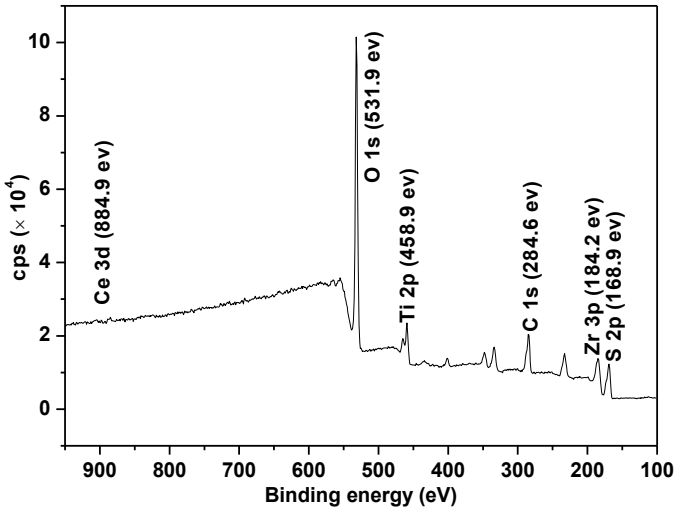

Fig. 3.6. Wide scan XPS spectra of 2-Ce/ZrO_2–TiO_2/SO_4^{2-}-600 catalyst.

3.3.2. Fatty acid alkyl ester characterization

3.3.2.1. FTIR Spectroscopy

In FTIR spectrum of oleic acid, the bands at 1710 and 1285 cm^{-1} appeared due to carboxylic C=O, and C—OH vibrational frequencies, respectively as shown in Fig. 3.7(a). Upon esterification, these bands shift to 1750 and 1170–1200 cm^{-1}, respectively Fig. 3.7(b) and 3.7(c), to support the formation of ester group.

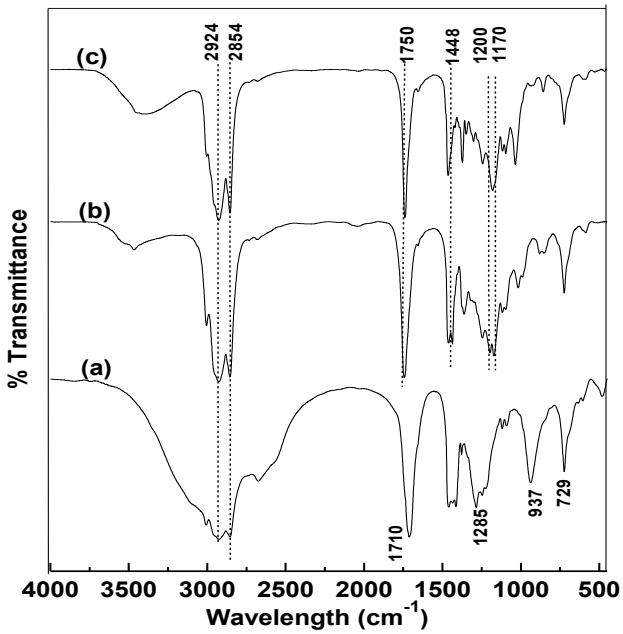

Fig. 3.7. FTIR spectra of (a) oleic acid, (b) methyl oleate and (c) ethyl oleate.

3.3.2.2. NMR Spectroscopy

In ^{1}H-NMR spectra of oleic acid and corresponding alkyl esters, peaks at 0.88, 1.25-1.31 and 2.3 ppm are due to the terminal methyl, backbone methylene and alpha methylene protons, respectively (Fig. 3.8). Presence of unsaturated protons (–CH=CH–) in all three molecules was supported by the presence of a signal at 5.35 ppm. Upon esterification of oleic acid, appearance of a singlet at 3.6 ppm, due to methoxy protons, supports the formation of methyl oleate (MO) (Fig. 3.8(b)). On the other hand, presence of a quartet at 4.1 ppm, due to $–OCH_2$-group, supports the formation of ethyl oleate (EO) (Fig. 3.8(c)).

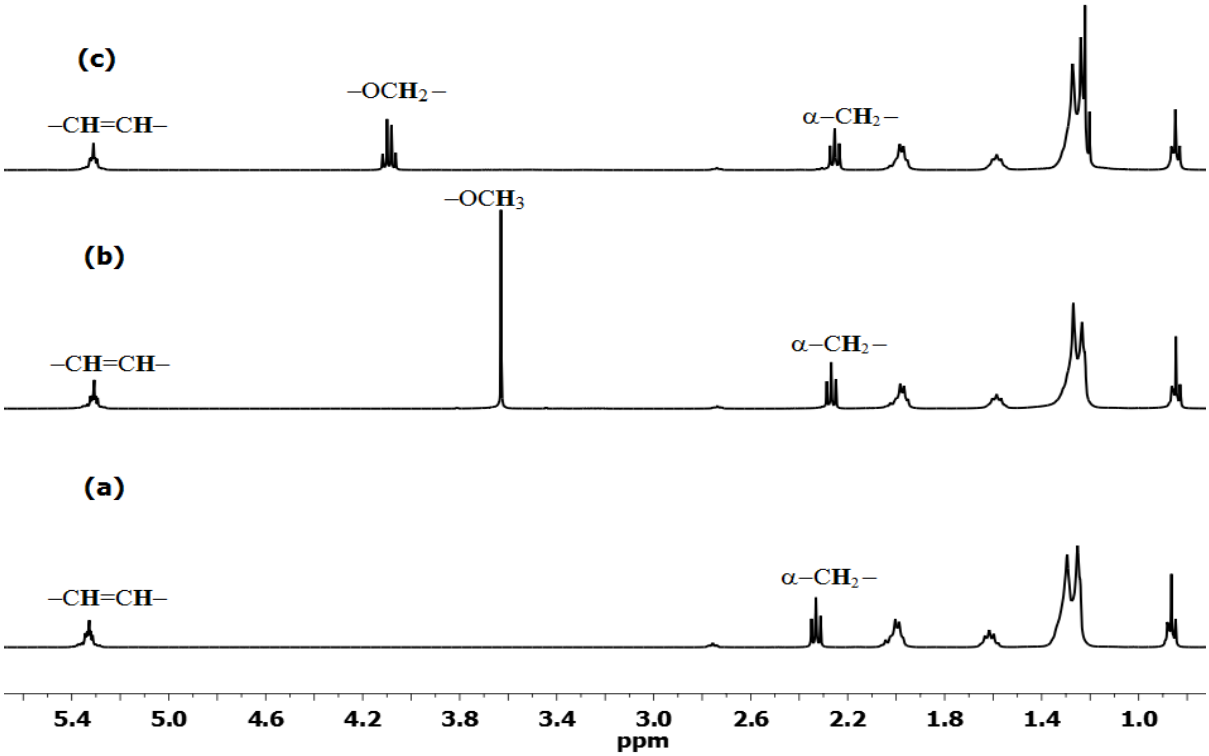

Fig. 3.8. ^{1}H-NMR spectra of (a) oleic acid, (b) methyl oleate and (c) ethyl oleate.

The ^{13}C-NMR spectra of OA, MO and EO are compared in Fig. 3.9. The peak appeared at 14 ppm is characteristic of the terminal methyl group and the signal due to unsaturated carbons appeared at 128–130 ppm for all three molecules. The appearance of new peak upon esterification at 50.8 ppm due to –O**C**H$_3$ and 60.0 ppm due to –O**C**H$_2$– supported the formation of methyl and ethyl esters, respectively. Further, carbonyl carbon of carboxylic acid was shifted from 180 ppm to 174-175 ppm upon esterification as shown in Fig. 3.8(b) and 3.8(c).

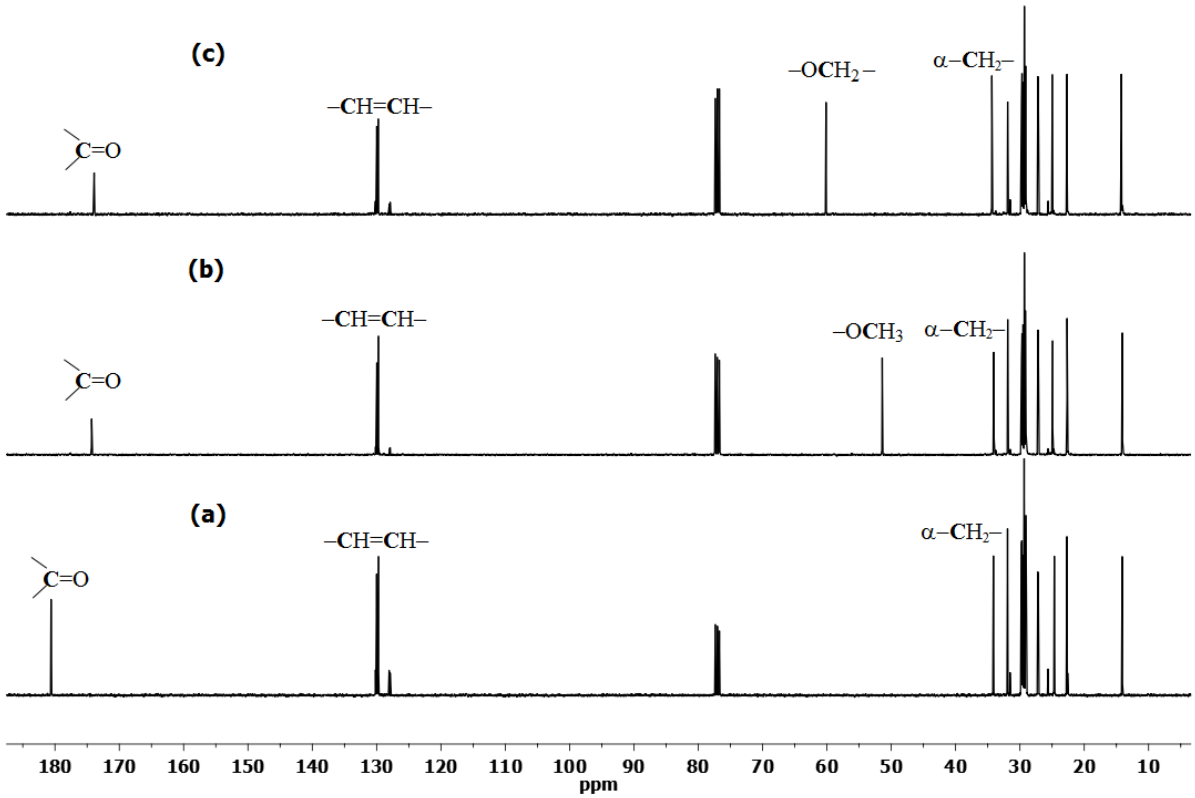

Fig. 3.9. ^{13}C-NMR spectra of (a) oleic acid, (b) methyl oleate and (c) ethyl oleate.

3.3.2.3. GC-MS study

The purity and molecular weight of the prepared EO and MO was established by GC-MS technique as shown in Fig. 3.10. Appearance of a single peak at 16.25 and 16.77 min in Fig. 3.10(a) supports the formation of single and pure product during esterification reaction. In MS spectrum, molecular ion peaks observed at m/z value of 296 and 310 supports the formation of MO and EO, respectively. Peak appeared at 264 m/z support the loss of $–OCH_3$ and $–OCH_2CH_3$ fragment from MO and EO, respectively.

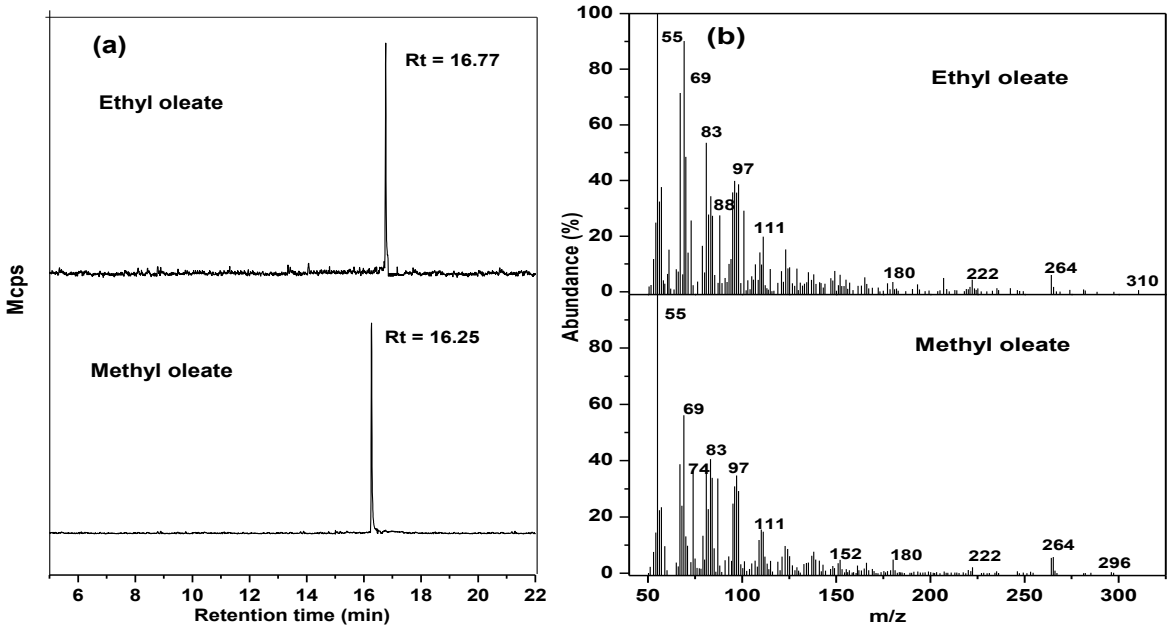

Fig. 3.10. GC-MS of methyl and ethyl oleate (a) GC spectra and (b) MS spectra.

Methyl oleate : **FT-IR** (ATR, cm^{-1})**:** 2924 (CH_3), 2854 (CH_2), 1750 (C=O), 1445 (O–CH_3) , 1170-1210 (C–O) cm^{-1}; **^{1}H–NMR** ($CDCl_3$, δ ppm): 5.34 (m, –C**H**=C**H**–), 3.6 (s, –OC**H**$_3$), 2.3 (m, –C**H**$_2$–CO–), 2.03 (m, =CH–C**H**$_2$–), 1.29 (m, –(C**H**$_2$)$_n$–), 0.88 (m, –CH_2–C**H**$_3$); **^{13}C–NMR** ($CDCl_3$, δ ppm): 174.09 (–**C**O–CH_2–), 129.9 (–**C**H=**C**H–), 51.4 (–O**C**H_3), 34.1 (–CO–**C**H_2–), 31.9 (ω3 –**C**H_2–), 29.66–29.08 (–CH=CH–**C**H_2–, –**C**H_2–), 27.2 (–CH=CH–**C**H_2–CH=CH–), 25.6–24.80 (–CO–CH_2–**C**H_2–), 22.70, 22.47 (ω2 –**C**H_2–) and 14.16 (ω1 –**C**H_3); **GC-MS**: Rt: 16.25 min; positive ion *m/z*: 296$[M]^+$, 264$[M-32]^+$(loss of methoxy ion + H^+), 180$[M-116]^+$(loss of carboxyl group by cleavage between carbon 5 and 6), 74$[M-222]^+$ (loss of Maclefferty ion), 55 (loss of $C_4H_7^+$), 69 (loss of $C_5H_9^+$) 83 (loss of $C_6H_{11}^+$), 97 ((loss of $C_7H_{13}^+$), 111(loss of $C_8H_{15}^+$).

Ethyl oleate : **FT-IR** (ATR, cm^{-1}): 2924 (CH_3), 2854 (CH_2), 1750 (C=O), 1445 (O–C_2H_5) , 1170-1210 (C–O) cm^{-1}; **^{1}H–NMR** ($CDCl_3$, δ ppm): 5.34 (m, –C**H**=C**H**–), 4.1–4.2 (q, –OC**H**$_2$–),2.3 (m, –C*H*$_2$–CO–), 2.03 (m, =CH–C**H**$_2$–), 1.29 (m, –(C**H**$_2$)$_n$– , –CO–CH_2–C**H**$_3$), 0.88 (m, –CH_2–C**H**$_3$); **^{13}C–NMR** ($CDCl_3$, δ ppm): 174.09 (–**C**O–CH_2–), 129.9 (–**C**H=**C**H–),60 (–O**C**H_2–), 34.1 (–CO–**C**H_2–), 31.9 (ω3 –**C**H_2–), 29.66–29.08 (–CH=CH–**C**H_2–, –**C**H_2–), 27.2 (–CH=CH–**C**H_2–CH=CH–), 25.6–24.80 (–CO–CH_2–**C**H_2–), 22.70, 22.47 (ω2 –**C**H_2–) and 14.16 (ω1 –**C**H_3, –OCH_2–**C**H_3); **GC-MS**: Rt: 16.77 min; positive ion *m/z*: 310$[M]^+$, 264$[M-46]^+$ (loss of ethoxy ion + H^+), 180$[M-130]^+$ (loss of carboxyl group by cleavage between carbon 5 and 6), 88$[M-222]^+$ (loss of Maclefferty ion), 55 (loss of $C_4H_7^+$), 69 (loss of $C_5H_9^+$) 83 (loss of $C_6H_{11}^+$), 97 ((loss of $C_7H_{13}^+$), 111(loss of $C_8H_{15}^+$).

The FT–IR, NMR (^{1}H and ^{13}C) and GC–MS spectra of other esters prepared using 2-Ce/ZrO_2–TiO_2/SO_4^{2-}-600 catalyst is provided in Appendix A (A.1-A.12).

3.3.3. Catalytic activity

3.3.3.1. Structure-Activity correlation

The activity of the solid acid catalyst was found to be a function of their acidic strength (Lopez *et al.*, 2005). In order to enhance the acidity of the catalysts, for the optimum activity, cerium concentration and calcination temperature were varied during the catalyst preparation. The activity of the prepared catalyst was compared by performing the esterification of oleic acid with methanol and ethanol.

$Zr(OH)_4$–$Ti(OH)_4$, and 2-Ce/ZrO_2-TiO_2-600 show negligible esterification activity owing to their poor acidic strength (entry 1 and 2; Table 3.2). Similarly $Zr(OH)_4$–$Ti(OH)_4$ having SO_4^{2-} but not cerium ions, was also found less effective towards the esterification reaction (entry 3; Table 2). As could be seen from Table 3.2, simultaneous incorporation of up to 2 wt% cerium and sulfate was found to enhance the total as well as Bronsted acidic sites of the catalyst which resulted > 8 fold increase in activity in comparison to the catalyst having sulfate group without cerium. Our results are in line with the literature report (Li *et al.*, 2010) which claims that lanthanum impregnation, as an assistant component, enhances the activity of sulfated ZrO_2–TiO_2. Thus activity of the prepared catalyst was mainly found to be a function of its acidic strength, which in turn depends upon the cerium and sulfate concentration.

Although, significant difference in catalyst structure was not observed during 400–600 °C calcination temperature, however, ~ 4 fold increases in activity was observed in the same calcination temperature range. This could be due to the presence of relative lesser Bronsted acidic sites in catalyst prepared at low calcination temperature (entry 8 and 9; Table 3.2). At 600 °C calcination temperature relatively higher $Zr(SO_4)_2$ concentration ($Zr(SO_4)_2/Ti_2(SO_4)_3$ = 2.15) was observed, which could also be another reason for the enhanced activity of 2-Ce/ZrO_2–TiO_2/SO_4^{2-}-600. However, a further increase in calcination temperature (700 °C) decomposes the catalyst to form $ZrTiO_4$ phase which has shown poor acidic strength as well as activity (entry 10; Table 3.2).

Table 3.2. Comparison of acidic strength, acidity distribution, TOFs and Bronsted/Lewis ratio of the prepared catalysts.

S.No.	Catalyst	Acidic strength	Bromothymol blue (pK_a=7.2)	Neutral red (pK_a=6.8)	Methyl red (pK_a=4.8)	Methyl orange (pK_a=3.1)	Total acidity (mmol g^{-1})	TOF(h^{-1}) M/E	B/L ratio
1	$Zr(OH)_4$-$Ti(OH)_4$	$3.1<pK_a<4.8$	0.09	0.08	0.04	0.00	0.21	0.006/0.003	-
2	2-Ce/ZrO_2-TiO_2-600	$3.1<pK_a<4.8$	0.32	0.30	0.24	0.00	0.86	0.41/0.33	-
3	SO_4^{2-}/ZrO_2-TiO_2 -600	$0.8< pK_a<3.1$	0.74	0.72	0.68	0.15	2.29	0.70/0.44	1.33
4	0.5-Ce/ZrO_2-TiO_2/SO_4^{2-}-600	$0.8<pK_a<3.1$	2.14	2.13	2.00	0.53	6.80	0.83/0.62	1.39
5	1-Ce/ZrO_2-TiO_2/SO_4^{2-}-600	$0.8<pK_a<3.1$	2.35	2.31	2.12	0.63	7.41	1.06/0.76	N.D
6	2-Ce/ZrO_2-TiO_2/SO_4^{2-}-600	$0.8<pK_a<3.1$	2.79	2.73	2.40	0.89	8.81	4.62/3.30	1.55
7	3-Ce/ZrO_2-TiO_2/SO_4^{2-}-600	$0.8<pK_a<3.1$	2.54	2.53	2.32	0.65	8.04	1.80/1.26	1.48
8	2-Ce/ZrO_2-TiO_2/SO_4^{2-}-400	$3.1<pK_a<4.8$	1.71	1.68	1.20	0.00	4.59	1.34/0.55	1.36
9	2-Ce/ZrO_2-TiO_2/SO_4^{2-}-500	$0.8<pK_a<3.1$	1.85	1.83	1.60	0.32	5.60	1.73/1.06	1.44
10	2-Ce/ZrO_2-TiO_2/SO_4^{2-}-700	$4.8<pK_a<6.8$	0.28	0.26	0.00	0.00	0.54	0.40/0.24	-

M and E are TOFs for the esterification of oleic acid with methanol and ethanol, respectively; B/L is the ratio of Bronsted and Lewis acid sites; - = Bronsted sites remains absent; N.D – Not determined.

3.3.3.2. Effect of reaction conditions on the conversion efficiency

The effect of various reaction parameters such as catalyst concentration, alcohol/acid molar ratio and reaction temperature on catalytic performance was studied to establish the reaction conditions for better catalytic performance.

The optimum catalyst concentration for esterification reaction was determined by performing the reactions in presence of 1–6 wt% catalyst (with respect to OA) as shown in Fig. 3.11(a) and 3.11(b). Increase in catalyst concentration up to 5 wt% was found to increase the overall esterification rate gradually, due to increase in number of active acidic sites. However, a further increase in catalyst concentration was not found to enhance the overall reaction rate to significant extent due to mass transfer resistance in liquid–liquid–solid phases (Song *et al.*, 2011).

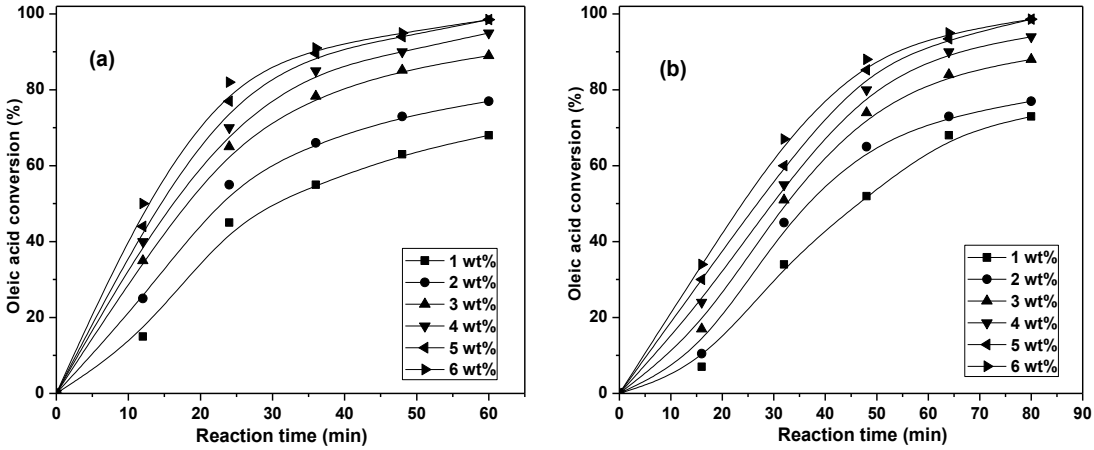

Fig. 3.11. Effect of catalyst concentration on 2-Ce/ZrO_2–TiO_2/SO_4^{2-}-600 catalyzed esterification of OA. **Reaction conditions:** (a) methanol:OA molar ratio of 6:1 at 65 ºC reaction temperature, and (b) ethanol:OA molar ratio of 6:1 at 75 ºC reaction temperature.

Although, 2-Ce/ZrO_2-TiO_2/SO_4^{2-}-600 catalyst was found to be efficient for the esterification of OA with methanol as well as ethanol, however, reaction rate was found to be slower in case of ethanol. This could be due to the lower mobility of the larger ethoxide ions in comparison to the smaller methoxide ions (Brunschwig *et al.*, 2012).

In order to demonstrate that catalytic activity is independent from the diffusion limitations, the Koros-Nowak criterion was employed (Madon and Boudart, 1982). As described in literature (Song *et al.*, 2011), the esterification reactions were carried out on two catalysts having different cerium loading but maintaining the constant fractional exposure of active sites to the substrates. The reaction time to yield the similar conversion levels of oleic acid into respective esters was recorded in presence of both the catalysts. The results exhibited in Fig. 3.12 showed that at same conversion levels, the TOFs of two catalysts were found to be almost similar to indicate that the reaction has followed the Koros-Nowak criterion.

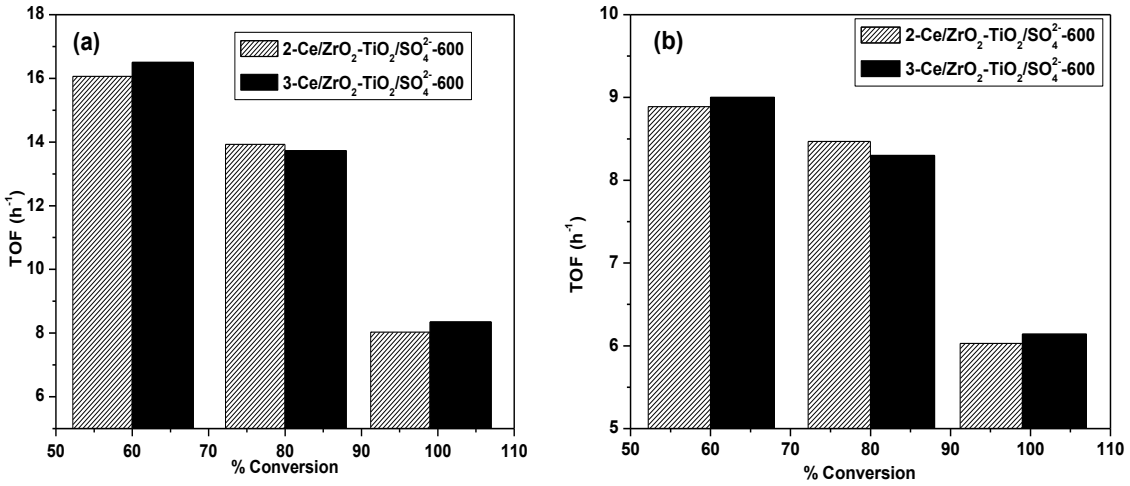

Fig. 3.12. TOFs of 2-Ce/ZrO_2-TiO_2/SO_4^{2-}-600 and 3-Ce/ZrO_2-TiO_2/SO_4^{2-}-600 with different conversions. **Reaction conditions:** (a) methanol:OA molar ratio of 6:1 at 65 ºC reaction temperature, and (b) ethanol:OA molar ratio of 6:1 at 75 ºC reaction temperature with 5 wt% of 2-Ce/ZrO_2-TiO_2/SO_4^{2-}-600 or 6 wt% of 3-Ce/ZrO_2 TiO_2/SO_4^{2-}-600 catalyst.

In order to determine the optimum alcohol to OA molar ratio, reactions were performed in presence of 5 wt% catalyst by varying the alcohol to OA molar ratio from 1:1 to 7:1 as shown in Fig. 3.13(a) and 3.13(b). The reaction rate enhances gradually on increasing alcohol/OA molar ratio from 1 to 6. A further increase in the molar ratio was not found to increase the reaction rate to significant extent as shown in Fig. 3.13. The excess alcohol used during the reaction was recovered by distillation and reused in next cycle.

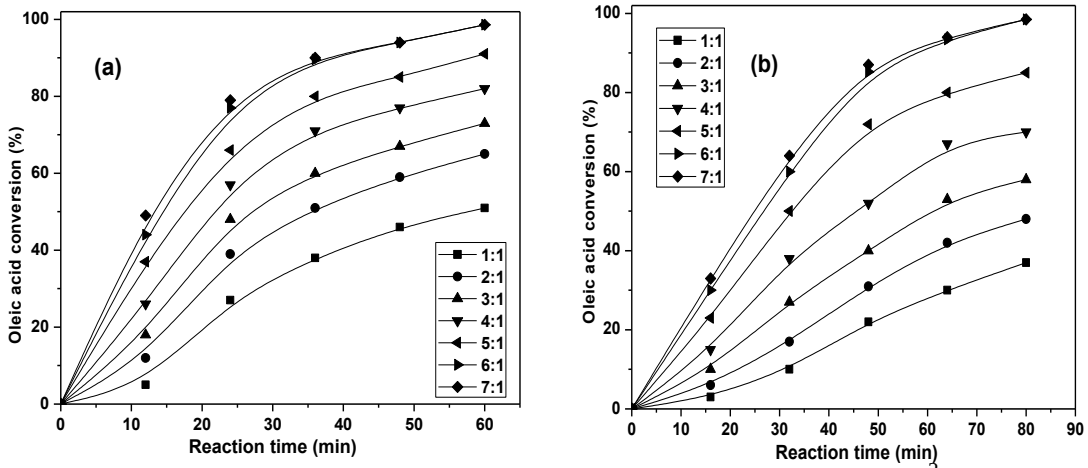

Fig. 3.13. Effect of alcohol:OA molar ratio on 2-Ce/ZrO_2–TiO_2/SO_4^{2-}-600 catalyzed esterification of OA. **Reaction conditions:** Reaction temperature in case of (a) methanol at 65 ºC, and (b) ethanol at 75 ºC, catalyst amount = 5 wt% of catalyst with respect to OA in both cases.

To determine the temperature for the optimum catalyst activity, esterification reactions were performed by varying the temperature in the range of 35-85 ºC. The conversion and reaction rate was found to increase with the increase in reaction temperature However, no significant increase in reaction rate was observed on increasing the temperature above 65 °C and 75 °C in case of methanol and ethanol, respectively (Fig. 3.14(a) and 3.14(b)). It is worth to mention that catalyst was also found to be effective even at room temperature (35 ºC), although longer reaction duration of 5 and 6 h was required, for the esterification of OA, with methanol and ethanol, respectively.

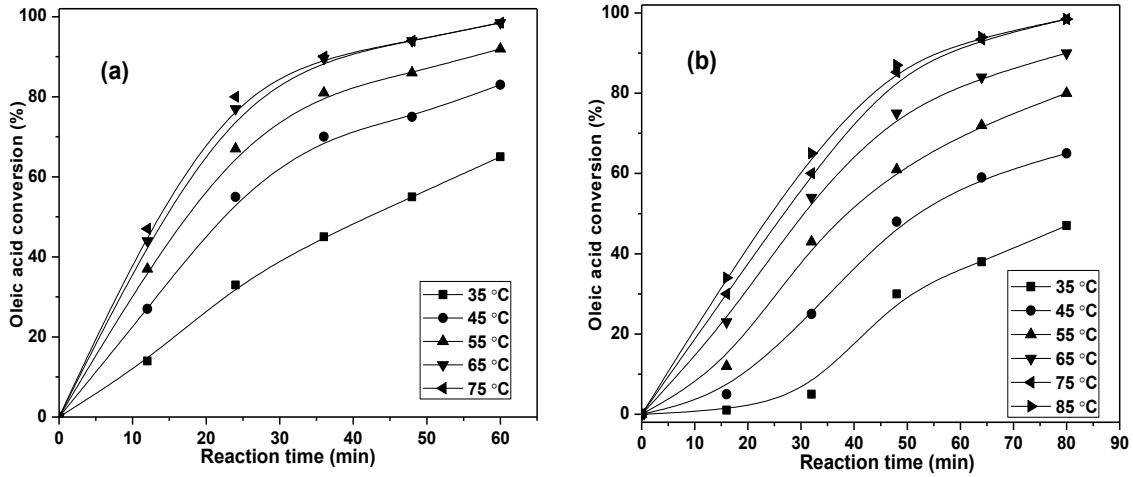

Fig. 3.14. Effect of reaction temperature on 2-Ce/ZrO_2–TiO_2/SO_4^{2-}-600 catalyzed esterification of OA. **Reaction conditions:** (a) methanol: OA molar ratio of 6:1, and (b) ethanol:OA molar ratio of 6:1, both reactions were performed in presence of 5 wt% of catalyst with respect to OA.

In order to evaluate the external mass transfer resistance, OA esterification with methanol was carried out by varying the stirring speed 100-700 rpm. As could be seen from Fig. 3.15, at mixing speed of ≥ 500 rpm, the initial reaction rate become constant to support that above 500 rpm reaction rate is not limited by the external mass diffusion.

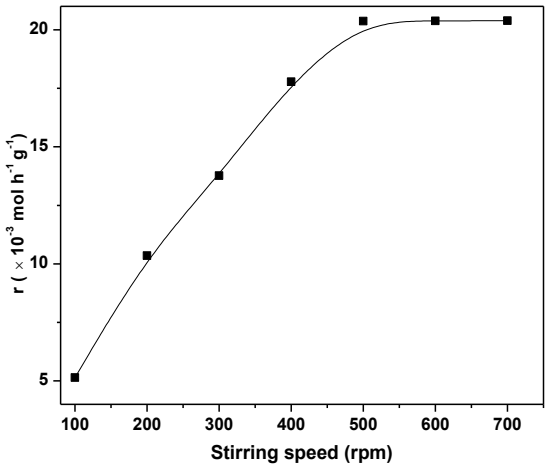

Fig. 3.15. Effect of stirring speed on initial rate of reaction. **Reaction conditions:** Reaction temperature = 65 ºC, methanol to oleic acid ratio = 6:1 and catalyst amount = 5 wt% with respect to OA.

Thus a 6:1 methanol to oil molar ratio at 65 ºC or 6:1 ethanol to oil molar ratio at 75 ºC in presence of 5 wt% catalyst (with respect to fatty acid) and a stirring speed of 500 rpm, were found to be optimum conditions for the 2-Ce/ZrO_2-TiO_2/SO_4^{2-}-600 catalyzed esterification of oleic acid.

3.3.3.3. Effect of moisture content

Being a by-product of the esterification reaction, presence of water is inevitable. The activity of homogeneous acid catalysts was found to be reduced by the presence of moisture (Liu *et al.*, 2006a; Liu *et al.*, 2006b). The reduction in catalytic activity by the moisture may be due to (i) increase in rate of backward reaction *via* hydrolysis of ester, and (ii) deactivation of the catalyst through interaction of water and active sites of catalyst (Marchetti and Errazu, 2008). Thus for better activity, a moisture sensitive catalyst requires pre-dried reagents and efficient removal of the water; formed as a by-product during the esterification reaction. In order to gauge the moisture resistance of 2-Ce/ZrO_2-TiO_2/SO_4^{2-}-600 catalyst, esterification of OA with methanol was performed in presence of externally added moisture contents. As shown in Fig. 3.16, the catalyst was found to be effective even in presence of 12 wt% (with respect to OA) moisture contents however the efficacy of the catalyst (TOF) decreases on increasing

the moisture content in reaction mixture. Nonetheless, even in presence of 12 wt% moisture the catalyst was able to complete (> 98% FAME yield) the esterification of OA in 8.5 h. It is worth mentioning that in reaction mixture 36 mmol of OA is present and presence of water, approximately double to the substrate molar concentration (66 mmol or 12 wt%), was not able to hinder the catalytic activity completely. In literature, addition of merely 2000 ppm water in sulfated zirconia catalyzed esterification of myristic acid was found to decrease the conversion level from 98 to 91% (Saravanan *et al.*, 2012). On increasing the water content from 0 to 10 wt% (with respect to substrate) in Amberlyst-15 catalyzed esterification, FAME yield was found to decrease from 91 to 76% in 6 h of reaction duration (Park *et al.*, 2010b). On the other hand in present study, > 98% FAME yield was obtained in 8.5 h of reaction duration even in presence of 12 wt% moisture content.

Thus prepared catalyst neither required simultaneous removal of water nor anhydrous alcohol or fatty acid to catalyze the reaction.

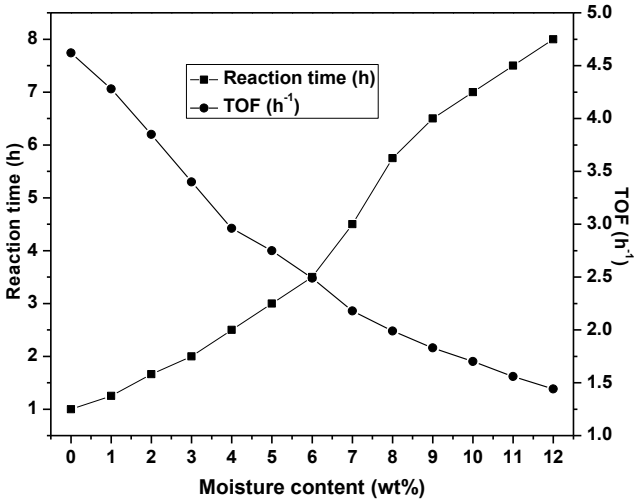

Fig. 3.16. Effect of moisture content upon reaction time for complete esterification (> 98% FAME yield) of oleic acid.

3.3.3.4. Effect of carboxylic acid and alcohol carbon chain length on reaction rate

To demonstrate the versatility of the catalyst, it was employed for the esterification (with methanol) of organic acids having C_2-C_{18} alkyl carbon chain length. The efficiency of 2-Ce/ZrO_2-TiO_2/SO_4^{2-}-600 catalyst was compared by calculating the TOFs of esterification of various carboxylic acid at ~ 25% conversion levels. A decrease in reaction rate was observed on increasing the carbon chain length of organic acids as shown in Fig. 3.17. To correlate the carbon chain length of organic acid with its esterification rate in presence of acidic catalyst, Charton (1976) has used the modified Taft equation 3.1.

$$\log r = \psi v + h \quad (3.1)$$

where, v is the van der Waals radii associated with alkyl groups (Liu *et al.*, 2006c) and ψ and h are constants. Since, v values for acids > C_8 remains constant, hence, rate of esterification reaction or TOFs should be stable for carboxylic acids having more than eight carbon atoms. However, experimentally the rate of reaction as well as TOFs decreases gradually on increasing the carbon chain length as shown in Fig. 3.17.

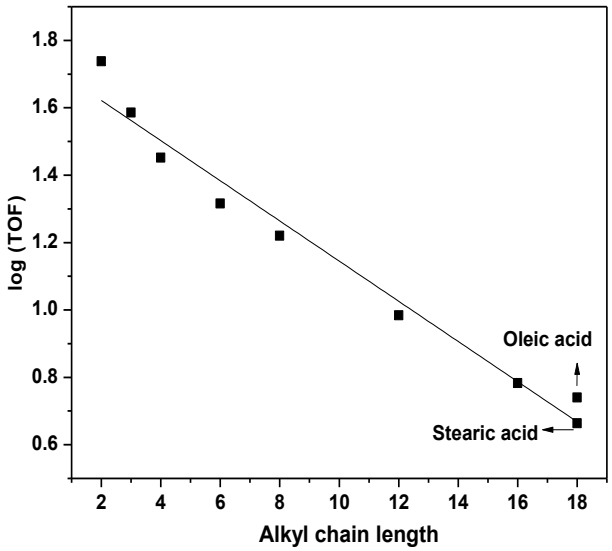

Fig. 3.17. Plot of $\log_{10}$(TOF) as a function of carboxylic acid alkyl chain length (C_2-C_{18}) for 2-Ce/ZrO_2-TiO_2/SO_4^{2-}-600 catalyzed esterification reaction (C_2 - Acetic acid, C_3 - Propionic acid, C_4 - Butyric acid, C_6 - Caproic acid, C_8 - Caprylic acid, C_{12} - Lauric acid, C_{16} - Palmitic acid, C_{18} - Stearic and Oleic acid).

Thus, the rate of organic acid esterification was found to follow the linear relationship (equation 3.2), with alkyl chain lengths (l) in absence of diffusion limitations.

$$\log_{10}(\text{TOF}) = -0.059l + 1.74 \quad (3.2)$$

Eze *et al*. (2013) and Pirez *et al.* (2012) also reported similar trends for the $PrSO_3H$-SBA-15 and $PrSO_3H$-KIT-6 catalyzed esterification of carboxylic acids of varying alkyl chain lengths. Since electronic properties for chain length > C_4 do not change significantly, hence decrease in esterification rates could be attributed to the steric or mixing effect (Eze *et al*., 2013). Steric hindrance increases with carbon chain length of the carboxylic acid, however, in case of homogeneous catalysts to counter the steric constrain, molecule may orient itself in so called "preferential conformation" (Pirez *et al.*, 2012). In case of heterogeneous catalyst adsorbed carboxylic acid could not adopt preferential conformation and hence, steric factor increases gradually with alkyl chain length, and influences the esterification rate negatively (Lilja *et al.*, 2002).

The effect of alcohol carbon chain length on esterification activity is not frequently reported in literature. To study the effect of alcohol carbon chain length, esterification of OA was performed with C_1-C_{10} alcohols. Here again increasing alkyl chain length of alcohol was found to reduce the reaction rate as shown in Fig. 3.18.

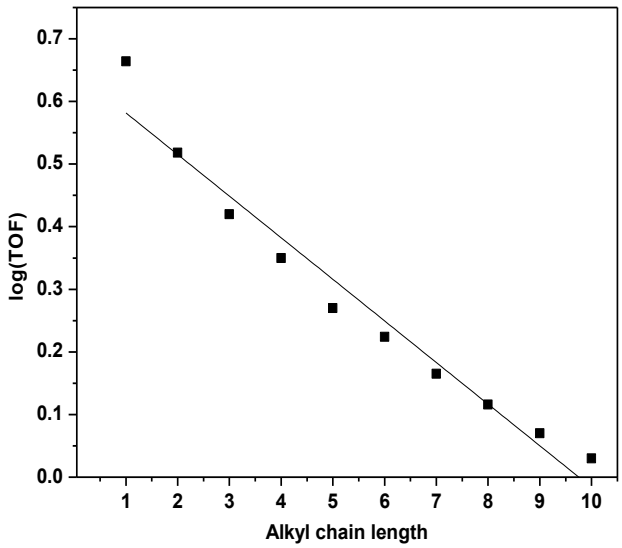

Fig. 3.18. Plot of $\log_{10}$(TOF) as a function of alcohol alkyl chain length (C_1-C_{10}) for 2-Ce/ZrO_2-TiO_2/SO_4^{2-}-600 catalyzed esterification reaction of oleic acid (C_1 - Methanol, C_2 - Ethanol, C_3 - Propanol, C_4 - Butanol, C_5 - Pentanol, C_6 - Hexanol, C_7 - Heptanol, C_8 - Octanol, C_9 - Nonanol, C_{10} - Decanol).

Thus, the rate of alcohol esterification was found to follow, as observed in case of carboxylic acids, the linear relationship (equation 3.3) with alkyl chain lengths (*l*).

$$\log_{10}(\text{TOF}) = -0.066l + 0.65 \qquad (3.3)$$

Thus, reduced reaction rate could be attributed to increase in steric hindrance on increasing the carboxylic acid or alcohol alkyl chain length (Ghiaci *et al.*, 2011).

Nevertheless, 2-Ce/ZrO_2-TiO_2/SO_4^{2-}-600 catalyst was found to complete the esterification (> 98 % conversion) of all organic acids and alcohols employed for the study.

3.3.4. Reusability and stability of the catalyst

In order to prove the reusability of 2-Ce/ZrO_2–TiO_2/SO_4^{2-}-600, esterification of the OA was performed with methanol under optimized reaction conditions. After the completion of reaction, catalyst was separated from the reaction mixture by filtration, washed with hexane, dried at 120 °C and finally calcined at 600 °C. The regenerated catalyst was employed in six successive runs under same experimental conditions and regeneration methods. As shown in Fig. 3.19, no significant loss in the catalyst activity was observed until fifth cycle. However, only 70% conversion was achieved during sixth run.

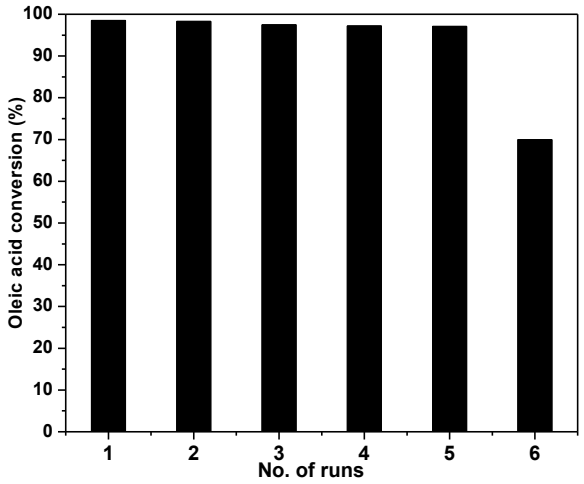

Fig. 3.19. Reusability study of 2-Ce/ZrO_2–TiO_2/SO_4^{2-}-600 catalyst.

To analyze the cause(s) behind the drop in activity after five cycles, XRD patterns of fresh and reused catalysts were compared. As shown in Fig. 3.20(a), an additional peak at 25° was observed in the diffraction pattern of the reused catalyst due to the formation of *anatase* phase of titanium oxide (TiO_2; JCPDS card no. 84-1286). Thus upon continuous reuse a small portion of TiO_2 has separated from the catalyst to alter its regular structure.

Comparison of the FTIR spectra (Fig. 3.19(b)) of fresh and reused catalysts supported that SO_4^{2-} moiety has not dissociated from the catalyst and remains intact even after five catalytic runs. Additionally, no vibration bands corresponding to the FFA or FAME were observed in the FTIR spectrum of reused catalyst to support that organic molecules have not accumulated over the catalyst surface to block the active sites. This is expected as catalyst was calcined at 600 °C before every consecutive run.

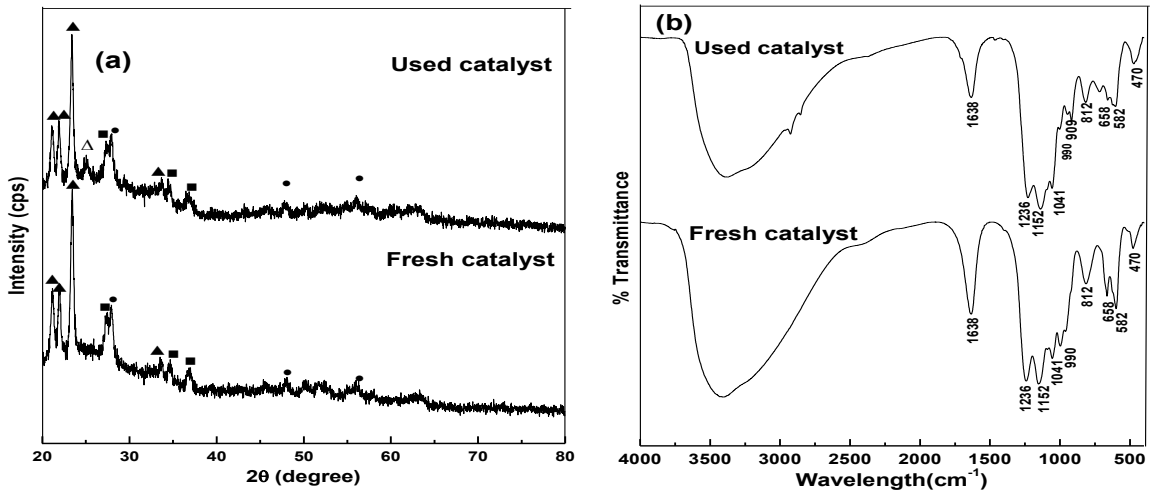

Fig. 3.20. Comparison of (a) XRD and (b) FT-IR of fresh and used catalyst. (▲- $Zr(SO_4)_2$, ■ - $Ti_2(SO_4)_3$, •- CeO_2, Δ - anatase TiO_2).

The possibility of the sulfate ion dissolution in reaction mixture was also tested by adding the $BaCl_2$ solution to the methanol contacted with catalyst for 2 h under stirring. A negative test ruled out the leaching of sulfate ions in reaction mixture. Moreover, total sulfur concentration in fresh (16.69 wt%) and spent (16.49 wt%) catalysts was also found to be almost similar to further exclude the leaching of sulfate species from catalyst.

In order to demonstrate that there is no homogeneous contribution in catalytic activity, hot filtration test was performed. The esterification reaction was performed under optimized reaction conditions but catalyst was removed after 20 min by filtration. The reactants were again heated and further conversion was monitored for another 3 h. As could be seen from Fig. 3.21, no significant gain in ester yield was obtained to rule out homogeneous contribution in catalytic activity.

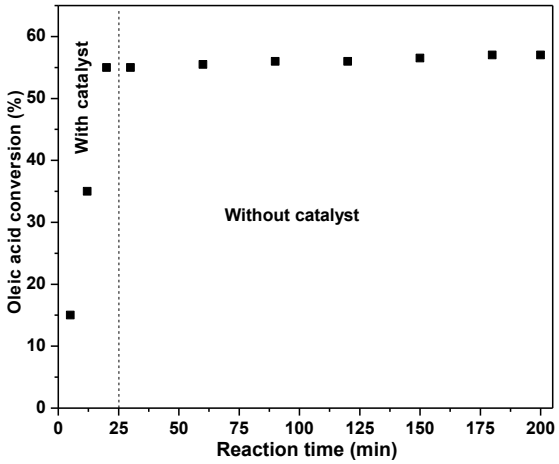

Fig. 3.21. Hot filtration test for esterification of oleic acid with methanol over 2-$Ce/ZrO_2–TiO_2/SO_4^{2-}$-600 (**Reaction conditions**:- Methanol:oleic acid molar ratio = 6:1, catalyst amount = 5 wt% with respect to oleic acid, and reaction temperature = 65 °C).

Sulfur content was not detected during the elemental analysis of MO and very less leaching of Ce (0.23 ppm), Zn (0.16 ppm) and Ti (4.71 ppm) supported the highly stable nature of the catalyst.

All these studies confirm the true heterogeneous mode of action of the catalyst and absence of any significant homogeneous contribution in the activity of 2-$Ce/ZrO_2–TiO_2/SO_4^{2-}$-600 catalyst. Thus, loss in catalytic activity may be attributed to the partial change in catalyst structure upon its repeated reuse.

3.3.5. Esterification of free fatty acids in the presence of triglycerides

As discussed in previous sections, 2-Ce/ZrO_2-TiO_2/SO_4^{2-}-600 catalyst was found effective for the esterification of a variety of carboxylic acids. In order to demonstrate the application of

the catalyst for the real system, it was employed for the esterification of high FFA containing VOs. Reduction of FFA in VOs is significant from commercial point of view as high FFA containing oils could not be employed directly for the transesterification reaction in presence of homogeneous catalyst. In conventional method, strong mineral acids (e.g., H_2SO_4, HCl etc.) are employed as homogeneous catalyst to reduce the FFA contents of VOs *via* esterification reaction. On the other hand, esterification activity of heterogeneous catalyst was found to decrease in presence of triglycerides. Therefore, in literature only few reports (Srilatha *et al.*, 2011; Kulkarni *et al.*, 2006; Park *et al.*, 2010a; Srilatha *et al.*, 2009) are available where heterogeneous catalyst was employed for esterification of fatty acids, present in VOs. Srilatha *et al.* (2009) reported that Nb_2O_5 showed better activity towards the esterification of pure fatty acid, but a decrease in activity was observed when a mixture of fatty acids were employed as a feedstock. Moreover, none of the report has demonstrated further transesterification of ester rich oil.

In this work, the catalyst was employed for the esterification of VOs having up to 15.2 wt% FFA. The proton and carbon-13 NMR spectra as shown in Fig. 3.22 and 3.23 supports the esterification of fatty acids present in VOs.

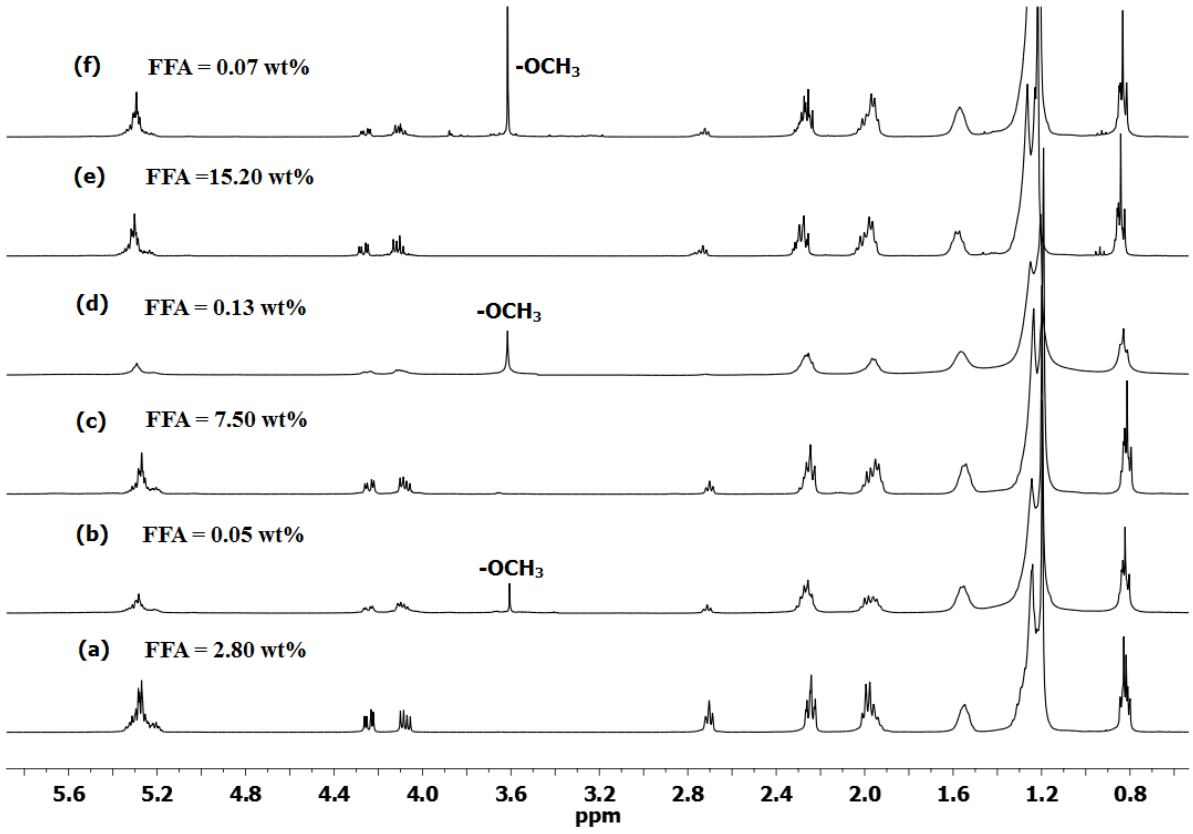

Fig. 3.22. ^{1}H-NMR of (a) waste cotton seed oil, (b) esterified waste cotton seed oil, (c) jatropha oil, (d) esterified jatropha oil, (e) karanja oil and (f) esterified karanja oil.

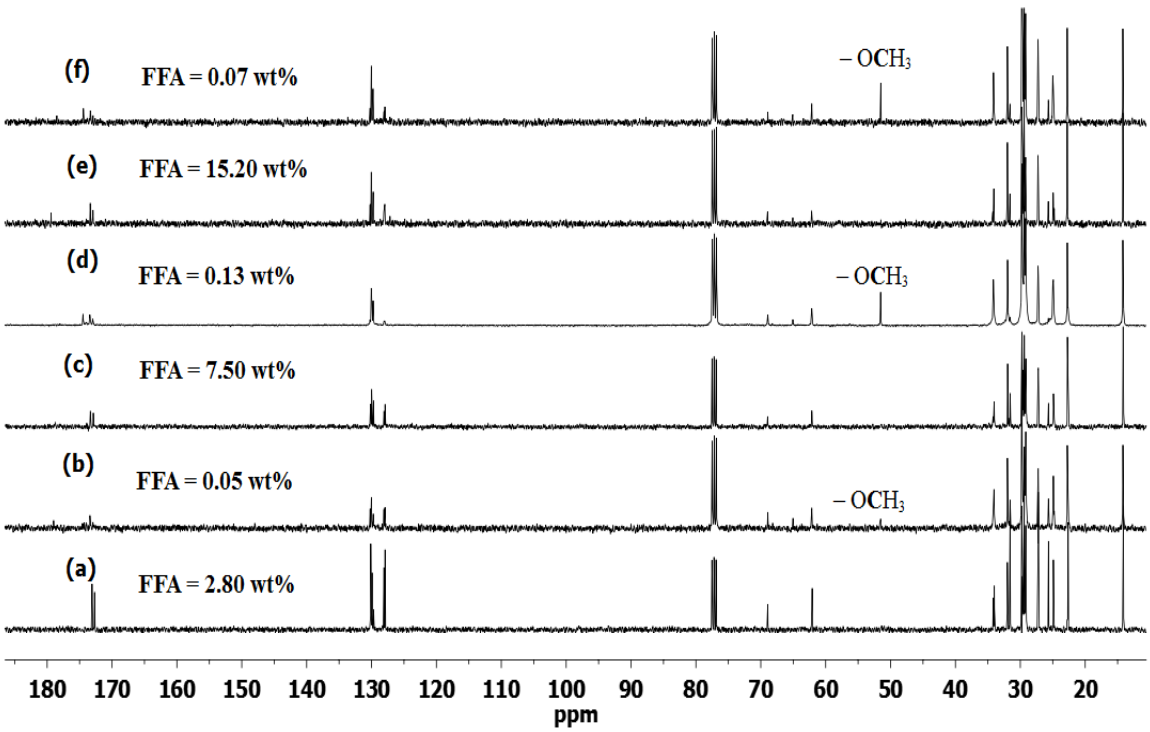

Fig. 3.23. ^{13}C-NMR of (a) waste cotton seed oil, (b) esterified waste cotton seed oil, (c) jatropha oil, (d) esterified jatropha oil, (e) karanja oil and (f) esterified karanja oil.

Fatty acid value calculation supported > 98% esterification of FFA present in VOs as shown in Table 3.3. Thus no significant drop in catalyst activity was observed even in presence of triglycerides.

Table 3.3. Esterification of free fatty acids present in vegetable oils.

Vegetable oils	FFA (wt%) in VOs		Fatty acid conversion (%)	Reaction time (h)
	Original	After esterification		
WO	2.80	0.05	98.21	1.0
JO	7.50	0.13	98.26	2.5
KO	15.20	0.07	99.53	3.0

Reaction conditions: Methanol:oil molar ratio – 6:1, Catalyst amount – 5 wt% (with respect to oil), Reaction temperature – 65 °C.

After the esterification reaction, catalyst was recovered by centrifugation and ester rich oil was directly employed for the transesterification reaction in presence of homogeneous catalyst (NaOH). As evident from Table 3.4, the transesterification of ester rich oils by homogeneous catalyst was able to give > 98% FAMEs yield.

Table 3.4. Transesterification of esterified oil using homogeneous (NaOH) catalyst.

Esterified oil	Reaction temperature (°C)	Methanol:oil molar ratio	NaOH (wt%, with respect to VO)	Reaction time (h)	FAME yield (%)
WO	65	3:1	1	0.35	98.30
JO	65	3:1	1	0.75	98.60
KO	65	3:1	1	1.00	99.10

The advantage of the developed 2-Ce/ZrO_2–TiO_2/SO_4^{2-}-600 catalyst, over homogeneous acid one, in esterification of high FFA containing VOs is evident from Scheme 3.1. The oil esterified by the heterogeneous catalyst was successfully employed for the transesterification reaction without requiring any acid neutralization and washing step. On the other hand prior to their transesterification, VOs esterified by sulfuric acid required acid neutralization followed by water washing to remove salt contamination. The removal of salt from esterified oil not only requires huge quantity of water but also generates significant amount of industrial effluents. More importantly, recovered heterogeneous catalyst was reused in 5 successive catalytic cycles and same is not possible with its homogeneous counterparts.

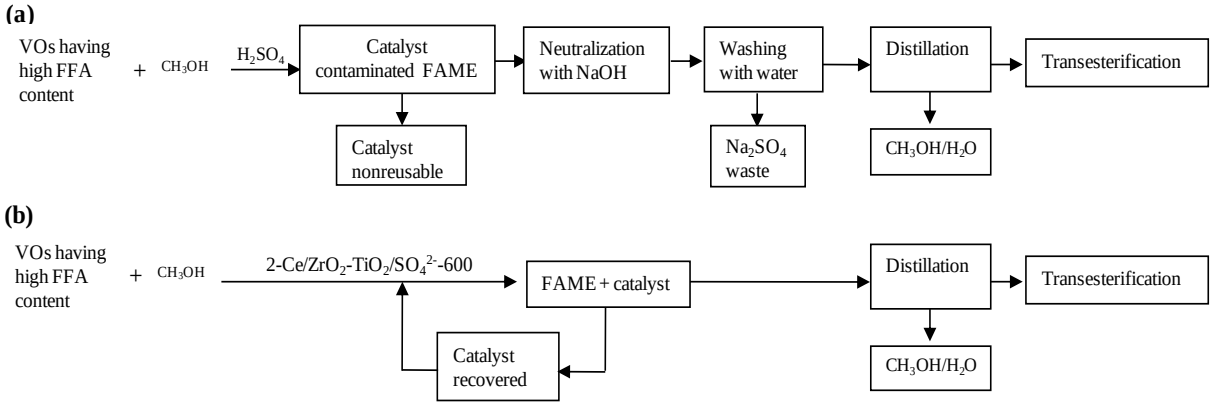

Scheme 3.1. Comparison of the reaction schemes for the production of biodiesel from high FFA containing vegetable oil. Esterification is catalyzed by (a) homogeneous acid (H_2SO_4), and (b) 2-Ce/ZrO_2–TiO_2/SO_4^{2-}-600, followed by the transesterification.

Hence, use of 2-Ce/ZrO_2–TiO_2/SO_4^{2-}-600 as heterogeneous catalyst for the esterification is clearly advantageous as it is (i) able to complete the esterification of FFA in presence and absence of triglycerides, (ii) effective for a variety of carboxylic acids, and alcohol, (iii) reusable, and stable as no significant leaching was observed, (iv) required in lesser amount (5 wt%), and (v) required relatively milder conditions of temperature, pressure, and moderate alcohol to carboxylic acid molar ratio.

3.3.6. Kinetic studies

Stoichiometrically, one mole of mono carboxylic acid required one mole of alcohol for the esterification and hence, the reaction should follow second order kinetics. In present work, optimum catalytic activity was achieved in presence of 6:1 alcohol to oleic acid molar ratio. Hence, the rate of reaction is independent from alcohol concentration and 2-Ce/ZrO_2–TiO_2/SO_4^{2-}-600 catalyzed esterification could safely be assumed to follow pseudo first order kinetics as given in equation 2.3 (Chapter 2).

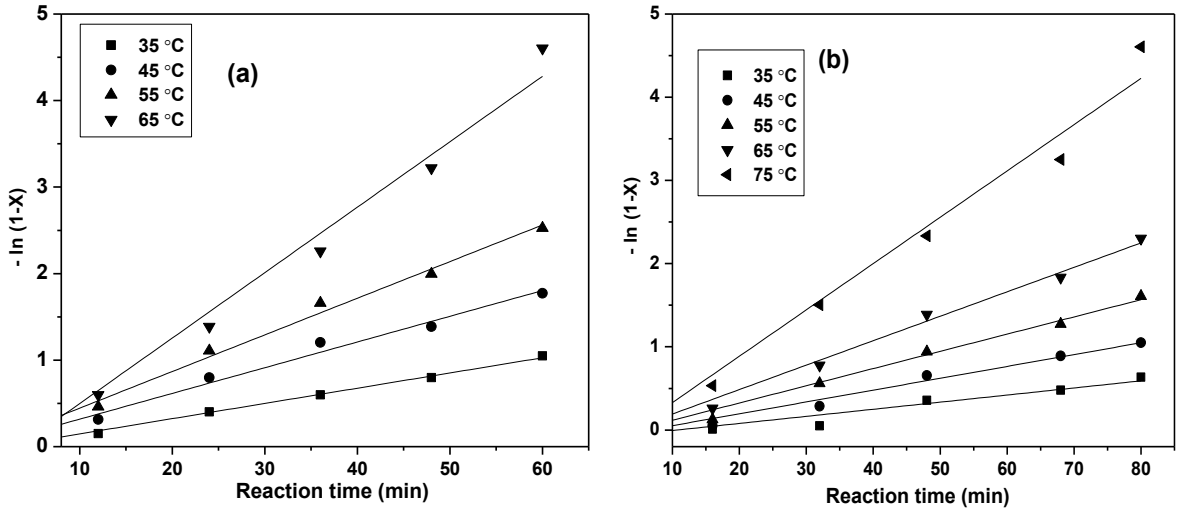

Fig. 3.24. Plots of –ln (1-X) versus reaction time at different temperatures using (a) methanol and (b) ethanol.

The linear nature of –ln (1-X) versus time plot (Fig. 3.24), in the temperature range of 35–75 °C further verified that the reaction has followed the pseudo first order kinetics. For the esterification of OA with methanol and ethanol, the maximum value of apparent first order rate constant was observed at 65 °C (7.56×10^{-2} min^{-1}) and 75 °C (5.56×10^{-2} min^{-1}) respectively.

From the Arrhenius plot (Fig. 3.25), the value of E_a for OA esterification with methanol and ethanol was observed 32.7 and 37.1 kJ mol^{-1}, respectively. These values are > 25 kJ mol^{-1} to support that reactions are chemically controlled and not by diffusion or mass transfer limitations (Patel and Brahmkhatri, 2013).

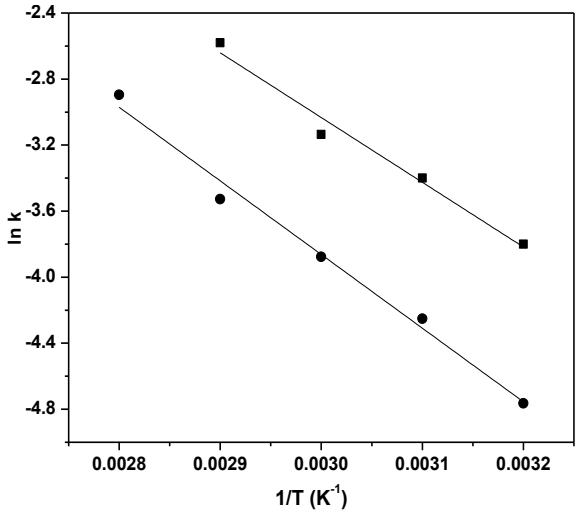

Fig. 3.25. Arrhenius plot of *ln k* versus 1/T for oleic acid esterification with methanol (■) and ethanol (•) over the 2-Ce/ZrO_2–TiO_2/SO_4^{2-}-600 catalyst.

3.4. Conclusions

The prepared catalyst, 2-Ce/ZrO_2–TiO_2/SO_4^{2-}-600, has demonstrated efficacy towards the esterification of various organic carboxylic acids and alcohols. The esterification activity of catalyst was found to be influenced by cerium loading in catalyst and calcination temperature along with the reaction parameters such as alcohol to oleic acid molar ratio, catalyst loading, reaction temperature and stirring speed. The catalyst with higher number of Bronsted acid sites shows better activity and could be re-used five times without significant loss in activity. The catalytic activity was not found to be effected by the presence of triglycerides and hence it was successfully employed for the reduction of FFA present in vegetable oils. The ester rich oil has been directly employed for the transesterification reaction without requiring any pre-washing step. Thus application of the prepared catalyst could be advantageous for the esterification of high FFA containing non edible or waste cooking oils as it may prevent the generation of huge industrial effluents, which is inevitable in case of homogeneous acid catalyzed esterification process.

References

Brunschwig, C. W.; Moussavou, W.; Blin, J.; Use of bioethanol for biodiesel production. *Prog. Energ. Combust.*, **2012**, 38, 283-301.

Charton, M.; Steric effects. Additional *v* constants. *J. Org. Chem.*, **1976**, 41, 2217-2220.

Das, D.; Mishra, H. K.; Parida, K. M.; Dalai, A. K.; Preparation, physico-chemical characterization and catalytic activity of sulphated ZrO_2–TiO_2 mixed oxides. *J. Mol. Catal. A: Chem.*, **2002**, 189, 271-282.

Eze, V. C; Phan, A. N.; Pirez, C.; Harvey, A. P.; Lee, A. F.; Wilson, K.; Heterogeneous catalysis in an oscillatory baffled flow reactor. *Catal. Sci. Technol.*, **2013**, 3, 2373-2379.

Ghiaci, M.; Aghabarari, B.; Gil, A.; Production of biodiesel by esterification of natural fatty acids over modified organoclay catalysts. *Fuel*, **2011**, 90, 3382-3389.

Kaur, N.; Ali, A.; Kinetics and reusability of Zr/CaO as heterogeneous catalyst for the ethanolysis and methanolysis of Jatropha crucas oil. *Fuel Process Technol*., **2014**, 119, 173-184.

Kulkarni, M. G.; Gopinath, R.; Meher, L. C.; Dalai, A. K.; Solid acid catalyzed biodiesel production by simultaneous esterification and transesterification. *Green Chem.*, **2006**, 8, 1056-1062.

Li, Y.; Zhang, X. D.; Sun, L.; Zhang, J.; Xu, H. P.; Fatty acid methyl ester synthesis catalyzed by solid superacid catalyst SO_4^{2-}/ZrO_2–TiO_2/La^{3+}. *Appl. Energ.*, **2010**, 87, 156-159.

Li, Z.; Wnetrzak, R.; Kwapinski, W.; Leahy, J. J.; Synthesis and characterization of sulfated TiO_2 Nanorods and ZrO_2/TiO_2 nanocomposites for the esterification of biobased organic Acid. *ACS Appl. Mater. Interfaces*, **2012**, 4, 4499-4505.

Lilja, J.; Murzin, D. Y.; Salmi, T.; Aumoa, J.; Arvela, P. M.; Sundell, M.; Esterification of different acids over heterogeneous and homogeneous catalysts and correlation with the Taft equation. *J. Mol. Catal. A: Chem.*, **2002**, 182-183, 555-563.

Liu, Y.; Lotero, E.; Goodwin, J. G.; A comparison of the esterification of acetic acid with methanol using heterogeneous versus homogeneous acid catalysis. *J. Catal.*, **2006a**, 242, 278-286.

Liu, Y.; Lotero, E.; Goodwin, J. G; Effect of water on sulfuric acid catalyzed esterification. *J. Mol. Catal. A: Chem.*, **2006b,** 245, 132-140.

Liu. Y.; Lotero, E.; Goodwin, J. G.; Effect of carbon chain length on esterification of carboxylic acids with methanol using acid catalysis. *J. Catal.*, **2006c**, 243, 221-228.

Lopez, D. E.; Goodwin, J. G.; Bruce, D. A.; Lotero, E.; Transesterification of triacetin with methanol on solid acid and base catalysts. *Appl. Catal. A: Gen.*, **2005**, 295, 97-105.

Madon, R. J.; Boudart, M.; Experimental criterion for the absence of artifacts in the measurement of rates of heterogeneous catalytic reactions. *Ind. Eng. Chem. Fundam.*, **1982**, 21, 438-447.

Marchetti, J. M; Errazu, A. F.; Comparison of different heterogeneous catalysts and different alcohols for the esterification reaction of oleic acid. *Fuel,* **2008**, 87, 3477-3480.

Park, J. Y.; Kim, D. K.; Lee, J. S.; Esterification of free fatty acids using water-tolerable Amberlyst as a heterogeneous catalyst. *Bioresour. Technol.*, **2010a**, 101, S62-S65.

Park, J. Y.; Wang, Z. M.; Kim, D. K.; Lee, J. S.; Effects of water on the esterification of free fatty acids by acid catalysts. *Renew. Energ*., **2010b**, 35, 614-618.

Patel, A.; Brahmkhatri, V.; Kinetic study of oleic acid esterification over 12-tungstophosphoric acid catalyst anchored to different mesoporous silica supports. *Fuel Process. Technol.*, **2013**, 113, 141-149.

Pirez, C.; Caderon, J. M.; Dacquin, J. P; Lee, A. F; Wilson, K.; Tunable KIT-6 mesoporous sulfonic acid catalysts for fatty acid esterification. *ACS Catal.*, **2012**, 2, 1607-1614.

Reddy, B. M.; Reddy, G. K.; Ganesh, I.; Ferreira, J. M. F.; Single step synthesis of nanosized CeO_2-M_xO_y mixed oxides (M_xO_y = SiO_2, TiO_2, ZrO_2, and Al_2O_3) by microwave induced solution combustion synthesis: characterization and CO oxidation. *J. Mater. Sci.*, **2009a**, 44, 2743-2751.

Reddy, B. M.; Reddy, G. K.; Rao, K. N.; Katta, L.; Influence of alumina and titania on the structure and catalytic properties of sulfated zirconia: Beckmann rearrangement. *J. Mol. Catal. A: Chem.*, **2009b**, 306, 62-68.

Saravanan, K.; Tyagi, B.; Bajaj, H. C.; Sulfated zirconia: an efficient solid acid catalyst for esterification of myristic acid with short chain alcohols. *Catal. Sci. Technol.*, **2012**, 2, 2512-2520.

Sarkar, A.; Ghosh, S. K.; Pramanik, P.; Investigation of the catalytic efficiency of a new mesoporous catalyst SnO_2/WO_3 towards oleic acid esterification. *J. Mol. Catal. A: Chem.*, **2010**, 327, 73-79.

Song, R.; Tong, D.; Tang, J.; Hu, C.; Effect of composition on the structure and catalytic properties of KF/Mg-La solid base catalysts for biodiesel synthesis via transesterification of cottonseed oil. *Energy Fuels*, **2011,** 25, 2679-2686.

Srilatha, K.; Kumar, R.; Devi, B. L. A. P.; Prasad, R. B. N.; Prasad, P. S. S.; Lingaiah, N.; Efficient solid acid catalysts for esterification of free fatty acids with methanol for the production of biodiesel. *Catal. Sci. Technol.*, **2011**, 1, 662-668.

Srilatha, K.; Lingaiah, N.; Prasad, P. S. S.; Devi, B. L. A. P.; Prasad, R. B. N.; Venkateswar, S.; Influence of carbon chain length and unsaturation on the esterification activity of fatty acids on Nb_2O_5 catalyst. *Ind. Eng. Chem. Res.*, **2009**, 48, 10816-10819.

Sudarsanam, P.; Mallesham, B.; Reddy, P. S.; Reddy, B. M.; Highly promising sulfate ion promoted M–ZrO_2 (M=Al_2O_3 and CeO_2) heterogeneous solid acids for biodiesel-derived glycerol esterification. *J. Chem. Sci. Technol.*, **2013**, 2, 161-168.

Thiruvengadaravi, K. V.; Nandagopal, J.; Baskaralingam, P.; Bala, V. S. S.; Sivanesan, S.; Acid-catalyzed esterification of karanja (Pongamia pinnata) oil with high free fatty acids for biodiesel production. *Fuel*, **2012**, 98, 1-4.

Yang, Q.; Xie, C.; Xu, Z.; Gao, Z.; Du, Y.; Synthesis of highly active sulfate-promoted rutile titania nanoparticles with a response to visible light. *J. Phys. Chem. B*, **2005**, 109, 5554-5560.

Zhang, J.; Jiang, L.; Acid-catalyzed esterification of Zanthoxylum bungeanum seed oil with high free fatty acids for biodiesel production. *Bioresour. Technol.*, **2008**, 99, 8995-8998.

Kinetics and Reusability of Zr/CaO as Heterogeneous Catalyst for the Ethanolysis and Methanolysis of *Jatropha Crucas* Oil

Contents — *Page No.*

Abstract: Zirconium impregnated (5–20 wt%) calcium oxide (Zr/CaO) was prepared by a simple wet chemical method followed by calcination up to 900 °C. The prepared Zr/CaO was employed as a heterogeneous catalyst for the transesterification of Jatropha crucas oil with ethanol and methanol for the production of fatty acid ethyl and methyl esters, respectively. The catalysts were characterized by powder X-ray diffraction, Fourier transform infrared spectroscopy, Brunauer–Emmett–Teller surface area measurement, scanning electron microscopy, transmission electron microscopy techniques and basic strength of the catalyst were established by acid–base titration. The catalytic activity was found to be a function of basic sites which in turn depend on calcinations temperature and zirconium concentration. The catalyst with 15 wt% zirconium concentration and calcined at 700 °C, showed the highest catalytic activity among the prepared catalysts. A pseudo first order kinetic equation was applied to evaluate the kinetic parameters of Zr/CaO catalyzed transesterification. The activation energy (E_a) for the Zr/CaO catalyzed methanolysis and ethanolysis was found to be 29.8 kJ mol^{-1} and 42.5 kJ mol^{-1}, respectively. The Koros–Nowak test was performed to demonstrate that catalytic activity was independent from the mass transport phenomenon and follows the kinetic regime.

4.1. Introduction

In previous chapter, high free fatty acid containing VOs were initially esterified in presence of Ce/ZrO_2-TiO_2/SO_4^{2-} catalyst and later esterified VOs were transesterified in presence of homogeneous catalyst (NaOH) to produce biodiesel. To remove the catalyst, biodiesel thus produced must be washed with water and hence, huge amount of industrial effluents are generated during the process.

Another issue related with the conventional biodiesel production technology is the use of methanol which is not only highly toxic but also a refinery residue and hence, FAME produced will not be completely carbon neutral. In this regard, application of ethanol could be advantageous as it is renewable and also considered as non toxic and green chemical. However, due to the lesser reactivity in comparison to methanol, ethanol has not been frequently employed for the transesterification reaction in presence of heterogeneous catalysts (Brunschwig *et al.*, 2012). To produce biodiesel in a single step utilizing ethanol, in present chapter, Zr/CaO catalyst was prepared by wet impregnation method and employed as heterogeneous catalyst for the transesterification of jatropha oil.

4.2. Experimental section

4.2.1. Catalyst preparation

A series of zirconium impregnated CaO was prepared by the wet impregnation method. In a typical preparation, 10 g of CaO was suspended in 40 mL of deionized water, and to this 10 mL aqueous solution of $ZrOCl_2.8H_2O$ of desired concentration was added. The resulted slurry was stirred for 4 h, then evaporated to dryness, and heated at 120 °C for 24 h. A series of Zr/CaO was prepared by varying zirconium concentration in the range of 5-20 wt% and calcination temperature 300-900 ºC. Prepared catalysts were labelled as *x*-Zr/CaO-T, where *x* and T represent the zirconium concentration (wt%) and calcination temperature (ºC), respectively.

4.2.2. Determination of total catalyst basic sites

Total basic sites of the catalysts were evaluated by measuring the acidity of conjugate acid, by acid-base titration method (Singh and Fernando, 2008). In a typical experiment, 25 mg catalyst was dissolved in 25 mL of 0.1 M HCl and resulting mixture was stirred for an hour. The catalyst would neutralize HCl equivalent to its basicity. The resulted solution was titrated against standard NaOH solution to determine the exact concentration of excess HCl. Finally,

the amount of HCl neutralized by the catalyst was determined and represented as basicity of the catalyst as mmol of HCl/g of catalyst.

4.2.3. Transesterification reaction

Transesterification reactions of JO were carried out in a 50 mL two-neck round bottom flask, equipped with a water bath, magnetic stirrer and a water-cooled reflux condenser. In a typical reaction 10 g of JO was stirred with desired molar concentration of methanol or ethanol and catalyst, and heated at desired temperature for specific duration. To monitor the progress of reaction, sample (0.25 mL) from the reaction mixture were withdrawn after every 15 min with the help of glass dropper, centrifuged and subjected to proton NMR analysis to quantify the FAAE produced. After the completion of reaction, the solid catalyst was recovered through filtration and liquid phase was kept in a separating funnel for 24 h to separate the lower glycerol layer from the upper FAAE layer.

4.3. Results and Discussion

4.3.1. Characterization of fatty acid alkyl esters

The ^{1}H-NMR spectrum of JO shows the characteristic glyceridic proton peaks at 4.15-4.35 ppm and 5.23 ppm, as shown in Fig 4.1(a). On transesterification, same peaks were no longer found in the proton NMR spectrum of FAME or FAEE (Fig 4.1(a)). The formation of FAME and FAEE were further supported due to the appearance of new peaks at 3.6 ppm (singlet) and 4.1-4.2 ppm (quartet), respectively. In ^{13}C-NMR spectrum of JO, signals due to glyceridic carbon appear at 62.2 and 69.0 ppm, as shown in Fig. 4.1(b). The formation of FAME and FAEE further supported by the appearance of peaks at 51.4 and 60.0 ppm, due to $–OCH_3$ and $–OCH_2–$ carbons, respectively. Moreover, peaks corresponding to the glyceridic carbons were no longer found in the ^{13}C-NMR spectrum of FAME and FAEE (Fig. 4.1(b)).

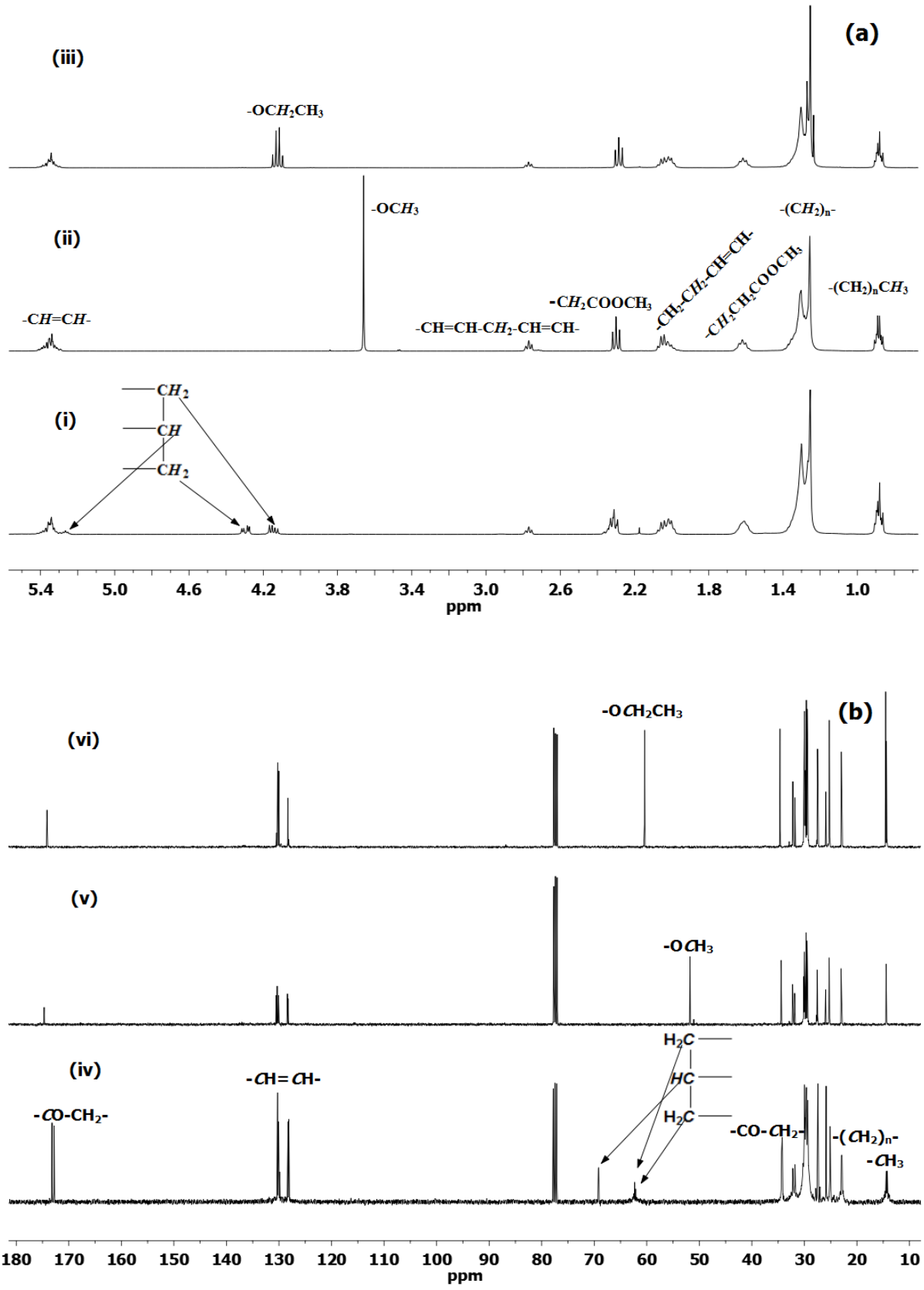

Fig. 4.1. Comparison of (a) ^{1}H-NMR and (b) ^{13}C-NMR spectra of jatropha oil (i and iv) with its methyl (ii and v) and ethyl esters (iii and vi).

Methyl esters of JO: **^{1}H-NMR** ($CDCl_3$, δ ppm): 5.34 (m, –C*H*=C*H*–), 3.6 (s, –OC*H*$_3$), 2.77 (m, –CH=CH–C*H*$_2$–CH=CH–), 2.3 (m, –C*H*$_2$–CO–), 2.03 (m, =CH–C*H*$_2$–), 1.29 (m, –(C*H*$_2$)$_n$–), 0.88 (m, –CH$_2$–C*H*$_3$); **^{13}C-NMR** ($CDCl_3$, δ ppm): 174.09 (–*C*O–CH$_2$–), 129.9 (–*C*H=*C*H–), 51.4 (–O*C*H$_3$), 34.1 (–CO–*C*H$_2$–), 31.9 (ω3 –*C*H$_2$–), 29.66–29.08 (–CH=CH–*C*H$_2$–, –*C*H$_2$–), 27.2 (–CH=CH–*C*H$_2$–CH=CH–), 25.6–24.80 (–CO–CH$_2$–*C*H$_2$–), 22.70, 22.47 (ω2 –*C*H$_2$–) and 14.16 (ω1 –*C*H$_3$).

Ethyl esters of JO: **^{1}H-NMR** ($CDCl_3$, δ ppm): 5.34 (m, –C*H*=C*H*–), 4.1–4.2 (q, –OC*H*$_2$–), 2.77 (m, –CH=CH–C*H*$_2$–CH=CH–), 2.3 (m, –C*H*$_2$–CO–), 2.03 (m, =CH–C*H*$_2$–), 1.29 (m, –(C*H*$_2$)$_n$– , –CO–CH$_2$–C*H*$_3$), 0.88 (m, –CH$_2$–C*H*$_3$); **^{13}C-NMR** ($CDCl_3$, δ ppm): 174.09 (–*C*O–CH$_2$–), 129.9 (–*C*H=*C*H–),60 (–OCH$_2$–), 34.1 (–CO–*C*H$_2$–), 31.9 (ω3 –*C*H$_2$–), 29.66–29.08 (–CH=CH–*C*H$_2$–, –*C*H$_2$–), 27.2 (–CH=CH–*C*H$_2$–CH=CH–), 25.6–24.80 (–CO–CH$_2$–*C*H$_2$–), 22.70, 22.47 (ω2 –*C*H$_2$–) and 14.16 (ω1 –*C*H$_3$, –OCH$_2$–*C*H$_3$).

The ^{1}H and ^{13}C-NMR of FAAE prepared by other oils is shown in Fig. A.13 and A.14 (Appendix A).

4.3.2. Catalyst characterization

4.3.2.1. X-ray diffraction

The catalyst structure and crystallite size were determined by powder XRD study. The effect of calcination temperature on structure was studied by calcining the prepared samples in the temperature range of 300-900 °C but maintaining a fix zirconium concentration of 15 wt%. As could be seen from Fig. 4.2(a), up to 400 °C calcination temperature the zirconia phase remains absent due to the homogeneous solid solution formation of ZrO_2-$Ca(OH)_2$. The thermal decomposition of $Ca(OH)_2$ into *cubic*-CaO phase (JCPDS 82–1691) was initiated at 500 °C and completed at 600 °C, as supported by the absence of $Ca(OH)_2$ diffraction patterns. As a consequence of increasing calcination temperature, *tertragonal*-ZrO_2 (JCPDS card no. 88-1007), *monoclinic*-ZrO_2 (JCPDS card no. 88-2390), and *perovskite*-$CaZrO_3$ (JCPDS card no. 76-240) phases were also formed above 600 °C calcination temperature.

The effect of the zirconium concentration (5-20 wt%) on Zr/CaO structure was studied at a fixed calcination temperature of 700 °C. As could be seen from Fig. 4.2(b), a variation in zirconium concentration has not initiated any new phase formation in Zr/CaO. However, the ratio between tetragonal to monoclinic phases was found to decrease with an increase in zirconium concentration, as given in Table 4.1. This may be due to the formation of mainly

monoclinic-ZrO_2 with increasing zirconium concentration in Zr/CaO at 700 °C calcination temperature.

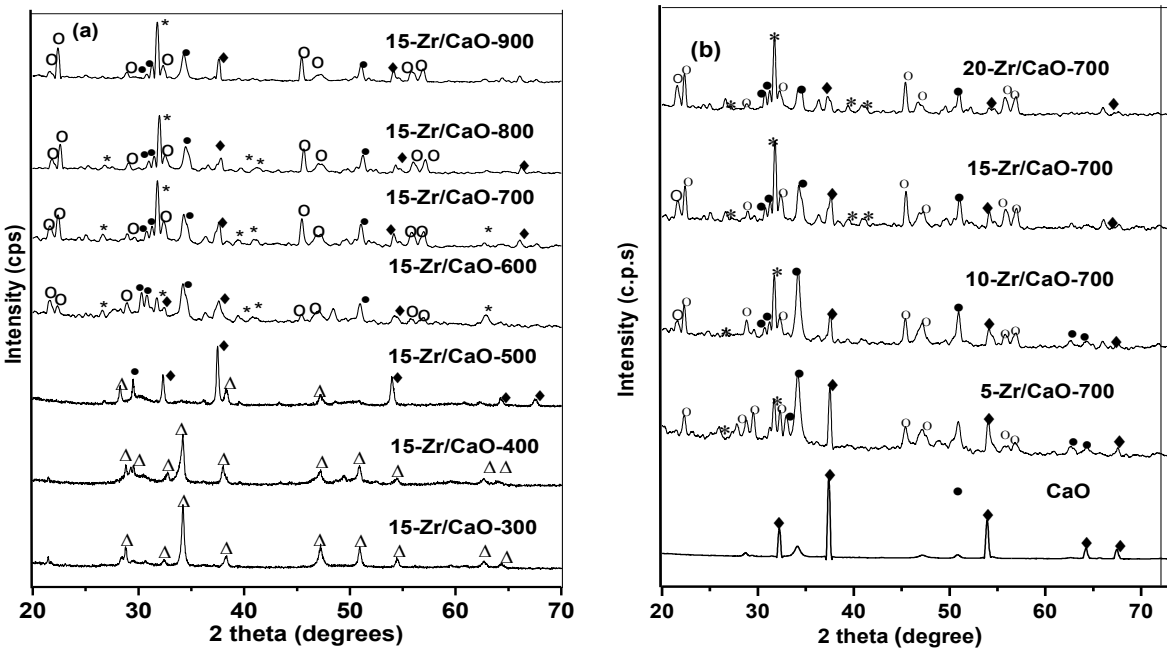

Fig. 4.2. Comparison of powder XRD patterns of (a) 15-Zr/CaO calcined in the temperature range of 300-900 ºC and (b) Zr/CaO having zirconium concentration in the range of 0-20 wt% (* = *monoclinic* ZrO_2, • = *tetragonal* ZrO_2, o = *perovskite* $CaZrO_3$, ♦ = *cubic* CaO, Δ = $Ca(OH)_2$).

The effect of the calcination temperature on crystallite size of *tetragonal and monoclinic*-ZrO_2 phases were studied following the Debye-Scherrer method as given in Table 4.1. At 500 °C calcination temperature, only *tertragonal*-ZrO_2 phase exist with a crystallite size of ~ 36 nm and monoclinic phase was not observed. At 600 °C calcination temperature, besides tetragonal phase, *monoclinic*-ZrO_2 was also formed with a crystallite size of ~ 27 nm. The formation of *monoclinic*-ZrO_2 was accompanied with the reduction in crystallite size of *tetragonal* phase to 16 nm. This observation supports that *monoclinic*-ZrO_2 might have formed from the existing *tetragonal* phase. A further increase in calcination temperature (≥ 700 °C) has neither initiated the formation of any new phase of ZrO_2, nor changed the crystallite size significantly.

Table 4.1. Effect of calcination temperature and Zr concentration on Zr/CaO structure and crystallite size.

Catalyst	Crystallite size[a] (nm)		Tetragonal phase[b] (%)	Ratio between tetragonal and monoclinic phase
	$(002)_{tetragonal}$ ($2\theta = 34.1$)	$(111)_{monoclinic}$ ($2\theta = 31.6$)		
Effect of calcination temperature				
15-Zr/CaO-300	Absence of phase	Absence of phase	-	-
15-Zr/CaO-400	Absence of phase	Absence of phase	-	-
15-Zr/CaO-500	35.77	Absence of phase	100	1:0
15-Zr/CaO-600	16.01	27.50	69	2.23:1
15-Zr/CaO-700	13.87	28.53	54	1.17:1
15-Zr/CaO-800	14.35	28.54	54	1.17:1
15-Zr/CaO-900	17.30	28.50	55	1.22:1
Effect of Zr concentration				
5-Zr/CaO-700	15.41	26.68	70	2.33:1
10-Zr/CaO-700	16.65	28.52	68	2.13:1
15-Zr/CaO-700	13.87	28.53	54	1.17:1
20-Zr/CaO-700	11.25	27.57	48	0.92:1

[a] calculated by Debye-Sherrer method; [b] calculated by following the method as given in Sahu and Rao, 2000.

4.3.2.2. Fourier Transformation Infrared Spectroscopy (FTIR)

The formation of ZrO_2 phase in Zr/CaO is further supported by the FT-IR study as shown in Fig. 4.3. Appearance of the bands at 535 and 684 cm^{-1} due to Zr-O and Zr-O_2-Zr vibrations, respectively (Sahu and Rao, 2000; Powers and Gray, 1973), support the formation of ZrO_2 species above 400 °C calcination temperature.

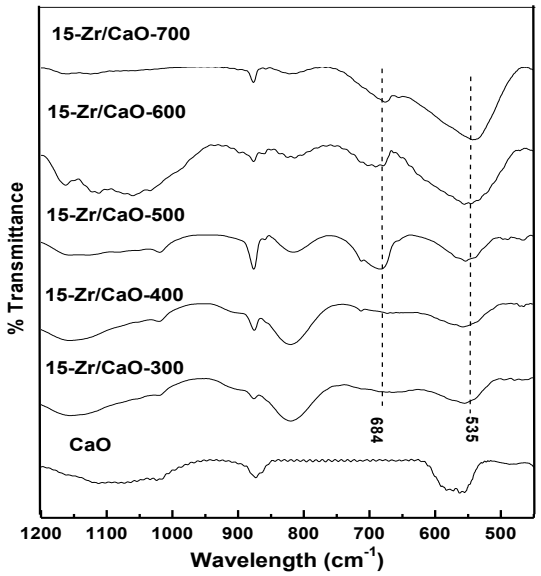

Fig. 4.3. Comparison of FTIR spectra of CaO and 15-Zr/CaO calcined at 300-700 ºC.

4.3.2.3. Scanning and Transmission Electron Microscopic Studies

The surface morphology and particle size of 15-Zr/CaO-700 was studied by SEM and TEM studies, respectively. As could be seen from SEM image (Fig. 4.4(a)), Zr/CaO has formed in the form of 0.5-2 μm sized particles with irregular shape. TEM analysis reveals that Zr/CaO particles are actually the clusters of further smaller particles with an average size of ~30 nm in quasi-spherical shape as shown in Fig. 4.4(b). Thus powder XRD as well as TEM study

supports the formation of nano structures of Zr/CaO. Qualitative analysis by SEM-EDS study supported the presence of ~17 wt% Zr in 15-Zr/CaO-700 catalyst.

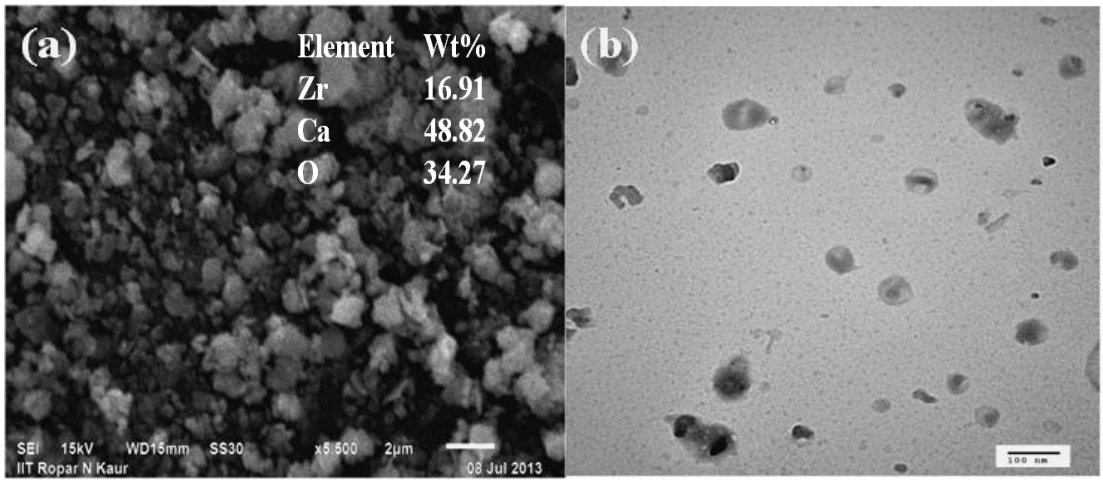

Fig. 4.4. (a) FE-SEM image and (b) TEM image of 15-Zr/CaO-700.

4.3.2.4. BET Surface area measurements

The specific surface area of Zr/CaO catalysts, prepared either by varying the zirconium concentration (10-20 wt%) or calcination temperature (600-800 °C) is compared in Table 4.3. Minimum surface area (1.86 m^2/g) was observed in case of Zr/CaO prepared with 15 wt% zirconium at 700 °C calcination temperature. Interestingly, same catalyst was found to show the best activity among the prepared catalysts. Thus activity of the catalyst was found to be a function of its basic strength rather than surface area. These results are in line with that of literature reports where activity of the catalysts towards transesterification reaction was found to be a function of basic strength rather than surface area (Singh and Fernando, 2008; Patil and Deng, 2009; Sankaranarayanan *et al.*, 2012).

4.3.3. Catalytic activity of Zr/CaO

In this work, in order to improve the activity, CaO has been impregnated with varying amount of zirconium. An increase in Lewis base sites was observed on increasing the zirconium concentration (from 5 to 15 wt%) followed by an increase in calcination temperature (from 300 to 700 °C). At high calcination temperature (≥ 600 °C), due to the thermal decomposition of hydroxides into corresponding oxides, the strong Lewis basic sites were created in catalyst as given in Table 4.2. The maximum basic strength as well as basic sites was observed in 15 wt% Zr impregnated CaO, prepared at 700 °C calcination temperature. On the basis of structural and activity analysis of Zr/CaO it was observed (Table

4.1 and 4.2) that better activity (in terms of the reaction rate) is shown by the catalysts having tetragonal/monoclinic ratio close to unity (e.g. 15-Zr/CaO-700, 20-Zr/CaO-900, 15-Zr/CaO-800 and 15-Zr/CaO-900).

The efficacy of Zr/CaO catalysts towards the methanolysis and ethanolysis of JO was compared on the basis of reaction rate and TOF. The reaction rate is found to be a function of basic sites present in Zr/CaO. However, the increase in reaction rate didn't follow the linear relationship with the basic sites, and hence, 15-Zr/CaO-700 catalyzed reaction exhibited maximum rate of reaction but not the highest TOF (Table 4.2). Since, 15-Zr/CaO-700 was found to enhance the reaction rate to the maximum extent; hence, it was selected to optimize various reaction parameters for the transesterification reaction. As evident from the Table 4.2, owing to higher mobility of methoxide nucleophile, due to its shorter carbon chain length, the rate of methanolysis was always found higher than that of ethanolysis (Brunschwig *et al.*, 2012).

Table 4.2. Comparison of basic strengths, basicity, BET surface areas, rate of reactions and TOFs for the Zr/CaO catalyzed transesterification reactions.

Catalyst	Basic strength	Basicity (mmoles of HCl/ g of catalyst)	BET surface area (m^2/g)	Methanolysis		Ethanolysis	
				TOF ($\times 10^{-3}$ s^{-1})	Rate of reaction ($\times 10^{-6}$ moles s^{-1} g^{-1} of catalyst)	TOF ($\times 10^{-4}$ s^{-1})	Rate of reaction ($\times 10^{-7}$ moles s^{-1} g^{-1} of catalyst)
CaO	9.8< pK_a<10.1	9.48	3.90	0.33	0.80	1.29	3.22
5-Zr/CaO-700	10.1< pK_a<11.1	9.71	ND	0.79	1.93	1.65	4.02
10-Zr/CaO-700	10.1< pK_a<11.1	14.24	6.40	0.60	2.15	1.50	5.37
15-Zr/CaO-700	11.1< pK_a<15.0	20.21	1.86	0.54	2.76	1.37	6.90
20-Zr/CaO-700	10.1< pK_a<11.1	11.91	3.26	0.77	2.32	1.62	4.83
15-Zr/CaO-300	10.1< pK_a<11.1	6.01	ND	0.95	1.20	1.93	3.43
15-Zr/CaO-400	10.1< pK_a<11.1	6.23	ND	0.91	1.40	1.90	3.65
15-Zr/CaO-500	10.1< pK_a<11.1	7.36	ND	0.83	1.89	1.85	4.00
15-Zr/CaO-600	10.1< pK_a<11.1	9.94	4.99	0.80	2.00	1.77	4.39
15-Zr/CaO-800	10.1< pK_a<11.1	15.67	5.68	0.60	2.38	1.29	5.08
15-Zr/CaO-900	10.1< pK_a<11.1	14.44	ND	0.66	2.41	1.64	5.93

(Reaction conditions: *Methanolysis*: methanol to oil molar ratio of 15:1 at 65 ºC reaction temperature; *Ethanolysis*: ethanol to oil molar ratio of 21:1 at 75 ºC reaction temperature, and 5 wt% of 15-Zr/CaO-700 with respect to oil in both the cases, ND- Not determined).

To find out the reaction conditions for the optimum catalytic activity of 15-Zr/CaO-700, transesterification reactions were carried out by varying one parameter at a time out of the followings: (i) catalyst amount with respect to oil, (ii) reaction temperature and (iii) alcohol to oil molar ratio. Further, transesterification reactions were also performed in presence of varying amount of moisture and FFA contents in order to evaluate the maximum tolerance of the catalyst toward them. Under optimized reaction conditions, reusability of the catalyst and kinetics of the Zr/CaO catalyzed transesterification were also studied.

4.3.3.1. Effect of catalyst amount with respect to oil

In order to optimize the catalyst concentration, a series of transesterification reactions of JO with methanol (15:1 molar ratio) and ethanol (21:1 molar ratio) were performed in presence of 1-6 wt% (with respect to oil) of 15-Zr/CaO-700. The FAME and FAEE yield was found to increases as the catalyst concentration was increased from 1 to 5 wt% as shown in Fig. 4.5(a) and 4.5(b), respectively. A 5 wt% catalyst concentration required 105 and 420 min for the complete conversion of JO into corresponding FAME and FAEE, respectively. However, a further increase in catalyst concentration (≥ 5 wt%) was not found to change the conversion significantly. This could be due to the fact that at higher catalyst loading, reaction mixture becomes more viscous which could resist the mass transfer in the liquid-liquid-solid system (Wang *et al.*, 2011).

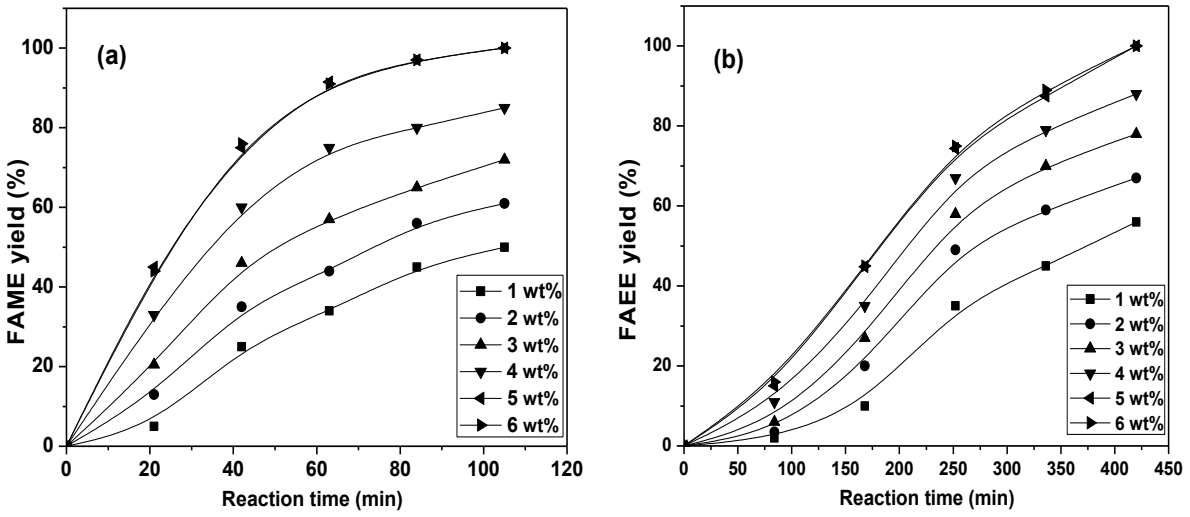

Fig. 4.5. Influence of catalyst concentration on 15-Zr/CaO-700 catalyzed transesterification of JO. **Reaction conditions:** (a) methanol to oil molar ratio of 15:1 at 65 ºC reaction temperature and (b) ethanol to oil molar ratio of 21:1 at 75 ºC reaction temperature.

4.3.3.2. Effect of reaction temperature

Heterogeneous catalysts, due to the phase difference from reagents, usually required high temperature and pressure and longer reaction period to yield the significant conversion. Such reaction conditions demand complicatedly designed costlier reactor which in turn may increase the biodiesel production cost (Ma and Hanna, 1999).

The optimum reaction temperature for 15-Zr/CaO-700 was determined by performing the transesterification of JO in the temperature range of 35-85 ºC. As increase in FAME and FAEE yield was observed with the increase in reaction temperature from 35 to 65 ºC and 45 to 75 ºC, respectively (Fig. 4.6(a) and 4.6(b)). A further increase in reaction temperature was

not found to influence the FAME and FAEE yield significantly. Although catalyst was found to be more effective at 65 ºC, however, even at room temperature (35 ºC) complete conversion of JO into corresponding FAME were achieved in 5 h of reaction period. High basic strength and presence of more number of basic sites could be responsible behind the moderate activity of catalyst even at ambient temperature.

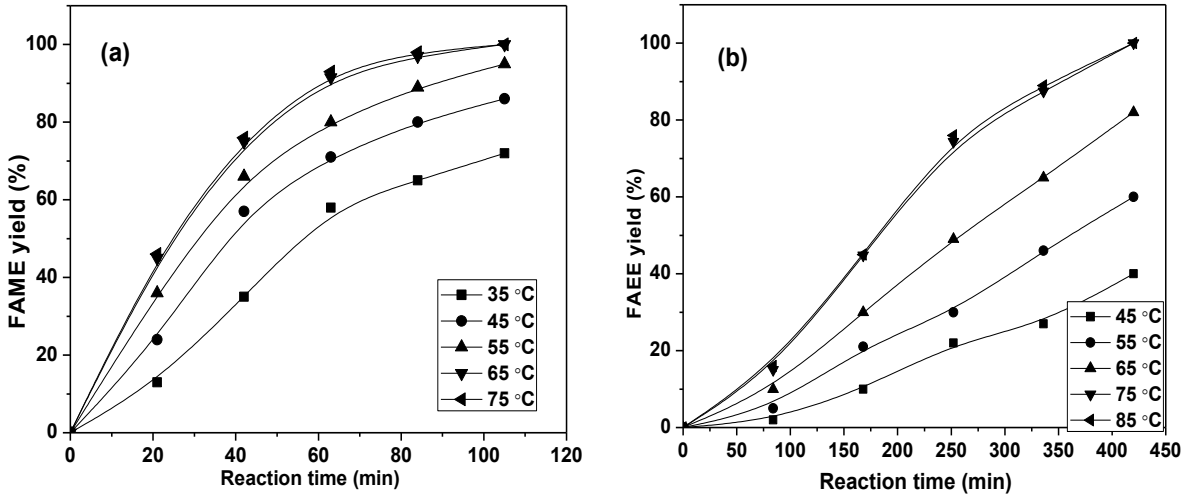

Fig. 4.6. Effect of reaction temperature on 15-Zr/CaO-700 catalyzed transesterification of JO. **Reaction conditions:** (a) methanol to oil molar ratio of 15:1 and (b) ethanol to oil molar ratio of 21:1 and 5 wt% of 15-Zr/CaO-700 with respect to oil in both the cases.

4.3.3.3. Effect of alcohol to oil molar ratio

The effect of alcohol/oil molar ratio on transesterification reaction is one of the important parameter which not only affects the alkyl ester yield but also the cost of biodiesel production. Stoichiometrically, a 3:1 alcohol to oil molar ratio is required for the complete transesterification of vegetable oil into corresponding alkyl esters. Transesterification, being a reversible reaction, usually performed with an excess of alcohol to shifts the equilibrium in forward direction and to achieve the maximum alkyl ester yield in relatively short reaction duration (Wang *et al.*, 2011). Excess alcohol not only promotes the transesterification rate but also removes product molecules from the catalyst surface to regenerate the active sites (Xie *et al.*, 2006; Furuta *et al.*, 2004).

To determine the optimum alcohol/oil molar ratio for 15-Zr/CaO-700, the reactions were performed by varying the alcohol/oil molar ratio from 3:1 to 18:1 in case of methanolysis and 3:1 to 24:1 in case of ethanolysis. The FAME yield increases from 60 to 99 % on increasing the methanol/oil molar ratio up to 15:1, as shown in Fig. 4.7(a). Similar trend was observed in case of ethanolysis (Fig. 4.7(b)) and 99 % FAEE yield was observed with a 21:1 ethanol/oil molar ratio.

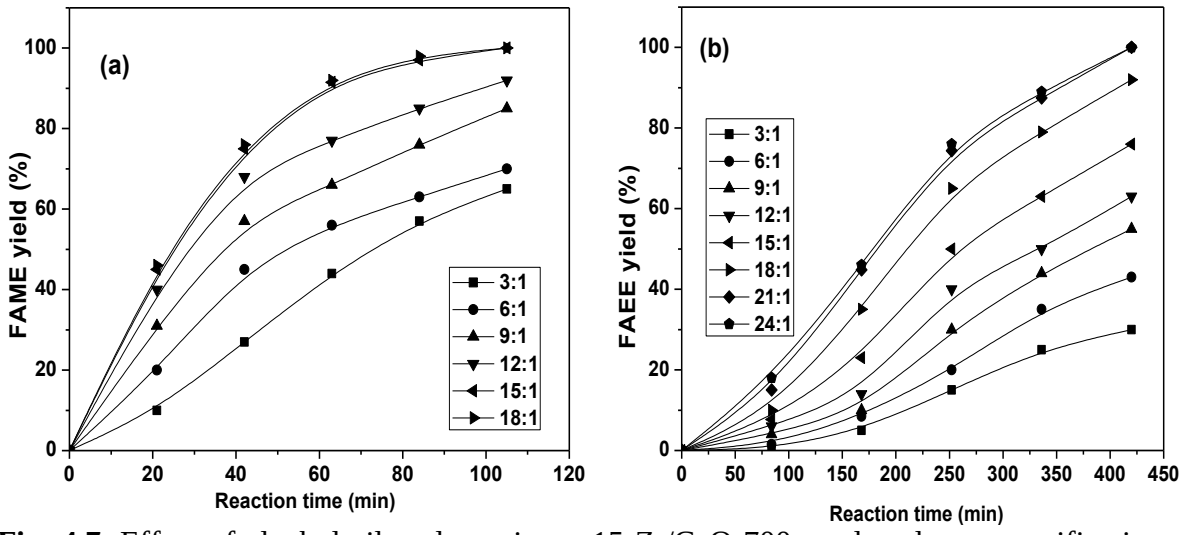

Fig. 4.7. Effect of alcohol:oil molar ratio on 15-Zr/CaO-700 catalyzed transesterification of JO. **Reaction conditions:** Reaction temperature (a) methanolysis at 65 ºC and (b) ethanolysis at 75 ºC, both reactions were performed in presence of 5 wt% of 15-Zr/CaO-700 with respect to oil.

Thus a 15:1 methanol to oil molar ratio at 65 ºC or 21:1 ethanol to oil molar ratio at 75 ºC in presence of 5 wt% catalyst (with respect to oil), were found to be optimum conditions for the 15-Zr/CaO-700 catalyzed transesterification of JO.

4.3.3.4. Effect of moisture and FFA content

Homogeneous catalyst required costlier refined vegetable oil for the transesterification reactions as presence of > 0.3 wt% moisture and/or > 0.5 wt% FFA contents in feedstock deactivates the catalyst due to the saponification (Kumar and Ali, 2012). In present study, JO employed as feedstock was found to have 7.5 and 0.35 wt% FFA and moisture contents, respectively. In order to demonstrate the advantage of developed Zr/CaO catalyst over homogeneous one, methanolysis of JO was also performed in presence of NaOH. Although saponification of JO was observed in presence of homogeneous catalyst, however, > 99 % FAME yield was observed in presence of Zr/CaO catalyst. In order to determine the maximum moisture resistance of the developed catalyst, transesterification reactions of JO were performed by adding up to 6.0 wt% of water (with respect to oil) in reaction mixture. The Zr/CaO activity was not found to be effected by the presence of up to 2 wt% of moisture contents as shown in Fig. 4.8(a). Nevertheless, a further increase in moisture concentration (3-6 wt%) was found to effect the catalytic activity adversely as more time was required by the catalyst for the complete methanolysis of oil. Lesser activity of Zr/CaO catalyst in

presence of high moisture concentration could be due to the reaction between water and catalyst support (CaO), which could convert the stronger Lewis basic (–O–) sites back into weaker Bronsted basic (–OH) sites (Yan *et al.*, 2009). A further increase in moisture content (> 6 wt%), results high degree of deactivation of the catalyst and hence, only ~30% FAME yield was achieved.

In order to determine the maximum FFA tolerance of the prepared catalyst, transesterification reactions of CO, WO, JO and KO (having 1–15 wt% FFA) were performed with methanol. As shown in Fig. 4.8(b), Zr/CaO catalyst was able to complete the transesterification of oil having up to 15 wt% FFA. Increase in FFA content was also found to reduce the catalytic activity and hence, Zr/CaO catalyst required more time for the complete transesterification of oils having higher FFA concentration.

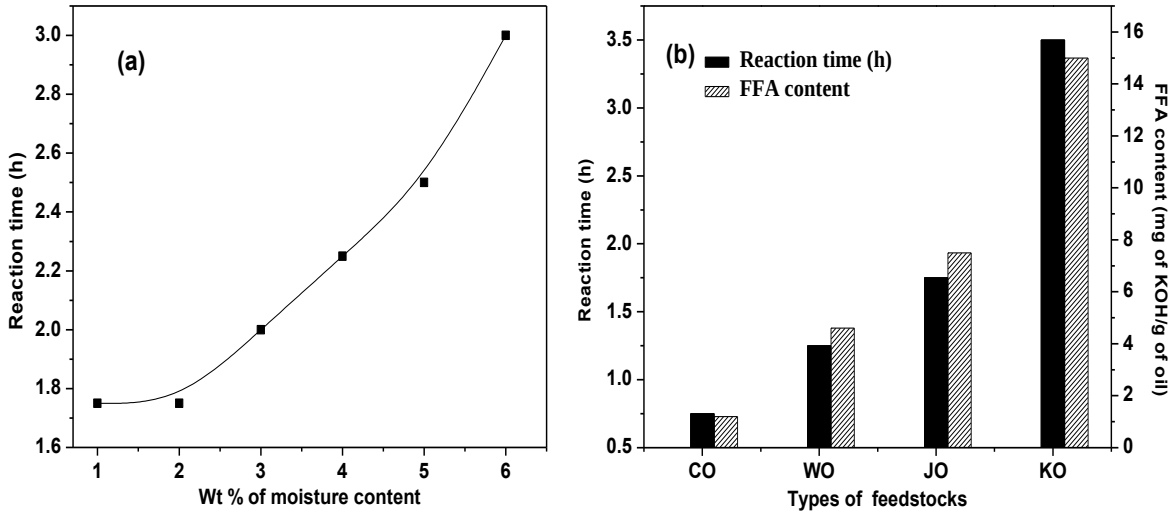

Fig. 4.8. Effect of (a) moisture content and (b) FFA contents on the 15-Zr/CaO-700 catalyzed transesterification of JO (reaction time is the time required for the completion of the reaction). **Reaction conditions:** Methanol to oil molar ratio of 15:1 at 65 ºC reaction temperature in presence of 5 wt% (catalyst/oil) catalyst.

Thus, prepared Zr/CaO catalyst has demonstrated not only better moisture and FFA resistance but also found to be effective for the transesterification of a variety of low quality feedstock in single step without any pre-treatment.

4.3.4. Reusability and Homogeneous contribution of catalyst

The repeated use of a heterogeneous catalyst is expected to reduce the overall processing cost of a chemical reaction. To test the reusability of 15-Zr/CaO-700, transesterification of the JO was performed with methanol under optimized reaction conditions. After the completion of the reaction, Zr/CaO was recovered from the reaction mixture by filtration, washed with

hexane and finally regenerated at 700 °C calcination temperature. The catalyst hence recovered and regenerated was employed for 4 successive catalytic cycles under the same experimental and regeneration methods. As shown in Fig. 4.9, the reused catalyst was also found to yield > 99 % FAME in second run. However, 80 % and 40 % FAME yields were achieved during third and fourth run, respectively. The gradual loss in catalytic activity may be due to, (i) the blockage of active sites either due to the adsorption of organic molecules or due to the contamination by atmospheric O_2, H_2O, and CO_2 (ii) the structural changes occurred during catalytic and regeneration process and (iii) the partial leaching of active species from the catalyst.

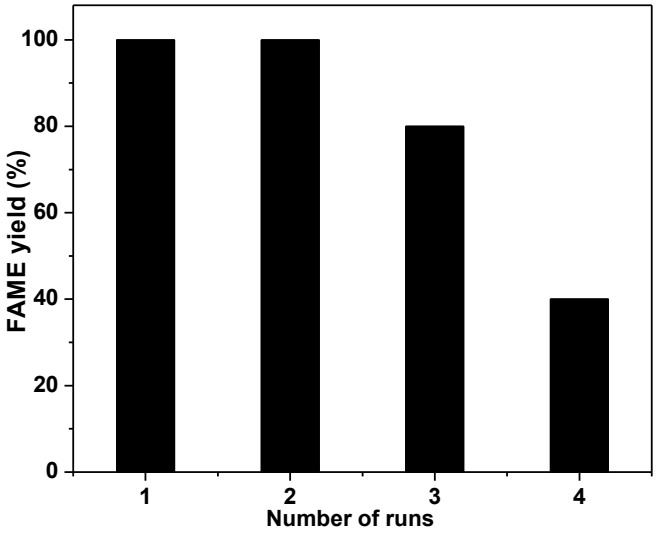

Fig. 4.9. Reusability study of 15-Zr/CaO-700. **Reaction conditions:** methanol to oil molar ratio of 15:1 at 65 ºC reaction temperature in presence of 5 wt % catalyst.

In order to evaluate the structural changes occurred in Zr/CaO, the XRD patterns of the fresh and regenerated Zr/CaO are compared in Fig. 4.10(a). In the XRD patterns of regenerated Zr/CaO, peaks corresponding to *cubic*-CaO phase, *tetragonal*-ZrO_2 phase and few peaks corresponding to *perovskite*-$CaZrO_3$ phase were no longer found. Further, presence of a new diffraction peak at $2\theta \sim 30.06$, in regenerated catalyst supports the formation of *orthorhombic*-ZrO_2 phase (JCPDS-87-2105) during the catalyst activation step.

The deposition of the adsorbed organic species on catalyst support could partially deactivate the catalyst due to the blockage of catalyst active sites (Serio *et al.*, 2008). The FTIR spectrum (Fig. 4.10(b)), of the regenerated catalyst didn't show vibrations corresponding to any adsorbed organic molecules to indicate that FAME or glycerol have not been adsorbed on the surface of regenerated Zr/CaO.

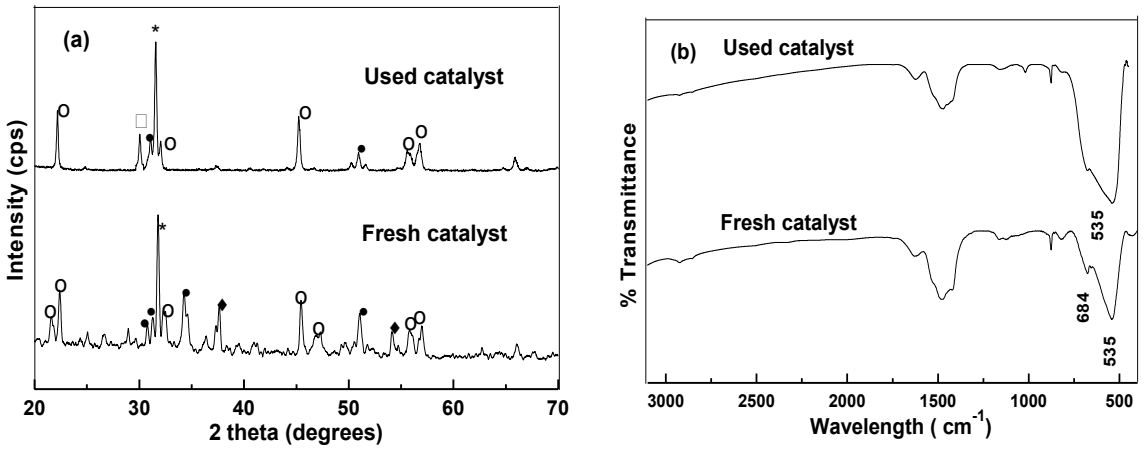

Fig. 4.10. Comparision of (a) XRD and (b) FT-IR of fresh and used catalyst.
(* = *monoclinic* ZrO_2, • = *tetragonal* ZrO_2, o = *perovskite* $CaZrO_3$, ♦ = *cubic* CaO, □ = *orthorhombic* zirconia).

The metal analysis supported the presence of Zr (120 ppm) and Ca (700 ppm) in FAME. Thus during the catalytic cycle metal is gradually lost and could also be another reason for the loss of catalytic activity. Hence, the gradual loss of the catalytic activity, upon repeated use, could be attributed to the (i) structural changes occurred in catalyst, and (ii) partial loss of the Zr from Zr/CaO catalyst.

Metal ions, found in reaction mixture could catalyze the reaction similar to a homogeneous catalyst. To investigate whether the leached metal ions have catalyzed the reaction, 15-Zr/CaO-700 (500 mg) was stirred vigorously with refluxing methanol (13 mL) for 105 min. After the stipulated time, the catalyst was removed by filtration and recovered methanol was mixed with JO (15:1 molar ratio) and heated at 65 °C for another 105 min. Under mentioned reaction conditions, not more than 5 % FAME yield was obtained. Thus it is safe to assume that leached metal ions have not catalyzed the reaction to the significant extent and heterogeneous Zr/CaO catalyst is mainly responsible for the catalytic activity.

4.3.5. Kinetic study

To study the kinetics of the reaction, samples from the reaction mixture were withdrawn after every 15 min with the help of glass dropper, centrifuged and subjected to proton NMR analysis. Fig. 4.11 and 4.12 show a typical ^{1}H-NMR plot for the methanolysis and ethanolysis, respectively. FAME and FAEE yield from these plots were calculated using equation 2.8 and 2.9 (Chapter 2) respectively.

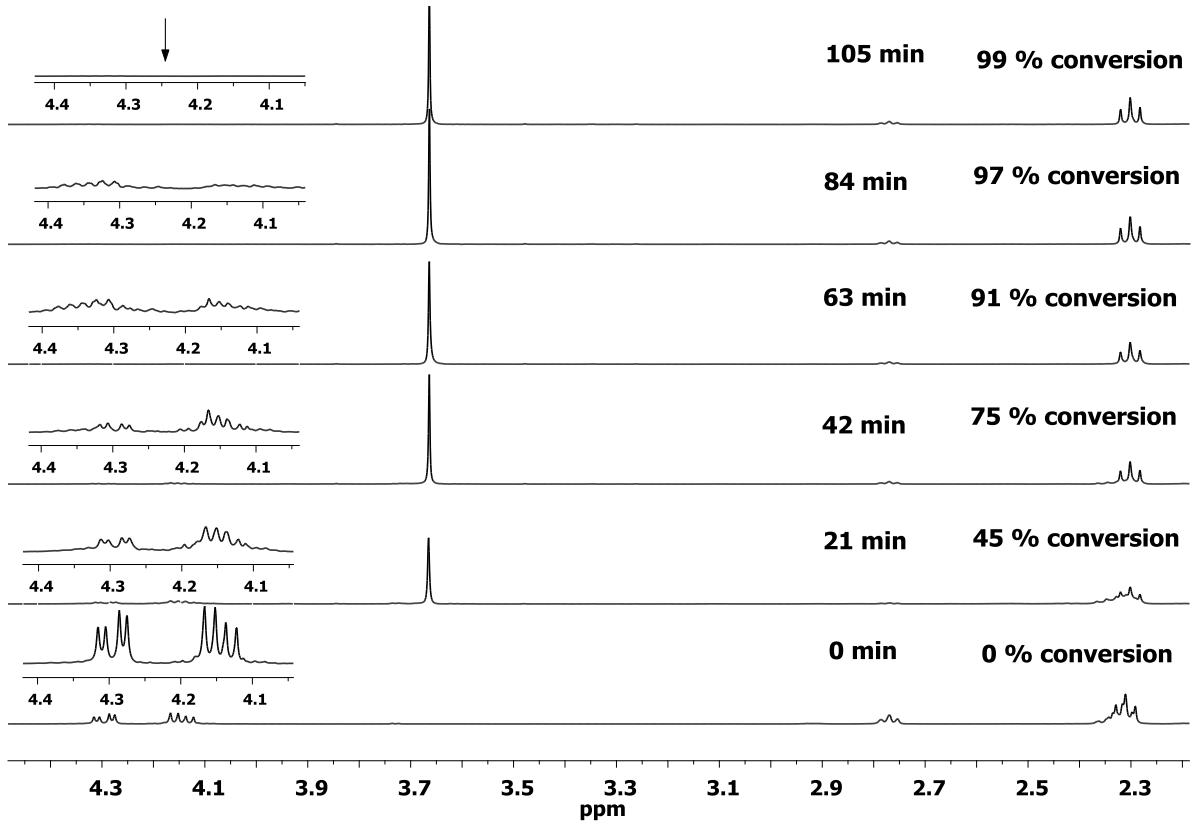

Fig. 4.11. Representative proton NMR spectra (2.2-4.5 ppm) of reaction mixture at various time intervals to study the kinetics of methanolysis reaction.

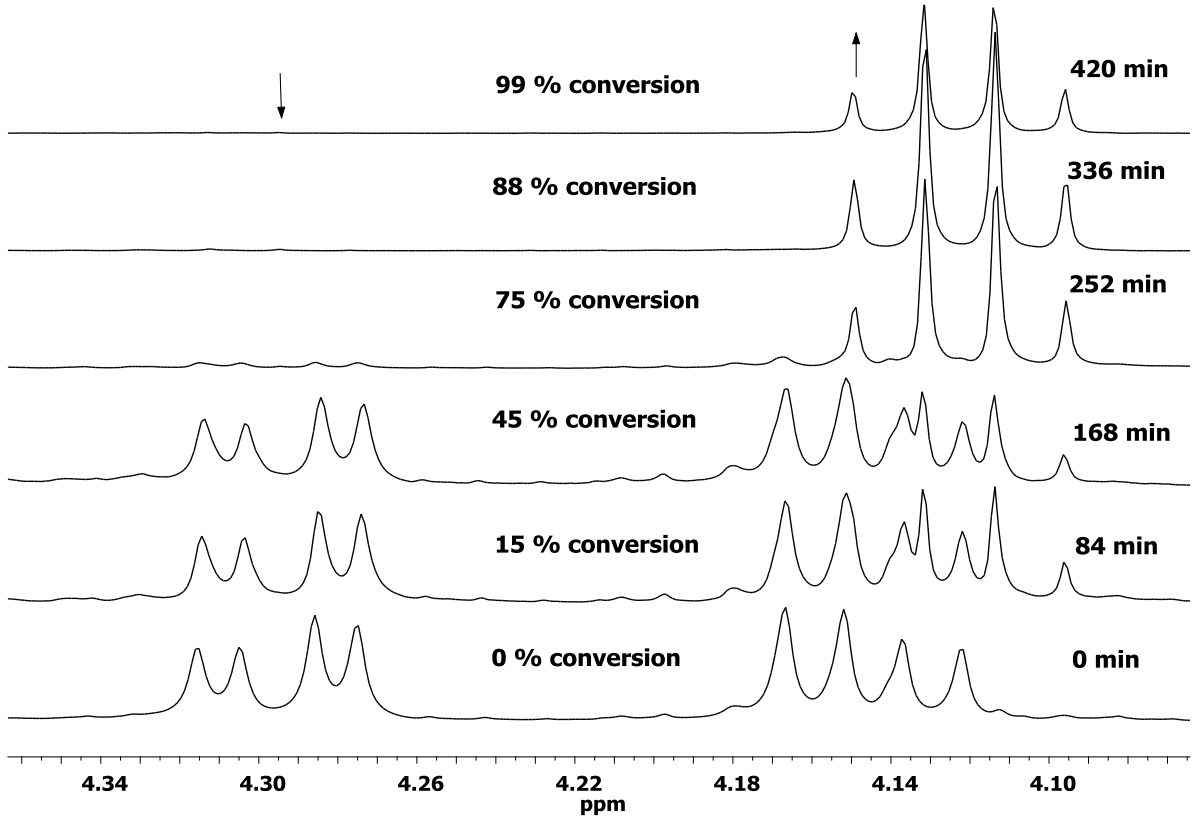

Fig. 4.12. Representative proton NMR spectra (3.80-4.36 ppm) of reaction mixture at various time intervals to study the kinetics of ethanolysis reaction.

During the kinetic experiments an alcohol to oil molar ratio of 15 and 21 was employed for methanolysis and ethanolysis, respectively. Thus both the reactions may be assumed to follow pseudo-first order kinetics. The kinetics of the 15-Zr/CaO-700 catalyzed methanolysis and ethanolysis of JO were studied at different temperatures using equation 2.3 (Chapter 2) and corresponding graphs between $-ln(1 - X)$ *vs t* are shown in Fig. 4.13(a) and 4.13(b) respectively.

The linear nature of these plots supported that both reactions followed the (pseudo) first order rate law. The apparent first order rate constants form these plots were found to be 0.062 min^{-1} at 65 ºC for the methanolysis and 0.012 min^{-1} at 75 ºC for the ethanolysis reaction.

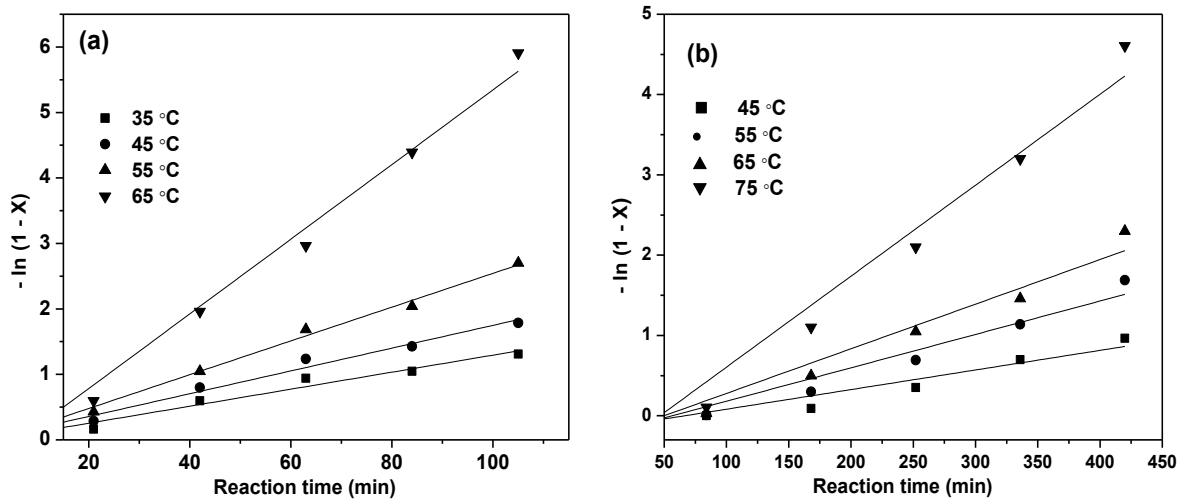

Fig. 4.13. Plots of –ln(1–X) *vs* time at different temperatures. **Reaction conditions:** (a) methanol to oil molar ratio of 15:1 (b) ethanol to molar oil ratio of 21:1 and 5 wt% of 15-Zr/CaO-700 with respect to oil in both the cases.

The Arrhenius model was employed to estimate the activation energy (E_a) and pre-exponential factor (A) for both the reactions followed the equation 2.4 (Chapter 2). A plot between ln k *vs* 1/T is shown in Fig. 4.14, and the values of E_a and A from this plot was found to be 29.8 kJ mol^{-1} and 1.8×10^3 min^{-1}, respectively for methanolysis and 42.5 kJ mol^{-1} and 2.2×10^4 min^{-1}, respectively for ethanolysis.

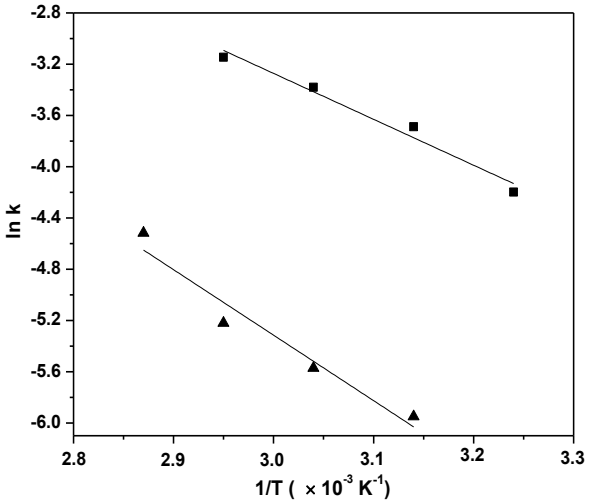

Fig. 4.14. Arrhenius plot for the transesterification of JO with methanol (■) and ethanol (▲) over 15-Zr/CaO-700 catalyst.

The literature reported activation energy for the methanolysis and ethanolysis in presence of homogeneous and heterogeneous catalysts has been compared with that of observed in present work as given in Table 4.3.

Table 4.3. Activation energy comparison for the transesterification reaction catalyzed by homogeneous and heterogeneous catalysts.

Oil	Catalyst/quantity (wt % with respect to oil)	Alcohol:oil molar ratio (Alcoholysis)	FAAE yield (%)	Reaction temperature (°C)	Order of reaction	Activation energy (kJ mol^{-1})	Reference
Homogeneous catalysts							
Palm	KOH/1	6:1(M)	98	55-65	second-order	26.8-61.5	Darnoko and Cheryan, 2000
Soybean	$NaOCH_3$/0.5	6:1(M)	98	20-60	2^{nd} and 4^{th} order for consecutive and shunt reactions	56.8-83.8	Freedman *et al.*, 1986
Soybean	NaOH/0.2	6:1(M)	93	30-70	second-order	21.7-83.1	Noureddini and Zhu, 1997
Brassica carinata	KOH/0.5-1.5	6:1(M)	98	25-65	second-order	12-104.8	Vicente *et al.*, 2006
Sunflower	KOH/0.5-1.5	6:1(M)	98	25-65	second-order	6-41.6	Vicente *et al.*, 2005
Sunflower	NaOH/0.75-1.25	6:1 12:1(E)	98	25-75	irreversible pseudo second-order	3.4-43.9	Marjanovic *et al.*, 2010
Castor	C_2H_5ONa/1	16:1(E)	99	30-70	first-order	70.6	Silva *et al.*, 2009
Heterogeneous catalysts							
Soybean	CaO.ZnO/2	10:1(M)	98	60-96	pseudo first-order	26.5	Lukic *et al.*, 2008
Used vegetable	CaO.ZnO/2	10:1(M)	98	60-96	pseudo first-order	16.6	Lukic *et al.*, 2008
Soybean	Zeolite Linde Type A/50	20:1(M)	97±3	40-63	pseudo first-order	14.09	Dang *et al.*, 2013
Palm	Zeolite Linde Type A/10	10:1(M)	95.4± 3.7	50-63	pseudo first-order	48.87	Dang *et al.*, 2013
Soybean	SrO/2	12:1(M)	98	40-65	pseudo first-order	40.12	Liu *et al.*, 2010
Soybean	CaO/2	12:1(M)	98	40-65	pseudo first-order	81.09	Liu *et al.*, 2010
Waste frying	CaO/2	6.03:1(M)	99.58	50-65	pseudo first-order	79	Birla *et al.*, 2012
Waste cottonseed	K-CaO/7.5	12:1(M)	98±2	35-65	pseudo first-order	54	Kumar and Ali, 2012
Jatropha	Zr/CaO/5	15:1(M)	99	35-65	pseudo first-order	29.8	In this chapter
Rapeseed	Mg_2CoAl/2	16:1(E)	97	140-200	irreversible first order	60.5	Soldi *et al.*, 2009
Jatropha	Zr/CaO/5	21:1(E)	99	45-75	pseudo first-order	42.5	In this chapter

M – Methanolysis; E- Ethanolysis

It is evident from the comparison, for heterogeneous catalysts, the activation energy for methanolysis was observed within the range of reported values and for ethanolysis lower than the literature reported values.

4.3.6. Koros-Nowak Criterion test

In order to study the kinetics of the reaction, the catalytic data should be independent from all transport influences. To prove that measured catalytic activity was independent of the influence of transport phenomena, the Koros–Nowak criterion test modified by Madon-Boudart was applied (Madon and Boudart, 1982; Song *et al.*, 2011). The reactions were carried out in the presence of two catalysts with similar fractional exposures of basic sites but having different Zr loadings. In present study, 5 wt% of 15-Zr/CaO-700 or 7 wt% of 10-Zr/CaO-700 catalyst dosages were employed with a methanol/oil ratio of 15:1 at 65 °C or ethanol/oil ratio of 21:1 at 75 °C as shown in Fig. 4.15. Alkyl esters formed during the course of reaction were quantified with a time gap of 15 min by ^{1}H-NMR technique. The time required for the similar conversions of JO into alkyl esters were determined and a plot between TOF *vs* % conversion is drawn as shown in Fig 4.15. The results supported that TOFs were found to be almost similar for the identical conversions in presence of catalyst having varying zirconium concentration. Hence, it could be concluded that the reaction obeyed the Koros-Nowak Criterion and reaction rates were not masked by the rates of transport.

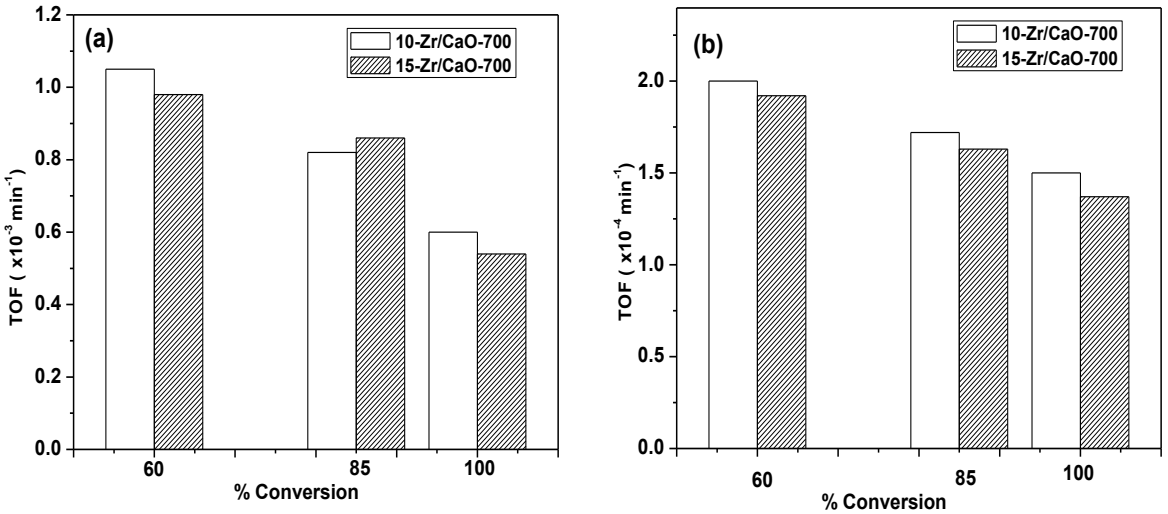

Fig. 4.15. A plot of TOF *vs* % conversion for the 10-Zr/CaO-700 and 15-Zr/CaO-700 catalyzed (a) methanolysis and (b) ethanolysis of JO. **Reaction conditions:** (a) methanol to oil molar ratio; 15:1 at 65 °C (b) ethanol to oil molar ratio; 21:1 at 75 °C and catalyst concentration; either 7 wt% of 10-Zr/CaO-700 or 5 wt% of 15-Zr/CaO-700 in both the cases.

The physicochemical properties of the prepared FAME and FAEE are shown in Table B.1 (Appendix B) and observed values were found within the limits of EN 14214 specifications.

4.4. Conclusions

In summary, a series of the Zr/CaO was prepared by varying the calcination temperature and zirconium loading in CaO. The catalyst prepared with 15 wt% zirconium in CaO at 700 °C calcination temperature (15-Zr/CaO-700), owing to higher basicity, has demonstrated better catalytic activity towards the methanolysis and ethanolysis of jatropha oil. The catalyst has shown high moisture and FFA tolerance and found to be effective for the transesterification of feedstocks having up to 6 and 15 wt% moisture and FFA contents, respectively. The optimum values of the parameters, to achieve > 99 % fatty acid alkyl ester yield, were: catalyst concentration of 5 wt%, methanol/oil molar ratio of 15:1 at 65 °C or ethanol/oil molar ratio of 21:1 at 75 °C. Following the pseudo first order kinetic equation, activation energy for the methanolysis and ethanolysis of jatropha oil was found to be 29.8 and 42.5 kJ mol^{-1}, respectively. The catalyst was reusable and its catalyst activity was persistent for two catalytic runs. The lixiviation study supports the negligible homogeneous contribution in catalytic activity, and the Koros-Nowak test demonstrates that activity is independent of the influence of transport phenomenon.

References

Birla, A.; Singh, B.; Upadhyay, S. N.; Sharma, Y. C.; Kinetics studies of synthesis of biodiesel from waste frying oil using a heterogeneous catalyst derived from snail shell. *Bioresour. Technol.*, **2012**, 106, 95-100.

Brunschwig, C.; Moussavou, W.; Blin, J.; Use of bioethanol for biodiesel production. *Prog. Energ. Combust. Sci.*, **2012**, 38, 283-301.

Dang, T. H.; Chen, B. H.; Lee, D. J.; Application of kaolin-based catalysts in biodiesel production via transesterification of vegetable oils in excess methanol. *Bioresour. Technol.*, **2013**, 145, 175-181.

Darnoko, D.; Cheryan, M.; Kinetics of palm oil transesterification in a batch reactor. *J. Am. Oil Chem. Soc.*, **2000**, 77, 1263-1267.

Faria, E. A.; Marques, J. S.; Dias, I. M.; Andrade, R. D. A.; Suareza, P. A. Z.; Prado, A. G. S.; Nanosized and reusable SiO_2/ZrO_2 catalyst for highly efficient biodiesel production by soybean transesterification. *J. Braz. Chem. Soc.*, **2009**, 20, 1732-1737.

Freedman, B.; Butterfield, R.; Pryde, E.; Transesterification kinetics of soybean oil. *J. Am. Oil. Chem. Soc.*, **1986**, 63, 1375-1380.

Furuta, S.; Matsuhashib, H.; Arata, K.; Biodiesel fuel production with solid superacid catalysis in fixed bed reactor under atmospheric pressure. *Catal. Commun.*, **2004**, 5, 721-723.

Kumar, D.; Ali, A.; Nanocrystalline K-CaO for the transesterification of a variety of feedstocks: structure, kinetics and catalytic properties. *Biomass Bioenerg.*, **2012**, 46, 459-468.

Liu, X.; Piao, X.; Wang, Y.; Zhu, S.; Model study on transesterification of soybean oil to biodiesel with methanol using solid base catalyst. *J. Phys. Chem. A*, **2010**, 110, 3750-3755.

Lukic, I.; Kesic, Z.; Maksimovic, S.; Zdujic, M.; Liu, H.; Krstic, J.; Skala, D.; Kinetics of sunflower and used vegetable oil methanolysis catalyzed by CaO.ZnO. *Fuel*, **2013**, 113, 367-378.

Ma, F.; Hanna, M. A.; Biodiesel production: a review. *Bioresour. Technol.*, **1999**, 70, 1-15.

Madon, R. J.; Boudart, M.; Experimental criterion for the absence of artifacts in the measurement of rates of heterogeneous catalytic reactions. *Ind. Eng. Chem. Fundam.*, **1982**, 21, 438-447.

Marjanovic, A. V.; Stamenkovic, O. S.; Todorovic, Z. B; Lazic, M. L.; Veljkovic, V. B.; Kinetics of the base-catalyzed sunflower oil ethanolysis. *Fuel*, **2010**, 89, 665-671.

Noureddini, H.; Zhu, D.; Kinetics of transesterification of soybean oil. *J. Am. Oil Chem. Soc.*, **1997**, 74, 1457-1463.

Patil, P. D.; Deng, S.; Transesterification of *Camelina Sativa* oil using heterogeneous metal oxide catalysts. *Energy Fuel*, **2009**, 23, 4619-4624.

Powers, D. A.; Gray, H. B.; Characterization of the thermal dehydration of zirconium oxide halide octahydrates. *Inorg. Chem.*, **1973**, 12, 2721-2726.

Sahu, H. R.; Rao, G. R.; Characterization of combustion synthesized zirconia powder by UV-vis, IR and other techniques. *Bull. Mater. Sci.*, **2000**, 23, 349-354.

Sankaranarayanan, S.; Antonyraj, C. A.; Kannan, S.; Transesterification of edible, non-edible and used cooking oils for biodiesel production using calcined layered double hydroxides as reusable base catalysts. *Bioresour. Technol.*, **2012**, 109, 57-62.

Serio, M. D.; Tesser, R.; Pengmei, L.; Heterogeneous catalysts for biodiesel production. *Energy Fuel*, **2008**, 22, 207-217.

Silva, N. L.; Batistella, C. B.; Filho, R. M.; Maciel, M. R. W.; Biodiesel production from castor oil: optimization of alkaline ethanolysis. *Energy Fuel*, **2009**, 23, 5636-5642.

Singh, A. K.; Fernando, S. D.; Transesterification of soybean oil using heterogeneous catalysts. *Energy Fuel*, **2008**, 22, 2067-2069.

Soldi, R. A; Oliveira, A. R. S.; Ramos, L. P; Oliveira, M. A. F. C; Soybean oil and beef tallow alcoholysis by acid heterogeneous catalysis, *Appl. Catal. A: Gen.*, **2009**, 361, 42–48.

Vicente, G.; Martinez, M.; Aracil, J.; Esteban, A.; Kinetics of sunflower oil methanolysis. *Ind. Eng. Chem. Res.*, **2005**, 44, 5447-5454.

Vicente, G.; Martinez, M.; Aracil, J.; Kinetics of *Brassica carinata* oil methanolysis. *Energy Fuel*, **2006**, 20, 1722-1726.

Wang, J. X.; Chen, K. T.; Huang, S. T.; Chen, C. C.; Application of Li_2SiO_3 as a heterogeneous catalyst in the production of biodiesel from soybean oil. *Chinese Chem. Lett.*, **2011**, 22, 1363-1366.

Xie, W.; Peng, H.; Chen, L.; Calcined Mg-Al hydrotalcites as solid base catalysts for methanolysis of soybean oil. *J. Mol. Catal. A: Chem.*, **2006**, 246, 24-32.

Yan, S.; Kim, M.; Mohan, S.; Salley, S. O.; Ng, K. Y. S.; Oil transesterification over calcium oxides modified with lanthanum. *Appl. Catal. A: Gen.*, **2009**, 360, 163-170.

Biodiesel Production v*ia* Ethanolysis of Jatropha Oil Using Molybdenum Impregnated Calcium Oxide as Solid Catalyst

Contents — *Page No.*

Abstract: Molybdenum impregnated calcium oxide (Mo/CaO) was prepared via wet impregnation method by varying Mo loading (1-5 wt%) and calcination temperature (300-800 °C). Powder X-ray diffraction study of Mo/CaO catalyst supported the homogeneous doping of Mo in CaO as no peak corresponding to molybdenum oxide was obtained.

The prepared catalyst was successfully employed for the ethanolysis of high free fatty acid (up to 18 wt%) containing vegetable oils with ethanol to give > 99% fatty acid ethyl ester (FAEE) yield under the optimal reaction conditions of ethanol to oil molar ratio of 12:1, catalyst concentration of 5 wt% (catalyst/oil) and reaction temperature of 65 °C. The catalyst was recovered and reused five times without significant loss in its activity. The Koros-Nowak criterion test demonstrated that catalytic activity was independent from the mass transport phenomenon. Under optimized reaction conditions the activation energy (E_a) for Mo/CaO catalyzed ethanolysis was found to be 66.02 kJ mol^{-1}. Thermodynamic activation parameters of the reactions were evaluated based on activation complex theory (ACT) and obtained values of $\Delta G^{\ddagger}$ = 43.62 kJ mol^{-1}, $\Delta H^{\ddagger}$ = 64.10 kJ mol^{-1} and $\Delta S^{\ddagger}$ = -60.58 J $mol^{-1}K^{-1}$ supported unspontaneous, endothermic and associative mechanism of reaction.

5.1. Introduction

In previous chapter, Zr/CaO catalyst demonstrated poor reusability due to the leaching of Zr into the reaction mixture while catalyzing the reaction and thus issue of catalyst stability needs to be addressed. In present chapter, to further improve the reusability and stability of CaO based catalyst, Mo impregnated CaO catalyst was prepared and employed as reusable catalyst for the ethanolysis of non edible oils.

5.2. Experimental Section

5.2.1. Catalyst preparation

A series of molybdenum impregnated CaO was prepared by the wet impregnation method. In a standard preparation method, 10 g of calcium oxide was suspended in 40 mL of deionized water, and to this 10 mL $(NH_4)_6Mo_7O_{24}.4H_2O$ solution of desired concentration was added and stirred for 4 h. After the molybdenum incorporation over CaO, the slurry was evaporated to dryness at 120 °C for 24 h and finally calcined at 300-800 ºC. A series of Mo/CaO samples was prepared by varying the molybdenum concentration 1 to 5 wt% and calcination temperature 300 to 800 ºC. Prepared Mo/CaO was abbreviated as xMo/CaO-T, where x and T represent the molybdenum concentration (wt%) and calcination temperature (ºC), respectively.

The transesterification reactions of JO were carried out by following the method given in Chapter 4 but using the Mo/CaO catalyst. The FAEE composition as well as yield was determined by GC-MS technique. Ethyl esters obtained upon ethanolysis of JO was also characterized by ^{1}H and ^{13}C-NMR techniques as shown in Fig. A.15 and A.16 (Appendix A).

5.2.2. Catalysts reusability and leaching tests

To examine the reusability of Mo/CaO catalyst, it was employed during six successive reaction cycles under the optimized reaction conditions. Prior to the next reaction cycle, catalyst was separated from the reaction mixture by filtration, washed thoroughly with hexane to remove adsorbed compound from catalyst surface, and finally regenerated at 700 °C calcination temperature.

The concentration of dissolved catalyst into the reaction mixture was investigated by ICP-AES study. To ensure the heterogeneous nature of the catalyst, and to prove that leached metal ion has not acted like a homogeneous catalyst, a hot filtration test was carried out under optimized reaction conditions. During the test, the catalyst was removed from reaction

mixture by filtration after 1.5 h of reaction duration, and reactants were heated again for an additional period of 3.5 h.

5.3. Results and Discussion

5.3.1. Catalyst characterization

5.3.1.1. X-ray diffraction

Powder XRD patterns of CaO and Mo/CaO containing different molybdenum concentrations in the range of 0-5 wt% at 700 °C calcination temperature are illustrated in Fig. 5.1(a). The appearance of sharp peaks in diffraction patterns indicates the formation of highly crystalline materials. Commercial CaO used as support material revealed the characteristic diffraction patterns of *cubic*-calcium oxide (JCPDS 82-1691) as a major phase and *hexagonal*-$Ca(OH)_2$ as a minor phase (JCPDS 84-1275) is also present. Molybdenum impregnation in CaO was not able to initiate the formation of any new phase. No diffraction peak corresponding to molybdenum oxide or any other phase of molybdenum was observed up to 5 wt% Mo loading in CaO. This indicates that Mo has been incorporated into CaO lattice to form a solid solution of molybdenum oxide in calcium oxide.

During Mo/CaO catalyst preparation by wet chemical method in aqueous medium reaction between CaO and H_2O leads to the formation of $Ca(OH)_2$ in *hexagonal* phase as supported by the XRD pattern of catalyst heated up to 400 °C (Fig. 5.1(b)). At 500 °C calcination temperature, $Ca(OH)_2$ decomposition was initiated into CaO phase and hence both CaO and $Ca(OH)_2$ phases were observed. A further increase in calcination temperature (≥ 600 °C) leads to the formation of a pure *cubic*-CaO phase which indicated the completion of $Ca(OH)_2$ decomposition. Similar XRD patterns were observed for Mo/CaO calcined up to 800 °C to indicate that an increase in the calcination temperature beyond 600 °C has not initiated any phase change in Mo/CaO.

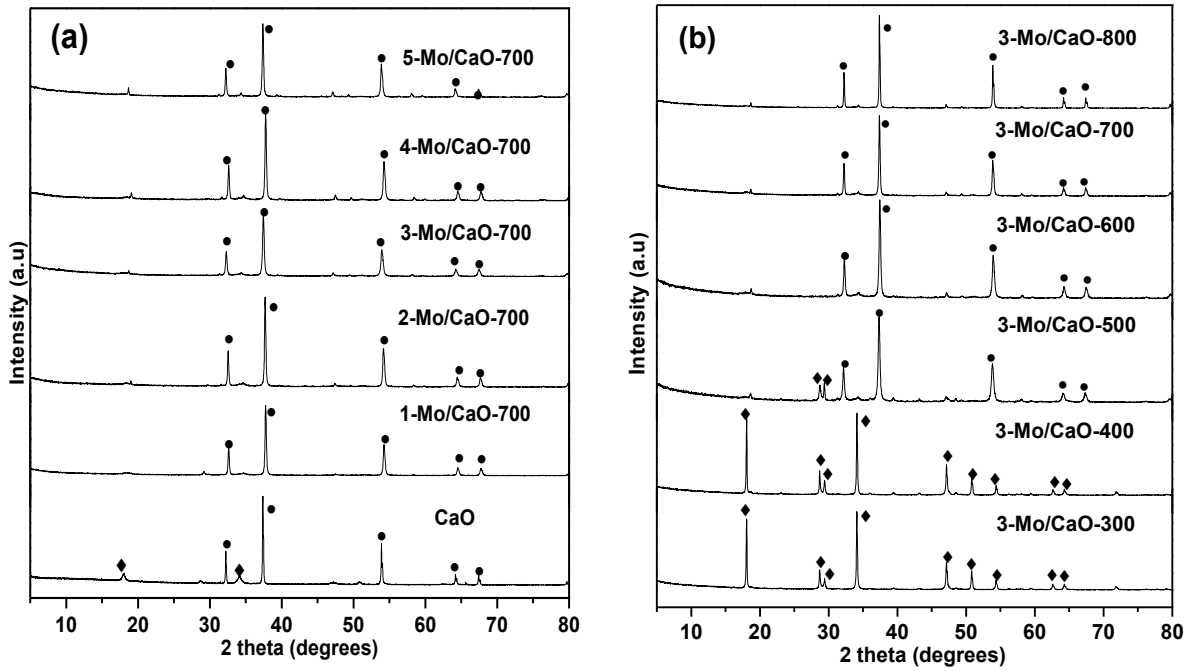

Fig. 5.1. XRD pattern of Mo/CaO with varying (a) Mo concentration (0-5%) and (b) calcination temperature (300-800 °C) (♦ = $Ca(OH)_2$; • = CaO).

The crystallize size of catalysts at varying Mo loadings and calcination temperature was calculated by Scherrer equation. The catalytic support CaO has crystallite size of 33.0 nm. With increase in molybdenum loading (1-3 wt%) on CaO the crystallite size of the catalyst decreases (33.0-22.5 nm) as shown in Table 5.1. This may be due to the small ionic radius of molybdenum (79 pm) as compared to calcium (114 pm). With increase in calcination temperature (300-500 °C) the crystallite size of the catalyst decreases may be due to the removal of water molecules from the vacant sites of Mo/CaO lattice as well as partial decomposition of $Ca(OH)_2$ at 500 °C (Wong *et. al.*, 2014). Further increase in calcination temperature (600-800 °C) was not found to bring any significant variation in crystallite size as no change in catalyst structure or phase was observed in this temperature range.

Table 5.1. Comparison of crystallite size of Mo/CaO at varying loadings of molybdenum and calcination temperature.

Catalyst	Crystallite size (nm)
CaO	33.0
1Mo/CaO-700	26.8
2Mo/CaO-700	26.8
3Mo/CaO-700	22.5
4Mo/CaO-700	25.2
5Mo/CaO-700	25.2
3Mo/CaO-300	33.1
3Mo/CaO-400	32.6
3Mo/CaO-500	22.8
3Mo/CaO-600	22.5
3Mo/CaO-800	21.5

5.3.1.2. Thermogravimetric analysis

TG curve of uncalcined Mo/CaO catalyst is illustrated in Fig. 5.2, which shows two weight loss regions in the temperature ranges of 437-500 °C and 500-700 °C. The first or major weight loss region (19.22 %) corresponds to the decomposition of $Ca(OH)_2$ into CaO phase. The second weight loss region (5.79 %) ascribed to the decomposition of $CaCO_3$ which may form due to the reaction of surface CaO with atmospheric CO_2. In order to avoid the presence of $CaCO_3$, catalyst was prepared at 700 °C calcination temperature.

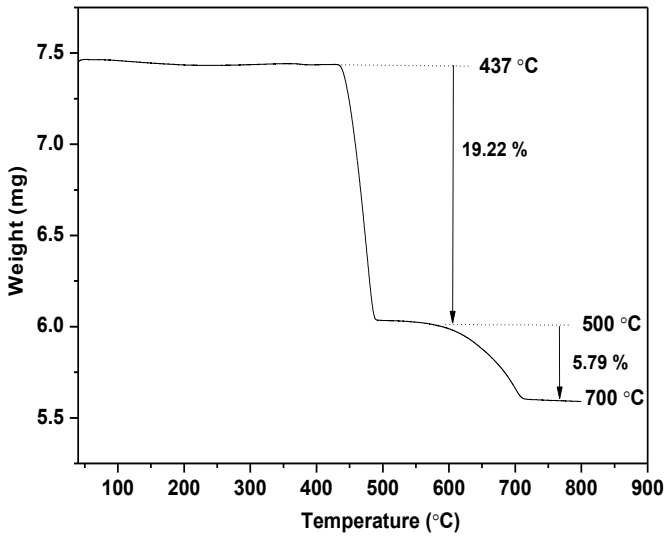

Fig. 5.2. TG curve of uncalcined 3Mo/CaO catalyst.

5.3.1.3. Electron Microscopy studies

The SEM and TEM images were recorded to determine the morphology and particle size of prepared catalyst. The SEM micrograph shows the clusters of irregular shaped crystalline

particles ranging from 0.2-1.0 μm in size which has formed due to the agglomeration of Mo/CaO particles as shown in Fig. 5.3(a). TEM image of these particles indicates that each cluster consist of even smaller particles of 25-40 nm size with inconsistent geometries as shown in Fig. 5.3(b). Thus powder XRD as well as TEM study supported the formation of nano structures of Mo/CaO catalyst. Qualitative analysis by SEM-EDS study supported the presence of ~2.7 wt% Mo in 3-Mo/CaO-700 catalyst.

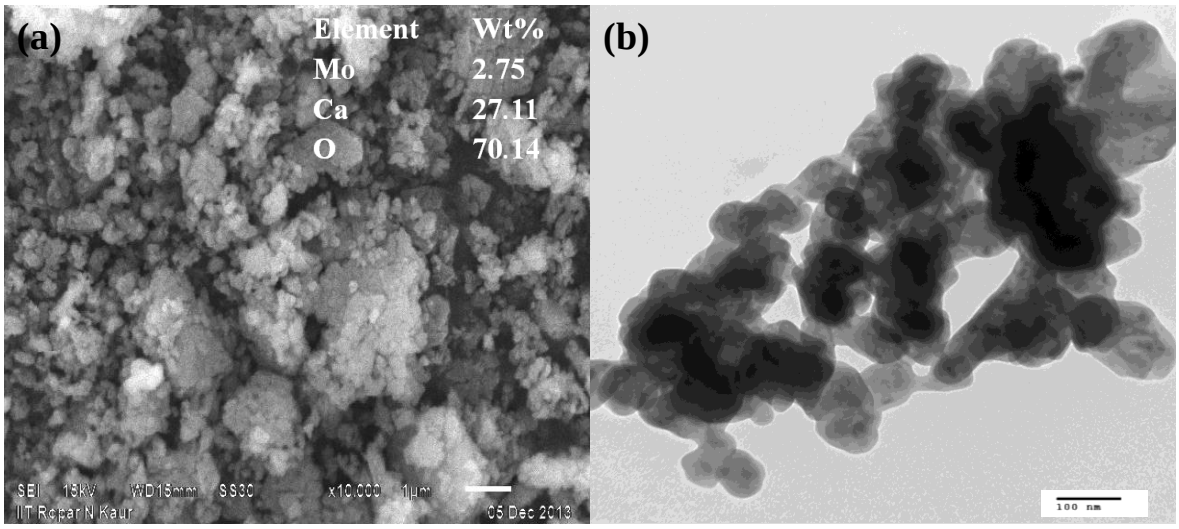

Fig. 5.3. (a) SEM and (b) TEM image of 3Mo/CaO-700 catalyst.

5.3.1.4. BET surface area and porosity measurements

As given in Table 5.2, the measured BET surface area of the commercially available CaO was found to be 3.90 m^2/g and an increase in surface area was observed upon Mo impregnation. It can be clearly seen from Table 5.2, that the addition of 0-3 wt% molybdenum increases the surface area from 3.90 to 44.29 m^2/g, however, a further increase of Mo content (up to 5 wt%) resulted in a decrease in surface area. Thus, up to 3 wt% molybdenum dispersed homogeneously into the CaO matrix and a further increase in Mo concentration blocked the micropores of the catalyst. The blockage of pore size is further supported by the larger pore size with 5 wt% Mo loading.

Table 5.2. Surface properties of Mo/CaO catalyst.

Catalyst	Surface area (m^2/g)	Pore size (nm)	Pore volume (cm^3/g)
CaO	3.90	Not determined	Not determined
1-Mo/CaO-700	27.80	32.68	0.227
3-Mo/CaO-700	44.29	20.14	0.223
5-Mo/CaO-700	28.83	28.76	0.207

The nitrogen adsorption-desorption isotherms (Fig. 5.4) indicate a type IV isotherm profile for Mo/CaO catalysts at different loading of molybdenum with hysteresis loop H3, at relative pressure of about 0.7-1.0; characteristic to the mesoporous materials.

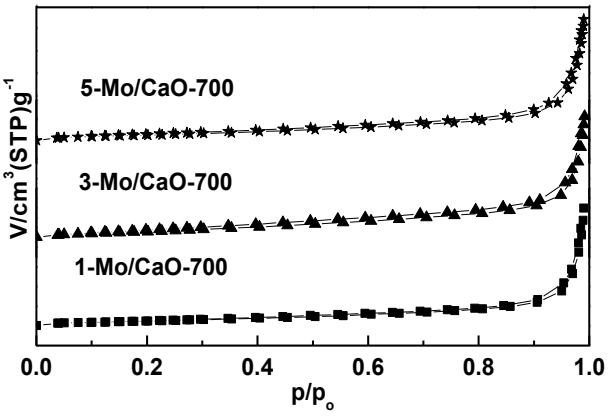

Fig. 5.4. N_2 adsorption-desorption isotherms for Mo/CaO catalyst at varying molybdenum loading.

5.3.1.5. XPS analysis

The electronic state of the metal ions present in catalyst was determined by XPS analysis as shown in Fig. 5.5. The peaks corresponding to O^{2-} (1s), Ca^{2+} (2p) and Mo^{6+} (3d) were observed at 533, 351 and 231 eV, respectively (Xie and Zhao, 2014). Thus XPS study supported the presence of molybdenum over catalyst surface, although same could not be detected by XRD study due to the homogeneous solid solution formation of molybdenum in calcium oxide.

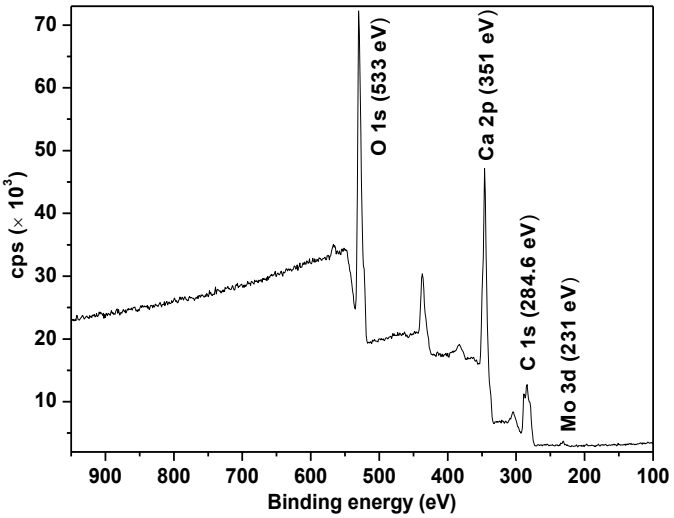

Fig. 5.5. Wide scan XPS spectra of 3Mo/CaO-700.

5.3.2. Catalytic activity

The commercially available CaO was found to show poor activity towards the ethanolysis of non-edible oils and hence, required relatively longer reaction duration (> 10 h) to achieve the equilibrium. Moreover, due to relatively high solubility of CaO in alcohol biodiesel must be washed to remove the dissolved catalyst (TeO *et al.*, 2014). The activity as well as stability of CaO was improved upon molybdenum impregnation. As shown in Table 5.3, with the increase in molybdenum loading from 1 to 3 wt% at 700 °C calcination temperature, the catalytic activity (TOF) was found to increase due to the increase in catalyst basic sites as well as surface area. A further increase in molybdenum concentration was not found to increase the basic sites and hence, no gain in activity was observed.

The optimized calcination temperature for the catalytic activity was established by preparing the catalyst in the range of 300-800 °C calcination temperature. Up to 400 °C, Bronsted site predominated in the catalyst due to the presence of $Ca(OH)_2$ and at ≥ 600 °C , these sites converted into Lewis site due to the decomposition of $Ca(OH)_2$ into CaO. Transesterification reaction could be effectively catalyzed by Lewis base sites rather than Bronsted sites (Yan *et al.*, 2009). In order to remove the possibility of active site blockage due to $CaCO_3$ formation, the catalyst was prepared at 700 °C calcination temperature, although its activity as well as basic site strength was found to be similar to the catalyst prepared at 600 °C (Table 5.3).

Table 5.3. Comparison of basicity and TOF of Mo/CaO at varying loadings of molybdenum and calcination temperature.

Catalyst	Indicators						TOF (h^{-1})
	Neutral red pK_a = 6.8	Bromothymol blue pK_a = 7.2	Phenolphthalein pK_a = 9.3	Nile blue pK_a = 10.1	Trapeolin pK_a =11.1	f_m (mmol/g of catalyst)	
CaO	0.28	0.22	0.10	0.14	-	0.74	0.95
1Mo/CaO-700	0.58	0.47	0.25	0.35	-	1.65	1.35
2Mo/CaO-700	1.34	0.82	0.50	0.48	0.73	3.87	2.47
3Mo/CaO-700	1.56	1.40	1.28	0.56	1.04	5.84	3.05
4Mo/CaO-700	1.54	1.42	1.29	0.56	1.02	5.80	3.03
5Mo/CaO-700	1.51	1.43	1.27	0.52	1.00	5.76	3.00
3Mo/CaO-300	0.32	0.25	0.14	0.17	-	0.88	1.12
3Mo/CaO-400	0.59	0.48	0.27	0.38	-	1.72	1.81
3Mo/CaO-500	1.00	0.70	0.57	0.43	0.64	3.34	2.79
3Mo/CaO-600	1.53	1.43	1.26	0.57	1.01	5.80	3.02
3Mo/CaO-800	1.55	1.42	1.26	0.57	1.03	5.83	3.03

$TOF = mol_{actual}/(f_m \times m_{cat} \times t)$ where mol_{actual}, m_{cat}, t and f_m were the moles of FAEE, mass of catalyst, reaction time and total basicity of catalyst (in mmol/g of catalyst). **Reaction conditions:** ethanol to oil molar ratio of 12:1 at 65 ºC in presence of 5 wt% catalyst (catalyst/oil).

The catalyst prepared with 3 wt% molybdenum loading at 700 °C calcination temperature was found to be most active and hence selected for detailed study.

5.3.3. Mass transfer limitation study

Vegetable oils and ethanol are completely immiscible and hence mass transfer limitations could affect the FAEE yield (Dube *et al.*, 2007). To establish the stirring speed at which the mass transfer limitations are minimal during 3Mo/CaO-700 catalyzed transesterification reaction, a series of ethanolysis reaction were performed at 50-650 rpm stirring speed. As could be seen from Fig. 5.6, initially the reaction rate increases with the increase in stirring speed and at ≥ 450 rpm the reaction rate was found to be maximum and constant. Thus all experiments in present study were carried out at a stirring speed of 450 rpm to exclude the effect of mass transfer phenomenon on reaction rate.

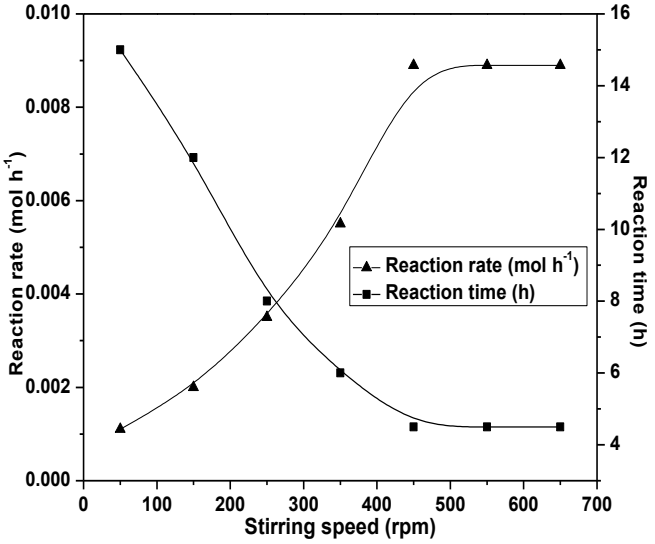

Fig. 5.6. Effect of stirring speed on 3Mo/CaO-700 catalyzed transesterification of JO. **Reaction conditions:** ethanol to oil molar ratio of 12:1 at 65 ºC in presence of 5 wt% catalyst (catalyst/oil).

5.3.4. Effect of the reaction parameters

To optimize the reaction parameters for the better catalytic activity, transesterification reactions were conducted by varying catalyst concentration (1-6 wt%), ethanol to oil molar ratio (3:1-15:1) and reaction temperature (35-75 ºC). The effect of these parameters on the FAEE yield are provided in Fig. 5.7 and on the basis of this study, a 12:1 ethanol to oil molar ratio, 65 ºC reaction temperature and 5 wt% catalyst (with respect to oil) were found to be the optimum conditions for 3Mo/CaO-700 catalyzed transesterification of JO.

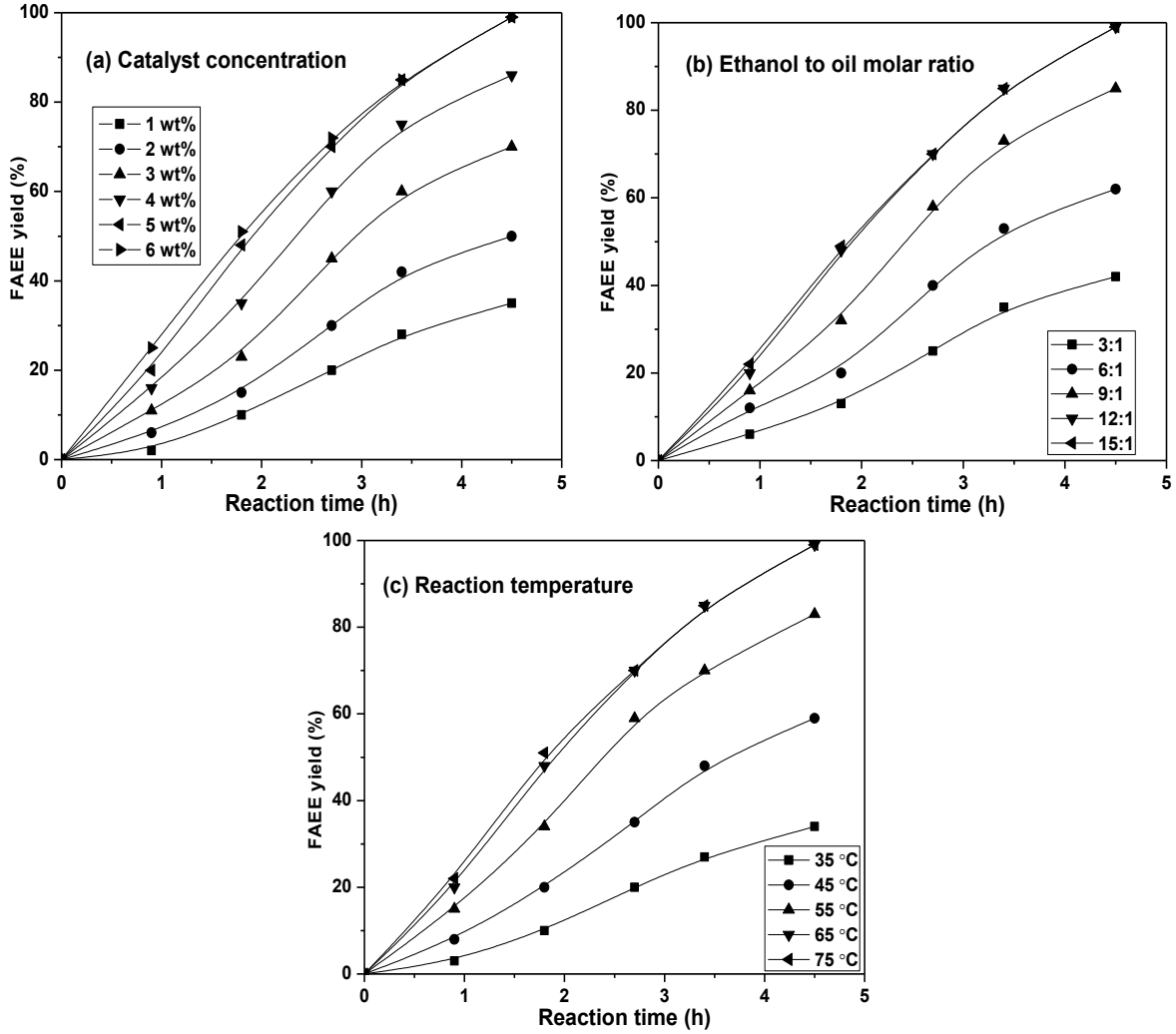

Fig. 5.7. Effect of reaction parameters on 3Mo/CaO-700 catalyzed transesterification of JO. **Reaction conditions:** (a) ethanol to oil molar ratio of 12:1 at 65 ºC reaction temperature (b) Reaction temperature at 65 ºC, in presence of 5 wt% of catalyst with respect to oil (c) ethanol to oil molar ratio of 12:1 in presence of 5 wt% of catalyst with respect to oil.

5.3.5. Tolerance towards water and FFA

The presence of water and FFA in case of low quality feedstock, such as nonedible or waste cooking oils, is inevitable although both are found to deactivate the homogeneous base catalysts *via* saponification in traditional biodiesel production processes. Presence of soap emulsifies the reaction mixture, which make the separation of fatty acid ester, glycerol and catalyst extremely difficult (Yan *et al.*, 2009).

In order to examine the moisture tolerance of catalyst, transesterification reaction of JO was performed in presence of 0.5-6.5 wt% water contents (with respect to oil). Fig. 5.8(a) indicates that presence of up to 2.5 wt% water was not found to make any negative effect on catalyst activity. A further increase in water (3.0-6.5 wt%) was found to reduce the catalyst activity owing to the conversion of Lewis basic sites (–O–) into Bronsted basic sites (–OH)

due to the reaction of water molecules with catalyst. The Bronsted basic sites were found to be less active towards the transesterification than corresponding Lewis basic sites. A comparison of XRD patterns (Fig. 5.8(b)) of fresh catalyst with the catalyst exposed to moisture also supported the conversion of CaO phase into $Ca(OH)_2$ phase.

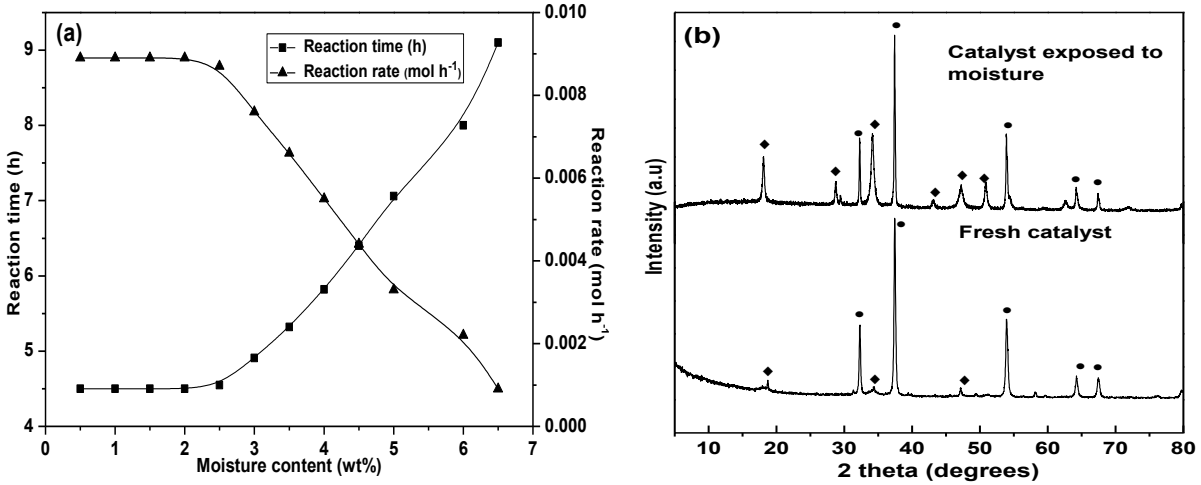

Fig. 5.8. (a) Effect of moisture content on the 3Mo/CaO-700 catalyzed transesterification of JO (reaction time is the time required to achieve > 99% FAEE yield) (b) Comparison of XRD spectra of fresh catalyst and catalyst exposed to moisture (● = CaO, ◆ = $Ca(OH)_2$).

FFA content in oils not only deactivates the homogeneous alkali catalyst *via* saponification but also found to reduce the activity of heterogeneous catalysts. To evaluate the effect of presence of FFA on 3Mo/CaO-700 activity, transesterification of VOs containing up to 18.1 wt% FFA was performed and results are shown in Fig. 5.9. The activity of the catalyst was found to decrease as FFA content in oil increases, nevertheless > 99% FAEE yield could be maintained by increasing the reaction duration. The reduction in catalytic activity may be attributed to the strong interaction of highly polar acetate group (of fatty acid) with the catalyst surface (Ca^{2+}) to result the partial blocking of the active sites (Kaur and Ali, 2014a).

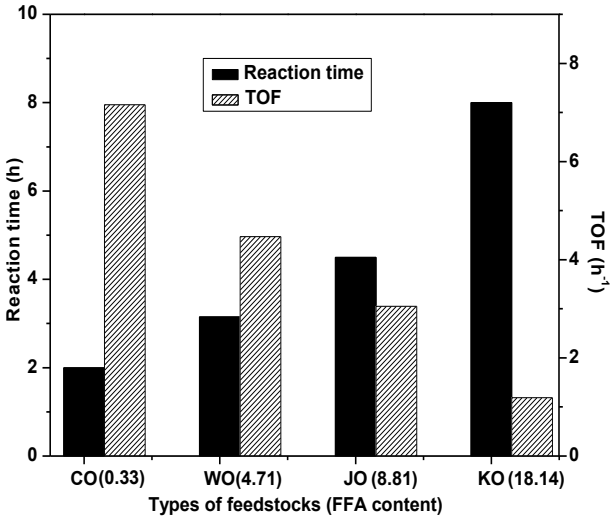

Fig. 5.9. Effect of FFA contents on the 3Mo/CaO-700 catalyzed transesterification of different feed stocks (reaction time is the time required to achieve > 99% FAEE yield). **Reaction conditions:-** Ethanol to oil molar ratio of 12:1 at 65 ºC reaction temperature in presence of 5 wt% (catalyst/oil) catalyst.

5.3.6. Reusability and stability

Reusability and ease of separation from the reaction mixture are few important advantages of a heterogeneous catalyst over homogeneous one. As shown in Fig. 5.10, the catalyst could be reused up to five times without significant loss in activity, however, in sixth run only partial conversion was achieved.

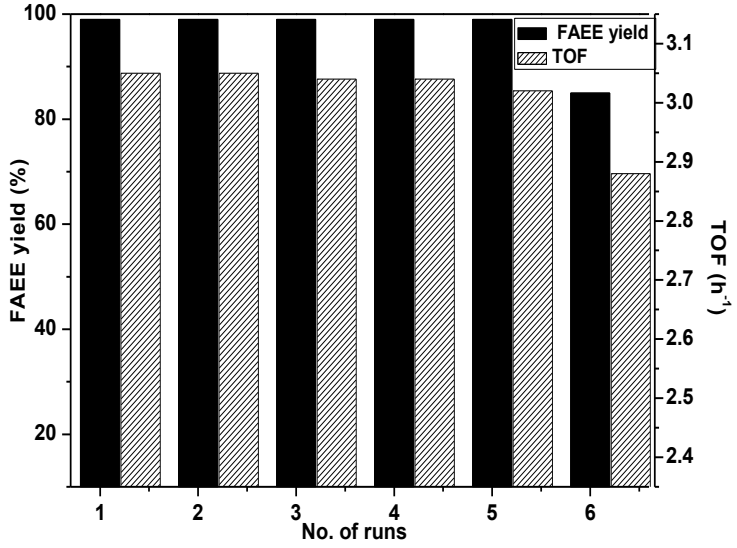

Fig. 5.10. Reusability study of catalyst.

A comparison of IR spectrum (Fig. 5.11(a)) of the fresh and used catalyst rule out the possibility of adsorption of organic molecule over the catalyst surface, which otherwise was found to reduce the catalytic activity (Singh *et al.*, 2014). Change in catalyst structure, during

repeated use and activation process, could be another reason for the loss of activity. The XRD study (Fig. 5.11(b)) of fresh and used catalyst validated that upon repeated use CaO phase has partially changed into $Ca(OH)_2$.

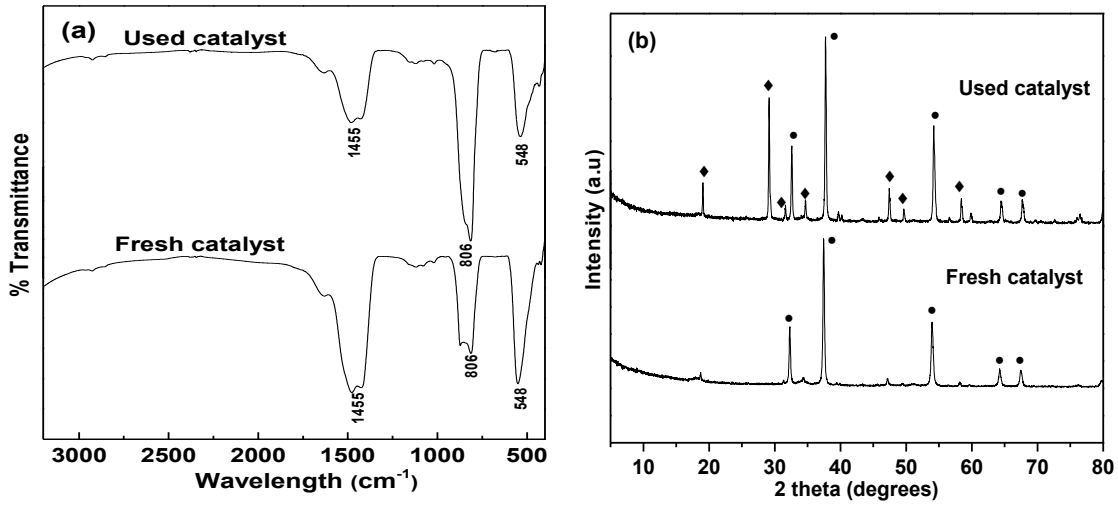

Fig. 5.11. Comparison of (a) XRD and (b) FT-IR of fresh and used catalyst. (● = CaO, ◆ = $Ca(OH)_2$).

The metal analysis supported minute leaching of Mo and Ca in FAEE (1.23 and 0.25 ppm, respectively) as well as in glycerol (4.12 and 2.28 ppm, respectively). Thus catalyst is stable although small amount of metal is lost during the catalytic run, which could be another reason for the loss of activity. To validate that dissolved metal ions have not acted as homogeneous catalyst, hot filtration test was performed (Fig. 5.12). No significant gain in FAEE yield was obtained when the reaction was continued after filtering out the catalyst to rule out the possibility of homogeneous contribution in catalytic activity by the dissolved metal ions and to support a truly heterogeneous mode of action of Mo/CaO catalyst.

Therefore, the gradual loss of the catalytic activity could be attributed to the (i) structural changes in catalyst and (ii) partial loss of the Mo and Ca from 3Mo/CaO-700 during its repeated use.

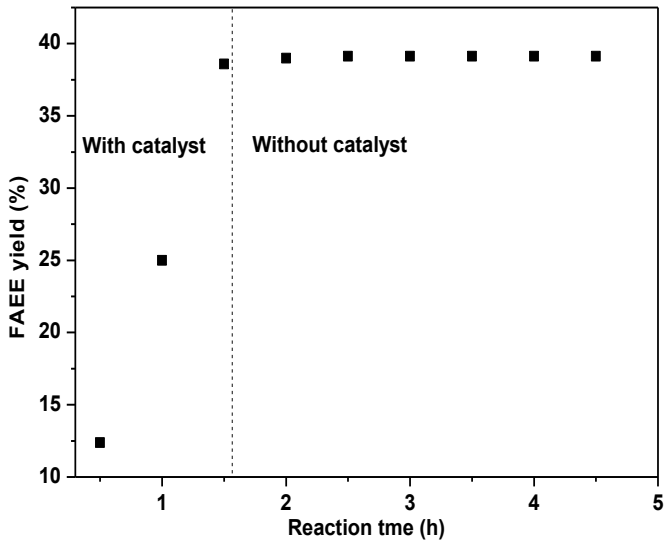

Fig. 5.12. Hot filtration test for 3Mo/CaO-700 catalyzed transesterification of JO.

5.3.7. Kinetics and thermodynamic studies

Transesterification is generally assumed to follow pseudo-first-order kinetics as alcohol in such reactions are employed in excess to the required stoichiometric amount of 3:1 alcohol to oil molar ratio. In this study, ethyl esters yield with respect to time was followed to study the reaction kinetics by performing the reaction under optimized reaction conditions. Since a 12:1 ethanol to oil molar ratio was employed during the reaction, the kinetics of 3Mo/CaO-700 catalyzed ethanolysis could safely be assumed to follow (pseudo) first order.

The linear nature of *– ln(1–X) versus t* plot supported that the reaction has followed the (pseudo) first order rate law (Fig. 5.13(a)). The apparent first order rate constant from the plot was observed 1.01 h^{-1} at 65 ºC.

To calculate the activation energy, reactions were carried out in the temperatures range of 35-65 ºC. The values of E_a and A from ln k *versus* 1/T plot (Fig. 5.13(b)) were found to be 66.02 kJ mol^{-1} and 9.2×10^9 h^{-1}, respectively.

The observed E_a value in present study (66.02 kJ mol^{-1}) was found within the range of reported values (26-82 kJ mol^{-1}) for transesterification reaction catalyzed by heterogeneous catalysts (Kaur and Ali, 2014b). A value of E_a > 25 kJ mol^{-1} also supported that 3Mo/CaO-700 catalyzed transesterification is a chemically controlled reaction and not controlled by mass transfer limitations (Patel and Brahmkhatri, 2013).

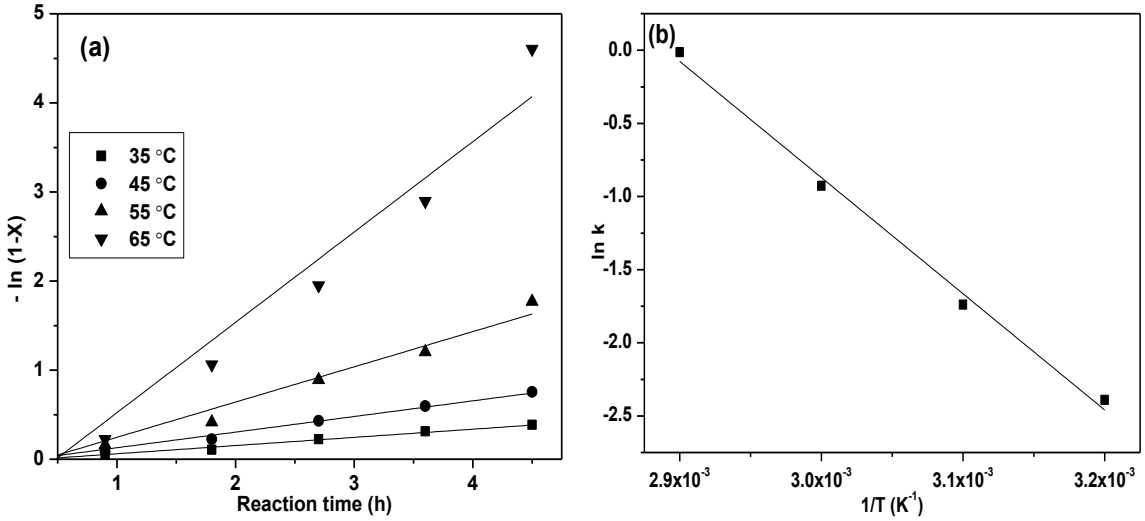

Fig. 5.13. Kinetic study of transesterification of JO with ethanol over 3Mo/CaO-700 catalyst. (a) Plots of –ln(1–X) *vs* time at different temperatures (b) Arrhenius plot of ln k *vs* 1/T. **Reaction conditions:** ethanol to oil molar ratio of 12:1 and 5 wt% of 3Mo/CaO-700 with respect to oil.

The thermodynamic parameters such as enthalpy ($\Delta H^{\ddagger}$) and entropy ($\Delta S^{\ddagger}$), were not frequently studied for the transesterification reactions catalyzed by heterogeneous catalyst. In present study to evaluate these parameters Eyring equation 2.6 (Chapter 2) was applied.

Fig. 5.14 depicts the Eyring plot of Mo/CaO catalyzed transesterification of JO and from this plot the value of $\Delta H^{\ddagger}$ was found to be 64.10 kJ mol^{-1}. The positive value indicates that reaction is endothermic and thus an external heating source is needed to raise the energy level of reactants so that they could be transformed to the transition state. The value of $\Delta S^{\ddagger}$ was found to be negative (-60.58 J $mol^{-1}K^{-1}$) to suggest that associative mechanism is followed in which reactant species might have joined together over catalyst surface to form a more ordered transition state.

The Gibb's free energy of activation ($\Delta G^{\ddagger}$) was determined (Galvan *et al.*, 2013) at 65 °C from fundamental thermodynamics equation 5.1:

$$\Delta G^{\ddagger} = \Delta H^{\ddagger} - T\Delta S^{\ddagger} \qquad (5.1)$$

The $\Delta G^{\ddagger}$ value was found to be 43.62 kJ mol^{-1}, to indicate unspontaneous nature of the reaction in which transition state is having higher energy level than reactants.

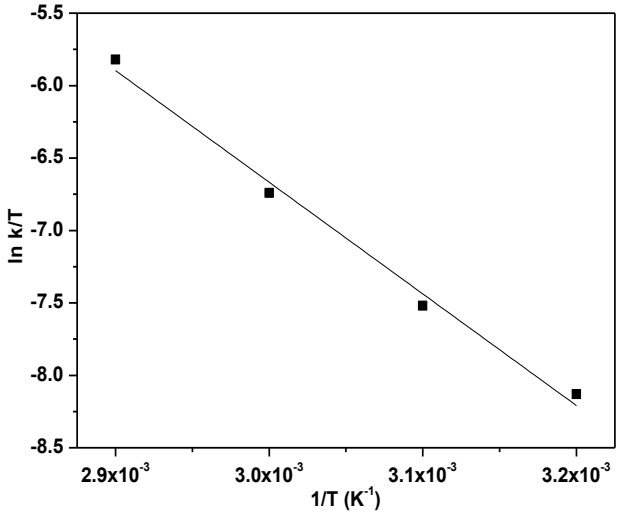

Fig. 5.14. The Eyring plot of 3Mo/CaO-700 catalyzed transesterification of JO.

5.3.8. Koros–Nowak Criterion test

Koros–Nowak criterion test was performed to find out whether reaction rates were free from mass transfer effects (Madon and Boudart, 1902). In present study the reactions were carried out in presence of two catalysts in which concentration of active sites over the catalyst has been changed without changing the total active (basic) sites. As shown in Fig. 5.15, at similar conversion levels, TOFs of both the catalysts were found to be almost similar to prove the absence of mass diffusion limitations in Mo/CaO catalyzed reaction.

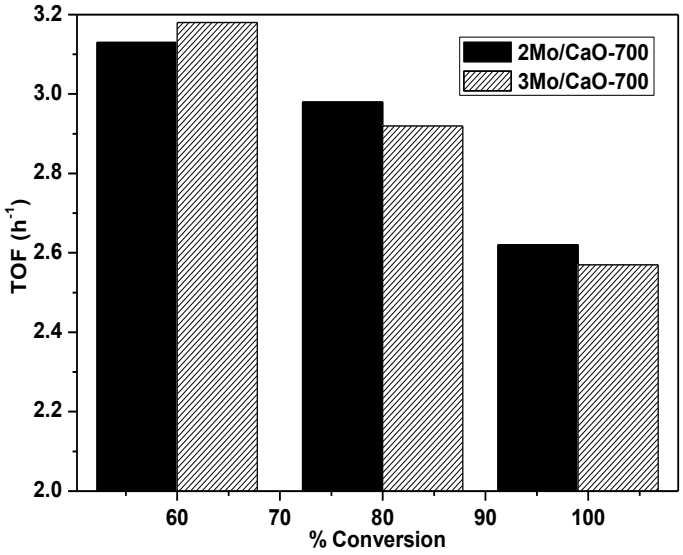

Fig. 5.15. A plot of TOF *vs* % conversion for the 2Mo/CaO-700 and 3Mo/CaO-700 catalyzed ethanolysis of JO. **Reaction conditions:** ethanol to oil molar ratio; 12:1 at 65 °C and catalyst concentration; either 5 wt% of 3Mo/CaO-700 or 7.5 wt% of 2Mo/CaO-700.

5.3.9. Fuel properties of biodiesel

Physicochemical properties of the biodiesel depend upon their fatty acid composition which could be evaluated by GC-MS study. Gas chromatogram of FAEE prepared from JO is provided in Fig. 5.16 and corresponding fatty acid ester composition is listed in Table 5.4.

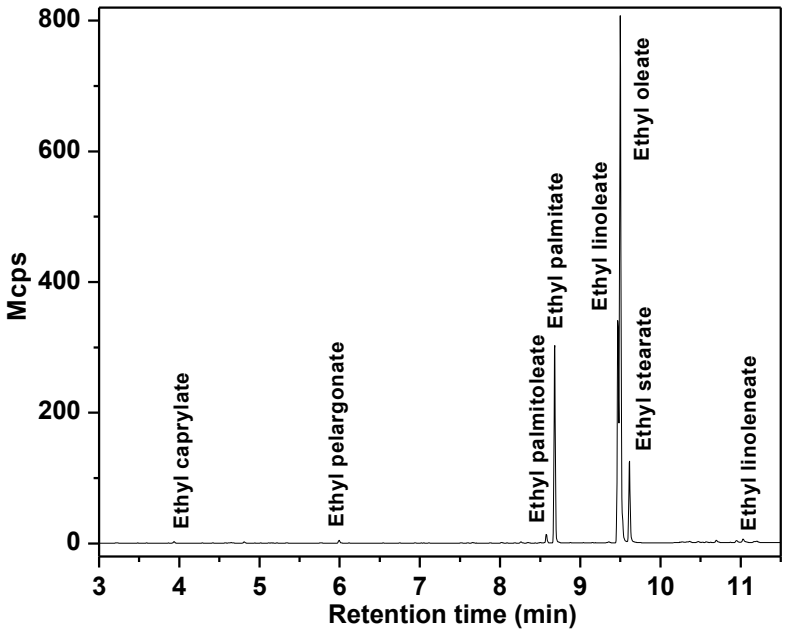

Fig. 5.16. Gas chromatogram of FAEE.

Total FAEE content was observed as high as 99.37 wt%, consisting of 26.66 wt% saturated and 72.71 wt% unsaturated fatty acid esters. A high percentage of unsaturated fatty acid ester indicates better cold flow properties of biodiesel even at low temperature (Lotero *et al.*, 2005).

Table 5.4. Composition of JO derived FAEE.

S.No.	Retention time (min)	Composition; Molecular formula	Corresponding acid (Cx:y)	Wt %
1	3.93	Caprylic acid ethyl ester; $C_{10}H_{20}O_2$	Caprylic acid (C8:0)	0.24
2	5.99	Pelargonic acid ethyl ester; $C_{11}H_{22}O_2$	Pelargonic acid (C9:0)	0.36
3	8.57	Palmitoleic acid ethyl ester; $C_{18}H_{34}O_2$	Palmitoleic acid (C16:1)	1.04
4	8.68	Palmitic acid ethyl ester; $C_{18}H_{36}O_2$	Palmitic acid (C16:0)	18.04
5	9.47	Linoleic acid ethyl ester; $C_{20}H_{36}O_2$	Linoleic acid (C18:2)	20.36
6	9.49	Oleic acid ethyl ester; $C_{20}H_{38}O_2$	Oleic acid (C18:1)	50.67
7	9.61	Stearic acid ethyl ester; $C_{20}H_{40}O_2$	Stearic acid (C18:0)	8.02
8	11.03	Linolenic acid ethyl ester;$C_{20}H_{34}O_2$	Linolenic acid (C20:3)	0.64

x:y = number of carbon atoms:number of double bods

5.4. Conclusions

Molybdenum impregnated calcium oxide has been synthesized *via* wet impregnation method and found effective for the transesterification of non edible oils having FFA contents as high as 18.1 wt%. The prepared catalyst under mild reaction conditions (Reaction temperature 65 °C, catalyst amount 5 wt% and ethanol to oil molar ratio of 12:1) demonstrated > 99 % FAEE yield in 4.5 h of reaction duration with low leaching amounts of Mo and Ca in the reaction mixture. The catalyst was recovered and reused during 5 successive catalytic runs; maintaining > 99% activity. The Koros-Nowak test demonstrated that catalytic activity was independent from the diffusion limitations. The values of thermodynamic activation parameters $\Delta G^{\ddagger}$, $\Delta H^{\ddagger}$ and $\Delta S^{\ddagger}$ were found out to be 43.62 kJ mol^{-1}, 64.10 kJ mol^{-1} and -60.58 J $mol^{-1}K^{-1}$, respectively, which show that reaction was unspontaneous, endothermic and endergonic in nature.

References

Dube, M. A.; Tremblay, A. Y.; Liu, J.; Biodiesel production using a membrane reactor. *Bioresour. Technol.*, **2007**, 98, 639-647.

Galvan, D.; Orives, J. R.; Coppo, R. L.; Silva, E. T.; Angilelli K. G.; Borsato, D.; Determination of the kinetics and thermodynamics parameters of biodiesel oxidation reaction obtained from an optimized mixture of vegetable oil and animal fat. *Energy Fuel*, **2013**, 27, 6866-6871.

Kaur, N.; Ali, A.; Kinetics and reusability of Zr/CaO as heterogeneous catalyst for the ethanolysis and methanolysis of *Jatropha crucas* oil. *Fuel Process. Technol*., **2014a**, 119, 173-184.

Kaur, N.; Ali, A.; One-pot transesterification and esterification of waste cooking oil via ethanolysis using Sr:Zr mixed oxide as solid catalyst. *RSC Adv.*, **2014b**, 4, 43671-43681.

Lotero, E.; Liu, Y.; Lopez, D. E.; Suwannakarn, K.; Bruce, D. A.; Goodwin, J. G.; Synthesis of biodiesel via acid catalysis. *Ind. Eng. Chem. Res.*, **2005**, 44, 5353-5363.

Madon, R. J.; Boudart, M.; Experimental criterion for the absence of artifacts in the measurement of rates of heterogeneous catalytic reactions. *Ind. Eng. Chem. Fundam*., **1902**, 21, 438-447.

Patel, A.; Brahmkhatri, V.; Kinetic study of oleic acid esterification over 12 tungstophosphoric acid catalyst anchored to different mesoporous silica supports. *Fuel Process. Technol.*, **2013**, 113, 141-149.

Singh, D.; Bhoi, R.; Ganesh, A.; Mahajani, S.; Synthesis of biodiesel from vegetable oil using supported metal oxide catalysts. *Energy Fuel*, **2014**, 28, 2743-2753.

Teo, S. H.; Rashid, U.; Yap, Y. H. T.; Biodiesel production from crude *Jatropha Curcas* oil using calcium based mixed oxide catalysts. *Fuel*, **2014**, 136, 244-252.

Wong, Y. C.; Tan, Y. P.; Yap, Y. H. T.; Ramli, I.; Effect of calcination temperatures of CaO/Nb_2O_5 mixed oxides catalysts on biodiesel production. *Sains Malays.*, **2014**, 43, 783-790.

Xie, W.; Zhao, L.; Heterogeneous $CaO\text{-}MoO_3$-SBA-15 catalysts for biodiesel production from soybean oil. *Energy Convers. Manage*., **2014**, 79, 34-42.

Yan, S.; Kim, M.; Salley, S. O.; Ng, K. Y. S.; Oil transesterification over calcium oxides modified with lanthanum. *Appl. Catal. A: Gen.*, **2009**, 360, 163-170.

Yan, S.; Salley, S. O.; Simon, K. Y.; Simultaneous transesterification and esterification of unrefined or waste oils over $ZnO\text{-}La_2O_3$ catalysts *Appl. Catal. A: Gen.*, **2009**, 353, 203-212.

Lithium Zirconate as Solid Catalyst for Simultaneous Esterification and Transesterification of Low Quality Triglycerides

Contents *Page No.*

Abstract: Alkali metals (Li, Na and K) doped zirconium oxide were prepared (Li/ZrO_2, Na/ZrO_2 and K/ZrO_2) by wet chemical route and used as active heterogeneous catalyst for the transesterification of waste cottonseed oil with ethanol and methanol to produce fatty acid ethyl and methyl esters, respectively. The catalyst characterization supports the formation of lithium zirconate single phase in case of Li/ZrO_2 and it was able to catalyze simultaneous esterification and transesterification of high free fatty acid containing vegetable oils. The reaction conditions, such as catalyst concentration, reaction temperature, the molar ratio of alcohol/oil, and stirring speed were optimized in presence of Li/ZrO_2 catalyst. The catalyst activity was found to be a function of its basic sites which in turn depend on calcinations temperature and lithium content of the catalyst. A pseudo first order kinetic equation was applied to evaluate the kinetic parameters for the transesterification of waste cottonseed oil with methanol and ethanol. The activation energy (E_a) for the Li/ZrO_2 catalyzed methanolysis and ethanolysis was found to be 40.8 kJ mol^{-1} and 43.1 kJ mol^{-1}, respectively. The catalyst could be reused up to 9 cycles without significant loss of performance as > 90 % fatty acid alkyl ester yield was maintained.

6.1. Introduction

In order to develop a catalyst which could catalyze the simultaneous esterification as well as transesterification of vegetable oil having high concentration of FFA, lithium doped ZrO_2 was prepared *via* wet impregnation method. The prepared Li/ZrO_2 catalyst was successfully employed for one-pot production of biodiesel from vegetable oil having FFA content as high as 18.1 wt% via esterification and transesterification.

6.2. Experimental Section

6.2.1. Catalyst preparation

Alkali doped zirconia was prepared *via* wet chemical route and in a typical preparation 10 g of zirconium oxide was suspended in 50 ml deionized water and to this 30 ml aqueous solutions of lithium hydroxide, or sodium nitrate, or potassium nitrate of desired concentrations was added. The resulted mixture was stirred for 4 h, initially dried at 120 ºC for 12 h, and finally calcined at desired temperature (300–800 ºC) for 4 h.

Prepared samples were designated as x-M/ZrO_2-T, where M, x and T represent the type of alkali dopant, its content (wt%) and calcination temperature (ºC), respectively.

The transesterification reactions of WO were carried out by following the same procedure as given in Chapter 4, but using Li/ZrO_2 catalyst. The FAME and FAEE yield obtained upon methanolysis and ethanolysis of WO respectively, was characterized and quantified by ^{1}H-NMR techniques as shown in Fig. A.17 (Appendix A).

6.3. Results and Discussion

6.3.1 Catalyst characterization

6.3.1.1. X-ray diffraction

The XRD patterns of Li/ZrO_2 with varying lithium content (5-25 wt%) are shown in Fig 6.1(a). At 5 wt% lithium content mixed phases of *monoclinic* (JCPDS card no. 75-2157) and *tetragonal*-lithium zirconate (JCPDS card no. 41-0324) and *monoclinic* zirconia (JCPDS card no. 88-2390) has formed. A gradual increase in lithium content was found to increase the amount of *monoclinic* and *tetragonal*-lithium zirconate and at 20 wt% Li content only these two phases remain present. Comparison of the XRD patterns of 20 wt% Li doped ZrO_2 at varying calcination temperature (300-800 °C) is shown in Fig. 6.1(b). At 300 °C mixed phases of the ZrO_2 and LiOH (JCPDS card no. 85-1064) were found to exist. An increase in calcination temperature found to initiate the formation of lithium zirconate (Li_2ZrO_3) due to

the solid state reaction between ZrO_2 and LiOH. A similar diffraction pattern for the Li_2ZrO_3, prepared by chemical method, was reported by Xiao *et al.* (2011). At 700 °C a mixed phase of *monoclinic* and *tetragonal*-lithium zirconate forms and other phases remain absent, thus supporting the completion of reaction between ZrO_2 and LiOH. A further increase in calcination temperature (800 °C) was found to initiate the formation of a new phase of *monoclinic* Li_4ZrO_4 (JCPDS card no. 20-0645).

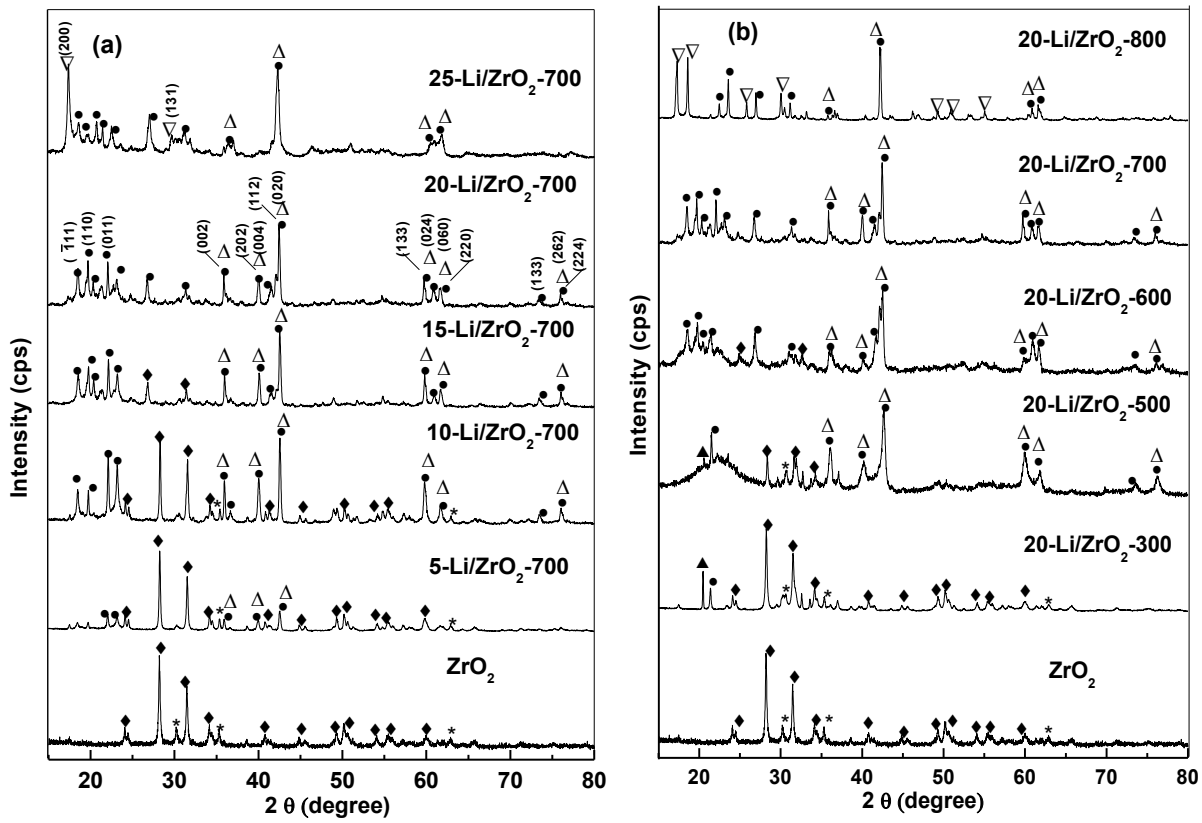

Fig. 6.1. Comparison of XRD patterns of Li/ZrO_2 at varying (a) lithium concentration (b) calcination temperature. (♦ = *monoclinic* zirconia, ∗ = *tetragonal* zirconia, • = *monoclinic* Li_2ZrO_3, Δ = *tetragonal* Li_2ZrO_3,∇ = *monoclinic* Li_4ZrO_4, ▲ = LiOH).

The XRD patterns of 20 wt% Li, or Na or K doped zirconium oxide (calcined at 700 °C) are compared in Fig. 6.2. Clear demarcation in XRD patterns could be seen as in case of Na/ZrO_2, a mixture of *monoclinic*-Na_2ZrO_3 (JCPDS card no. 35-0770) and zirconia was observed. On the other hand the diffraction patterns of K/ZrO_2, indicate the presence of *monoclinic and tetragonal* ZrO_2 phases and no peak either corresponding to the K_2O or K_2ZrO_3 was observed, thus supporting the formation of a homogeneous solution of K_2O and ZrO_2 in the solid state. Our findings are in line with the literature reported (Intrapong *et al.*, 2014) one where 10-15 wt% K loaded ZrO_2 has shown the XRD patterns almost similar to that of pure ZrO_2.

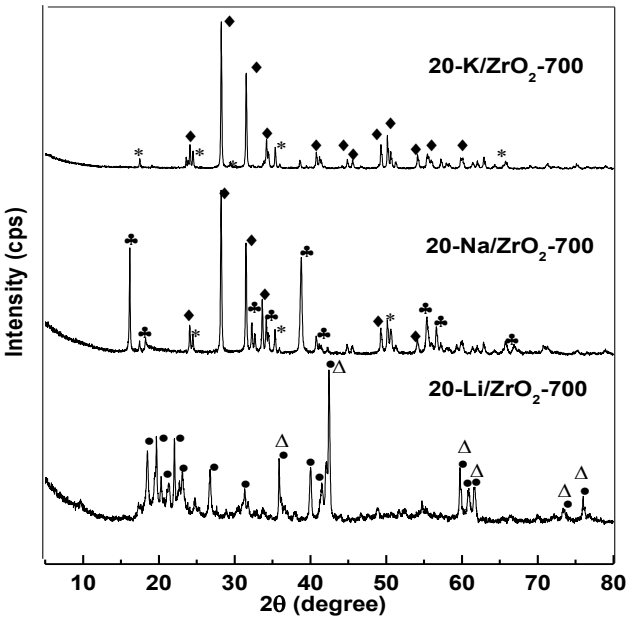

Fig. 6.2. Comparison of XRD patterns of different alkali metal impregnated on ZrO_2 (♦ = *monoclinic* ZrO_2, ∗ = *tetragonal* ZrO_2, • = *monoclinic* Li_2ZrO_3, Δ = *tetragonal* Li_2ZrO_3, ♣ = *monoclinic* Na_2ZrO_3).

The crystallite size of Li, Na and K doped ZrO_2, was found to increase with the increase in ionic radii of doped metal ion as given in Table 6.1. An increase in calcination temperature (500-800 °C) was found to increase the crystallite size of Li/ZrO_2 particles may be due to the sintering of the particles at high calcination temperature.

Table 6.1. Effect of calcination temperature and different alkali metals on crystallite size of 20-M/ZrO_2-T.

Catalyst	Crystallite size (nm) (2θ = 31.5°)
ZrO_2	24.3
20-Li/ZrO_2-500	13.5
20-Li/ZrO_2-600	16.5
20-Li/ZrO_2-700	25.2
20-Li/ZrO_2-800	30.5
20-Na/ZrO_2-700	26.7
20-K/ZrO_2-700	28.5

6.3.1.2. Electron Microscopic studies

The surface morphology and particle size of catalysts have been studied by SEM and TEM studies, respectively. As could be seen from SEM image (Fig. 6.3), the commercially available ZrO_2, used as support, was observed as agglomerates of 2-4 μm sized particles. Doping of Li or Na or K in this support has created relatively smaller sized particles of irregular geometries. The size of these particles was observed less than 1 μm in case of

Li/ZrO_2 with relatively homogeneous size distribution. In case of Na/ZrO_2 and K/ZrO_2, agglomerates of flake like structure, and polydisperse sample of 0.5-4 µm sized particles, respectively, has formed. The EDS analysis could not detect lithium in 20-Li/ZrO_2-700 because of atomic mass detection limitation of the instrument. In 20-Na/ZrO_2-700 and 20-K/ZrO_2-700, 18.05 wt% Na and 19.67 wt% K, was observed respectively. These values are closer to the theoretical doped amount of 20 wt% metal in both the cases.

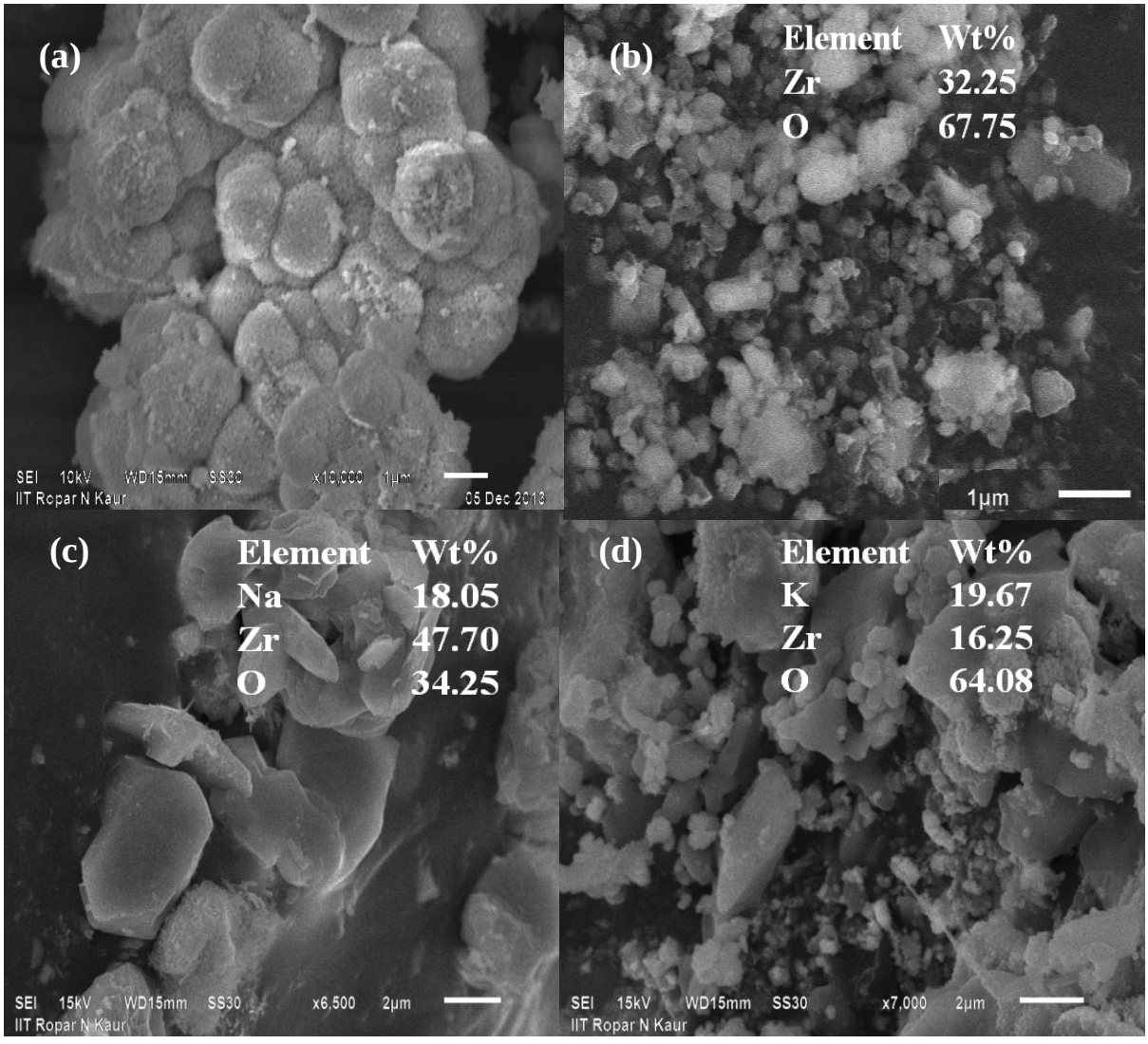

Fig. 6.3. SEM image of (a) commercially available ZrO_2 (b) 20–Li/ZrO_2–700 (c) 20–Na/ZrO_2–700 (d) 20–K/ZrO_2–700.

TEM analysis reveals that Li/ZrO_2, Na/ZrO_2 and K/ZrO_2 particles are the clusters of further smaller particles with an average size of ~ 80 nm, in quasi-spherical shape as shown in Fig. 6.4. In case of K/ZrO_2 formation of uniform dark colored particles also supported the creation

of homogeneous solid solution, as also evidenced by XRD study, of potassium and zirconium oxide.

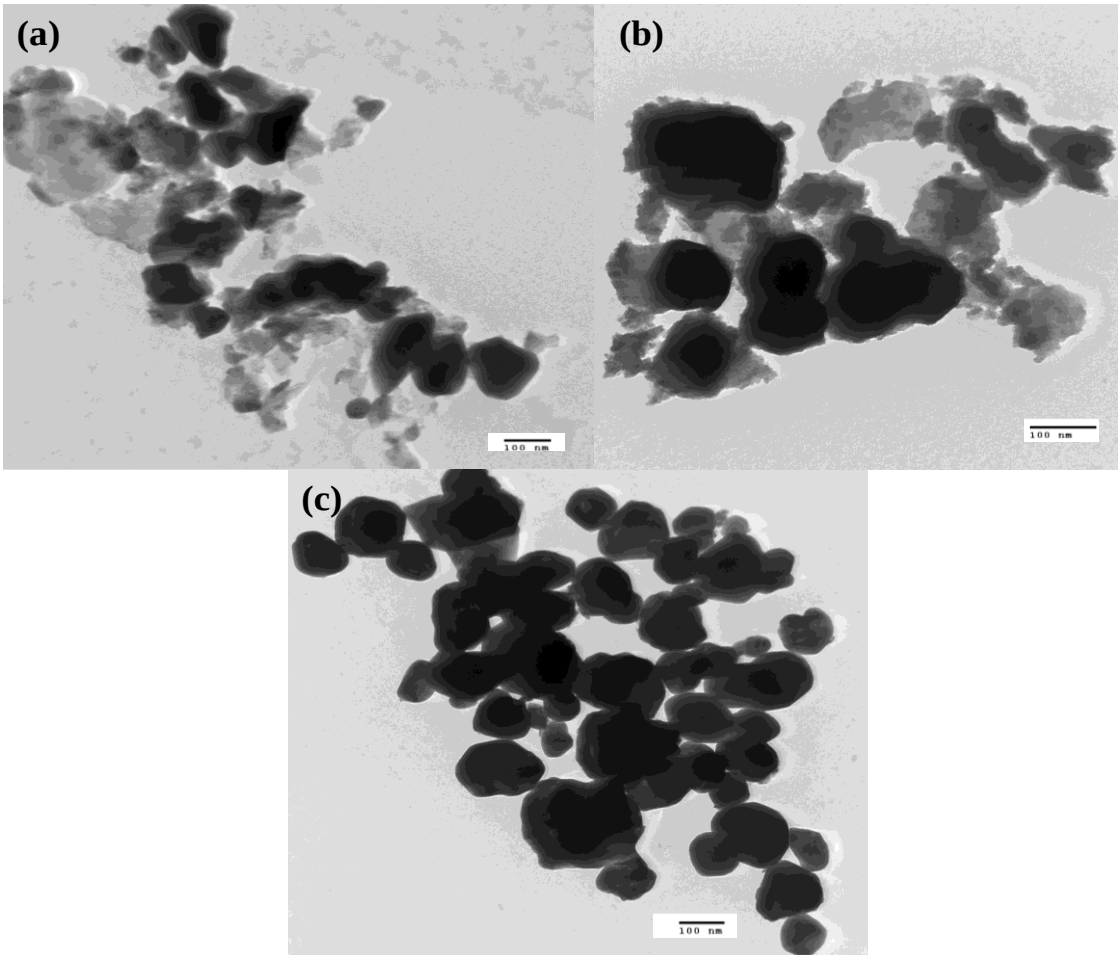

Fig. 6.4. TEM image of (a) 20–Li/ZrO_2–700, (b) 20–Na/ZrO_2–700 and (c) 20–K/ZrO_2–700.

6.3.1.3. BET Surface area measurements

As given in Table 6.2, the measured BET surface area of the commercial ZrO_2 was found to be 12.27 m^2/g. The doping of Li, Na and K over the support was found to reduce the surface area in the order of doped metal ion radii. Relatively large decrease in pore size in case of K/ZrO_2, could be due to the efficient pore plugging by K in comparison to smaller sized Li and Na ions. Although, catalyst surface area was found to be lower, however, Li/ZrO_2 demonstrates reasonably high activity under ambient reaction conditions. In case of transesterification reaction, a catalyst with low surface area may demonstrate high activity as in such reaction basic site strength plays more significant role in catalytic activity than surface area as reported by our group as well as other researchers (Kaur and Ali, 2014a; Patil and Deng, 2009).

Table 6.2. Comparison of BET Surface area, pore size and pore volume of the catalysts.

Catalyst	Surface area (m^2/g)	Pore size (Å)	Pore volume (cm^3/g)
ZrO_2	12.27	-	-
20-Li/ZrO_2-700	1.18	41.69	0.010
20-Na/ZrO_2-700	0.99	34.92	0.006
20-K/ZrO_2-700	0.71	17.09	0.005

6.3.1.4. Carbon dioxide-Temperature Programmed Desorption

Carbon dioxide adsorption–desorption technique determines the strength of basic sites as well as total basicity of the catalyst. The CO_2-TPD profiles for Li, Na and K doped zirconia are compared in Fig. 6.5. The desorption peak observed at 100–425 °C can be attributed as weaker, 425-625 °C as moderate and more than 625 °C as stronger basic sites. The basic strength of the catalyst was generated due to oxide ions (Lewis base) of the mixed metal oxide surface (Yan *et al.*, 2009; Thitsartarn and Kawi, 2011). In CO_2-TPD of Li/ZrO_2 no sharp desorption peak was observed even up to 800 °C. This could be due to the reaction between Li_2ZrO_3 and CO_2 to form highly stable Li_2CO_3 (Xiao *et al.*, 2011) which have decomposition temperature > 800 °C. Two desorption peaks for Na/ZrO_2 were observed at 425-625 °C and > 625 °C thus supporting the formation of moderate and strong basic sites in this catalyst. On the other hand, a large desorption peak was observed at 750 °C for K/ZrO_2, indicating the presence of strong basic sites. Thus, TPD study suggested the presence of more basic sites in Na/ZrO_2 and K/ZrO_2 due to desorption of CO_2 below 800 °C. Due to the absence of pure Na_2ZrO_3 and K_2ZrO_3 phases (as described in XRD section) Na/ZrO_2 and K/ZrO_2, are not able to form stable carbonates of sodium or potassium upon CO_2 adsorption. Thus it is not expected from Na/ZrO_2 and K/ZrO_2 to follow the same trend as expected from pure Na_2ZrO_3 and K_2ZrO_3 phases, respectively.

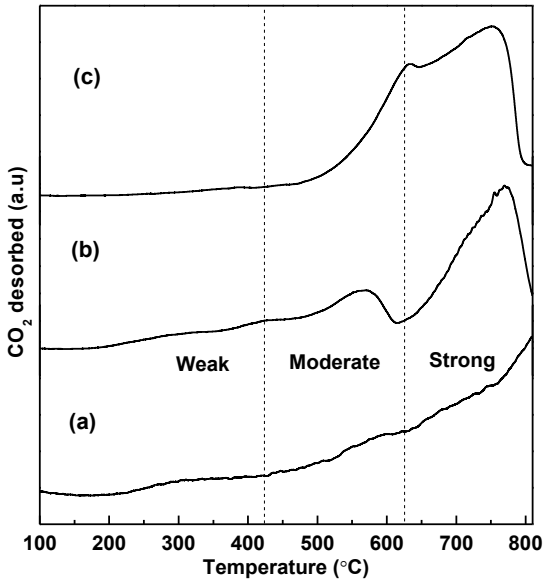

Fig. 6.5. CO_2-TPD profiles for (a) 20–Li/ZrO_2–700, (b) 20–Na/ZrO_2–700 and (c) 20–K/ZrO_2–700 catalysts.

To quantify the total basic site strength of the catalysts, Hammett indicator benzene carboxylic acid titration method (Table 6.3) was also employed. Titration method suggested that basic site strength increases in the order of: Li/ZrO_2 > Na/ZrO_2 > K/ZrO_2. This trend is exactly opposite to the order of basic strength observed by CO_2-TPD method. This difference is due to the fact that (i) in titration method total sites were calculated irrespective of their location while in case of TPD method only surface sites were quantified (Zhu *et al.*, 1998), and (ii) due to the high decomposition temperature of Li_2CO_3, desorption of CO_2 took place above 800 °C and thus corresponding basic sites were not observed in TPD profile of Li/ZrO_2.

6.3.2. Catalytic activity

The transesterification activity of solid bases mainly depends upon the Lewis base sites which in turn depend upon the type and content of doped metal as well as calcination temperature. The activity of various catalysts was compared by performing the transesterification (methanolysis and ethanolysis of WO) reactions under optimized reaction conditions and comparing their respective TOFs at 25% conversion level. The rate of methanolysis was always found higher than ethanolysis owing to the higher reactivity of methoxide ion (Brunschwig and Moussavou, 2012).

6.3.2.1. Effect of doped metal ion on catalytic activity

In order to study the effect of doped metal, ZrO_2 was doped with Li or Na or K metal ions and basic strength as well as activity of Li/ZrO_2, Na/ZrO_2 and K/ZrO_2 are compared in Table 6.3. The total basicity of the catalysts was evaluated by the Hammett indicator-benzene carboxylic acid titration in the presence of various indicators of pK_{BH+} = 6.8-18.4 as shown in Table 6.3. The maximum basic strength (2.38 mmol/g) as well as activity was observed in case of lithium doped zirconia. In present work the basicity of Li/ZrO_2, Na/ZrO_2 and K/ZrO_2 would depend on the chemical species present in each catalyst. The ionic radius of Zr^{4+} (0.72 Å) is almost similar to that of Li^+ (0.76 Å) but smaller than the radius of Na^+ (1.02 Å) and K^+ (1.38 Å). Due to this reason lithium doping in zirconia leads to the formation of a single Li_2ZrO_3 phase, a mixture of phases (Na_2ZrO_3 and ZrO_2) in case of Na/ZrO_2 and no K_2ZrO_3 phase formation in case of K/ZrO_2. Thus the reactivity of these catalysts could not be compared either with pure alkali metal or respective pure zirconates. Similar results were reported in case of alkali doped MgO catalysts as Li/MgO show better activity as well as basic strength than Na or K doped MgO (Macleod *et al.*, 2008).

Table 6.3. Comparison of basic strengths, basicity and TOFs for the Li/ZrO_2 catalyzed transesterification reactions.

Catalyst	Neutral red pK_a = 6.8	Bromothymol blue pK_a = 7.2	Phenolphthalein pK_a = 9.3	Nile blue pK_a = 10.1	Trapeolin pK_a = 11.1	2,4-dinitroaniline pK_a = 15.0	4-nitroaniline pK_a = 18.4	Total basicity (mmol/g of catalyst)	TOF (h^{-1}) M/E
ZrO_2	0.03	-	-	-	-	-	-	0.03	Negligible
5-Li/ZrO_2-700	0.05	0.12	0.16	0.22	0.30	-	-	0.85	21.43/1.94
10-Li/ZrO_2-700	0.06	0.23	0.20	0.26	0.41	-	-	1.16	25.31/4.92
15-Li/ZrO_2-700	0.08	0.32	0.26	0.28	0.49	-	-	1.43	32.74/7.51
20-Li/ZrO_2-700	0.08	0.40	0.30	0.32	0.56	0.48	0.24	2.38	45.62/9.72
25-Li/ZrO_2-700	0.07	0.36	0.36	0.26	0.46	0.44	0.23	2.21	37.76/8.56
20-Li/ZrO_2-300	0.03	0.11	0.14	0.20	-	-	-	0.48	17.55/1.79
20-Li/ZrO_2-500	0.04	0.16	0.22	0.26	-	-	-	0.68	22.24/4.59
20-Li/ZrO_2-600	0.06	0.30	0.27	030	0.48	-	-	1.41	34.10/6.01
20-Li/ZrO_2-800	0.09	0.38	0.28	0.34	0.50	0.44	0.26	2.29	39.37/7.87
20-Na/ZrO_2-700	0.16	0.24	0.28	0.31	0.26	0.19	0.17	1.61	29.50/5.04
20-K/ZrO_2-700	0.06	0.08	0.35	0.28	0.32	-	-	1.09	17.68/2.66

TOF – Turn over frequency at 25 % conversion levels; M – Methanolysis; E – Ethanolysis

6.3.2.2. Effect of content of lithium dopant on catalytic activity

Since maximum activity was shown by the Li/ZrO_2 hence further study of effect of content of lithium dopant as well as calcination temperature was performed by the Li/ZrO_2. As shown in Table 6.3, basic sites increases gradually on increasing the lithium content (from 5 to 20 wt%) due to the solid state reaction between LiOH and ZrO_2 to form Li_2ZrO_3.The maximum basic strength and basic sites were observed at 20 wt% Li doping and at 700 °C calcination temperature. It could be seen from Table 6.3 that TOFs of Li/ZrO_2 was found to increase with Li content and a maximum TOF was observed with the catalyst having 20 wt% Li content. A

further increase in Li content (up to 25 wt%) resulted the formation of less basic Li_4ZrO_4 (supported by the XRD study) to result a decrease in catalytic activity.

6.3.2.3. Effect of calcination temperature on catalytic activity

Activity of the solid base catalysts could be enhanced by increasing the Lewis base sites (O^{2-}) in case of metal oxides (Thitsartarn and Kawi, 2011). Calcination of metal hydroxides beyond their decomposition temperature leads to the formation corresponding oxides (Lewis base). Moreover, high temperature treatment may enhance the interactions among catalyst component due to solid state reaction to result the higher stability of the catalyst.

In order to optimize the calcination temperature, for better catalyst activity and stability, the catalysts were prepared at 300-800 °C. An increase in basic sites as well as activity was observed with the increase in calcination temperature from 300 to 700 °C as given in Table 6.3. The highest basicity as well as activity was observed for 20-Li/ZrO_2-700. At high calcination temperature (700 °C), Li_2ZrO_3 has formed due to the solid state reaction of LiOH with zirconia which has been reported to have strong basic sites (Xiao *et al.*, 2011). The activity of the catalyst decreases at 800 °C, due to the sintering of the catalyst particles which may result lesser active sites at the catalyst surface.

6.3.2.4. Effect of reaction parameters on FAAE yield

As evident from Table 6.3, the catalysts 20-Li/ZrO_2-700 was found to be more efficient and hence, used further to optimize the reaction parameters for the better catalytic activity. In order to determine the reaction conditions for the optimum catalytic activity, a series of transesterification reactions were carried out in presence of 20-Li/ZrO_2-700 by varying one parameter at a time out of the followings: (i) catalyst amount with respect to oil, (ii) alcohol to oil molar ratio (iii) reaction temperature and (iv) stirring speed. The effect of these parameters on the FAME and FAEE yield is shown in Fig. 6.6-6.9.

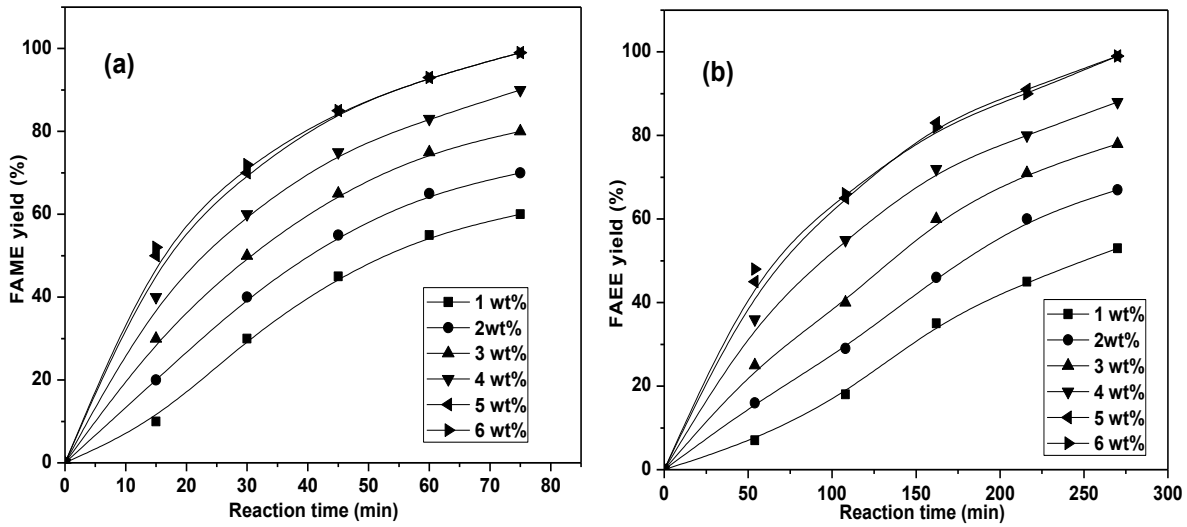

Fig. 6.6. Influence of catalyst concentration on 20–Li/ZrO_2–700 catalyzed transesterification of WO. **Reaction conditions:** (a) methanol to oil molar ratio of 12:1 at 65 ºC reaction temperature and (b) ethanol to oil molar ratio of 15:1 at 75 ºC reaction temperature.

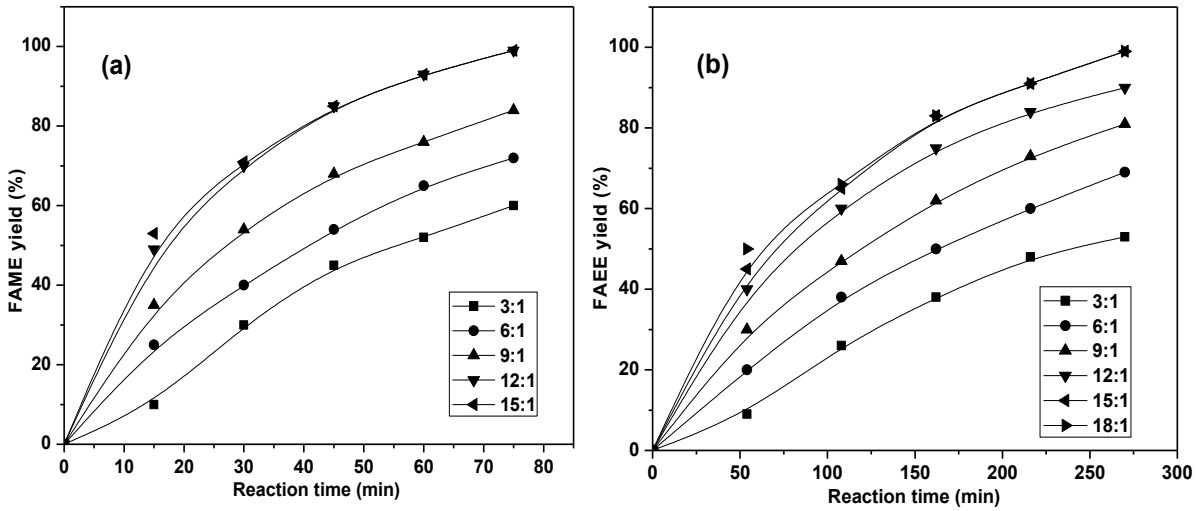

Fig. 6.7. Effect of alcohol:oil molar ratio on 20–Li/ZrO_2–700 catalyzed transesterification of WO. **Reaction conditions:** Reaction temperature (a) methanolysis at 65 ºC and (b) ethanolysis at 75 ºC, both reactions were performed in presence of 5 wt% of 20–Li/ZrO_2–700 with respect to oil.

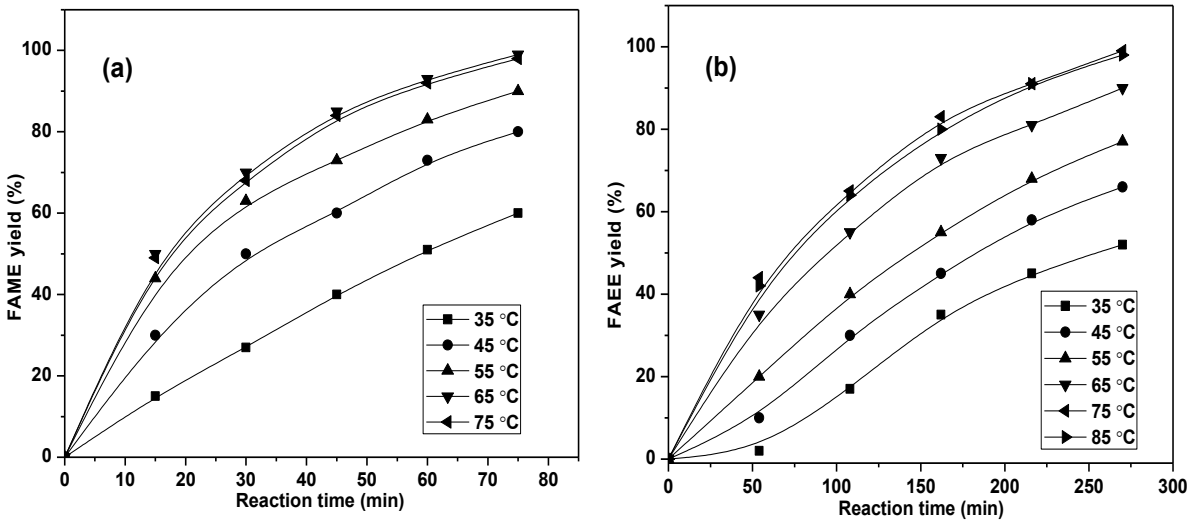

Fig. 6.8. Effect of reaction temperature on 20–Li/ZrO_2–700 catalyzed transesterification of WO. **Reaction conditions:** (a) methanol to oil molar ratio of 12:1 and (b) ethanol to oil molar ratio of 15:1 and 5 wt% of 20–Li/ZrO_2–700 with respect to oil in both the cases.

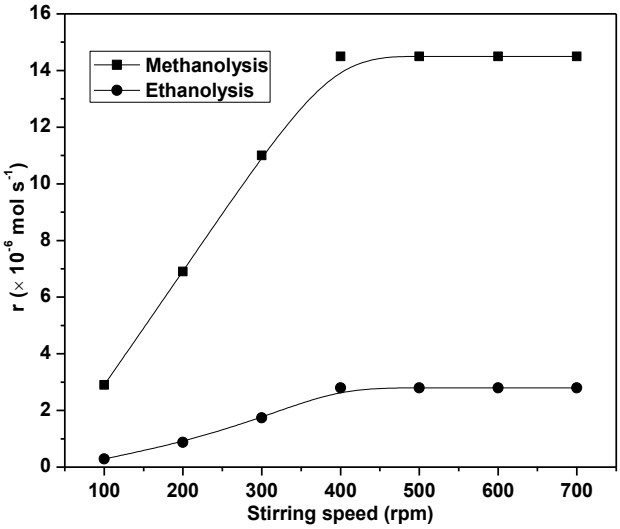

Fig.6.9. Effect of stirring speed on the 20–Li/ZrO_2–700 catalyzed transesterification of WO. **Reaction conditions:** (a) methanol to oil molar ratio of 12:1 at 65 ºC reaction temperature and (b) ethanol to oil molar ratio of 15:1 at 75 ºC reaction temperature and 5 wt% of 20–Li/ZrO_2–700 with respect to oil in both the cases.

Thus a 12:1 methanol to oil molar ratio at 65 ºC or 15:1 ethanol to oil molar ratio at 75 ºC in presence of 5 wt% catalyst (with respect to oil) and a stirring speed of 400 rpm, were found to be optimum conditions for the 20–Li/ZrO_2–700 catalyzed transesterification of WO to achieve >98 % FAAE yield.

6.3.3. Effect of moisture and FFA content

Water and FFA are usually considered as catalyst poisons for homogeneous as well as heterogeneous catalysts in transesterification process. As discussed in introduction section, the presence of > 0.3 wt% moisture and/or > 0.5 wt% FFA contents in feedstock deactivates the homogeneous base catalyst *via* saponification (Kumar and Ali, 2012). In the present study, activity of 20–Li/ZrO_2–700 catalyst was not found to be adversely affected by 4.6 and 0.35 wt% FFA and moisture contents, respectively, present in WO. In order to determine the maximum moisture resistance of the catalyst, the transesterification reactions of WO were performed by adding up to 4.0 wt% (water/oil) of water in the reaction mixture. As could be seen from Fig. 6.10, addition of up to 2 wt% water was not found to affect the catalysts efficacy to the significant extent. A further increase in moisture contents (2.5-4.0 wt%) was found to reduce the TOF and more reaction duration was required to achieve the completion of the reaction. Thus, use of prepared catalyst would be beneficial as it did not require pre dried moisture free feedstock or alcohol for the transesterification reaction.

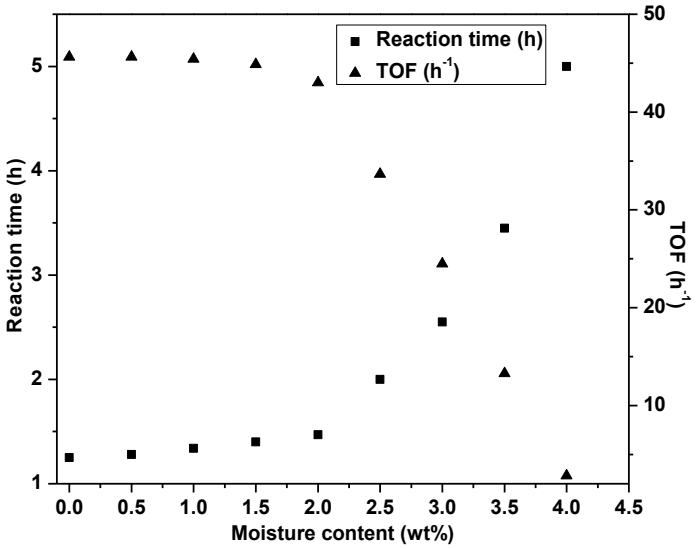

Fig. 6.10. Effect of moisture content on the 20–Li/ZrO_2–700 catalyzed transesterification of WO (reaction time is the time required for the completion of the reaction). **Reaction conditions:** Methanol to oil molar ratio of 12:1 at 65 ºC reaction temperature in presence of 5 wt% (catalyst/oil) catalyst.

In order to establish the reason behind the drop in catalyst efficacy in presence of moisture, FTIR and XRD of fresh catalyst was compared with the catalyst exposed to moisture. As could be seen from Fig. 6.11(a), exposure to the moisture leads to the formation of –OH group on catalyst surface which is supported by the appearance of a broad band at 3120 cm^{-1}

in FTIR spectrum. From XRD patterns of the catalyst exposed to moisture (Fig. 6.11(b)), peaks corresponding to the LiOH were observed, thus supporting the partial conversion of catalyst into LiOH.

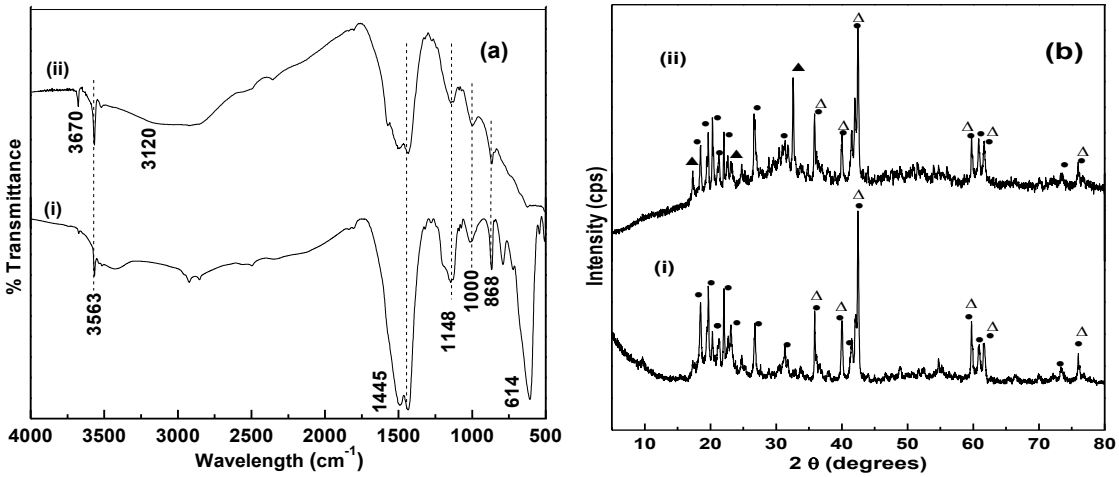

Fig. 6.11. Comparison of (a) FT-IR and (b) XRD of (i) fresh catalyst and (ii) catalyst exposed to moisture. (• = *monoclinic* Li_2ZrO_3, Δ = *tetragonal* Li_2ZrO_3, ▲ = LiOH).

In nonedible or waste oils, usually FFA contents are present in relatively higher concentration (4.6–18 wt% in present study). Conventionally transesterification of high FFA containing vegetable oils is performed in two step process involving acid-catalyzed pre esterification step in the presence of an acid catalyst followed by transesterification in presence of alkali catalyst (Yan *et al.*, 2009). In this process acid neutralization and salt removal from the product required huge quantity of water and also generate a significant amount of industrial effluent. Therefore, developing a catalyst which can simultaneously esterify FFA and transesterify triglyceride into biodiesel is important from commercial as well as environmental point of view. In order to determine the maximum FFA tolerance of the prepared catalyst, transesterification reactions of CO, WO, JO and KO (having 1–18 wt% FFA) were performed with methanol. As could be depicted from Fig. 6.12, Li/ZrO_2 catalyst was able to complete the transesterification of oil having up to 18 wt% FFA but a decrease in catalyst TOF was observed with the increase in FFA contents in feedstock. This may be due to the strong interactions of Bronsted base sites with fatty acids to result the partial blocking of catalyst active sites (Kaur and Ali, 2014b).

The ^{1}H and ^{13}C-NMR of FAAE prepared VOs is shown in Fig. A.18 and A.19 (Appendix A).

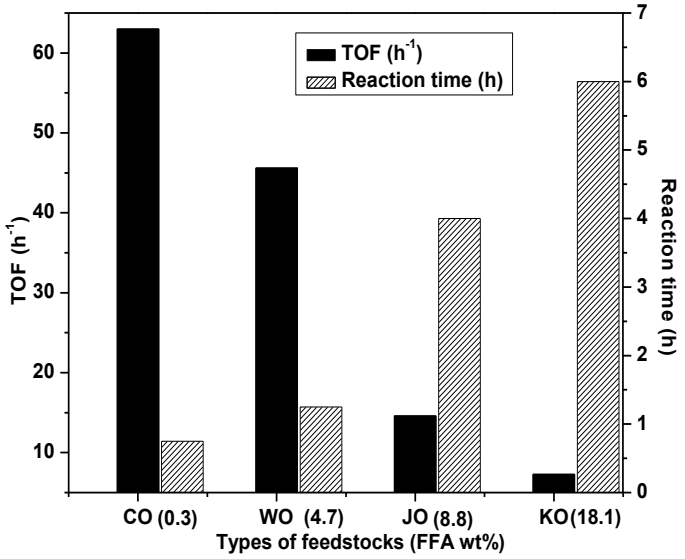

Fig. 6.12. Effect of FFA contents on the 20–Li/ZrO_2–700 catalyzed transesterification (reaction time is the time required for the completion of the reaction). **Reaction conditions:** Methanol to oil molar ratio of 12:1 at 65 ºC reaction temperature in presence of 5 wt% (catalyst/oil) catalyst.

It is vital to study the fate of FFA during the transesterification reaction as unreacted fatty acids would remain in biodiesel to increase the acid value of fuel beyond the acceptable limit. Lithium doping in zirconia leads to the formation of a single Li_2ZrO_3 phase having acidic (Li^+) as well as basic sites (ZrO_3^{2-}). Thus it is not unusual for this catalyst to show simultaneous esterification as well as transesterification activity. In order to prove the esterification activity of the catalyst, in a separate reaction oleic acid was treated with methanol (1:12 molar ratio) in the presence of 20-Li/ZrO_2-700 catalyst. As could be seen from Fig. 6.13, in 75 min of reaction duration 65.8% methyl oleate yield was obtained (Fig. A.20; Appendix A), to verify that catalyst was also effective for the esterification of fatty acids. Moreover, biodiesel prepared from high FFA containing oil was found to show significantly lesser acid value (0.3 mg KOH/g), to further support the esterification of fatty acids, present in triglyceride.

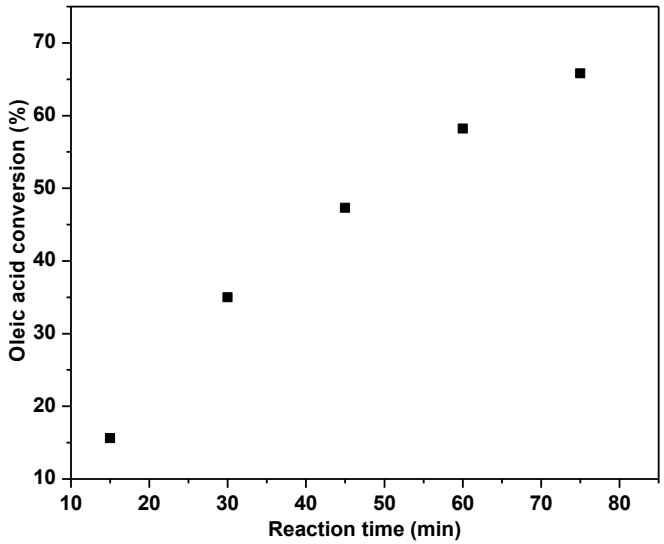

Fig. 6.13. Esterification of oleic acid. (**Reaction conditions:-** methanol to oleic acid molar ratio – 12:1 ; catalyst amount – 5 wt% with respect to oleic acid; reaction temperature – 65 °C; reaction duration – 75 min).

6.3.4. Recycling and homogeneous contribution of catalyst activity

The ease of separation and recycling of the heterogeneous catalyst is an important benefit from economical as well as environmental point of view over its homogeneous counterpart. To test the reusability of 20–Li/ZrO_2–700, transesterification of the WO was performed with methanol under optimized reaction conditions. Upon completion of reaction, Li/ZrO_2 was recovered from the reaction mixture by filtration, washed with hexane and finally regenerated at 700 °C calcination temperature. The catalyst hence recovered and regenerated was employed for 10 successive catalytic cycles under the same experimental and regeneration methods. As shown in Fig. 6.14, no significant loss in catalyst activity was observed up to ninth run as ≥ 90 % FAME yield was maintained. However, on further reuse a significant drop in activity was observed as 80 % FAME yield was achieved during tenth run. An almost similar trend was observed even in case of catalyst efficiency (TOF) and a significant drop in TOF was observed after 8^{th} cycle.

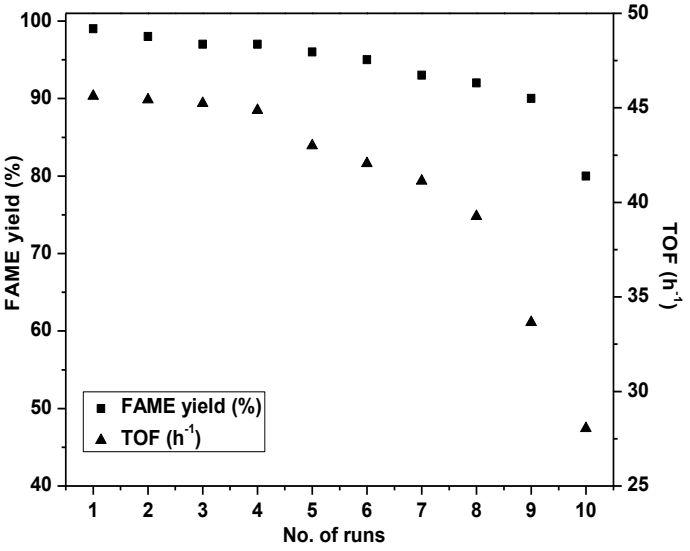

Fig. 6.14. Reusability study of 20–Li/ZrO_2–700. **Reaction conditions:** methanol to oil molar ratio of 12:1 at 65 ºC reaction temperature in presence of 5 wt % catalyst.

In order to evaluate reason behind the activity loss after nine cycles, the XRD patterns of fresh and reused Li/ZrO_2 are compared in Fig. 6.15(a). In the XRD pattern of reused Li/ZrO_2, few diffraction peaks (2θ = 20.21º, 21.20º and 60.92º) corresponding to Li_2ZrO_3 disappears and a new peak (2θ = 19.51º) due to *tetragonal* zirconia was observed. No significant difference in the crystallite size of fresh (25.2 nm) and used catalyst (27.6 nm), was observed.

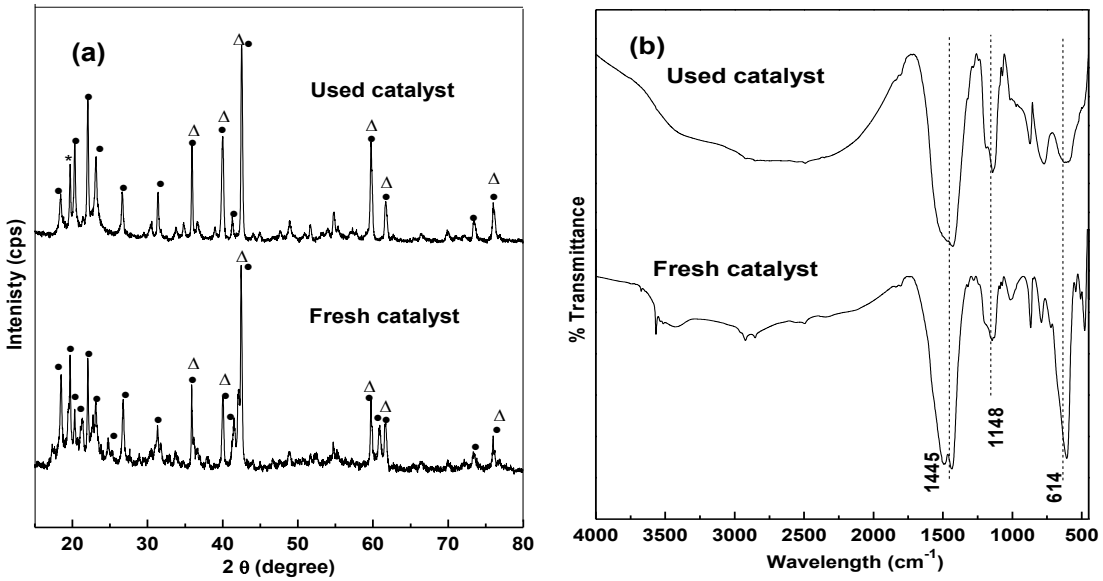

Fig. 6.15. Comparison of (a) XRD and (b) FT-IR of fresh and used catalyst. (∗ = tetragonal zirconia • = monoclinic Li_2ZrO_3, Δ = tetragonal Li_2ZrO_3).

The deposition of the adsorbed organic species on catalyst support may also partially deactivate the catalyst due to the blockage of catalyst active sites. The FTIR spectrum (Fig. 6.15(b)), of the regenerated catalyst did not show any band due to adsorbed organic molecules to indicate that FAME or glycerol have not been accumulated on the surface of the regenerated Li/ZrO_2 catalyst.

The leaching of the active species is a major problem among the alkali doped heterogeneous catalysts (Song *et al.*, 2011). The metal analysis supported the presence of 4.5 ppm of Li and 3.4 ppm of Zr in FAME while a relatively higher concentration of these metal ions in glycerol as shown in Table 6.4.

Table 6.4. Leaching of metal ions in biodiesel and glycerol.

	Concentration of metal ion in biodiesel (ppm)			Concentration of metal ion in glycerol (ppm)		
Metal	20-Li/ZrO_2-700	20-Na/ZrO_2-700	20-K/ZrO_2-700	20-Li/ZrO_2-700	20-Na/ZrO_2-700	20-K/ZrO_2-700
Lithium	4.5	-	-	8.3	-	-
Sodium	-	6.2	-	-	12.1	-
Potassium	-	-	8.3	-	-	16.7
Zirconium	3.4	4.5	6.7	15.3	8.4	49.8

In order to evaluate the relative leaching, transesterification reactions were also performed by Na/ZrO_2 and K/ZrO_2 catalysts. As shown in Table 6.5, relatively more metal contents were observed in FAME, prepared in presence of these two catalysts. Lesser metal leaching in case of Li/ZrO_2 could be due to the formation of a single phase of lithium zirconate.

To investigate whether the leached metal ions from the catalyst have contributed in catalytic activity, hot filtration test was performed. The transesterification reaction was performed under optimized reaction conditions in presence of Li/ZrO_2 and after 15 min the catalyst was removed by filtration. The reactants were again heated and further conversion was monitored for another 3 h. As could be seen from Fig. 6.16, no significant gain in FAME yield was obtained to rule out any considerable homogeneous contribution in catalytic activity. Thus reaction is mainly catalyzed by solid catalyst and the leached metal ions did not contribute to the transesterification activity.

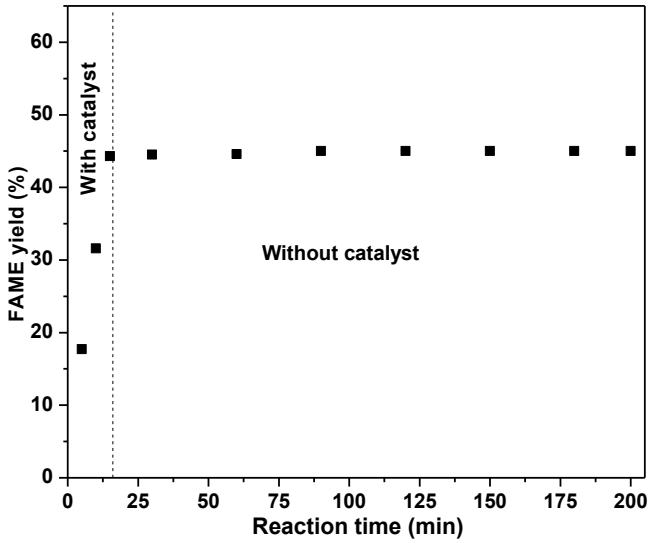

Fig. 6.16. Hot filtration test for transesterification of WO with methanol over 20-Li/ZrO_2-700 catalyst. (**Reaction conditions:** Methanol:oil molar ratio = 12:1, catalyst amount = 5 wt% with respect to oil, and reaction temperature = 65°C).

Hence, the gradual loss of the catalytic activity upon repeated use could be attributed to the change in catalyst structure and partial leaching of the metal ions on its repeated use.

6.3.5. Kinetic study

To follow the kinetics, methanolysis as well as ethanolysis of WO were performed in presence 20–Li/ZrO_2–700 catalyst at various reaction temperatures and corresponding graphs of $-\ ln(1-X)$ *vs* t are shown in Fig. 6.17(a) and 6.17(b). The linear nature of these plots supported that both reactions followed the (pseudo) first order rate law. The apparent first order rate constants form these plots were found to be 0.060 min^{-1} at 65 ºC for the methanolysis and 0.016 min^{-1} at 75 ºC for the ethanolysis reaction.

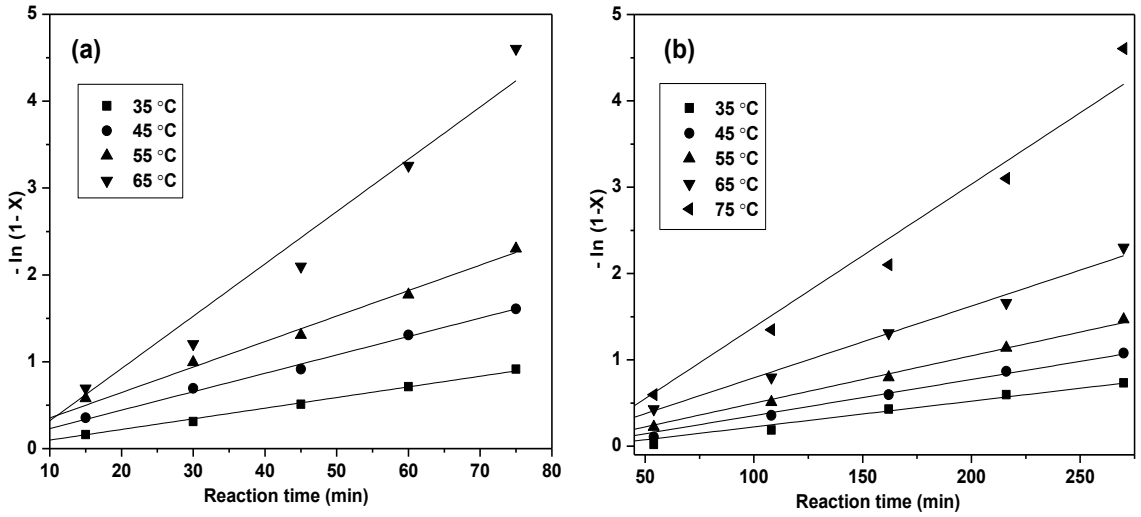

Fig. 6.17. Plots of –ln(1–X) *vs* time at different temperatures. **Reaction conditions:** (a) methanol to oil molar ratio of 12:1 (b) ethanol to oil molar oil ratio of 15:1 and 5 wt% of 20–Li/ZrO_2–700 with respect to oil in both the cases.

The Arrhenius model was employed to estimate the activation energy (E_a) and pre–exponential factor (A) for both the reactions following the equation 2.5 (Chapter 2). A plot between lnk *vs* 1/T is shown in Fig. 6.18, and the values of E_a and A from the plot was found to be 40.8 kJ mol^{-1} and 8.1 × 10^4 min^{-1}, respectively for methanolysis and 43.1 kJ mol^{-1} and 2.7 × 10^4 min^{-1}, respectively for ethanolysis.

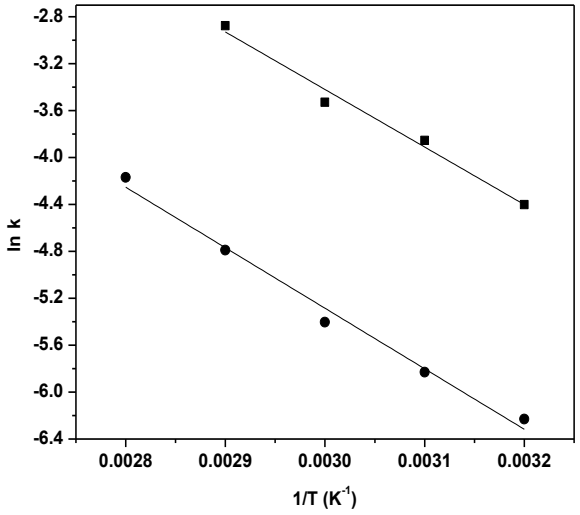

Fig. 6.18. Arrhenius plot of lnk *vs* 1/T for the transesterification of WO with methanol (■) and ethanol (•) over 20–Li/ZrO_2–700 catalyst.

The observed E_a values in present study for both the reactions were found within the range of values (26–84 kJ mol^{-1}) reported for heterogeneous catalysts (Freedman *et al.*, 1984). The observed activation energy was found > 25 kJ mol^{-1}, thus supporting that 20-

Li/ZrO_2-700 catalyzed transesterification is chemically controlled and not by diffusion/mass transfer limitations (Patel and Brahmkhatri, 2013).

6.3.6. Koros-Nowak Criterion

In order to demonstrate that catalytic activity is independent from the diffusion limitations, the Koros-Nowak criterion was employed. According to the literature procedure (Song *et al.*, 2011), reactions were carried out in the presence of two catalysts, separately, having different active sites. Fractional exposures of active sites to the substrates in both the reactions were kept constant. In the present study, ethanolysis as well as methanolysis of WO were performed with 5 wt% 20-Li/ZrO_2-700 and 5.5 wt% of 25-Li/ZrO_2-700 and the reaction time to yield the similar conversion levels were recorded. The results exhibited in Fig. 6.19 showed that at same conversion levels, the TOFs of two catalysts were found to be almost similar to indicate that the reaction has followed the Koros-Nowak criterion. Thus it is safe to assume that reaction rates under the mentioned experimental conditions are independent from the transport phenomenon.

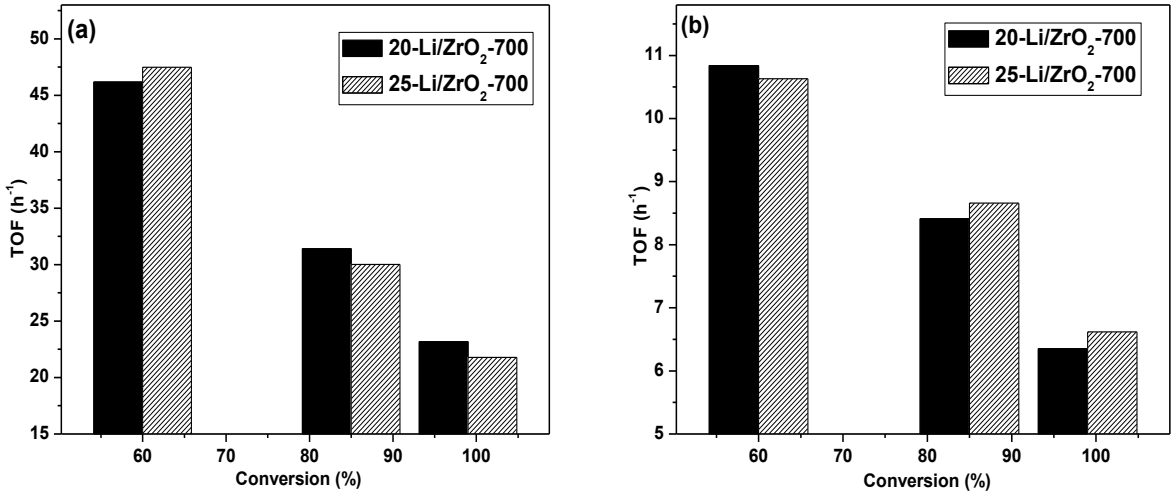

Fig. 6.19. TOFs of 20-Li/ZrO_2-700 and 25-Li/ZrO_2-700 with different conversions. **Reaction conditions**: (a) methanol:oil molar ratio of 12:1 at 65 ºC reaction temperature, and (b) ethanol:oil molar ratio of 15:1 at 75 ºC reaction temperature with 5 wt% 20-Li/ZrO_2-700 and 5.5 wt% of 25-Li/ZrO_2-700 of catalyst.

The physicochemical properties of FAME and FAEE prepared from WO are illustrated in Table B.2 (Appendix B) and observed values were found within the limits of EN 14214 specifications.

6.4. Conclusions

In present work, 20–Li/ZrO_2–700 has been prepared by wet chemical method and characterized by powder XRD, FT-IR, SEM-EDS and TEM techniques. Li/ZrO_2 catalyst was found to be an effective catalyst for simultaneous esterification and transesterification of a variety of feedstock having up to 4 and 18 wt% of moisture and FFA contents, respectively. Under optimized reaction conditions (catalyst concentration 5 wt%, methanol to oil molar ratio of 12:1 at 65 °C, ethanol to oil molar ratio 15:1 at 75 °C) the transesterification of the waste cottonseed oil was found to followed (pseudo) first order rate law. The activation energy for the methanolysis and ethanolysis of waste cottonseed oil was found to be 40.8 and 43.1 kJ mol^{-1}, respectively. The catalyst has been recovered and recycled without any significant loss in activity (≥90 % FAME yield) during nine cycles. The leaching study supported the negligible homogeneous contribution in catalytic activity, and Koros-Nowak test demonstrated that the activity is free from mass transfer phenomenon.

References

Brunschwig, C.; Moussavou, W.; Blin, J.; Use of bioethanol for biodiesel production. *Prog. Energ. Combust.*, **2012**, 38, 283-301.

Freedman, B.; Pryde, E. H.; Mounts, T. L.; Variables affecting the yields of fatty esters from transesterified vegetable oils. *J. Am. Oil Chem. Soc.*, **1984**, 61, 1638-1643.

Intarapong, P.; Iangthanarat, S.; Luengnaruemitchai, A.; In, S.; Biodiesel production from palm oil using potassium hydroxide loaded on ZrO_2 catalyst in a batch reactor. *Chiang Mai J. Sci.*, **2014**, 41, 128-137.

Kaur, N.; Ali, A.; Kinetics and reusability of Zr/CaO as heterogeneous catalyst for the ethanolysis and methanolysis of Jatropha crucas oil. *Fuel Process. Technol.*, **2014**, 119, 173-184.

Kaur, N.; Ali, A.; One-pot transesterification and esterification of waste cooking oil via ethanolysis using Sr:Zr mixed oxide as solid catalyst. *RSC Adv.*, **2014**, 4, 43671-43681.

Kumar, D.; Ali, A.; Nanocrystalline K-CaO for the transesterification of a variety of feedstocks: Structure, kinetics and catalytic properties. *Biomass Bioenerg.*, **2012**, 46, 459-468.

MacLeod, C. S.; Harvey, A. P.; Le, A. F.; Wilson, K.; Evaluation of the activity and stability of alkali-doped metal oxide catalysts for application to an intensified method of biodiesel production. *Chem. Eng. J.*, **2008**, 135, 63-70.

Patel, A.; Brahmkhatri, V.; Kinetic study of oleic acid esterification over 12-tungstophosphoric acid catalyst anchored to different mesoporous silica supports. *Fuel Process. Technol.*, **2013**, 113, 141-149.

Patil, P. D.; Deng, S.; Transesterification of Camelina Sativa oil using heterogeneous metal oxide catalysts. *Energy Fuel*, **2009**, 23, 4619-4624.

Song, R.; Tong, D.; Tang, J.; Hu, C.; Effect of composition on the structure and catalytic properties of KF/Mg-La solid base catalysts for biodiesel synthesis via transesterification of cottonseed oil. *Energy Fuel*, **2011**, 25, 2679-2686.

Thitsartarn, W.; Kawi, S.; An active and stable $CaO–CeO_2$ catalyst for transesterification of oil to biodiesel. *Green Chem.*, **2011**, 13, 3423-3430.

Xiao, Q.; Liu, Y.; Zhong, Y.; Zhu, W.; A citrate sol–gel method to synthesize Li_2ZrO_3 nanocrystals with improved CO_2 capture properties. *J. Mater. Chem.*, **2011**, 21, 3838-3842.

Yan, S.; Kim, M.; Salley, S. O.; Ng, K. Y. S.; Oil transesterification over calcium oxides modified with lanthanum. *Appl. Catal. A: Gen.*, **2009**, 360, 163-170.

Zhu, J. H.; Wang, Y.; Cun, Y.; Wang, X. S.; Dispersion of potassium nitrate and the resulting basicity on alumina and zeolite NaY. *J. Chem. Soc., Faraday Trans*., **1998**, 94, 1163-1169.

One Pot Transesterification and Esterification of Waste Cooking Oil via Ethanolysis Using Sr:Zr Mixed Oxide as Solid Catalyst

Contents *Page No.*

Abstract: Mixed oxide of Sr and Zr has been prepared by co-precipitation method and examined as heterogeneous catalyst for one pot esterification and transesterification of waste cooking oil with ethanol for the production of fatty acid ethyl esters (FAEE). Mixed oxide of Sr:Zr with 2:1 atomic ratio and calcined at 650 ºC showed the optimum activity among the prepared catalysts. The catalyst possesses both acidic and basic sites, and hence was able to perform simultaneous esterification and transesterification of free fatty acid containing vegetable oils. The transesterification activity was found to be a function of basic sites of catalyst which in turn depends on calcination temperature and Sr:Zr atomic ratio. A pseudo first order kinetic equation was applied to evaluate the kinetics of the 2Sr:Zr-650 catalyzed ethanolysis of waste cottonseed oil and activation energy (E_a) for the reaction was observed as 48.17 kJ mol^{-1}. Thermodynamic activation parameters of the reaction was evaluated from Eyring-Polanyi equation and the values of $\Delta G^{\ddagger}$, $\Delta H^{\ddagger}$ and $\Delta S^{\ddagger}$ were found to be 88.23 kJ mol^{-1}, 45.97 kJ mol^{-1} and -121.37 J $mol^{-1}K^{-1}$, respectively. These values suggest that 2Sr:Zr-650 catalyzed reaction is endothermic, unspontaneous and following the associative kind of mechanism. The catalyst was moderately stable as no significant loss of metal component or catalyst activity was observed in four successive runs.

7.1. Introduction

In previous chapter, Li/ZrO_2 was able to catalyze simultaneous esterification and transesterification with methanol. As discussed earlier methanol is a highly toxic chemical and itself a refinery residue (Brunschwig *et al.*, 2012). On the other hand, ethanol is nontoxic as well as renewable as it is mainly produced by the fermentation of biomass. However, due to low reactivity and difficulty in separation of FAEE from glycerol it could not be explored extensively for BD production in literature as well as at commercial level. To employ ethanol for biodiesel production, in present chapter, Sr:Zr catalyst is prepared via co-precipitation method and successfully employed for the ethanolysis of high free fatty acid containing vegetable oils. To the best of our knowledge, no report is available in literature where ethanol has been employed for the simultaneous esterification and transesterification of VOs in presence of heterogeneous catalyst.

7.2. Experimental Section

7.2.1. Catalyst preparation

The mixed oxide of strontium and zirconium with an atomic ratio 0.3-3 (Sr/Zr) was prepared by co-precipitation method. In a typical preparation, 5 g of $ZrOCl_2.8H_2O$ and appropriate amount of $Sr(NO_3)_2$ was mixed in 50 ml distilled water. To this 25 wt% ammonia solution was added until the pH of mixture reached ~ 10. The resulted mixture was stirred for 4 h, and then filtered to obtain white precipitate which was washed with distilled water to make it pH neutral. The white solid, thus obtained, was dried at 120 °C for 24 h and finally calcined at 650 °C for 5 h. Mixed oxide of magnesium, calcium and barium with zirconium were also prepared following the same experimental procedure but using appropriate metal precursors in place of $Sr(NO)_3$. Prepared catalysts were labelled as xM:Zr-T, where x, M and T represents the M/Zr atomic ratio, alkaline metal and calcination temperature (ºC), respectively.

The transesterification reactions of WO were carried out by following the method given in Chapter 4 but using Sr:Zr catalyst. The FAEE composition as well as yield was determined by GC-MS technique. Ethyl esters obtained upon ethanolysis of WO was also characterized by ^{1}H and ^{13}C-NMR techniques.

7.3. Results and Discussion

7.3.1. Catalyst characterization

7.3.1.1. X-ray diffraction

The XRD patterns of Sr:Zr with varying atomic ratio (0.5-3) are shown in Fig. 7.1(a). At low Sr:Zr atomic ratio (0.3-1.0) the diffraction patterns supported the presence of three species *viz.*, *monoclinic* zirconia (*m*-ZrO_2; JCPDS 88-2390), *cubic* strontium oxide (*c*-SrO; JCPDS 75-0263) and *tetragonal* strontium zirconate (*t*-$SrZrO_3$; JCPDS 70-0694). A further increase in Sr concentration (Sr/Zr = 2) leads to the formation of *t*-$SrZrO_3$ as major phase and a further increase in Sr/Zr atomic ratio was not found to initiate any new phase formation. Thus an atomic ratio of 2 (Sr/Zr) was considered as optimum ratio for the catalyst preparation.

Comparison of the XRD patterns of 2Sr:Zr at varying calcination temperature (350-750 °C) is shown in Fig. 7.1(b). At lower calcination temperature (350-550 °C), strontium nitrate phase ($Sr(NO_3)_2$; JCPDS 87-0557) is the major phase along with *m*-ZrO_2, *t*-$SrZrO_3$ and *c*-SrO as minor phases. At 650 °C, due to the solid state reaction between $Sr(NO_3)_2$ and ZrO_2, diffraction patterns supported the formation of *t*-$SrZrO_3$ as major phase and a further increase in calcination temperature was not found to initiate any major structural changes in catalyst structure. Thus 650 °C was considered as optimum temperature for the catalyst preparation.

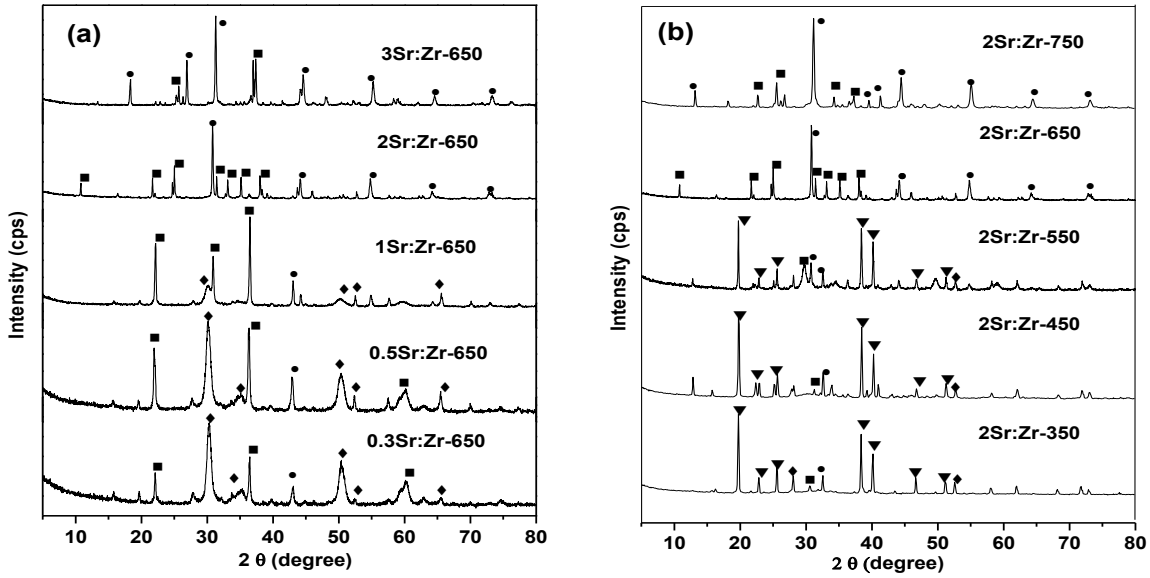

Fig. 7.1. XRD pattern of (a) varying Sr:Zr atomic ratio and (b) calcination temperature (• = *t*-$SrZrO_3$, ■ = *c*-SrO, ♦ = *m*-ZrO_2, ▼ = $Sr(NO_3)_2$).

As shown in Table 7.2, an increase in Sr/Zr ratio was also found to increase the crystallite size of the catalyst may be due to large ionic radii of Sr (1.27 Å) than Zr (0.76 Å). An increase in calcination temperature (350-650 °C) was found to increase the crystallite size due to the sintering of the catalyst particles at high calcination temperature.

7.3.1.2. Thermogravimetric and Differential scanning calorimetry analysis

TG and DSC curves of the uncalcined catalyst are illustrated in Fig. 7.2, which shows three endothermic weight loss regions existing in the temperature ranges of 25-200 °C, 200-350°C and 550–650 °C. The first weight loss of 7 wt% in 25-100 °C region may be ascribed to the loss of physically adsorbed water molecules over catalyst surface. The second weight loss of 23 wt% in 200-350 °C region corresponds to the loss of water molecule due to the decomposition of hydroxides of Sr and Zr. In third step, at 550-650 °C (endothermic), a weight loss of 21 wt% was observed due to the decomposition of $Sr(NO_3)_2$ into SrO and formation of $SrZrO_3$ phase. No significant weight loss or phase change in 2Sr:Zr was observed beyond 650 °C and hence the catalyst was prepared at 650 °C calcination temperature.

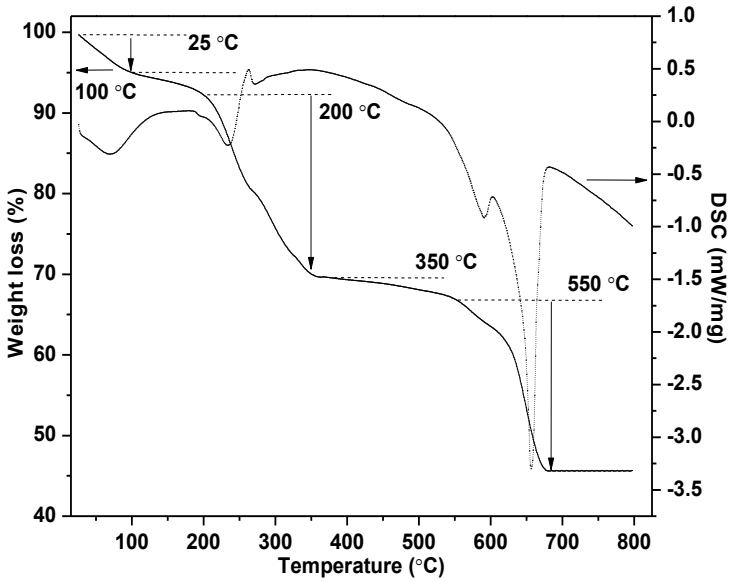

Fig. 7.2. Thermogravimetric analysis of 2Sr:Zr precursor.

7.3.1.3. Electron Microscopic studies

The surface morphology and particle size of catalysts have been studied by SEM and TEM studies, respectively. As could be seen from SEM image (Fig. 7.3(a)), 2Sr:Zr-650 particles

are either cubic or irregular shaped geometry within the range of 2-3 µm. EDS analysis supported the Sr:Zr atomic ratio of 1.7:1 which is close to the theoretical value of 2:1.

TEM picture (Fig. 7.3(b)) of these particles reveal these are the clusters of smaller particles of ~25-30 nm size with few large relatively large sized particles of ~130 nm. Thus a powder XRD as well as TEM study supports the formation of nano structures of 2Sr:Zr-650 particles.

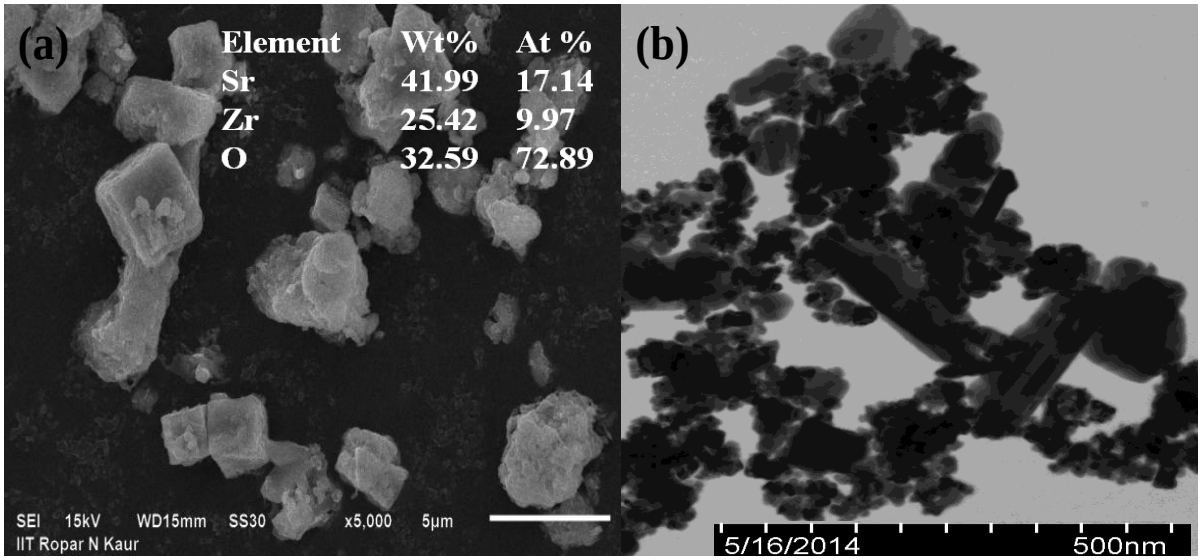

Fig. 7.3. (a) SEM and (b) TEM image of 2Sr:Zr-650 catalyst.

7.3.1.4. BET Surface area and porosity measurements

The surface properties of the catalysts at different calcination temperature were measured as shown in Table 7.1. The surface area and pore volume of the catalyst were observed higher at low calcination temperature, although no regular trend of surface properties with calcination temperature was obtained. The 2Sr:Zr-650 catalyst has low surface area and low pore volume, however, same catalyst was found to show the best activity among the prepared catalysts owing to highest basic strength (Table 7.2). Thus the activity of the catalyst was found to be a function of its basic strength rather than surface area. These results are in line with that of literature reports (Sankaranarayanan *et al.*, 2012; Patil and Deng, 2009) as well as with our own work reported in chapter 4 where the activity of the catalysts towards transesterification reaction was found to be a function of basic strength rather than surface area.

Table 7.1. Surface properties of the catalysts at different calcination temperature.

Catalyst	Surface area (m^2/g)	Pore diameter (nm)	Pore volume (cm^3/g)
2Sr:Zr-350	15.10	9.02	0.0298
2Sr:Zr-450	0.66	23.14	0.0049
2Sr:Zr-550	0.87	24.74	0.0093
2Sr:Zr-650	0.55	32.58	0.0043

The nitrogen adsorption-desorption isotherms (Fig. 7.4(a)) indicate a type IV isotherm profile for 2Sr:Zr catalysts at different calcination temperature with hysteresis loop H3, at relative pressure of about 0.7-1.0; characteristic to mesoporous materials. The Non Localized Density Functional Theory (NLDFT) and Grand Canonical Monte Carlo (GCMC) method was used to calculate the pore size distribution. Despite the smaller surface area of the catalysts has a larger pore diameter in accordance with Table 7.1. The catalyst at low calcination temperature (350 °C) show narrow pore size distribution with ~ 9 nm pore diameter. On increasing the calcination temperature (450-550 °C), the pore diameter increases to ~ 24 nm (Fig. 7.4(b)) and at 650 °C it reached to the maximum value of ~32 nm. At low calcination temperature $Zr(OH)_4$ might be occupying the pores of $Sr(NO_3)_2$/SrO to reduce the pore size of 2Sr:Zr. At high calcination temperature (650 °C) due to the solid state chemical reaction of ZrO_2 with $Sr(NO_3)_2$/SrO, the pores might have been vacated to form the material of relatively large pore sizes.

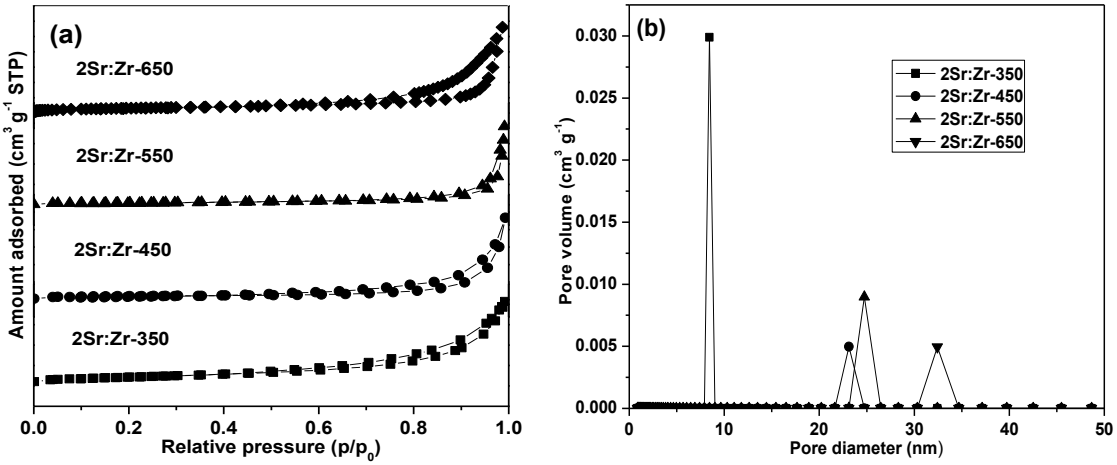

Fig. 7.4. (a) N_2 adsorption-desorption isotherms and (b) Pore size distribution curve for 2Sr:Zr catalyst at different calcination temperature.

7.3.2. Structure-activity relation of catalysts

The activities of the various catalysts were compared on the basis of their total basic sites, and TOFs of WO ethanolysis. The catalyst prepared using Mg or Ba show very less activity

while the catalyst having Ca was found to be lesser active in comparison to the Sr/Zr catalyst. There could be two reasons behind the activity difference viz., (i) difference in catalyst basic strength and (ii) difference in catalyst structure. It is evident from Table 7.2, basic strength of 2Sr:Zr-650 was found to be 22.7 mmol/g which is much higher in comparison to the 2Mg:Zr-650, 2Ca:Zr-650 and 2Ba:Zr-650 catalysts (9.7-17.8 mmol/g).

To compare the catalyst structure, 2Mg:Zr-650, 2Ca:Zr-650, 2Ba:Zr-650 and 2Sr/Zr-650 were prepared under the same experimental conditions and their powder XRD diffraction patterns were compared. As could be seen from Fig. 7.5, in case of Mg:Zr catalyst, diffraction patterns supported the formation of a single MgO phase, while in case of Ba:Zr, pure $BaZrO_3$ phase formation was observed. On the other hand in case of Ca:Zr, and Sr:Zr catalysts, XRD diffraction patterns supported the formation of mixed phases of $CaO/CaZrO_3$ and $SrO/SrZrO_3$, respectively. This structural disparity might also be responsible for the variation in catalytic activity of the material prepared with different alkaline earth metals. Nevertheless, Sr/Zr being highest in activity has been studied in detail in present manuscript.

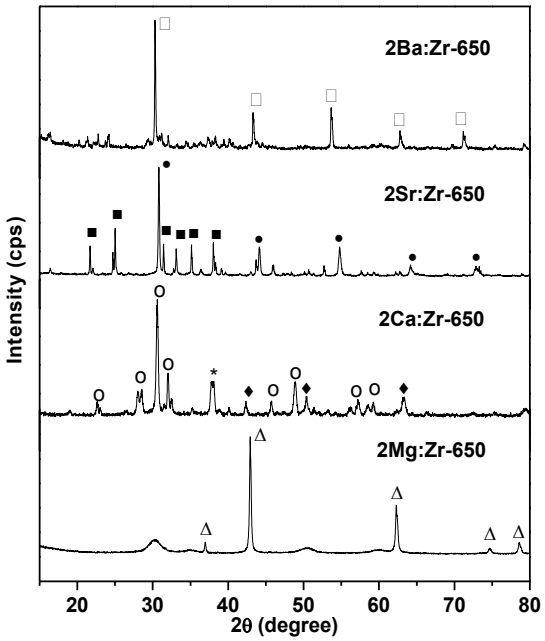

Fig. 7.5. XRD pattern of varying metal to zirconia atomic ratio (• = $SrZrO_3$, ■ = SrO, ♦= m-ZrO_2, o = $CaZrO_3$, * = CaO, Δ = MgO, □ = $BaZrO_3$).

As shown in Table 7.2, the basic sites of the catalysts increases gradually on increasing the Sr/Zr ratio and calcination temperature. The optimum atomic ratio of 2 (Sr/Zr) and calcination temperature of 650 °C was able to yield the catalyst with maximum basic sites. The increase in basicity may be due to the presence of *t*-$SrZrO_3$ as major phase at this ratio (Sr/Zr = 2) which is reported to be an active species for transesterification reaction

(Lima *et al.*, 2012). A further increase in strontium to zirconium ratio (≥ 3) was not found to increase the activity of the catalyst to significant extent as the total basic site remains almost similar to the catalyst having Sr/Zr ratio of 2.

Similarly, on increasing the calcination temperature, the basic site as well as activity of the catalyst was found to increase and a maximum activity was observed at 650 °C. At low calcination temperature (350-550 ºC), the lesser activity could be due to the presence of strontium nitrate which decomposed into SrO and reacted with ZrO_2 at 650 ºC to form the $SrZrO_3$. Since, 2Sr:Zr-650 catalyst was found to catalyze the reaction rate to the maximum extent, hence it was selected for optimizing the other reaction parameters for the transesterification reaction.

Table 7.2. Comparison of basic strengths, basicity and TOFs for the 2M:Zr-T catalyzed transesterification.

Catalyst	Crystallite size (nm)	Basic strength	Neutral red $pK_a = 6.8$	Bromothymol blue $pK_a = 7.2$	Phenolphthalein $pK_a = 9.3$	Nile blue $pK_a = 10.1$	Trapeolin $pK_a = 11.1$	Total basicity (mmol/g of catalyst)	TOF[a] (h^{-1})
0.3Sr:Zr-650	8.74	$9.3<pK_a<10.1$	2.0	2.6	3.8	4.0	2.4	14.8	0.30
0.5Sr:Zr-650	9.88	$9.3< pK_a <10.1$	2.2	2.9	4.1	4.3	3.2	16.7	0.35
1Sr:Zr-650	24.8	$10.1< pK_a <11.1$	2.5	3.3	4.3	4.7	3.8	18.9	0.48
2Sr:Zr-650	27.1	$11.1< pK_a <15.0$	3.6	4.3	5.0	5.5	4.3	22.7	0.71
3Sr:Zr-650	26.1	$11.1< pK_a <15.0$	3.4	4.3	4.9	5.4	4.1	22.1	0.68
2Sr:Zr-350	22.8	$7.2< pK_a <9.3$	1.2	1.5	2.3	2.8	1.8	9.60	0.28
2Sr:Zr-450	24.9	$9.3< pK_a <10.1$	1.9	2.0	2.8	3.4	2.2	12.3	0.35
2Sr:Zr-550	26.8	$10.1< pK_a <11.1$	2.4	2.7	3.2	3.7	3.0	15.0	0.47
2Sr:Zr-750	24.7	$11.1< pK_a <15.0$	3.3	3.8	4.7	5.2	4.1	21.1	0.65
2Mg:Zr-650	21.8	$9.3< pK_a <10.1$	2.2	3.0	3.6	2.5	1.8	13.1	NC
2Ca:Zr-650	22.4	$10.1< pK_a <11.1$	2.7	3.6	3.9	4.2	3.4	17.8	0.24
2Ba:Zr-650	32.3	$7.2< pK_a <9.3$	1.4	1.6	2.4	2.7	1.6	9.70	NC

[a]TOF is calculated at 25% conversion level; NC = negligible conversion. **Reaction conditions** = ethanol to oil molar ratio of 12:1 at 75 ºC reaction temperature, in presence of 5 wt% of catalyst with respect to oil with 400 rpm stirring speed.

Usually catalysts with both acidic as well as basic sites were found to show simultaneous esterification and transesterification activity (Yan *et al.*, 2009). The catalyst, 2Sr:Zr-650, was also found to have moderate acidic sites (3.9 mmol/g of catalyst; Acidic strength $3.3<H\_<4.8$) which can catalyze the fatty acid esterification. In order to show the esterification activity of 2Sr:Zr-650 catalyst, esterification of oleic acid with ethanol (1:12 molar ratio) was performed at 75 ºC. As could be seen from Fig. 7.6, in 3.5 h of reaction duration 70.6 % ethyl oleate yield was obtained, to prove the esterification activity of the catalyst. Moreover, biodiesel prepared from high FFA (up to 18 wt%) containing oil was found to show significantly lesser acid value (0.4 mg KOH/g) to further support the esterification of FFA present in triglyceride. To best of our knowledge this is the first report for the simultaneous esterification and transesterification of high FFA containing triglycerides ***with ethanol*** in presence of heterogeneous catalyst.

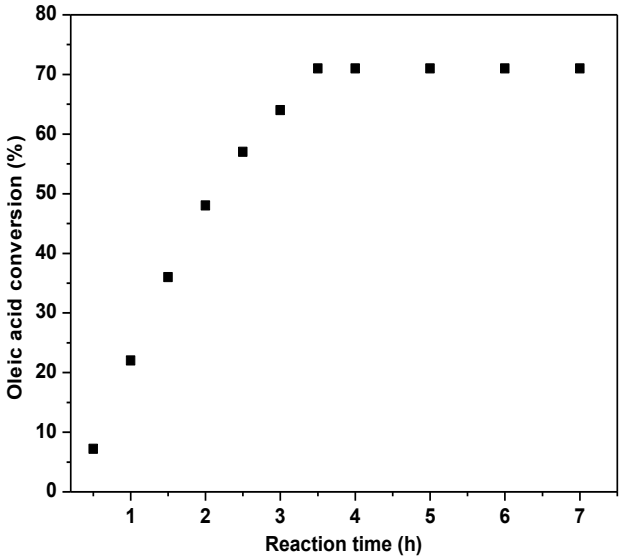

Fig. 7.6. Esterification of oleic acid with ethanol (**Reaction conditions:-** Ethanol to oleic acid ratio 12:1 in presence of 75 °C reaction temperature in presence of 5 wt% of catalyst with respect to oleic acid).

7.3.3. Optimization of the reaction parameters

In order to optimize the reaction parameters to achieve better catalytic performance following reaction parameters have been studied: (i) stirring speed (100-700 rpm), (ii) catalyst concentration (1-6 wt%), (iii) ethanol/oil molar ratio (3-15), and (iv) reaction temperature (35-85 ^{o}C). The effect of individual parameter on the FAEE yield is shown in Fig. 7.7. On the basis of study, a 12:1 ethanol to oil molar ratio at 75 ^{o}C in presence of 5 wt% catalyst (with respect to oil) at stirring speed of 400 rpm were found to be optimum conditions for the 2Sr:Zr-650 catalyzed transesterification of WO.

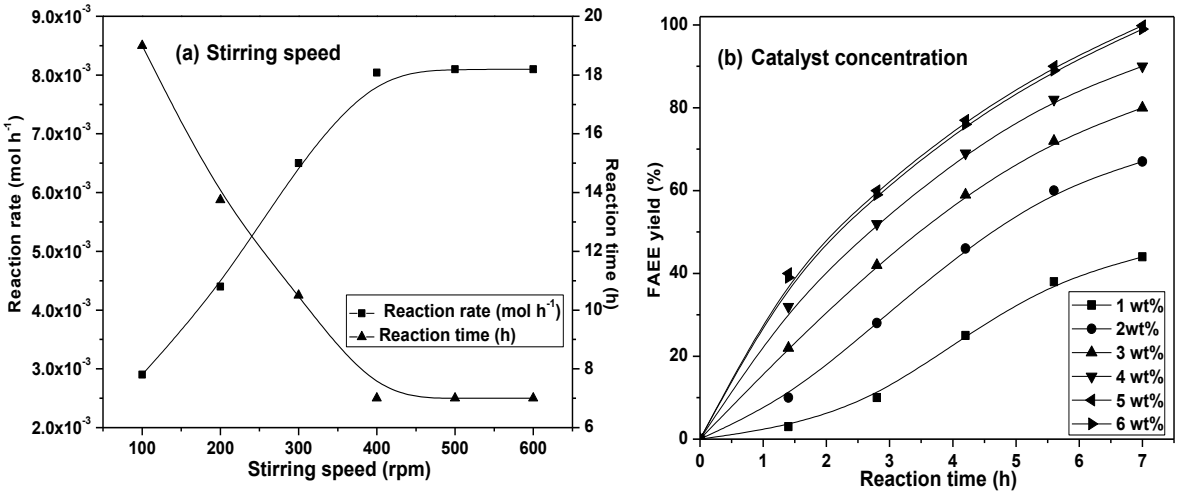

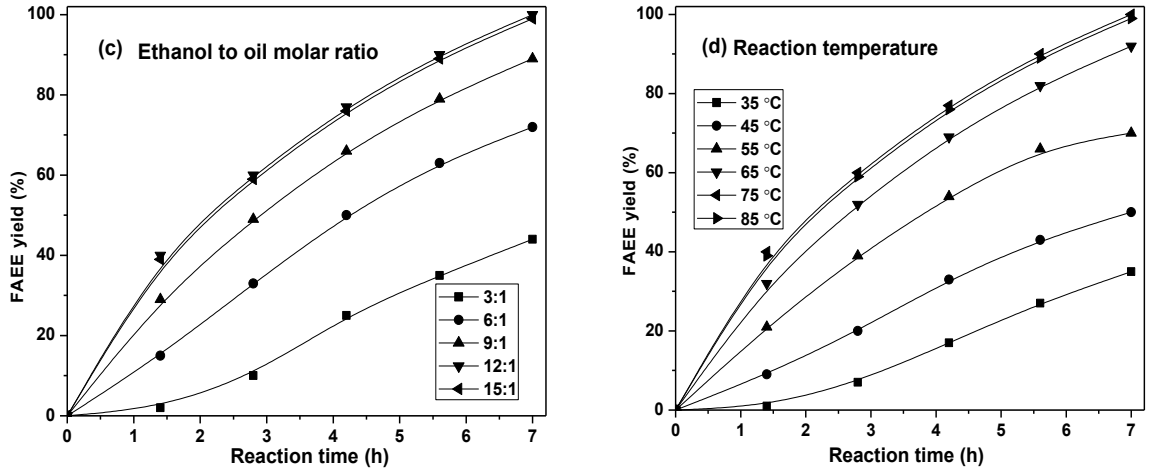

Fig. 7.7. Effect of reaction conditions on 2Sr:Zr-650 catalyzed transesterification of WO. **Reaction conditions:-** (a) ethanol to oil molar ratio of 12:1 at 75 ºC reaction temperature in presence of 5 wt% of catalyst with respect to oil. (b) ethanol to oil molar ratio of 12:1 at 75 ºC reaction temperature (c) Reaction temperature at 75 ºC, in presence of 5 wt% of catalyst with respect to oil (d) ethanol to oil molar ratio of 12:1 in presence of 5 wt% of catalyst with respect to oil.

7.3.4. Effect of moisture and FFA

Homogeneous catalyst required costlier refined feedstock for the transesterification reactions as presence of > 0.3 wt% moisture and/or > 0.5 wt% FFA contents in feedstock leads to the formation of soap instead of biodiesel (Yan *et al.*, 2008). In present study WO employed as feedstock was found to have 4.7 and 0.27 wt% FFA and moisture contents, respectively. When transesterification of the same oil in presence of homogeneous base catalyst (NaOH) was performed, catalyst deactivation occurred due to the soap formation. However, > 99 % FAEE yield was obtained in 2Sr:Zr-650 catalyzed transesterification of WO. In order to determine the maximum moisture resistance of the catalyst, the transesterification reactions of WO were performed by adding up to 4.5 wt% (water/oil) of water in reaction mixture. The 2Sr:Zr-650 was found to be effective for the transesterification of WO having up to 2.0 wt% of moisture contents as shown in Fig. 7.8(a). However, a further increase in water concentration (2.0-4.5 wt%) was found to decrease the catalyst efficiency. This could be attributed to the change of Lewis basic sites (–O–) into Bronsted basic sites (–OH) due to the reaction of water with catalyst. The Bronsted basic sites were found to be less active towards the transesterification than corresponding Lewis basic sites (Kaur and Ali, 2014). The conversion of oxides into respective hydroxides is also evident from the comparison of XRD of neat and moisture exposed catalyst as shown in Fig. 7.8(b).

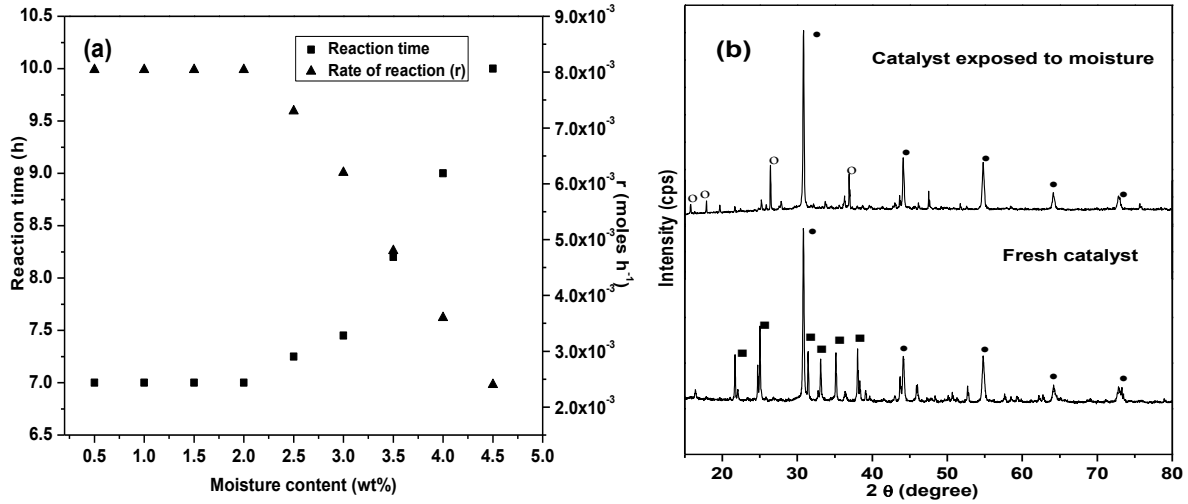

Fig. 7.8. (a) Effect of moisture content on the 2Sr:Zr-650 catalyzed transesterification of WO (reaction time is the time required to achieve > 99% FAEE yield) (b) Comparison of XRD spectra of fresh catalyst and catalyst exposed to water (● = $SrZrO_3$, o = $Sr(OH)_2$).

Non-edible or waste cooking oils, usually found to have FFA contents in relatively higher amount (4.6–18.1 wt% in present study). Conventionally transesterification of high FFA containing vegetable oils is performed in two step process involving acid-catalyzed pre esterification step in the presence of an acid catalyst followed by transesterification in presence of alkali catalyst. The 2Sr:Zr-650 catalyst was found to show the esterification as well as transesterification activity as discussed in previous section. In order to demonstrate the simultaneous esterification as well as transesterification activity of the catalyst in one pot, transesterification reactions of CO, WO, JO and KO (having 1–18.1 wt% FFA) were performed with ethanol as shown in Fig. 7.9. Although catalyst was found to be effective for the transesterification of high FFA containing VOs, however, a decrease in TOF was observed with the increase in FFA contents. This may be due to the strong interactions of highly polar acetate ($-COO^-$) functional group with catalyst (Sr^{2+}/Zr^{4+}) to result in the partial blocking of the active sites.

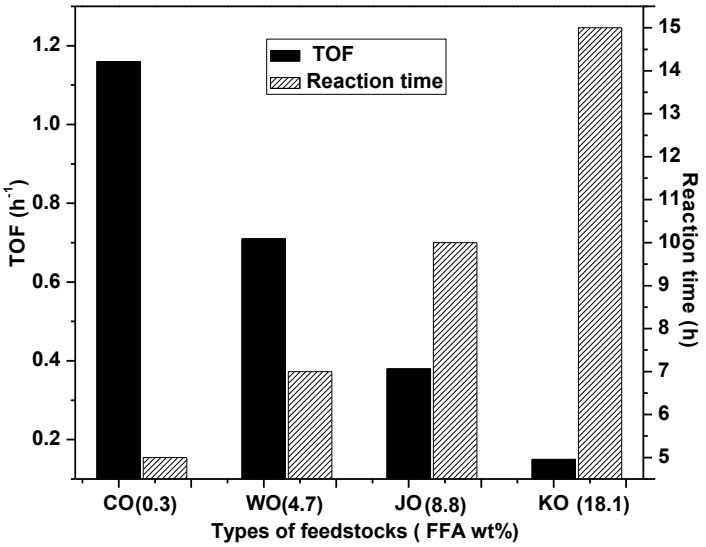

Fig. 7.9. Effect of FFA contents on the 2Sr:Zr-650 catalyzed transesterification of different feed stocks (reaction time is the time required to achieve > 99% FAEE yield). **Reaction conditions:**-Ethanol to oil molar ratio of 12:1 at 75 ºC reaction temperature in presence of 5 wt% (catalyst/oil) catalyst.

7.3.5. Reusability

Commercial success of BD production technologies depends on its production cost. Catalyst reusability could reduce the BD production cost to significant extent. In order to study the stability and reusability of catalyst, it was separated from the reaction mixture by centrifugation, washed with hexane and finally regenerated at 650 °C calcination temperature. The regenerated catalyst was employed in 5 successive catalytic cycles under the same experimental and regeneration methods. As could be seen from Fig. 7.10, no significant loss in catalytic activity was observed during first four runs, however, a partial decrease in activity was observed in fifth cycle.

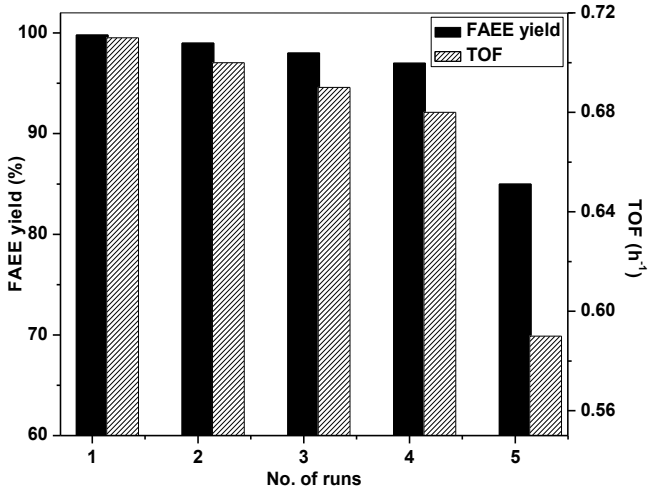

Fig. 7.10. Reusability study of catalyst.

The structural changes and/or leaching of the active catalysts ingredient or blockage/poisoning of active sites could be the reasons behind the activity loss of heterogeneous catalysts (Singh *et al.*, 2014). To identify the structural changes, XRD patterns of fresh and regenerated 2Sr:Zr-650 catalysts are compared in Fig. 7.11(a). In the XRD pattern of regenerated 2Sr:Zr-650 catalyst, diffraction peaks due to SrO were no longer found. The crystallite size of regenerated catalyst was found to be bigger (30.2 nm) than fresh catalyst (27.1 nm) to support partial agglomeration of catalyst during re-calcination process.

As shown from Fig. 7.11(b), in FTIR spectrum of fresh catalyst the stretching vibrations associated with Sr—O and Zr—O bonds appear at 550 and 648 cm^{-1}, respectively (Lima *et al.*, 2012). The bands appeared at 1453 and 1638 cm^{-1} supported the presence of hydroxide and water molecule due to catalyst surface hydration. In regenerated catalyst new bands appeared at 909 and 974 cm^{-1} , in addition to the original bands, to support the changes in catalyst structure which is also consistent with the XRD analysis of the reused catalyst. The spectrum of the regenerated catalyst didn't show vibrations corresponding to any adsorbed organic molecules to indicate that FAEE or glycerol have not been accumulated on the surface of regenerated catalyst.

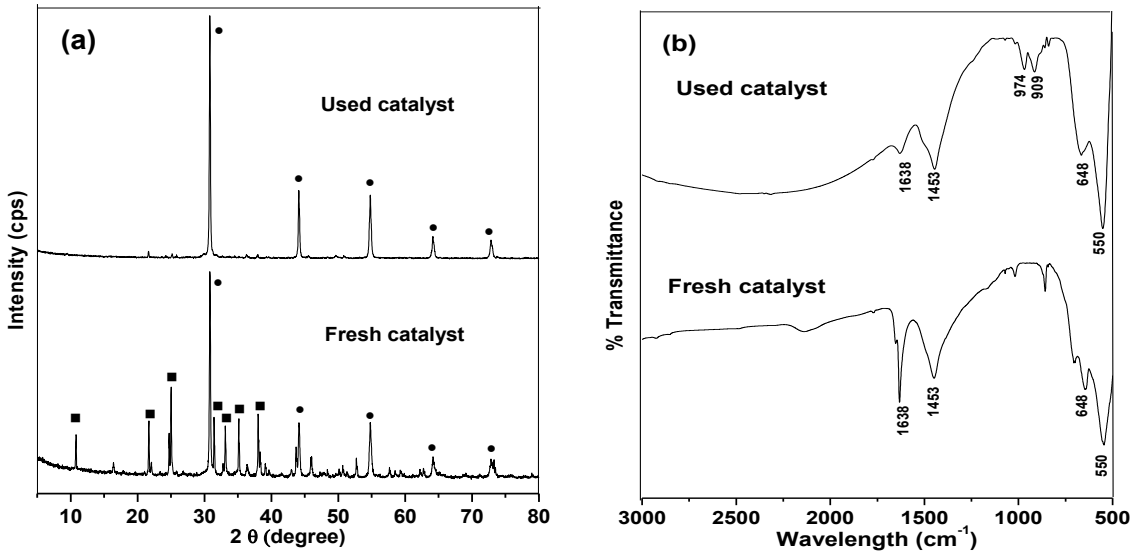

Fig. 7.11. Comparison of (a) XRD and (b) FT-IR of fresh and used catalyst. (■ = SrO; ● = $SrZrO_3$).

The metal analysis supported the presence of metal in FAEE (Sr =1.6 ppm and Zr = 0.8 ppm) as well as in glycerol (Sr = 4.6 ppm and Zr = 3.9 ppm). Thus metal is gradually lost during the catalytic run and could be another reason for the loss of activity. To ensure the

heterogeneous nature of the catalyst, and to prove that leached metal ion has not acted like a homogeneous catalyst, a hot filtration test was performed under optimized reaction conditions. After 1.5 h of reaction duration the catalyst was removed by filtration and reactants were heated again for additional 3.5 h. As could be seen from Fig. 7.12, no significant gain in FAEE yield was obtained after the catalyst removal to prove (i) a truly heterogeneous mode of action of Sr:Zr catalyst and (ii) that leached metal has no contribution in catalytic activity.

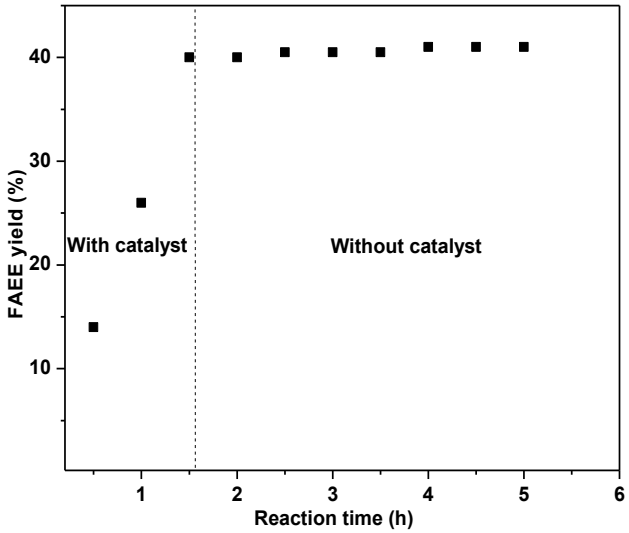

Fig. 7.12. Hot filtration test for 2Sr:Zr-650 catalyzed transesterification.

Therefore, the gradual loss of the catalytic activity could be attributed to the (i) structural changes occurred in catalyst structure and (ii) partial loss of the Sr and Zr from 2Sr:Zr-650 upon repeated use.

7.3.6. Koros–Nowak Criterion test

The absence of internal transfer limitations was demonstrated with the Koros–Nowak criterion test (Song *et al.*, 2011; Madon and Boudart, 1902). In present study the reactions were carried out in presence of two catalysts *viz.*, 5 wt% of 2Sr:Zr-650 or 6 wt% of 1Sr:Zr-650 catalyst dosages to maintain same fractional exposures of active (basic) sites. At similar conversion levels the TOF of both the catalysts were found to be almost similar as shown in Fig. 7.13. Thus Sr:Zr catalyzed reaction is free from mass diffusion limitations and is a chemically controlled reaction.

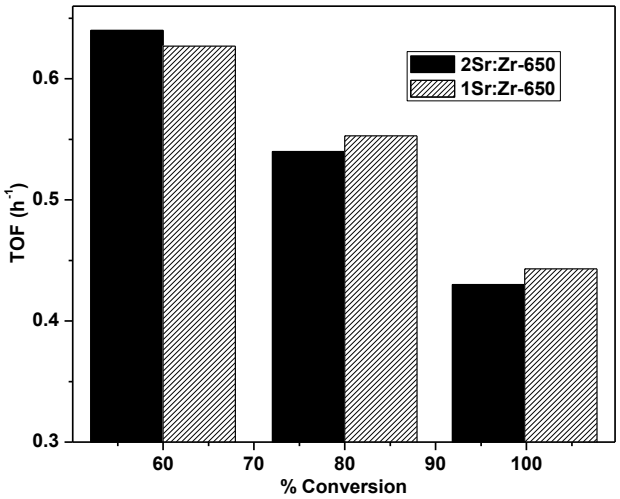

Fig. 7.13. A plot of TOF *vs* % conversion for the 1Sr:Zr-650 and 2Sr:Zr-650 catalyzed ethanolysis of WO. **Reaction conditions:** ethanol to oil molar ratio; 12:1 at 75 °C and catalyst concentration; either 5 wt% of 2Sr:Zr-650 or 6 wt% of 1Sr:Zr-650.

7.3.7. Kinetics and thermodynamic study

Transesterification is generally assumed to follow pseudo-first-order kinetics as alcohol in such reactions are employed in excess to the required stoichiometric amount of 3:1 alcohol to oil molar ratio. In present work also optimized alcohol to VO molar ratio was 12:1 and hence, the kinetics of 2Sr:Zr-650 catalyzed ethanolysis has been studied by following (pseudo) first order equation 2.3 (Chapter 2).

The linear nature of the plot between $-\ ln(1-X)$ *vs* t plot supported that the reaction has followed the (pseudo) first order rate law (Fig. 7.14(a)). The apparent first order rate constant from the plot was found to be 0.648 h^{-1} at 75 ºC.

To calculate the activation energy, reactions were carried out in temperatures range of 35-75 ºC. The Arrhenius equation was employed to estimate the activation energy (E_a) and pre–exponential factor (A) following the equation 2.4 (Chapter 2).

A plot between ln k *vs* 1/T is shown in Fig. 7.14(b), and the values of E_a and A from the plot was found to be 48.17 kJ mol^{-1} and 6.83 × 10^6 h^{-1}. The observed E_a value in present study (48.17 kJ mol^{-1}) was found within the range of the reported values (26-82 kJ mol^{-1}) for transesterification reaction catalyzed by heterogeneous catalysts (Kaur and Ali, 2014).

A value of E_a > 25 kJ mol^{-1} also supported that 2Sr:Zr-650 catalyzed transesterification is a chemically controlled reaction and not controlled by mass transfer limitations (Patel and Brahmkhatri, 2013).

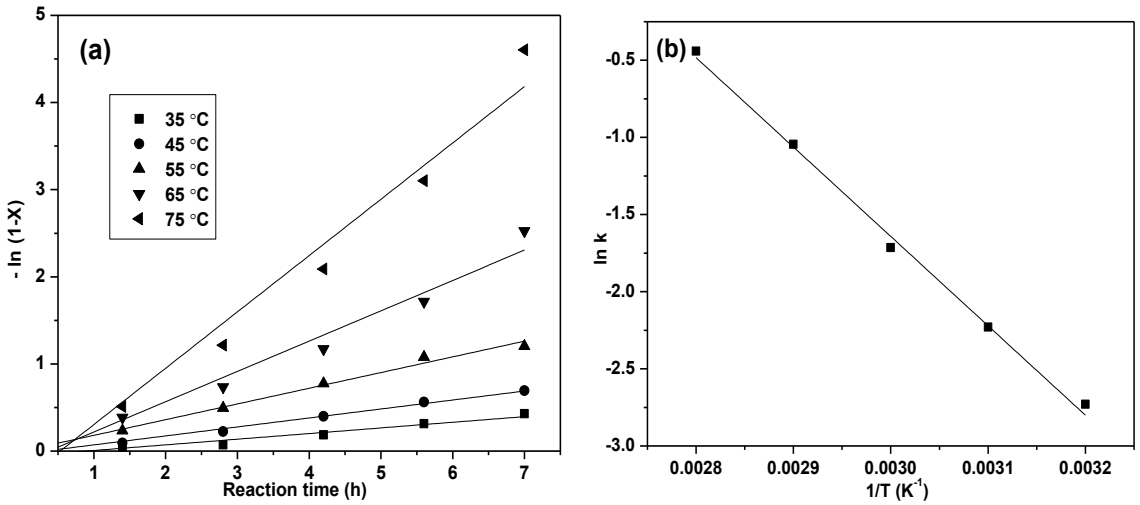

Fig. 7.14. Kinetic study of transesterification of WO with ethanol over 2Sr:Zr-650 catalyst. (a) Plots of –ln(1–X) *vs* time at different temperatures (b) Arrhenius plot of ln k *vs* 1/T. **Reaction conditions:** ethanol to oil molar ratio of 12:1 and 5 wt% of 2Sr:Zr-650 with respect to oil.

Thermodynamic analysis was addressed for evaluating the enthalpy ($\Delta H^{\ddagger}$), entropy ($\Delta S^{\ddagger}$), and the Gibb's free energy of activation ($\Delta G^{\ddagger}$), which are the important features for interpreting the behaviour of transesterification reactions. In this regard activation complex theory, developed by Eyring, was applied to evaluate thermodynamic parameters from temperature-dependent rate constants. These parameters are calculated from Eyring-Polanyi equation 2.6 (Chapter 2).

Fig. 7.15 depicts the Eyring plot of transesterification and the value of $\Delta H^{\ddagger}$ was found to be 45.97 kJ mol^{-1} indicating that energy input (heat) from external source is required to raise the energy level and transform the reactants to transition state. The value of $\Delta S^{\ddagger}$ was found to be -121.37 J $mol^{-1}K^{-1}$ and a negative value suggests associative mechanism in which reactant species have joined together to form a more ordered transition state. The $\Delta G^{\ddagger}$ value was found to be 88.23 kJ mol^{-1}, to indicate unspontaneous nature of the reaction having higher energy level of transition state than reactant species.

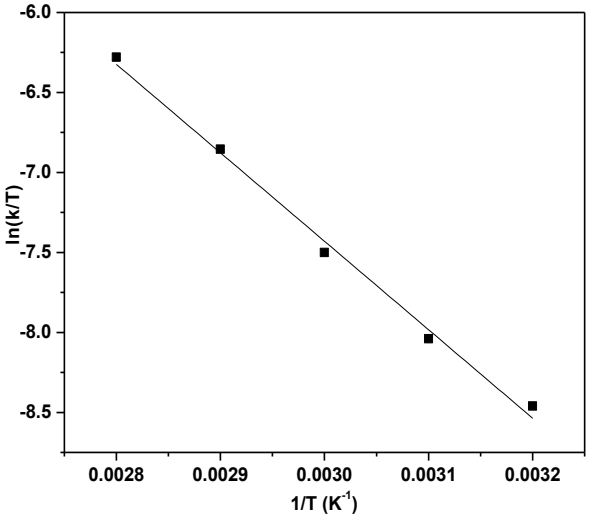

Fig. 7.15. The Eyring plot of 2Sr:Zr-650 catalyzed transesterification of WO.

7.3.8. GC/MS analysis of FAEE

Physicochemical properties such as viscosity, freezing point, cold flow properties of BD depends upon its chemical composition. GC/MS analysis was performed to quantify the FAEE yield as well as FAEE chemical composition. Seven peaks were observed in GC chromatogram (Fig. 7.16) of FAEE prepared from WO.

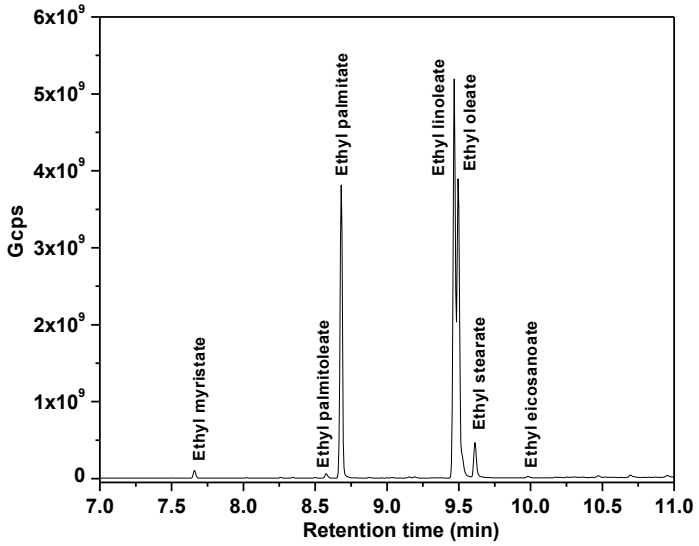

Fig. 7.16. Gas chromatogram of FAEE.

Each peak corresponds to a fatty acid ethyl ester which was identified on the basis of MS pattern from the library match software (NIST) and the component corresponding to individual peak is listed in Table 7.3. The total FAEE contents obtained through area normalization method was found 99.61 wt%. Out of which total saturated and unsaturated

fatty acid alkyl ester content was found to be 31.32 and 68.29 wt%, respectively. A higher unsaturated fatty acid alkyl ester contents reflects the better cold flow properties of BD even at low temperature (Lotero *et al.*, 2005).

Table 7.3. Analysis of compositions of FAEE.

S.No.	Retention time (min)	Composition; Molecular formula	Corresponding acid (Cx:y)	Wt %
1	7.66	Myristic acid ethyl ester; $C_{16}H_{32}O_2$	Myristic acid (C14:0)	0.86
2	8.57	Palmitoleic acid ethyl ester; $C_{18}H_{34}O_2$	Palmitoleic acid (C16:1)	0.62
3	8.68	Palmitic acid ethyl ester; $C_{18}H_{36}O_2$	Palmitic acid (C16:0)	26.64
4	9.46	Linoleic acid ethyl ester; $C_{20}H_{36}O_2$	Linoleic acid (C18:2)	37.77
5	9.49	Oleic acid ethyl ester; $C_{20}H_{38}O_2$	Oleic acid (C18:1)	29.90
6	9.61	Stearic acid ethyl ester; $C_{20}H_{40}O_2$	Stearic acid (C18:0)	3.44
7	9.90	Eicosanoic acid ethyl ester;$C_{22}H_{44}O_2$	Eicosanoic acid (C20:0)	0.38

Cx:y = x is number of carbon atom, y is number of double bonds.

7.4. Conclusions

In present work, 2Sr:Zr-650 catalyst has been prepared as ~ 25-30 nm sized particles as revealed by powder XRD and TEM techniques. The catalyst was found to be effective for the one pot esterification and transesterification of a variety of feedstock having up to 2.0 and 18 wt% of moisture and FFA contents, respectively. Under optimized reaction conditions (catalyst concentration 5 wt%, ethanol to oil molar ratio of 12:1 at 75 °C and 400 rpm) the transesterification of the waste cottonseed oil was found to follow (pseudo) first order rate law. Activation and Gibbs free energy for the ethanolysis of waste cottonseed oil was found to be 48.17 and 88.23 kJ mol^{-1}, respectively. The catalyst has been recovered and recycled without any significant loss in activity during first four catalytic cycles. The leaching test supports the negligible homogeneous contribution in catalytic activity, and Koros-Nowak test demonstrated that the activity is free from transport phenomenon.

References

Brunschwig, C.; Moussavou, W.; Blin, J.; Use of bioethanol for biodiesel production. *Prog. Energ. Combust. Sci.*, **2012**, 38, 283-301.

Kaur N.; Ali, A.; Kinetics and reusability of Zr/CaO as heterogeneous catalyst for the ethanolysis and methanolysis of Jatropha crucas oil. *Fuel Process. Technol*., **2014**, 119,173.

Lima, J. R. O.; Ghani, Y. A.; Silva, R. B.; Batista, F. M. C.; Bini, R. A.; Varanda, L. C.; Oliveira, J. E.; Strontium zirconate heterogeneous catalyst for biodiesel production: Synthesis, characterization and catalytic activity evaluation. *Appl. Catal. A: Gen*., **2012**, 445-446, 76-82.

Lotero, E.; Liu, Y.; Lopez, D. E.; Suwannakarn, K.; Bruce, D. A.; Goodwin, J. G.; Synthesis of biodiesel via acid catalysis. *Ind. Eng. Chem. Res.*, **2005**, 44, 5353.

Madon, R. J.; Boudart, M.; Experimental criterion for the absence of artifacts in the measurement of rates of heterogeneous catalytic reactions. *Ind. Eng. Chem. Fundam.*, **1982**, 21, 438-447.

Patel A.; Brahmkhatri, V.; Kinetic study of oleic acid esterification over 12 tungstophosphoric acid catalyst anchored to different mesoporous silica supports. *Fuel Process. Technol.*, **2013**, 113, 141.

Patil, P. D.; Deng, S.; Transesterification of Camelina Sativa oil using heterogeneous metal oxide catalysts. *Energy Fuel*, **2009**, 23, 4619-4624.

Sankaranarayanan, S.; Antonyraj, C. A.; Kannan, S.; Transesterification of edible, non-edible and used cooking oils for biodiesel production using calcined layered double hydroxides as reusable base catalysts. *Bioresour. Technol*., **2012**, 109, 57-62.

Singh, D.; Bhoi, R.; Ganesh A.; Mahajani, S.; Synthesis of biodiesel from vegetable oil using supported metal oxide catalysts. *Energy Fuel*, **2014**, 28, 2743-2753.

Song, R.; Tong, D.; Tang, J; Hu, C; Effect of composition on the structure and catalytic properties of KF/Mg_La solid base catalysts for biodiesel synthesis via transesterification of cottonseed oil. *Energy Fuel*, **2011**, 25, 2679-2686.

Yan, S.; Lu, H.; Liang, B.; Supported CaO catalysts used in the transesterification of rapeseed oil for the purpose of biodiesel production, *Energy Fuel*, **2008**, 22, 646-651.

Yan, S.; Salley, S. O.; Simon, K. Y.; Simultaneous transesterification and esterification of unrefined or waste oils over ZnO-La_2O_3 catalysts. *Appl. Catal. A: Gen.*, **2009**, 353, 203-212.

Conclusions and Futuristic Aspect

Abstract: The results given in chapter 3-7 have been concluded, compared and correlated in this chapter. A future scope of work with the prepared catalysts is also discussed.

8.1. Introduction

In the present thesis, work was carried out for the preparation and characterization of calcium and zirconium oxide based catalysts and their application as solid catalysts for the transesterification of a variety of feed stocks. Few catalysts are able to catalyze simultaneous esterification and transesterification of vegetable oils containing high FFA content. Efficacy of the prepared catalysts was also tested towards ethanolysis of VOs to utilize ethanol, non-toxic and green chemical, for biodiesel production.

8.2. Conclusions from present thesis

In ***Chapter 3***, Cerium and sulphate impregnated ZrO_2-TiO_2 catalyst was prepared and found to catalyzed esterification of various carboxylic acids using different alcohols. The catalyst with higher number of Bronsted acid sites shows better activity and excellent stability as negligible sulfate leaching was observed and recovered catalyst was reused in five successive runs without significant loss in activity. The catalyst was able to catalyze the esterification even in presence of up to 12 wt% moisture (with respect to fatty acids), however, a decrease in turn over frequency (TOF) was observed. The catalytic activity was not found to be effected by the presence of triglycerides and hence it was successfully employed for the reduction of FFA present in vegetable oils (Scheme 8.1).

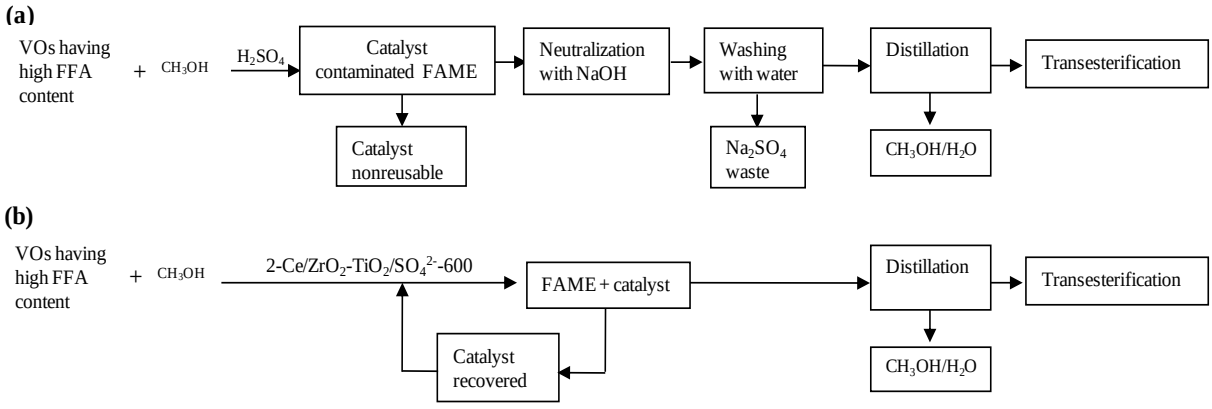

Scheme 8.1. Comparison of the reaction schemes for the production of biodiesel from high FFA containing vegetable oil. Esterification is catalyzed by (a) homogeneous acid (H_2SO_4), and (b) 2-Ce/ZrO_2–TiO_2/SO_4^{2-}-600, followed by the transesterification.

In ***Chapter 4***, Zr/CaO was prepared via wet impregnation method and found to be active for the methanolysis and ethanolysis of jatropha oil (Scheme 8.2). The catalyst has shown high moisture and FFA tolerance and found to be effective for the transesterification of feedstocks having up to 6 and 15 wt% moisture and FFA contents, respectively. The optimum values of

the parameters, to achieve > 99 % fatty acid alkyl ester yield, were: catalyst concentration of 5 wt%, methanol/oil molar ratio of 15:1 at 65 °C or ethanol/oil molar ratio of 21:1 at 75 °C. Following the pseudo first order kinetic equation, activation energy for the methanolysis and ethanolysis of jatropha oil was found to be 29.8 and 42.5 kJ mol^{-1}, respectively. The catalyst was reusable and its catalyst activity was persistent for two catalytic runs.

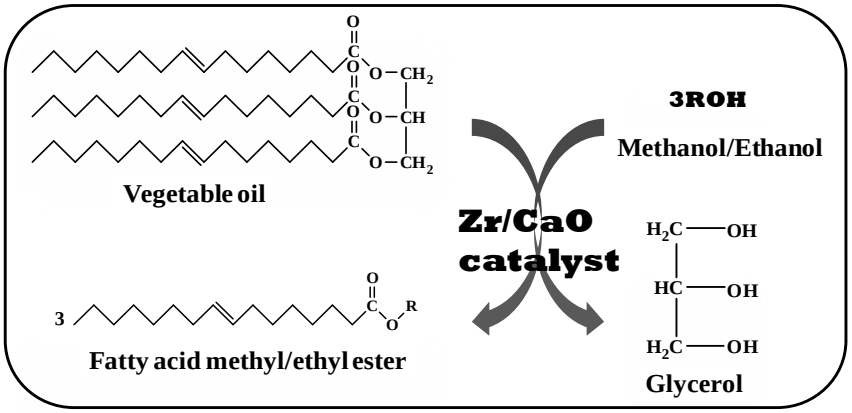

Scheme 8.2. Transesterification of vegetable oil with methanol or ethanol using Zr/CaO catalyst.

In ***Chapter 5***, Mo impregnated CaO was synthesized and found effective for the transesterification of non edible oils having FFA contents as high as 18.1 wt%. The catalyst was found to be reusable for five runs without significant leaching of metal ions. The Koros-Nowak test and mass transfer limitation study demonstrate that catalytic activity was independent from the diffusion limitations. The values of thermodynamic activation parameters $\Delta G^{\ddagger}$, $\Delta H^{\ddagger}$ and $\Delta S^{\ddagger}$ were found out to be 43.62 kJ mol^{-1}, 64.10 kJ mol^{-1} and -60.58 J $mol^{-1}K^{-1}$, respectively, which show that reaction was unspontaneous, endothermic and endergonic in nature.

In ***Chapter 6***, Li/ZrO_2 has been prepared by wet chemical method and characterized by powder XRD, FT-IR, SEM-EDS and TEM techniques. Li/ZrO_2 catalyst was found to be an effective catalyst for the simultaneous esterification and transesterification of a variety of feedstock having up to 4 and 18 wt% of moisture and FFA contents, respectively (Scheme 8.3). The activation energy for the methanolysis and ethanolysis of waste cottonseed oil was found to be 40.8 and 43.1 kJ mol^{-1}, respectively. The catalyst has been recovered and recycled without any significant loss in activity (≥90 % FAME yield) during nine cycles. The leaching study supported the negligible homogeneous contribution in catalytic activity.

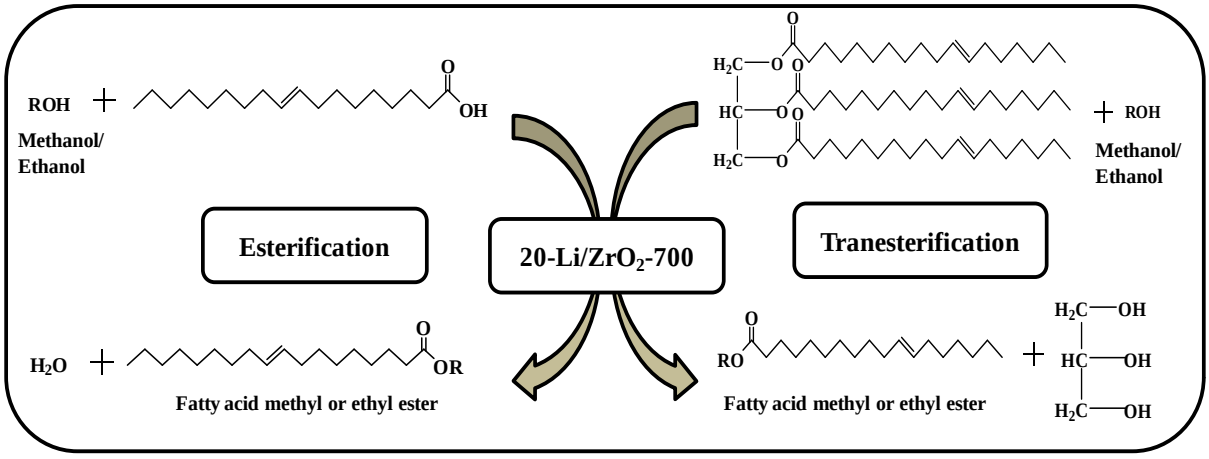

Scheme 8.3. Li/ZrO_2 catalyst showing simultaneous esterification and transesterification of high free fatty acid containing vegetable oils.

In ***Chapter 7***, Sr and Zr based mixed oxide catalyst was prepared by co-precipitation method and found to be effective for the one pot esterification and transesterification of a variety of feedstock having up to 2.0 and 18 wt% of moisture and FFA contents, respectively. Activation and Gibbs free energy for the ethanolysis of waste cottonseed oil was found to be 48.17 and 88.23 kJ mol^{-1}, respectively. The catalyst has been recovered and recycled without any significant loss in activity during first four catalytic cycles. The leaching test supports the negligible homogeneous contribution in catalytic activity, and Koros-Nowak test demonstrated that the activity is free from transport phenomenon.

The activity of the prepared catalysts, reported in present thesis is compared in Table 8.1.

Table 8.1. Comparison of reaction conditions of prepared catalysts used for the transesterification of vegetable oils.

Catalyst	Feedstock	Alcohol	Reaction conditions*						Activation energy (kJ mol^{-1})
			FFA/ Moisture tolerance(%)	Reaction temperature (°C)	Alcohol/ oil (m/m)	Reaction time (h)	FAAE yield (%)	Reusability	
Zr/CaO	Jatropha oil	Methanol	15/6	65	15:1	1.75	>99	2	29.8
		Ethanol	ND	75	21:1	7		ND	42.5
Mo/CaO	Jatropha oil	Ethanol	18.1/6.5	65	12:1	4.5	>99	5	66.0
Li/ZrO_2	Waste cotton seed	Methanol	18.1/4	65	12:1	1.25	>98	9	40.8
		Ethanol	ND	75	15:1	4.5	>98	ND	43.1
Sr:Zr	Waste cotton seed	Ethanol	18.1/4.5	75	12:1	7	>99	4	48.2

*All the reactions were performed in presence of 5 wt% catalyst (with respect to oil); ND – Not determined

Thus, all prepared catalysts have shown excellent activity and have the potential to use non edible oils or waste cooking oils having high FFA and moisture content, as feedstock for biodiesel preparation.

8.3. Futuristic aspects

Few futuristic suggestions related with the present work are listed below:

1. In future, other transition metals such as tungsten, nickel and iron based mixed oxide will be prepared and used as catalyst for simultaneous esterification and transesterification to produce biodiesel.
2. In present work mainly wet chemical route and co-precipitation method has been employed for the catalyst preparation. To further improve the stability of the catalyst other preparation methods such as sol-gel, template assisted, solvothermal, and hydrothermal, could also be explored.
3. To solve the problem of glycerol management, interesterification of triglycerides with methyl acetate (Scheme 8.4) *via* Saka-Isayama process (Saka and Isayama, 2009) in presence of prepared catalysts could also be explored. In this process glycerol is not produced and mixture of FAME and triacetin can be used directly as biodiesel.

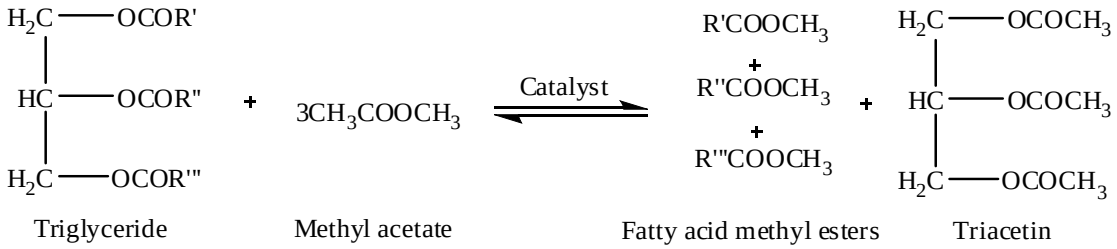

Scheme 8.4. Interesterification reaction between triglycerides and methyl acetate to produce fatty acid methyl esters (FAME) and triacetin.

4. Shape selective magnetic catalysts will be prepared for biodiesel production to simplify the separation process.
5. Non-conventional heating methods, such as microwave, will be used for the catalyst preparation as well as to biodiesel production to reduce the reaction time and production cost.

Reference

Saka, S.; Isayama, Y.; A new process for catalyst-free production of biodiesel using supercritical methyl acetate. *Fuel*, **2009**, 88, 1307-1313.

APPENDIX A

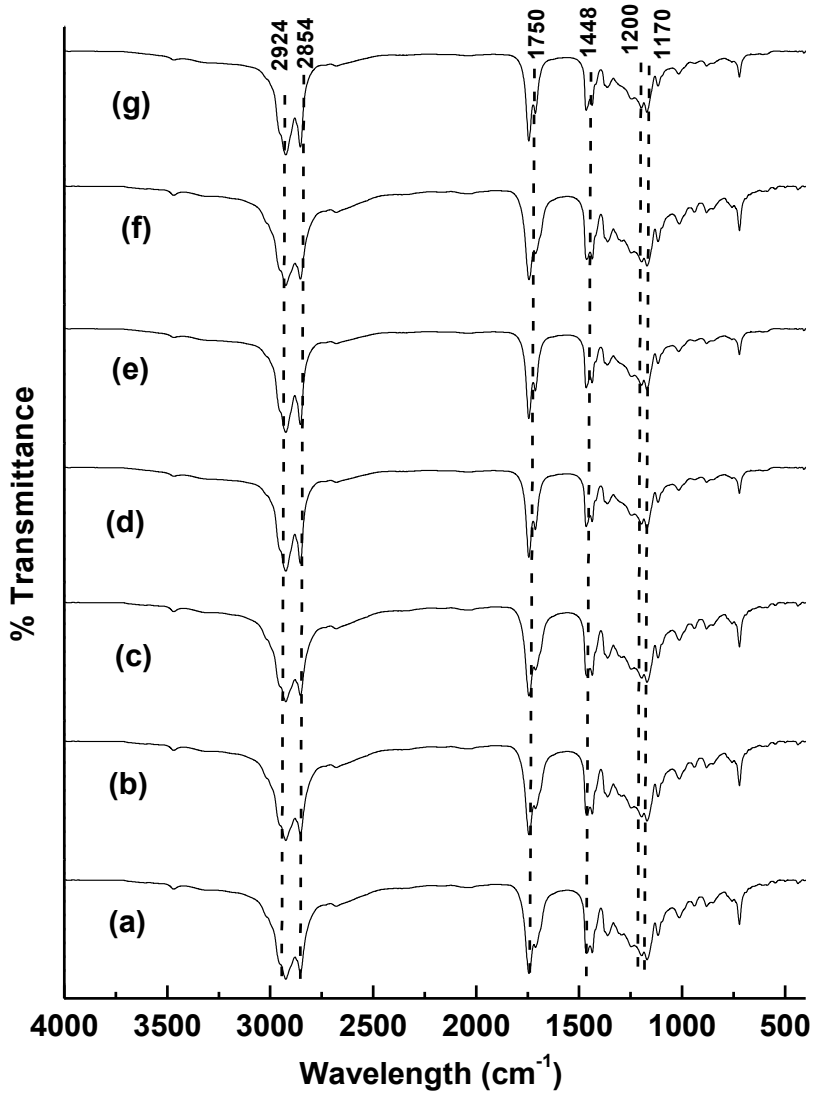

Fig.A.1. FT-IR of (a) methyl propanoate, (b) methyl butyrate, (c) methyl caproate, (d) methyl caprylate, (e) methyl laurate, (f) methyl palmitate and (g) methyl stearate.

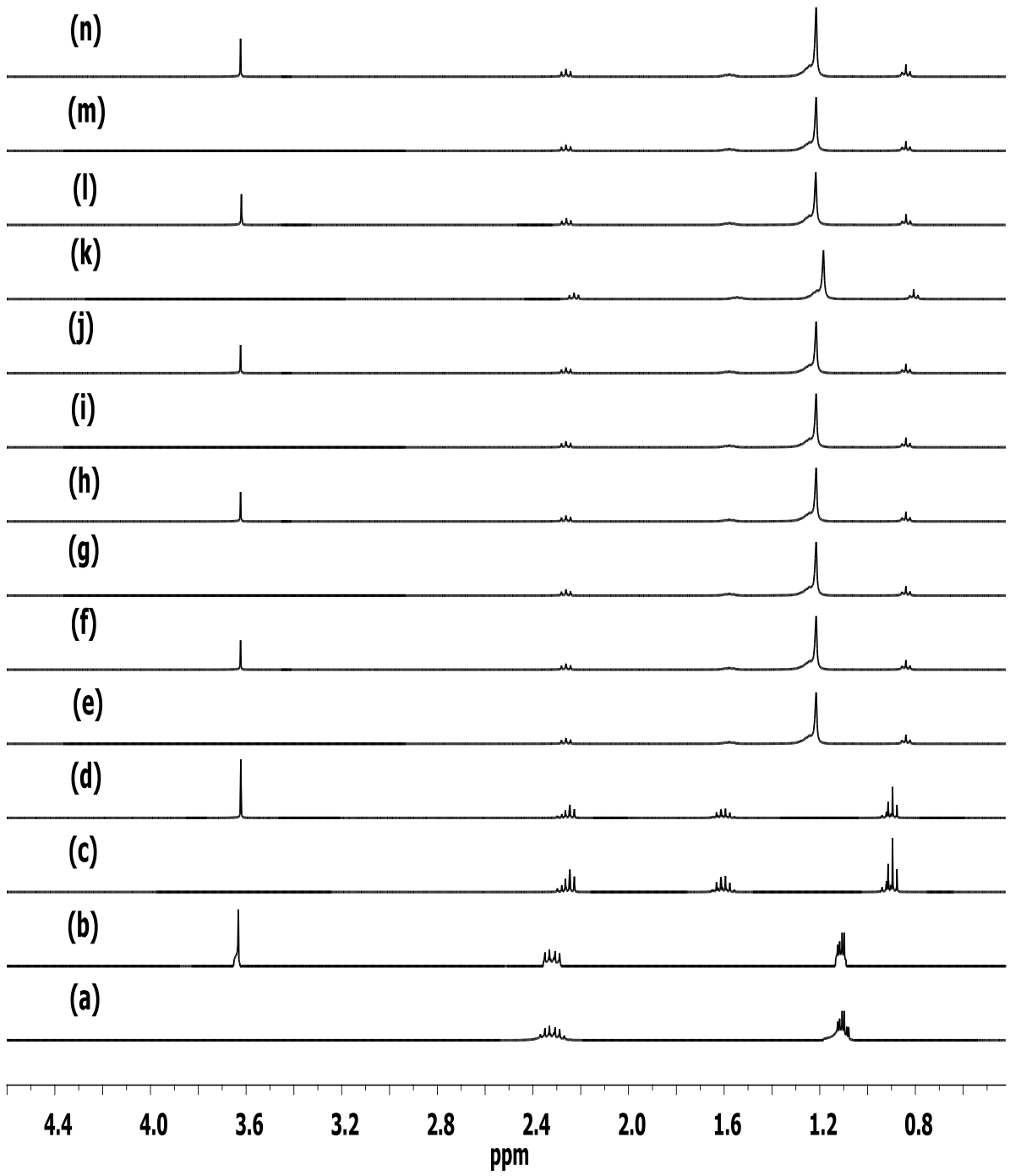

Fig.A.2. ^{1}H-NMR of (a) propanoic acid, (b) methyl propanoate, (c) butyric acid, (d) methyl butyrate, (e) caproic acid, (f) methyl caproate, (g) caprylic acid, (h) methyl caprylate, (i) lauric acid, (j) methyl laurate, (k) palmitic acid, (l) methyl palmitate, (m) stearic acid and (n) methyl stearate.

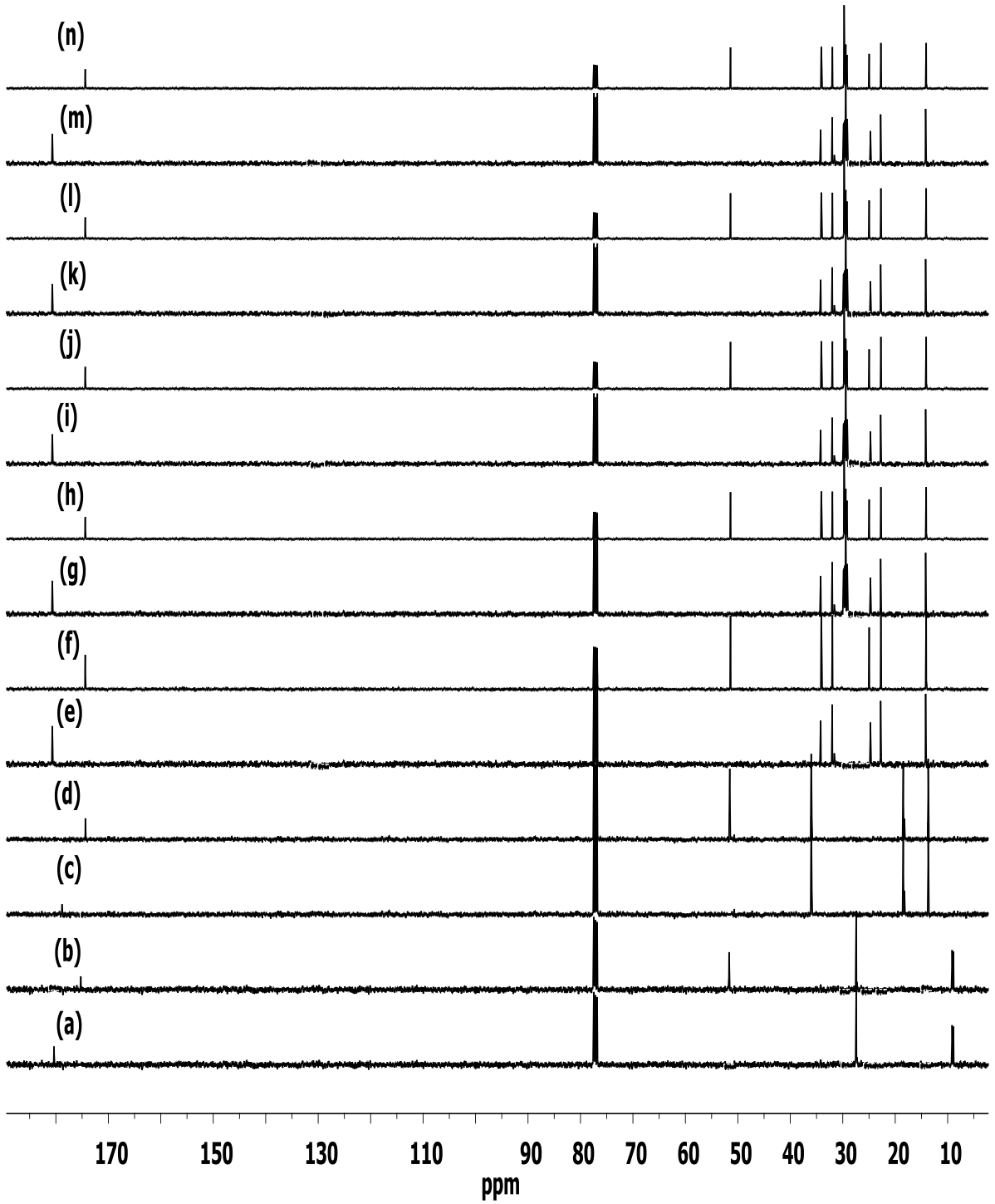

Fig.A.3. ^{13}C-NMR of (a) propanoic acid, (b) methyl propanoate, (c) butyric acid, (d) methyl butyrate, (e) caproic acid, (f) methyl caproate, (g) caprylic acid, (h) methyl caprylate, (i) lauric acid, (j) methyl laurate, (k) palmitic acid, (l) methyl palmitate, (m) stearic acid and (n) methyl stearate.

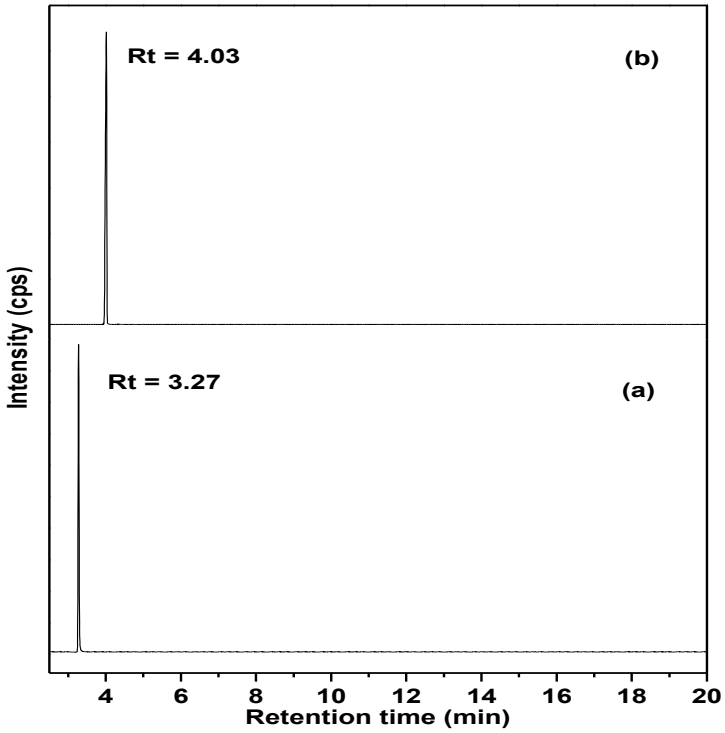

Fig.A.4. GC chromatogram of (a) methyl propanoate and (b) methyl butyrate.

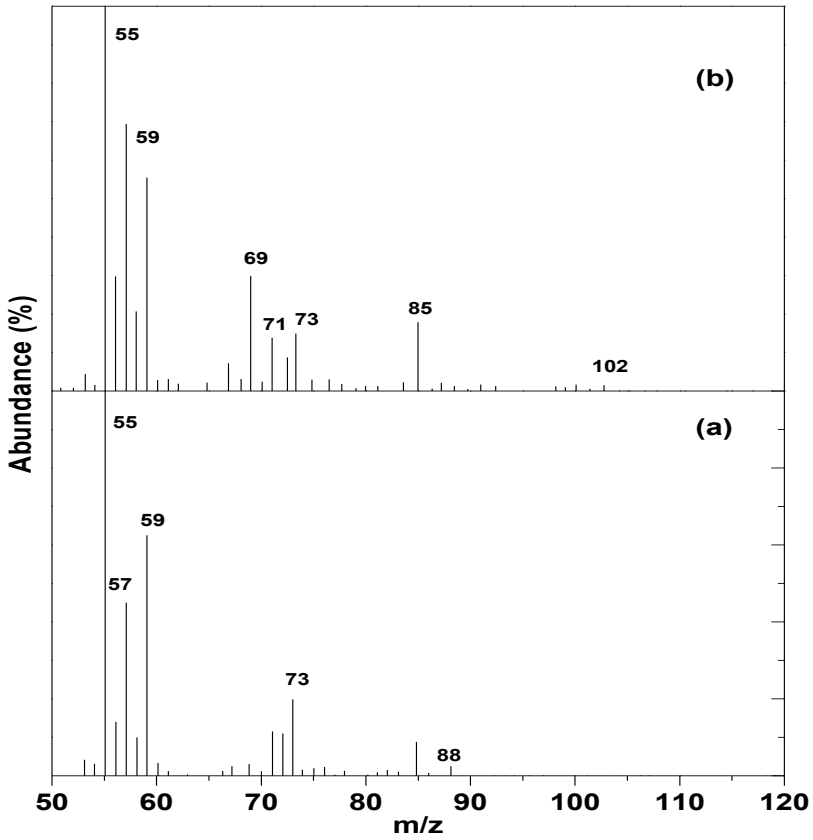

Fig.A.5. Mass spectra of (a) methyl propanoate and (b) methyl butyrate.

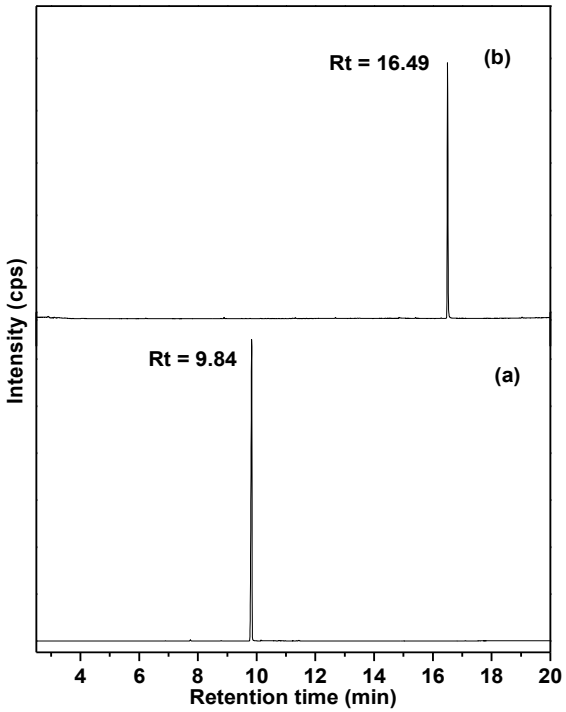

Fig.A.6. GC chromatogram (a) methyl palmitate and (b) methyl stearate.

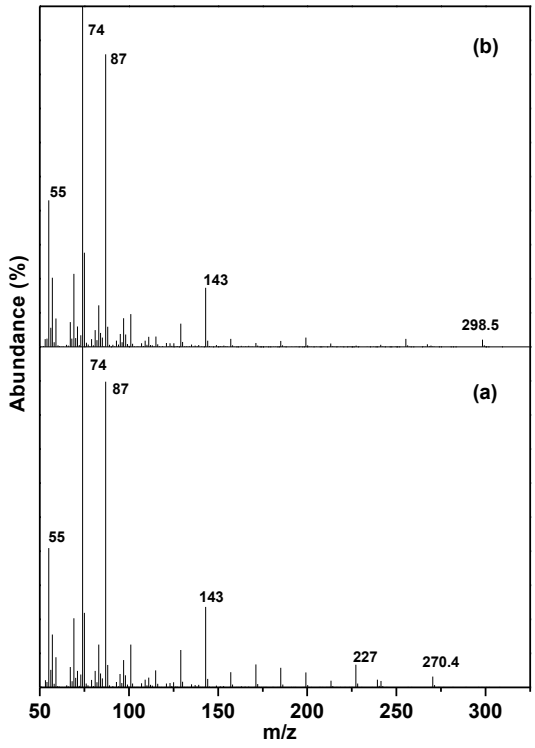

Fig.A.7. Mass spectra of (a) methyl palmitate and (b) methyl stearate.

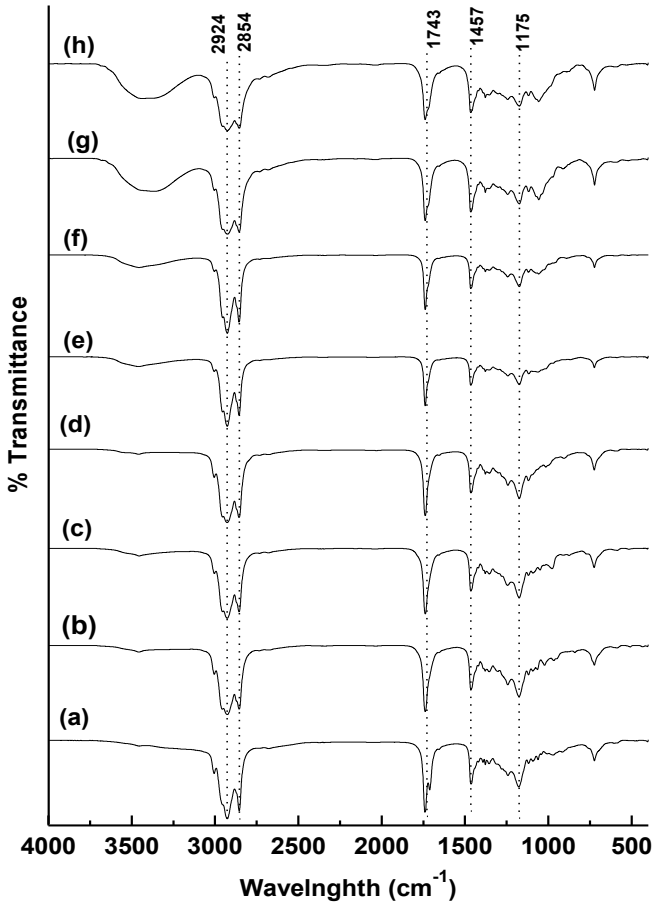

Fig.A.8. FT-IR of (a) propyl oleate, (b) butyl oleate, (c) pentyl oleate, (d) hexyl oleate, (e) heptyl oleate, (f) octyl oleate, (g) nonyl oleate and (h) decyl oleate.

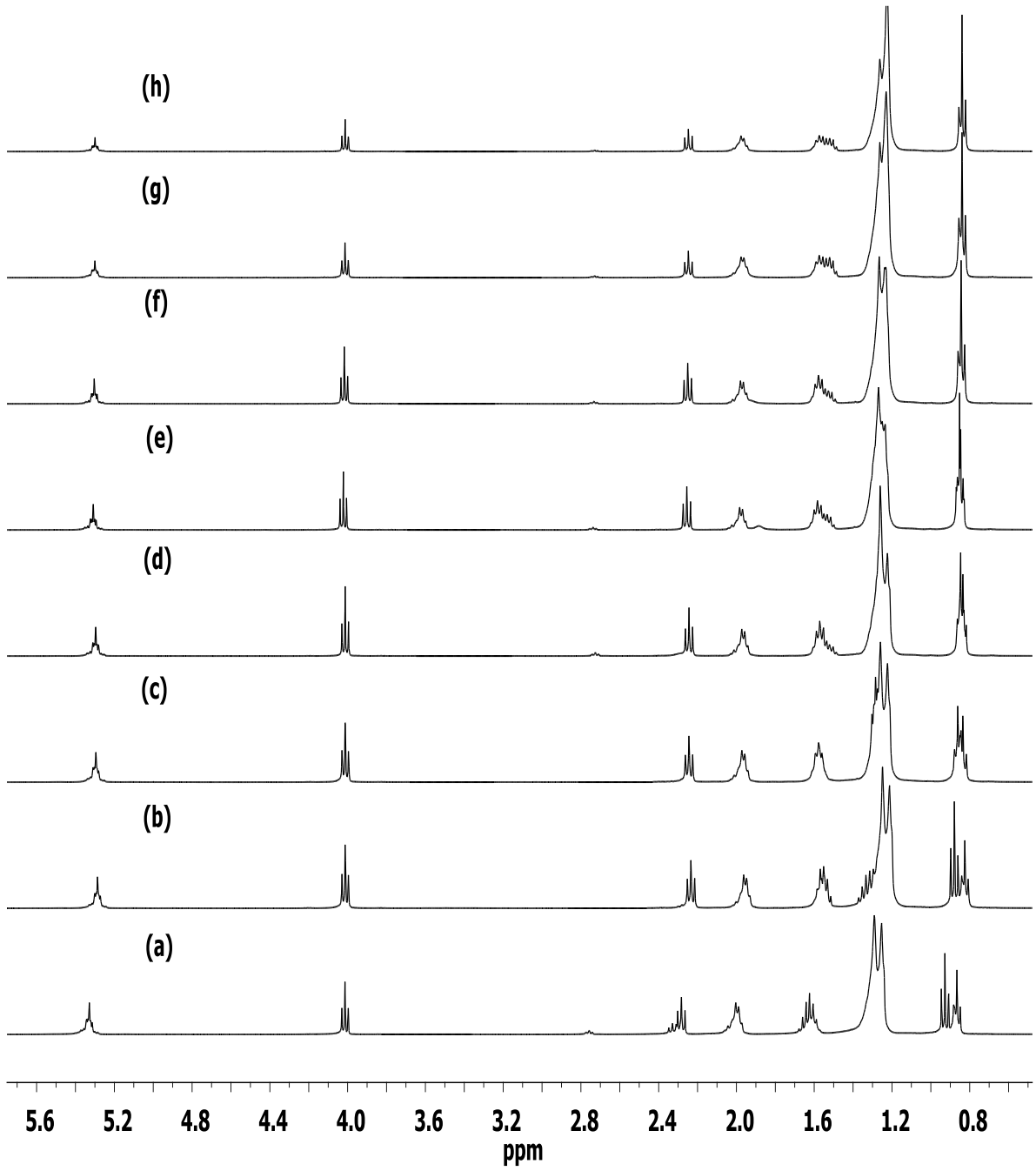

Fig.A.9. ^{1}H-NMR of (a) propyl oleate, (b) butyl oleate, (c) pentyl oleate, (d) hexyl oleate, (e) heptyl oleate, (f) octyl oleate, (g) nonyl oleate and (h) decyl oleate.

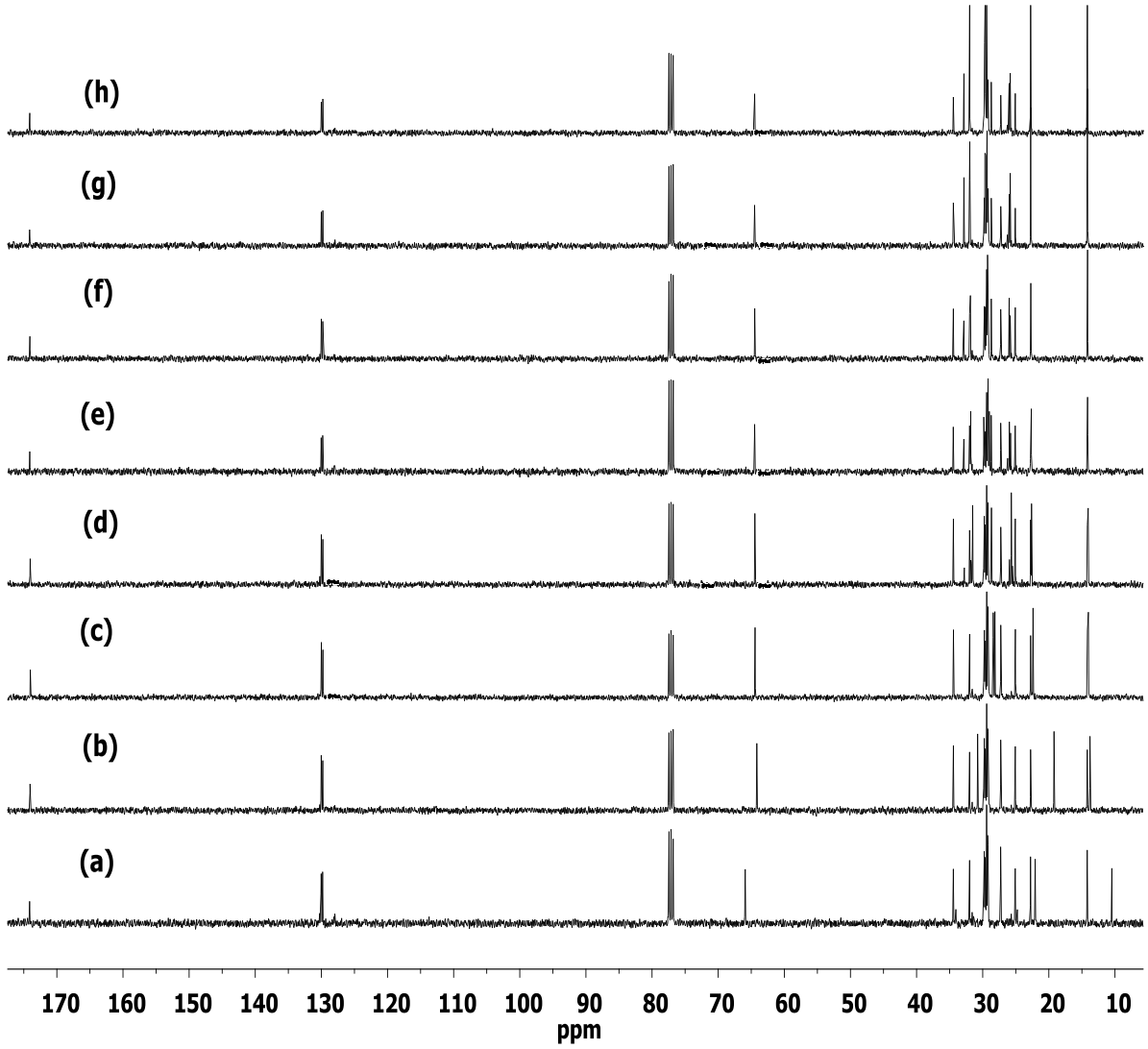

Fig.A.10. ^{13}C-NMR of (a) propyl oleate, (b) butyl oleate, (c) pentyl oleate, (d) hexyl oleate, (e) heptyl oleate, (f) octyl oleate, (g) nonyl oleate and (h) decyl oleate.

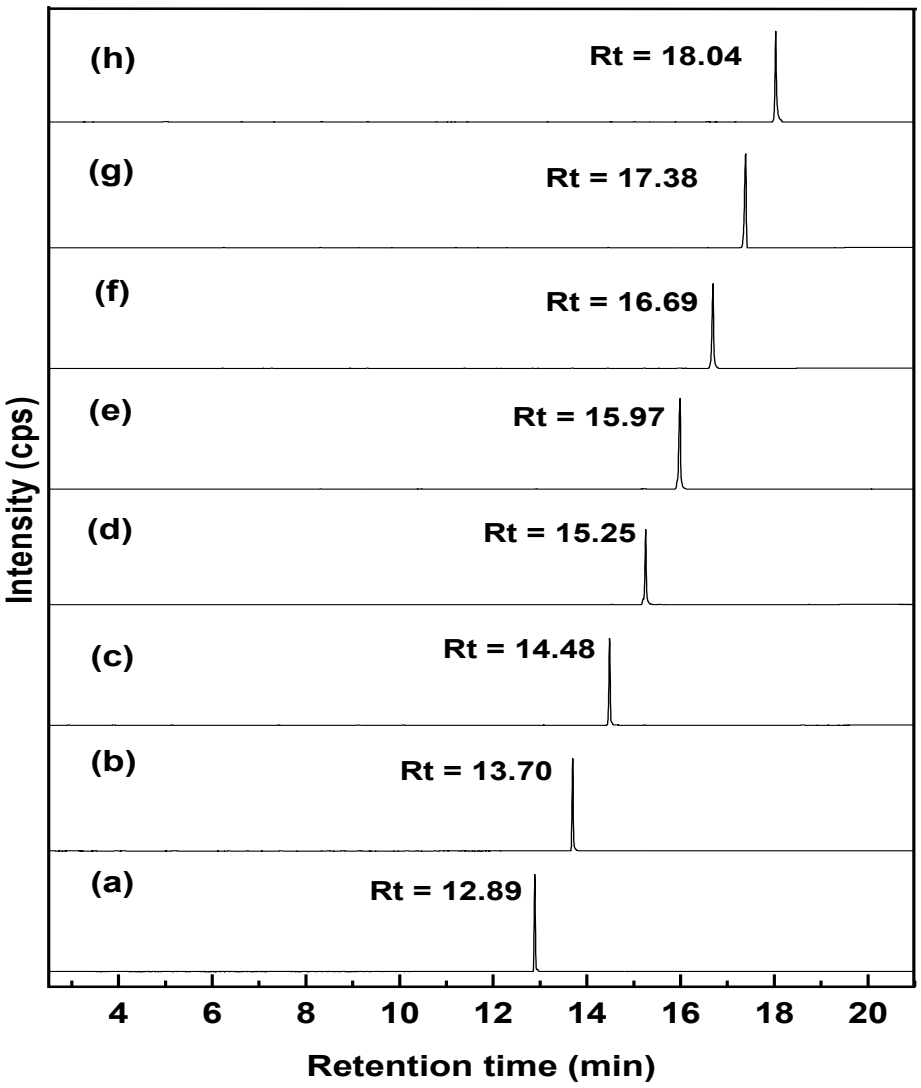

Fig.A.11. GC chromatogram of (a) propyl oleate, (b) butyl oleate, (c) pentyl oleate, (d) hexyl oleate, (e) heptyl oleate, (f) octyl oleate, (g) nonyl oleate and (h) decyl oleate.

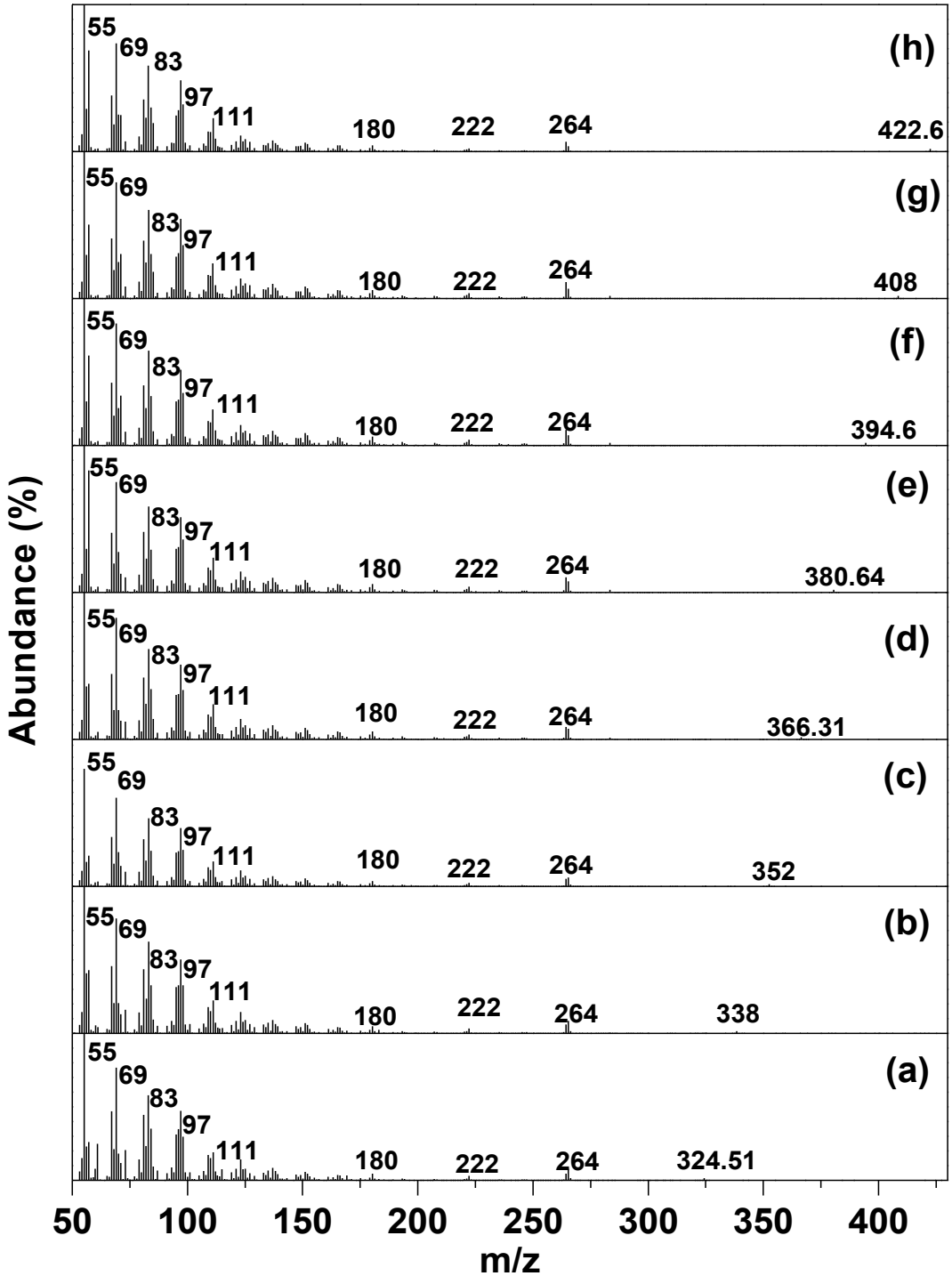

Fig.A.12. Mass spectra of (a) propyl oleate, (b) butyl oleate, (c) pentyl oleate, (d) hexyl oleate, (e) heptyl oleate, (f) octyl oleate, (g) nonyl oleate and (h) decyl oleate.

Propyl oleate: **FT-IR** (ATR, cm^{-1}): 2924 (CH_3), 2854 (CH_2), 1743 (C=O), 1457 (O–CH_3), 1170-1210 (C–O) cm^{-1}; **^{1}H–NMR** ($CDCl_3$, δ ppm): 5.34 (m, –C**H**=C**H**–), 4.1–4.2 (t, –OC**H**$_2$–), 2.18 (–CH=CH–C**H**$_2$), 2.3 (m, –C**H**$_2$–CO–), 1.29 (m, –(C**H**$_2$)$_n$– , 0.88 (m, –CH_2–C**H**$_3$), 0.90 (–O(CH_2)$_2$C**H**$_3$–), 1.73 (–OCH$_2$C**H**$_2$–), 1.64 (–CO–CH$_2$C**H**$_2$–); **^{13}C–NMR** ($CDCl_3$, δ ppm): 174.09 (–**C**O–CH_2–), 130.6 (–**C**H=**C**H–), 66.2 (–O**C**H$_2$–), 33.9 (–CO–**C**H$_2$–), 31.9 (ω3 –**C**H$_2$–), 22.7 (ω2 –**C**H$_2$–, H$_2$**C**–CH=CH–**C**H$_2$), 29.9 (H$_2$**C**–CH$_2$CH=CHCH$_2$–**C**H$_2$), 29.7-31.8 (–**C**H$_2$–), 25.0 (–CO–CH$_2$–**C**H$_2$–), 22.70 (ω2 –**C**H$_2$–), 14.16 (ω1 –**C**H$_3$), 10.3 (–O(CH_2)$_2$**C**H$_3$–), 21.9 (–OCH$_2$**C**H$_2$CH$_3$); **GC-MS**: Rt: 12.89 min; positive ion *m/z*: 324.51[M]$^+$, 264[M-59]$^+$(loss of propyloxy ion + H$^+$), 55 (loss of $C_4H_7^+$), 69 (loss of $C_5H_9^+$) 83 (loss of $C_6H_{11}^+$), 97 ((loss of $C_7H_{13}^+$), 111(loss of $C_8H_{15}^+$).

Butyl oleate: **FT-IR** (ATR, cm^{-1}): 2924 (CH_3), 2854 (CH_2), 1743 (C=O), 1457 (O–CH_3), 1170-1210 (C–O) cm^{-1}; **^{1}H–NMR** ($CDCl_3$, δ ppm): 5.34 (m, –C**H**=C**H**–), 4.1–4.2 (t, –OC**H**$_2$–), 2.18 (–CH=CH–C**H**$_2$), 2.3 (m, –C**H**$_2$–CO–), 1.29 (m, –(C*H*$_2$)$_n$–, 0.88 (m, –CH_2–C**H**$_3$, –O(CH_2)$_2$C**H**$_3$–), 1.64 (–CO–CH$_2$C**H**$_2$–, –OCH$_2$C**H**$_2$–); **^{13}C–NMR** ($CDCl_3$, δ ppm): 174.09 (–**C**O–CH_2–), 130.6 (–**C**H=**C**H–), 64.9 (–O**C**H$_2$–), 33.9 (–CO–**C**H$_2$–), 31.9 (ω3 –**C**H$_2$–), 22.7 (ω2 –**C**H$_2$–), 27.7 (H$_2$**C**–CH=CH–**C**H$_2$), 29.9 (H$_2$**C**–CH$_2$CH=CHCH$_2$–**C**H$_2$), 29.0-29.7 (–**C**H$_2$–), 25.0 (–CO–CH$_2$–**C**H$_2$–),14.16 (ω1 –**C**H$_3$), 18.9 (–O(CH_2)$_2$**C**H$_2$–), 13.8 (–O(CH_2)$_3$–**C**H$_3$); **GC-MS**: Rt: 13.70 min; positive ion *m/z*: 338[M]$^+$, 264 [M-74]$^+$ (loss of butoxy ion + H$^+$), 55 (loss of $C_4H_7^+$), 69 (loss of $C_5H_9^+$) 83 (loss of $C_6H_{11}^+$), 97 ((loss of $C_7H_{13}^+$), 111(loss of $C_8H_{15}^+$).

Pentyl oleate: : **FT-IR** (ATR, cm^{-1}): 2924 (CH_3), 2854 (CH_2), 1743 (C=O), 1457 (O–CH_3), 1170-1210 (C–O) cm^{-1}; **^{1}H–NMR** ($CDCl_3$, δ ppm): 5.34 (m, –C**H**=C**H**–), 4.1–4.2 (t, –OC**H**$_2$–), 2.18 (–CH=CH–C**H**$_2$), 2.3 (m, –C**H**$_2$–CO–), 1.25-1.31 (m, –(C**H**$_2$)$_n$–, 0.88 (m, –CH_2–C**H**$_3$, –O(CH_2)$_2$C**H**$_3$–), 1.64 (–CO–CH$_2$C**H**$_2$–, –OCH$_2$C**H**$_2$–); **^{13}C–NMR** ($CDCl_3$, δ ppm): 174.09 (–**C**O–CH_2–), 130.6 (–**C**H=**C**H–), 64.9 (–O**C**H$_2$–), 33.9 (–CO–**C**H$_2$–), 31.9 (ω3 –**C**H$_2$–), 22.7 (ω2 –**C**H$_2$–), 27.7 (H$_2$**C**–CH=CH–**C**H$_2$), 29.9 (H$_2$**C**–CH$_2$CH=CHCH$_2$–**C**H$_2$), 29.0-29.7 (–**C**H$_2$–), 25.0 (–CO–CH$_2$–**C**H$_2$–),14.16 (ω1 –**C**H$_3$, –O(CH_2)$_4$–**C**H$_3$), 22.4 (–O(CH_2)$_3$**C**H$_2$–), 28.0 (–O(CH_2)$_2$–**C**H$_2$–), 28.6 (–OCH$_2$**C**H$_2$–); **GC-MS**: Rt: 14.48 min; positive ion *m/z*: 352[M]$^+$, 264 [M-88]$^+$ (loss of pentoxy ion + H$^+$), 55 (loss of $C_4H_7^+$), 69 (loss of $C_5H_9^+$) 83 (loss of $C_6H_{11}^+$), 97 ((loss of $C_7H_{13}^+$), 111(loss of $C_8H_{15}^+$).

Hexyl oleate: **FT-IR** (ATR, cm^{-1})**:** 2924 (CH_3), 2854 (CH_2), 1743 (C=O), 1457 (O–CH_3), 1170-1210 (C–O) cm^{-1}; **^{1}H–NMR** ($CDCl_3$, δ ppm): 5.34 (m, –C**H**=C**H**–), 4.1–4.2 (t, –OC**H**$_2$–), 2.18 (–CH=CH–C**H**$_2$), 2.3 (m, –C**H**$_2$–CO–), 1.29 (m, –(C**H**$_2$)$_n$–, 0.88 (m, –CH_2–

C**H**$_3$, –O(CH$_2$)$_2$C**H**$_3$–), 1.64 (–CO–CH$_2$C**H**$_2$–, –OCH$_2$C**H**$_2$–); **^{13}C–NMR** (CDCl$_3$, δ ppm): 174.09 (–**C**O–CH$_2$–), 130.6 (–**C**H=**C**H–), 64.9 (–O**C**H$_2$–), 33.9 (–CO–**C**H$_2$–), 31.9 (ω3 –**C**H$_2$–), 22.7(ω2 –**C**H$_2$–, –O(CH$_2$)$_4$**C**H$_2$–), 27.7 (H$_2$**C**–CH=CH–**C**H$_2$), 29.9 (H$_2$**C**–CH$_2$CH=CHCH$_2$–**C**H$_2$), 29.0-29.7 (–**C**H$_2$–), 25.0 (–CO–CH$_2$–**C**H$_2$–), 14.16 (ω1 –**C**H$_3$,–O(CH$_2$)$_5$**C**H$_3$), 31.5 (–O(CH$_2$)$_3$**C**H$_2$–), 25.5 (–O(CH$_2$)$_2$**C**H$_2$–), 28.9 (–OCH$_2$**C**H$_2$–); **GC-MS**: Rt: 15.25 min; positive ion *m/z*: (+):366.31[M]$^+$, 264 [M-102]$^+$ (loss of hexoxy ion + H$^+$)55 (loss of C$_4$H$_7^+$), 69 (loss of C$_5$H$_9^+$) 83 (loss of C$_6$H$_{11}^+$), 97 ((loss of C$_7$H$_{13}^+$), 111(loss of C$_8$H$_{15}^+$)

Heptyl oleate: **FT-IR** (ATR, cm^{-1})**:** 2924 (CH$_3$), 2854 (CH$_2$), 1743 (C=O), 1457 (O–CH$_3$), 1170-1210 (C–O) cm^{-1}; **^{1}H–NMR** (CDCl$_3$, δ ppm): 5.34 (m, –C**H**=C**H**–), 4.1–4.2 (t, –OC**H**$_2$–), 2.18 (–CH=CH–C**H**$_2$), 2.3 (m, –C**H**$_2$–CO–), 1.29 (m, –(C**H**$_2$)$_n$–, 0.88 (m, –CH$_2$–C**H**$_3$, –O(CH$_2$)$_2$C**H**$_3$–), 1.64 (–CO–CH$_2$C**H**$_2$–, –OCH$_2$C**H**$_2$–); **^{13}C–NMR** (CDCl$_3$, δ ppm): 174.09 (–**C**O–CH$_2$–), 130.6 (–**C**H=**C**H–), 64.9 (–O**C**H$_2$–), 33.9 (–CO–**C**H$_2$–), 31.9 (ω3 –**C**H$_2$–, –O(CH$_2$)$_4$**C**H$_2$–), 22.7 (ω2 –**C**H$_2$–, –O(CH$_2$)$_5$**C**H$_2$–), 27.7 (H$_2$**C**–CH=CH–**C**H$_2$), 29.9 (H$_2$**C**–CH$_2$CH=CHCH$_2$–**C**H$_2$), 29.0-29.7 (–**C**H$_2$–), 25.0 (–COCH$_2$**C**H$_2$–), 14.16 (ω1–**C**H$_3$,–O(CH$_2$)$_6$**C**H$_3$), 29.0 (–O(CH$_2$)$_3$**C**H$_2$–), 25.8 (–O(CH$_2$)$_2$**C**H$_2$–), 28.9 (–OCH$_2$**C**H$_2$–); **GC-MS**: Rt: 15.97 min; positive ion *m/z*: 380.64[M]$^+$, 264 [M-116]$^+$ (loss of heptoxy ion + H$^+$) 55 (loss of C$_4$H$_7^+$), 69 (loss of C$_5$H$_9^+$) 83 (loss of C$_6$H$_{11}^+$), 97 ((loss of C$_7$H$_{13}^+$), 111(loss of C$_8$H$_{15}^+$).

Octyl oleate: **FT-IR** (ATR, cm^{-1})**:** 2924 (CH$_3$), 2854 (CH$_2$), 1743 (C=O), 1457 (O–CH$_3$) , 1170-1210 (C–O) cm^{-1}; **^{1}H–NMR** (CDCl$_3$, δ ppm): 5.34 (m, –C**H**=C**H**–), 4.1–4.2 (t, –OC**H**$_2$–), 2.18 (–CH=CH–C**H**$_2$), 2.3 (m, –C**H**$_2$–CO–), 1.29 (m, –(C**H**$_2$)$_n$–, 0.88 (m, –CH$_2$–C**H**$_3$, –O(CH$_2$)$_2$C**H**$_3$–), 1.64 (–CO–CH$_2$C**H**$_2$–, –OCH$_2$C**H**$_2$–); **^{13}C–NMR** (CDCl$_3$, δ ppm): 174.09 (–**C**O–CH$_2$–), 130.6 (–**C**H=**C**H–), 64.9 (–O**C**H$_2$–), 33.9 (–CO–**C**H$_2$–), 31.9 (ω3–**C**H$_2$–, –O(CH$_2$)$_5$**C**H$_2$–), 22.7(ω2 –**C**H$_2$–, –O(CH$_2$)$_6$**C**H$_2$–), 27.7 (H$_2$**C**–CH=CH–**C**H$_2$), 29.9 (H$_2$**C**–CH$_2$CH=CHCH$_2$–**C**H$_2$), 29.0-29.7 (–**C**H$_2$–), 25.0 (–CO–CH$_2$–**C**H$_2$–), 14.16 (ω1–**C**H$_3$,–O(CH$_2$)$_7$**C**H$_3$), 29.3 (–O(CH$_2$)$_3$**C**H$_2$–, –O(CH$_2$)$_4$**C**H$_2$–), 25.8 (–O(CH$_2$)$_2$**C**H$_2$–), 28.9 (–OCH$_2$**C**H$_2$–); Rt: 16.69 min; **GC-MS**: positive ion *m/z*: 394.6[M]$^+$, 264 [M-74]$^+$ (loss of octoxy ion + H$^+$), 55 (loss of C$_4$H$_7^+$), 69 (loss of C$_5$H$_9^+$) 83 (loss of C$_6$H$_{11}^+$), 97 (loss of C$_7$H$_{13}^+$), 111(loss of C$_8$H$_{15}^+$).

Nonyl oleate: **FT-IR** (ATR, cm^{-1})**:** 2924 (CH$_3$), 2854 (CH$_2$), 1743 (C=O), 1457 (O–CH$_3$), 1170-1210 (C–O) cm^{-1}; **^{1}H–NMR** (CDCl$_3$, δ ppm): 5.34 (m, –C**H**=C**H**–), 4.1–4.2 (t, –OC**H**$_2$–), 2.18 (–CH=CH–C**H**$_2$), 2.3 (m, –C**H**$_2$–CO–), 1.29 (m, –(C**H**$_2$)$_n$–, 0.88 (m, –CH$_2$–

C**H**$_3$, –O(CH$_2$)$_2$C**H**$_3$–), 1.64 (–CO–CH$_2$C**H**$_2$–, –OCH$_2$C**H**$_2$–); **^{13}C–NMR** (CDCl$_3$, δ ppm): 174.09 (–**C**O–CH$_2$–), 130.6 (–**C**H=**C**H–), 64.9 (–O**C**H$_2$–), 33.9 (–CO–**C**H$_2$–), 31.9 (ω3 –**C**H$_2$–, –O(CH$_2$)$_6$**C**H$_2$–), 22.7 (ω2 –**C**H$_2$–, –O(CH$_2$)$_7$**C**H$_2$–), 27.7 (H$_2$**C**–CH=CH–**C**H$_2$), 29.9 (H$_2$**C**–CH$_2$CH=CHCH$_2$–**C**H$_2$), 29.0-29.7 (–**C**H$_2$–), 25.0 (–CO–CH$_2$–**C**H$_2$–), 14.16 (ω1–**C**H$_3$,–O(CH$_2$)$_8$**C**H$_3$), 29.6(–O(CH$_2$)$_4$**C**H$_2$), 29.3 (–O(CH$_2$)$_5$**C**H$_2$–, –O(CH$_2$)$_3$**C**H$_2$), 25.8 (–O(CH$_2$)$_2$**C**H$_2$–), 28.9 (–OCH$_2$**C**H$_2$–); **GC-MS**: Rt: 17.38 min; positive ion *m*/*z*: 408[M]$^+$, 264 [M-144]$^+$ (loss of nonoxy ion + H$^+$), 55 (loss of C$_4$H$_7^+$), 69 (loss of C$_5$H$_9^+$) 83 (loss of C$_6$H$_{11}^+$), 97 ((loss of C$_7$H$_{13}^+$), 111(loss of C$_8$H$_{15}^+$).

Decyl oleate: **FT-IR** (ATR, cm^{-1})**:** 2924 (CH$_3$), 2854 (CH$_2$), 1743 (C=O), 1457 (O–CH$_3$) , 1170-1210 (C–O) cm^{-1}; **^{1}H–NMR** (CDCl$_3$, δ ppm): 5.34 (m, –C**H**=C**H**–), 4.1–4.2 (t, –OC**H**$_2$–), 2.18 (–CH=CH–C**H**$_2$), 2.3 (m, –C**H**$_2$–CO–), 1.29 (m, –(C**H**$_2$)$_n$–, 0.88 (m, –CH$_2$–C**H**$_3$, –O(CH$_2$)$_2$C**H**$_3$–), 1.64 (–CO–CH$_2$C**H**$_2$–, –OCH$_2$C**H**$_2$–); **^{13}C–NMR** (CDCl$_3$, δ ppm): 174.09 (–**C**O–CH$_2$–), 130.6 (–**C**H=**C**H–), 64.9 (–O**C**H$_2$–), 33.9 (–CO–**C**H$_2$–), 31.9 (ω3 –**C**H$_2$–, –O(CH$_2$)$_7$**C**H$_2$–), 22.7 (ω2 –**C**H$_2$–, –O(CH$_2$)**C**H$_2$–), 27.7 (H$_2$**C**–CH=CH–**C**H$_2$), 29.9 (H$_2$**C**–CH$_2$CH=CHCH$_2$–**C**H$_2$), 29.0-29.7 (–**C**H$_2$–), 25.0 (–CO–CH$_2$–**C**H$_2$–), 14.16 (ω1–*C*H$_3$,–O(CH$_2$)$_9$**C**H$_3$), 29.6 (–O(CH$_2$)$_4$**C**H$_2$–, –O(CH$_2$)$_4$**C**H$_2$–), 29.3 (–O(CH$_2$)$_6$**C**H$_2$–, –O(CH$_2$)$_3$**C**H$_2$), 25.8 (–O(CH$_2$)$_2$**C**H$_2$–), 28.9 (–OCH$_2$**C**H$_2$–) ; **GC-MS**: Rt: 18.04 min; positive ion *m*/*z*: 422.6[M]$^+$, 264 [M-158]$^+$ (loss of decoxy ion + H$^+$) 55 (loss of C$_4$H$_7^+$), 69 (loss of C$_5$H$_9^+$), 83 (loss of C$_6$H$_{11}^+$), 97 ((loss of C$_7$H$_{13}^+$), 111(loss of C$_8$H$_{15}^+$).

Methyl propanoate: **FT-IR** (ATR, cm^{-1})**:** 2924 (CH$_3$), 2854 (CH$_2$), 1750 (C=O), 1445 (O–CH$_3$) , 1170-1210 (C–O) cm^{-1}; **^{1}H–NMR** (CDCl$_3$, δ ppm): 3.6 (s, –OC**H**$_3$), 2.3 (m, –C**H**$_2$–CO–),1.09 (m, –CH$_2$–C**H**$_3$); **^{13}C–NMR** (CDCl$_3$, δ ppm): 174.09 (–**C**O–CH$_2$–), 51.4 (–O**C**H$_3$), 9.4 (ω1 –**C**H$_3$), 27.3 (–CO–**C**H$_2$–); **GC-MS**: Rt: 3.27 min; positive ion *m*/*z*: 88[M]$^+$, 55 (loss of methoxy ion), 73 [M-15] (loss of methyl radical).

Methyl butyrate: **FT-IR** (ATR, cm^{-1})**:** 2924 (CH$_3$), 2854 (CH$_2$), 1750 (C=O), 1445 (O–CH$_3$), 1170-1210 (C–O) cm^{-1}; **^{1}H–NMR** (CDCl$_3$, δ ppm): 3.6 (s, –OC**H**$_3$), 2.3 (m, –C**H**$_2$–CO–),0.88 (m, –CH$_2$–C**H**$_3$); 1.65 (m, –CO–CH$_2$–C**H**$_2$–) **^{13}C–NMR** (CDCl$_3$, δ ppm): 174.09 (–**C**O–CH$_2$–), 51.4 (–O**C**H$_3$), 13.5 (ω1 –**C**H$_3$), 18.4 (ω2 –**C**H$_2$), 35.8 (–CO–**C**H$_2$–); **GC-MS**: Rt: 4.03 min; positive ion *m*/*z*: 102[M]$^+$, 71(loss of methoxy ion), 73(loss of CH$_2$COOCH$_3$).

Methyl caproate: **FT-IR** (ATR, cm^{-1})**:** 2924 (CH$_3$), 2854 (CH$_2$), 1750 (C=O), 1445 (O–CH$_3$), 1170-1210 (C–O) cm^{-1}; **^{1}H–NMR** (CDCl$_3$, δ ppm): 3.6 (s, –OC**H**$_3$), 2.3 (m, –C**H**$_2$–CO–), 1.65 (m, –CO–CH$_2$–C**H**$_2$–), 1.29 (m, –(C**H**$_2$)$_n$– , 0.88 (m, –CH$_2$–C**H**$_3$); **^{13}C–NMR**

($CDCl_3$, δ ppm): 174.09 (–**C**O–CH_2–), 51.4 (–O**C**H_3), 34.1 (–CO–**C**H_2–), 31.9 (ω3 –**C**H_2–), 25.6–24.80 (–CO–CH_2–**C**H_2–) 22.7 (ω2 –**C**H_2–) and 14.16 (ω1 –**C**H_3).

Methyl caprylate: **FT-IR** (ATR, cm^{-1})**:** 2924 (CH_3), 2854 (CH_2), 1750 (C=O), 1445 (O–CH_3), 1170-1210 (C–O) cm^{-1}; **^{1}H–NMR** ($CDCl_3$, δ ppm): 3.6 (s, –OC**H**$_3$), 2.3 (m, –C**H**$_2$–CO–), 1.65 (m, –CO–CH_2–C**H**$_2$–), 1.29 (m, –(C**H**$_2$)$_n$– , 0.88 (m, –CH_2–C**H**$_3$); **^{13}C–NMR** ($CDCl_3$, δ ppm): 174.09 (–**C**O–CH_2–), 51.4 (–O**C**H_3), 34.1 (–CO–**C**H_2–), 31.9 (ω3 –**C**H_2–), 29.6 (–(**C**H_2)$_n$–), 25.6–24.80 (–CO–CH_2–**C**H_2–) 22.7 (ω2 –**C**H_2–) and 14.16 (ω1 –**C**H_3)

Methyl laurate: **FT-IR** (ATR, cm^{-1})**:** 2924 (CH_3), 2854 (CH_2), 1750 (C=O), 1445 (O–CH_3), 1170-1210 (C–O) cm^{-1}; **^{1}H–NMR** ($CDCl_3$, δ ppm): 3.6 (s, –OC**H**$_3$), 2.3 (m, –C**H**$_2$–CO–), 1.65 (m, –CO–CH_2–C**H**$_2$–), 1.29 (m, –(C**H**$_2$)$_n$– , 0.88 (m, –CH_2–C**H**$_3$); **^{13}C–NMR** ($CDCl_3$, δ ppm): 174.09 (–**C**O–CH_2–), 51.4 (–O**C**H_3), 34.1 (–CO–**C**H_2–), 31.9 (ω3 –**C**H_2–), 29.6 (–(**C**H_2)$_n$–), 25.6–24.80 (–CO–CH_2–**C**H_2–) 22.7 (ω2 –**C**H_2–) and 14.16 (ω1 –**C**H_3).

Methyl palmitate: **FT-IR** (ATR, cm^{-1})**:** 2924 (CH_3), 2854 (CH_2), 1750 (C=O), 1445 (O–CH_3), 1170-1210 (C–O) cm^{-1}; **^{1}H–NMR** ($CDCl_3$, δ ppm): 3.6 (s, –OC**H**$_3$), 2.3 (m, –C**H**$_2$–CO–), 1.65 (m, –CO–CH_2–C**H**$_2$–), 1.29 (m, –(C**H**$_2$)$_n$– , 0.88 (m, –CH_2–C**H**$_3$); **^{13}C–NMR** ($CDCl_3$, δ ppm): 174.09 (–**C**O–CH_2–), 51.4 (–O**C**H_3), 34.1 (–CO–**C**H_2–), 31.9 (ω3 –**C**H_2–), 29.6 (–(**C**H_2)$_n$–), 25.6–24.80 (–CO–CH_2–**C**H_2–) 22.7 (ω2 –**C**H_2–) and 14.16 (ω1 –**C**H_3); **GC-MS**: Rt: 9.84 min ; positive ion *m*/*z*: 270.4$[M]^+$, 74[M-22] (loss of Maclefferty ion), 55 (loss of $C_4H_7^+$), 143 (loss of $(CH_2)_6COOCH_3$), 87 (loss of $(CH_2)_2COOCH_3$).

Methyl stearate: **FT-IR** (ATR, cm^{-1})**:** 2924 (CH_3), 2854 (CH_2), 1750 (C=O), 1445 (O–CH_3), 1170-1210 (C–O) cm^{-1}; **^{1}H–NMR** ($CDCl_3$, δ ppm): 3.6 (s, –OC**H**$_3$), 2.3 (m, –C**H**$_2$–CO–), 1.65 (m, –CO–CH_2–C**H**$_2$–), 1.29 (m, –(C**H**$_2$)$_n$– , 0.88 (m, –CH_2–C**H**$_3$); **^{13}C–NMR** ($CDCl_3$, δ ppm): 174.09 (–**C**O–CH_2–), 51.4 (–O**C**H_3), 34.1 (–CO–**C**H_2–), 31.9 (ω3 –**C**H_2–), 29.6 (–(**C**H_2)$_n$–), 25.6–24.80 (–CO–CH_2–**C**H_2–) 22.7 (ω2 –**C**H_2–) and 14.16 (ω1 –**C**H_3); **GC-MS**: Rt: 16.49 min; positive ion *m*/*z*: 298.5$[M]^+$, 74[M-22] (loss of Maclefferty ion), 55 (loss of $C_4H_7^+$), 143 (loss of $(CH_2)_6COOCH_3$), 87 (loss of $(CH_2)_2COOCH_3$).

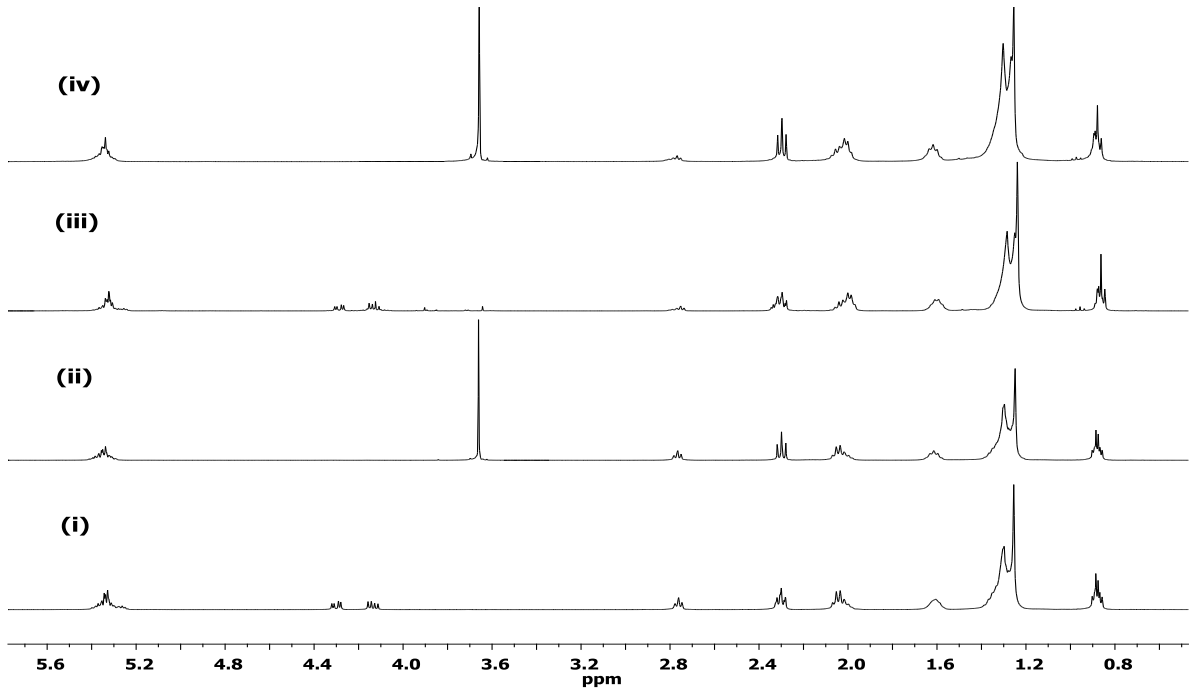

Fig.A.13. Comparison of ^{1}H-NMR spectra of (i) cottonseed oil with its (ii) methyl ester and (iii) karanja oil with its (iv) corresponding methyl esters.

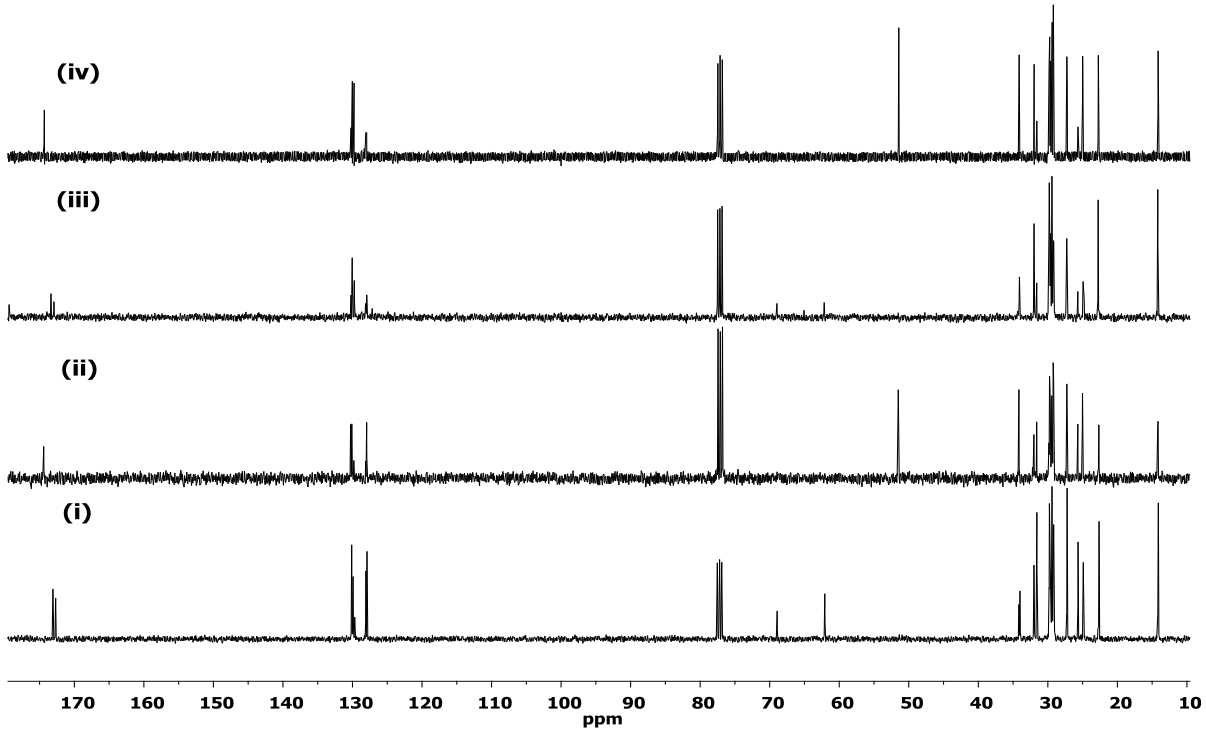

Fig.A.14. Comparison of ^{13}C-NMR spectra of (i) cottonseed oil with its (ii) methyl ester and (iii) karanja oil with its (iv) corresponding methyl esters.

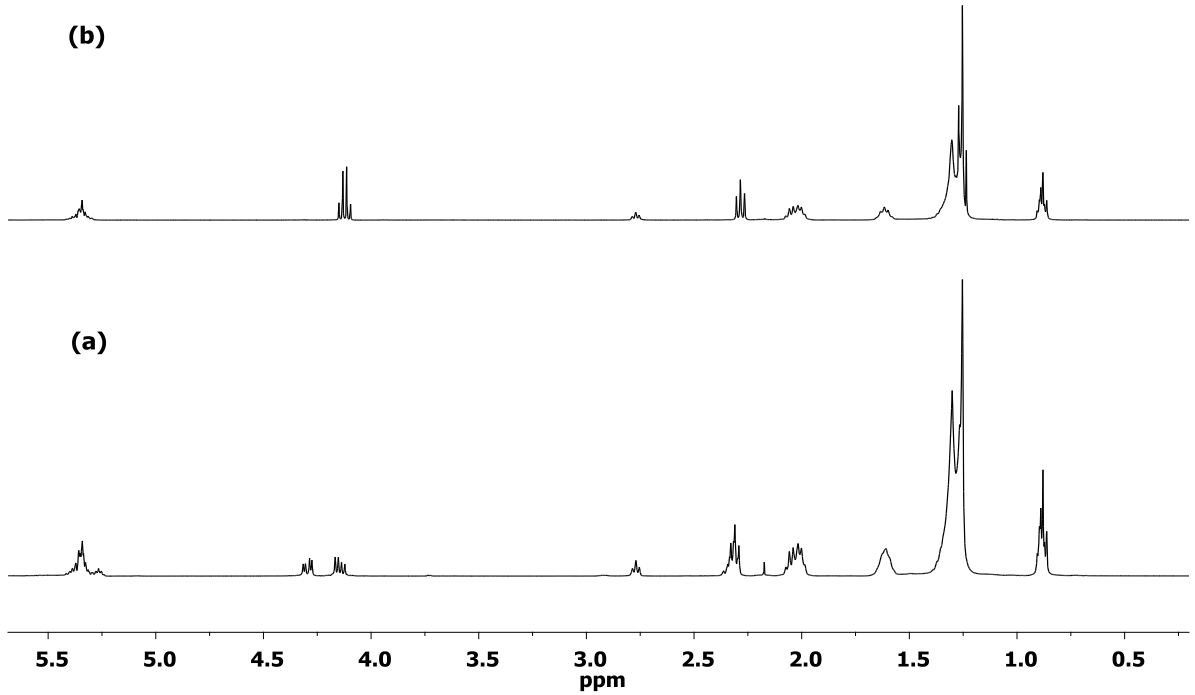

Fig. A.15. Comparison of ^{1}H-NMR spectra of (a) jatropha oil and (b) corresponding ethyl ester.

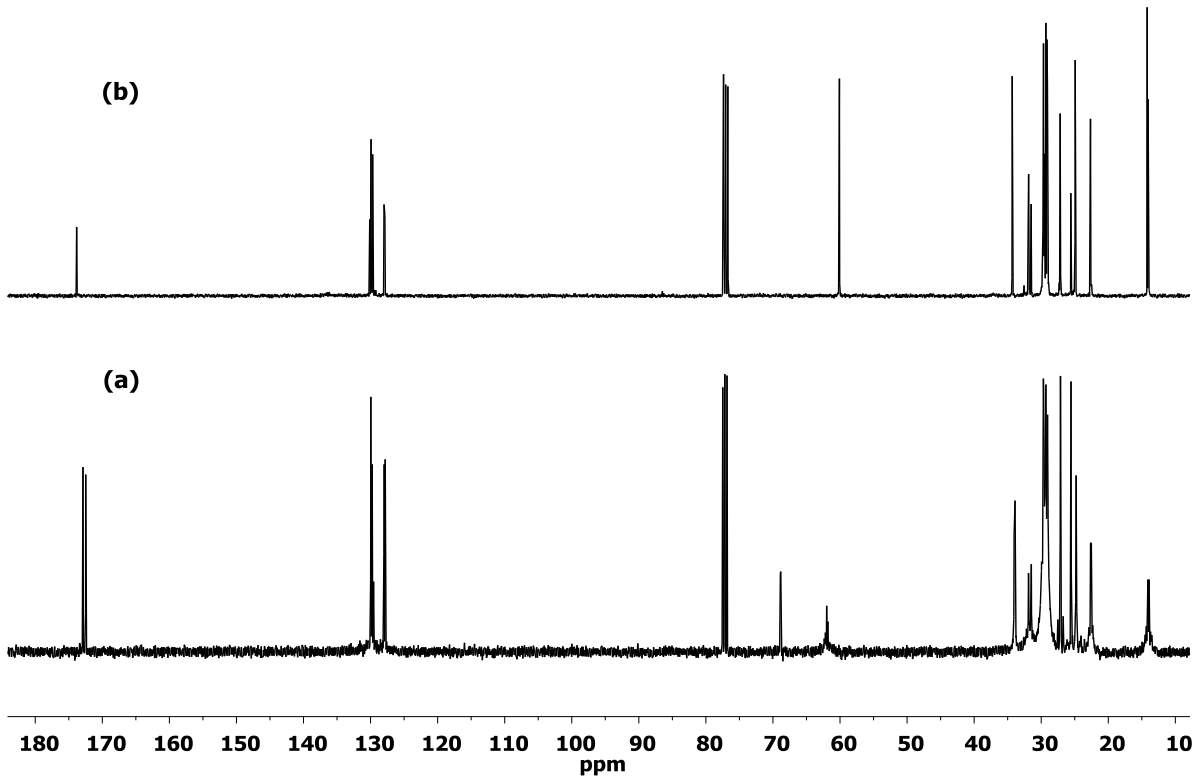

Fig. A.16. Comparison of ^{13}C-NMR spectra of (a) jatropha oil and (b) corresponding ethyl ester.

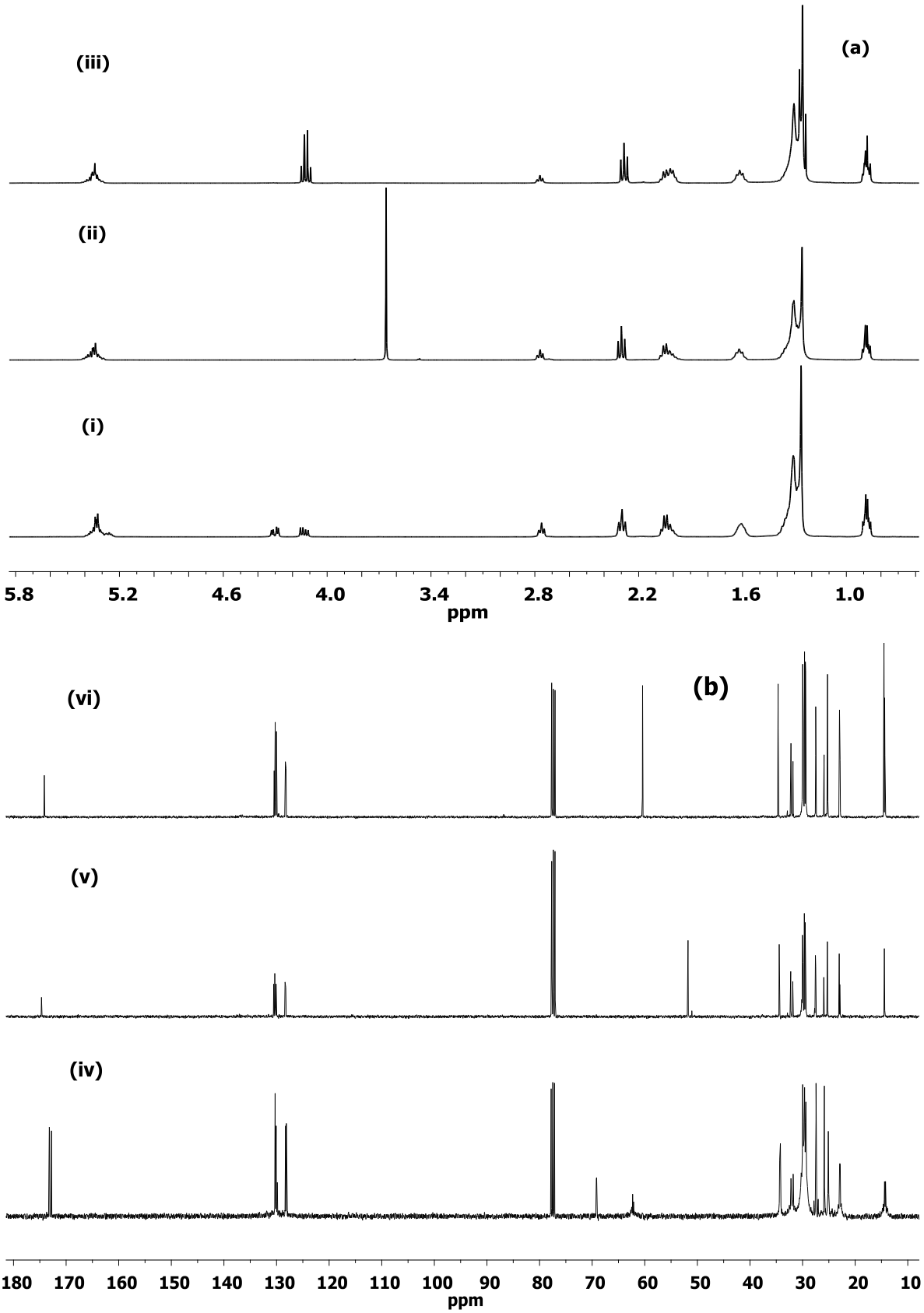

Fig.A.17. Comparison of (a) ^{1}H-NMR and (b) ^{13}C-NMR spectra of waste cottonseed oil (i and iv) with its methyl (ii and v) and ethyl esters (iii and vi).

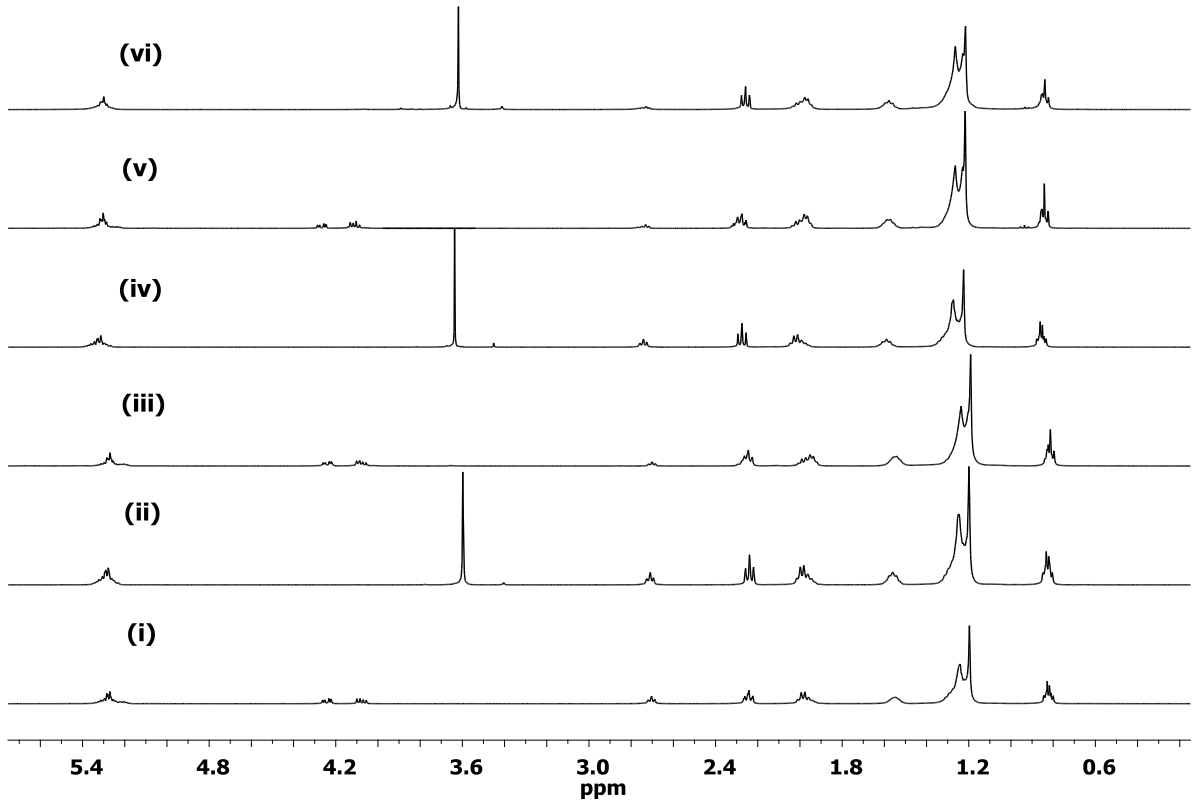

Fig.A.18. Comparison of ^{1}H-NMR (i) cotton seed oil with its (ii) methyl ester (iii) jatropha oil with its (iv) methyl ester (v) karanja oil with its corresponding (vi) methyl ester.

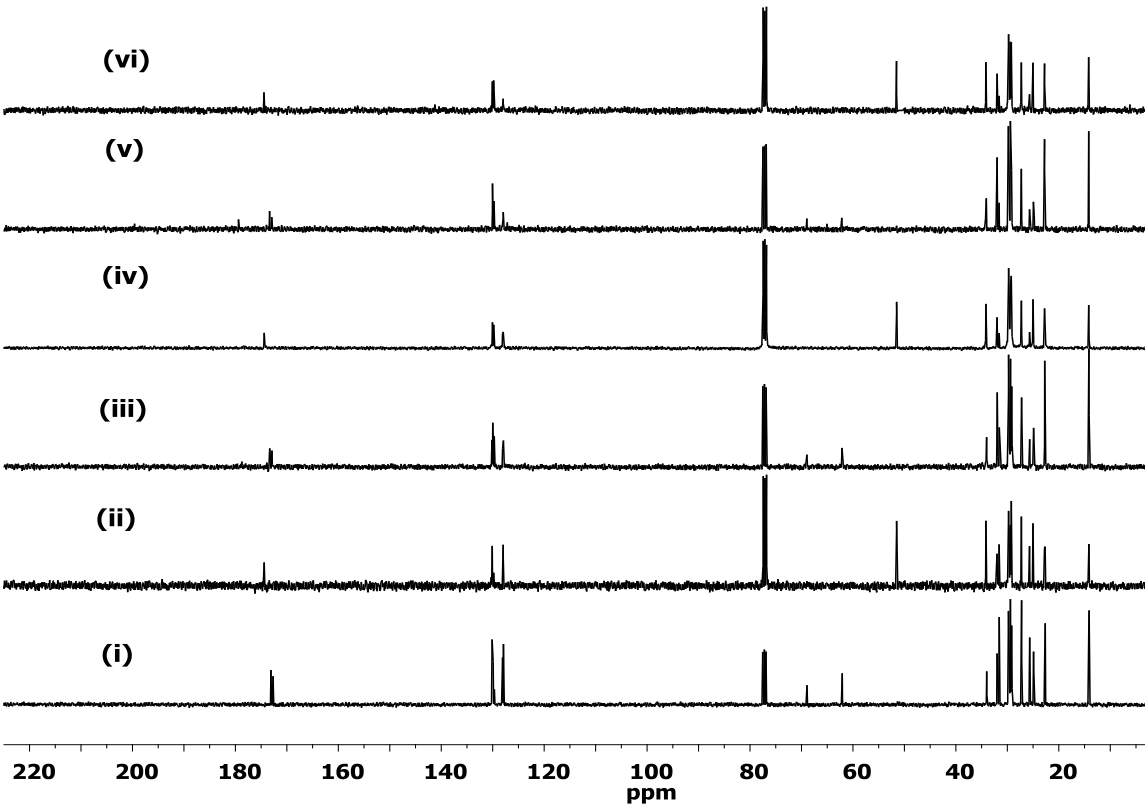

Fig.A.19. Comparison of ^{13}C-NMR (i) cotton seed oil with its (ii) methyl ester (iii) jatropha oil with its (iv) methyl ester (v) karanja oil with its corresponding (vi) methyl ester.

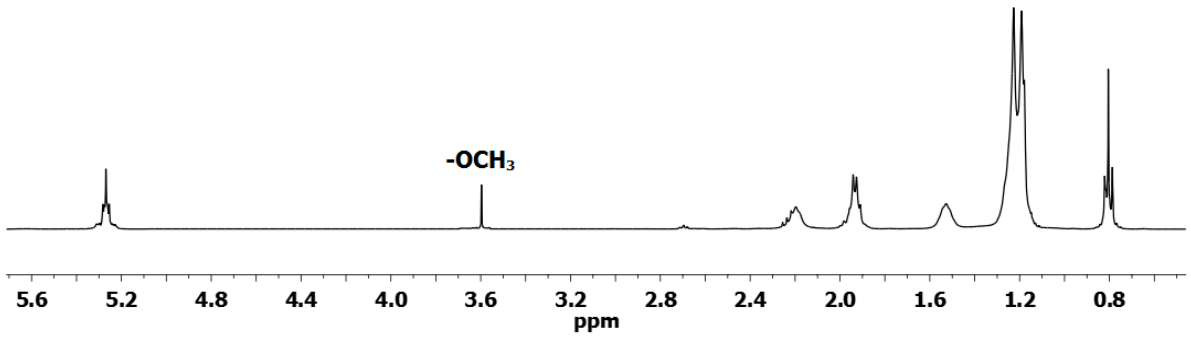

Fig.A.20. ^{1}H-NMR of methyl oleate. (**Reaction conditions:-** methanol to oleic acid molar ratio – 12:1 ; catalyst amount – 5 wt% with respect to oleic acid; reaction temperature – 65 °C; reaction duration – 75 min).

APPENDIX B

Table B.1. Physicochemical properties of the FAME and FAEE prepared from JO.

Parameters	Units	FAME	FAEE	EN14214	Test method
Ester content	%	>99 %	>99 %	≥96.5	^{1}H-NMR
Flash point	ºC	110	120	100-170	ASTM D93
Pour point	ºC	1	2	-5 to10	ASTM D2500
Kinematic viscosity at 40 ºC	cSt	4.50	4.83	1.9-6.0	ASTM D445
Density at 31 ºC	kg/mm^3	870	880	860-900	ISI448 P:32
Ash	%	NIL	0.01	≤0.02	ASTM D874
Iodine value	mg of I_2/g of sample	75.9	87.8	<120	^{1}H-NMR*
Acid value	mg of KOH/g of sample	0.4	0.5	≤0.5	ASTM D664
Saponification value	mg of KOH/g of sample	180	182.32	-	ASTM D5558

Table B.2. Physicochemical properties of the FAME and FAEE prepared from WO.

Parameters	Units	FAME	FAEE	EN14214	Test method
Ester content	%	99 %	99 %	≥96.5	^{1}H–NMR
Flash point	ºC	120	114	100–170	ASTM D93
Pour point	ºC	2	1	–5 to10	ASTM D2500
Water content	%	0.25	0.27	<0.5	ASTM D2709
Kinematic viscosity at 40 ºC	cSt	4.60	4.73	1.9–6.0	ASTM D445
Density at 31 ºC	kg/mm^3	867	870	860–900	ISI448 P:32
Ash	%	NIL	0.01	≤0.02	ASTM D874
Iodine value	mg of I_2/g of sample	78.9	80.1	<120	^{1}H–NMR*
Acid value	mg of KOH/g of sample	0.3	0.4	≤0.5	ASTM D664
Saponification value	mg of KOH/g of sample	180.5	181.23	-	ASTM D5558

* following the method given in Kumar *et al.*, 2012

Reference

Kumar, R.; Bansal, V.; Patel, M. B.; Sarpal, A. S.; 1H nuclear magnetic resonance (NMR) determination of the iodine value in biodiesel produced from algal and vegetable oils. *Energy Fuel*, **2012**, 26, 7005-7008.

LIST OF PUBLICATIONS

Kaur, N.; Ali, A.; Preparation and application of Ce/ZrO_2-TiO_2/SO_4^{2-} as solid catalyst for the esterification of fatty acids. *Renew. Energ.*, **2015**, 81, 421-43.

Kaur, N; Ali, A; Biodiesel prouction via ethaolysis of jatropha oil using molybdenum impregnated cacium oxide as solid ctaalyst. *RSC Adv.*, **2015**, 5, 13285-13295.

Kaur, N.; Ali, A.; Lithium zirconate as solid catalyst for simultaneous esterification and transesterification of low quality triglycerides. *Appl. Catal. A: Gen.*, **2015,** 489, 193-202.

Kaur, N.; Ali, A.; One pot transesterification and esterification of waste cooking oil via ethanolysis using Sr:Zr mixed oxide as solid catalyst. *RSC Adv*., **2014**, 4, 43671-43681.

Kaur, N.; Ali, A.; Kinetics and reusability of Zr/CaO as heterogeneous catalyst for the ethanolysis and methanolysis of Jatropha crucas oil, *Fuel Process. Technol*., **2014**, 119, 173-184.

Kaur, N.; Ali, A.; Lithium ions-supported magnesium oxide as nano-sized solid catalyst for biodiesel preparation from mutton fat. *Energ. Sourc. Part A,* **2013**, 35, 184-192.

MANUSCRIPT UNDER PREPARATION

Kaur, N.; Ali, A.; Cerium impregnated CaO based mixed oxide catalyst for the ethanolysis of waste cotton seed oil.

CONFERENCE PROCEEDINGS

Kaur, N; Ali, A; Methanolysis of Jatropha oil employing Mg-Zr/CaO as heterogeneous catalyst, proceedings of conference on Exploring Basic and Applied Sciences for Next Generation Frontiers, Elsevier publishers, ISBN: 9789351073130, **2014,** Chapter 49, 180-184.

Kaur, N; Ali, A; Sodium impregnated zirconia as a solid base catalyst for the transesterification of waste cotton seed oil, proceedings of conference on Exploring Basic and Applied Sciences for Next Generation Frontiers, Elsevier publishers, ISBN:9789351073130, **2014,** Chapter 50, 185-188.

CONFERENCES

N. Kaur and A. Ali, Synthesis and characterization of alkali/calcium mixed oxide as solid catalyst for the transesterification of triglycerides, *National Conference on "Emerging Trends in Chemistry-Biology Interface 2011" held at Kumaun University, Nainital during Nov. 03-05,* **2011**. **(Award for Best Poster Presentation in Biodiesel/Application of nanomaterial).**

N. Kaur and A. Ali, Preparation, Characterization and application of heterogeneous solid catalyst for biodiesel production from cotton seed oil, *International Conference on "Functional Materials for sustainable energy and advanced technology" held at Thapar University, Patiala during Feb,13-15,* **2012**.

N. Kaur and A. Ali, Synthesis and characterization of zirconium impregnated calcium oxide as solid catalyst for the transesterification of triglycerides, "*National Conference on Preservation of Environment: Challenges before Humanity" held at Sri Guru Granth Sahib World University, Fatehgarh Sahib on 14th March,* **2013 (Award for Best Poster).**

N. Kaur and A. Ali, Zirconium impregnated calcium oxide as solid catalyst for the ethanolysis of jatropha oil, *National Conference on* "*Innovative Molecules for Sustainable Future" held at Thapar University, Patiala during Oct. 24-26,* **2013**.

N. Kaur and A. Ali, Sodium impregnated zirconia as a solid base catalyst for the transesterification of waste cotton seed oil *National Conference on "Exploring Basic and Applied Sciences for Next Generation Frontiers" held at Lovely Professional University, Phagwara during Nov. 14-15,* **2014.**

N. Kaur and A. Ali, Methanolysis of jatropha oil employing Mg-Zr/CaO as heterogeneous catalyst, *National Conference on "Exploring Basic and Applied Sciences for Next Generation Frontiers" held at Lovely Professional University, Phagwara during Nov. 14-15,* **2014.**